University of Cape Town

Dissertation submitted in partial fulfilment of the requirements for the degree

Master of Science in Engineering

Department of Chemical Engineering

University of Cape Town

The use of model compounds to investigate the influence of fuel composition on the thermo-oxidative stability of FAME/diesel blends

---

Hundzukani Vukeya

Supervisor: Dr Chris Woolard January 2015

Plagiarism declaration

1. I know that plagiarism is wrong. Plagiarism is using another's work and to pretend that it is one's own.
2. Each significant contribution to, and quotation in, this project from the work, or works of other people has been attributed and has been cited and referenced.
3. This project is my own work.
4. I have not allowed, and will not allow, anyone to copy my work with the intention of passing it off as his or her own work.
5. I acknowledge that copying someone else's assignment or project, or part of it, is wrong, and declare that this is my own work.

Hundzukani Marvelous Vukeya

Signed by candidate

SIGNATURE: Signature Removed

DATE: January 2015

Acknowledgements

1. Firstly I would like to acknowledge Sasol Fuels Technology as well as the National Research Foundation of South Africa for their financial support. I enjoyed working on my project because I did not have any financial concerns and I thank you for that.
2. I would like to acknowledge and extend my honest gratitude to my supervisor, Dr Chris Woolard, for his encouragement and comments on my project. I would also like to thank him for guiding me throughout this study. I really appreciate the time he took to assist me. Further, I would like to thank him for giving me the opportunity to do the project at SAFL and for having faith in me. Last but not least, I would like to thank him for the journal club. I learnt a lot about my project and it raised awareness of what other people were working on for me and my fellow MSc students.
3. I would specially like to thank Jeanri Coetzee, Uyuendiwannyi Mandavha, Irenee Kaminuza and Gerhard Lourens for their backing throughout my project.
4. I would like to thank my SAFL colleagues for their livelihood.
5. Finally, I would like to give special thanks to my family for their care and words of encouragement.

Table of contents

List of illustrations

List of tables

List of abbreviations and acronyms

% m/m	percentage mass per mass
% v/v	percentage volume per volume
amu	atomic mass unit
ASTM	ASTM International, formerly American Society for Testing and Materials
ASTM D6751-14	ASTM - Standard specification for biodiesel fuel blend stock (B100) for middle distillate fuels
ASTM D7545-14	ASTM - Standard test method for oxidation stability of middle distillate Fuels — rapid small scale oxidation test (RSSOT
ASTM D7739-11	ASTM - Standard practice for thermo-oxidative stability measurement via quartz crystal microbalance
ATR	Attenuated total reflectance
Bx	an x % blend (% v/v) of biodiesel with petroleum diesel
bhp	Brake horsepower
BHT	Butylated hydroxy toluene
BPX90	[90% cyanopropyl] methyl-polysiloxane column [stationary phase: cyanopropyl-substituted polysilphenylene-siloxane]
BPX5	[5% diphenyl/90%dimethyl] polysiloxane column [stationary phase: chemically bonded 5% phenyl-95% dimethylpolysiloxane]
CeBER	Centre for Bioprocess Engineering Research
CFPP	Cold filter plugging point
CI	Compression ignition
DMC	Diesel model compound
EN 590:2013	European Union standard - Automotive fuels. Diesel. Requirements and test methods
EN 14112:2003	European Union standard - Fat and oil derivatives—fatty acid methyl esters (FAME)—determination of oxidation stability (accelerated oxidation test)
EN 14214:2013	European Union standard - Automotive fuels. Fatty acid methyl esters (FAME) for diesel engines.
ESI-MS	Electrospray ionisation-mass spectrometry
ESI-MS(+)	Electrospray ionisation-mass spectrometry (positive ion mode)
ESI-MS(-)	Electrospray ionisation-mass spectrometry (negative ion mode)
FAME	Fatty acid methyl ester
FTIR	Fourier transform infrared spectroscopy
GC-FID	Gas chromatography-flame ionisation detector
GC-MS	Gas chromatography-mass spectrometry
GPC	Gel permeation chromatography
HPLC	High performance liquid chromatography
HP-ULTRA 1	Methyl polysiloxane [stationary phase: bonded methyl polysiloxane]
ID	Internal diameter
MALDI-MS	Matrix-assisted laser desorption/ionisation-mass spectrometry
max	Maximum
min	Minimum

ML	Methyl linoleate
MLN	Methyl linolenate
MO	Methyl oleate
m/z	Mass to charge ratio
NMR	Nuclear magnetic resonance
NOx	Mono-nitrogen oxides
PM	Particulate matter
PM10	Particulate matter, 10 μm or less
PMCC	Pensky-Martens closed cup
ppm	Parts per million (mass), mg/kg
QCM	Quartz crystal microbalance
rpm	Revolutions per minute
RME	Rapeseed methyl ester
RMEMC	Rapeseed methyl ester model compound
SAFL	Sasol Advanced Fuels Laboratory
SANS 342-2006	South African national standard – Automotive diesel fuel
SME	Soybean methyl ester
SMORS	Soluble macromolecular oxidatively reactive species
SPK	Synthetic paraffinic kerosene
TAM	Toluene/acetone/methanol solvent (1:1:1 % v/v) mixture
TEM	Transmission electron microscopy
TOD	Thermo-oxidative deposit
UCT	University of Cape Town
USA	United States of America
UV/Vis	Ultra violet-visible
vol	Volume

Abstract

Biodiesel can be used in diesel engines without significant modification of the engine prior to use because it has properties similar to those of petroleum diesel. Biodiesel, however, exhibits lower stability compared to petroleum diesel. Small differences in fuel properties such as component concentration or total acidity can lead to the formation of deposits which can reduce engine performance and increase maintenance requirements and costs.

Thermo-oxidative stressing was performed in two reactor systems in this study. For comparative purposes both sets of experiments were performed at 140^{o}C. The systems used were a quartz crystal microbalance (QCM) in which oxygen was limited and open glass flasks under flowing air (unlimited oxygen). To simplify analysis, diesel model compound systems were used in which full boiling range diesel was replaced with single compounds representing the classes of compounds found in petroleum diesel. The model compounds were *n*-hexadecane, tetralin and decalin. Fuel analysis was performed using gas chromatography (GC) with mass spectrometric (MS) and flame ionisation (FID) detection. Further analytical methods included Fourier transform infrared (FTIR) and ultraviolet-visible (UV-Vis) spectroscopy as well as electrospray ionisation-mass spectrometry (ESI-MS).

This study represents the first application of QCM methodology to systems that contain fatty acid methyl esters (FAMEs). FAMEs with different degrees of unsaturation were investigated. The quantities of deposits formed were as follows: methyl linolenate (40.1 μg/cm^2) and methyl linoleate (19.2 μg/cm^2) when these were blended with diesel model compounds in a 20:80 ratio. These values are significantly higher than those typically reported for middle distillates. Increased polyunsaturation of the FAME led to increased deposit formation. Spectroscopic investigations revealed very small, if any, changes to bulk fuel composition during oxidation in a QCM. GC and ESI-MS analysis demonstrated the formation of oxygenates but in small concentrations. Nonetheless these were sufficient to initiate the formation of deposits.

More severe conditions used in open flask experiments led to greater quantities of, more types of, and more highly oxygenated products as seen by GC and, with respect to the latter, especially by ESI-MS. FTIR spectroscopy revealed the inclusion of oxygen-containing

functional groups. Increasing deposit precursor molecular mass and polarity led to phase separation in these experiments. Colour and UV-Vis changes were suggestive of the formation of conjugated systems. Examples of these species were identified by GC-MS.

The QCM was also useful in the exploration of fuel solvency. This study represents, as far as the author is aware, the first application of a QCM in this area. Fuels, with small quantities of biodiesel added, formed greater amounts of deposits than petroleum diesel model compounds or 100% biodiesel. Furthermore these systems consumed oxygen slightly faster. This points to a complex interaction between reactivity (faster oxygen uptake) and fuel polarity. This study has demonstrated the versatility of the QCM methodology for application to fuels beyond petroleum middle distillates.

FAME molecules were observed to be highly oxygenated and formed highly oxygenated dimers and a small quantity of trimers/tetramers during oxidation. It was observed that under severe oxidative conditions (flowing oxygen) the types of high molecular species formed differed from those formed during constrained oxygen stressing in a QCM.

Existing mechanisms for fuel oxidation were validated and in some cases extended. A possible soluble macromolecular oxidatively reactive species (SMORS), 1,4-naphthoquinone, was identified from the oxidation of tetralin by GC-MS and ESI-MS. Previously unobserved species such as 1,2-dicarboxylic acids, derived from tetralin and decalin, were reported and used to extend existing mechanistic schemes. The formation of higher molecular weight species that result from the interaction of alkenes (derived) from paraffin cracking with radicals such as the 1-tetralyl radical are also explained.

-

1. Introduction

1.1 Background and scope

Petroleum diesel is a mixture of hydrocarbons distilled from crude oil at temperatures between 160°C and 360°C. It is used as fuel in compression ignition (CI) engines which have the potential to achieve higher thermal efficiency due to their high compression ratio (*1*). Petroleum diesel is of great importance as it provides energy used for transportation, manufacturing, farming, *etc*.

Biodiesel is an alternative fuel for compression ignition engines. Its use reduces the dependence on fossil fuels which are expected to decrease in availability and affordability (*2*). Furthermore, biodiesel has the potential to reduce nett greenhouse gas emissions which would impact on potential global warming (*3*,*4*,*5*).

Because fatty acid methyl esters (FAMEs) have similar properties to those of the petroleum diesel, they can be used in compression ignition with little or no modification to the engine (*6*). Blends of biodiesel and petroleum diesel have been commercialised around the world with four feedstocks dominating production. These are rapeseed oil, sunflower oil, palm oil and soybean oil (*3*,*6*,*7*,*8*) . Various levels of biodiesel, *e.g.,* B5 (a 5% (% v/v) blend of biodiesel with petroleum diesel) are approved for operation in CI engines (*9*).

Concern has, however, been expressed about the stability of biodiesel. Degradation of fuel can lead to the formation of high molecular weight, soluble species and ultimately deposits (*10*,*11*). The formation of deposits and insoluble species within vehicular fuel lines is a very complex topic which involves bulk liquid-phase reactions, nucleation of particles through polymerisation or clustering reactions, solubility, transport phenomena and surface reactions (*12*).

FAMEs have reduced stability, compared to petroleum diesel, because of the presence of unsaturated methyl esters. FAME degradation may alter fuel properties by forming undesirable products such as soluble and insoluble oligomers (*13*) in addition to soluble epoxides, ketones, acids, alcohols and aldehydes (*14*).

Fuel may degrade by a variety of reaction pathways. These are dependent, among others, on the concentration of oxygen to which the fuel is exposed, the temperature and the composition of the fuel (*15*,*16*). Extensive studies have been conducted on the stability of FAMEs under storage conditions where the temperature is below 80°C. The mechanism by which neat FAME degrades under these conditions is well established (*17*,*18*). Storage stability may be improved by the addition of antioxidants (*19*). Antioxidants contain highly labile hydrogen atoms that are more easily abstracted by peroxy radicals than the most labile hydrogen atoms in the FAME molecules (*2*).

Thermo-oxidative stability (typically understood to refer to stability of fuels when exposed to oxygen in the temperature range 110-300°C) is a very complex set of phenomena. The mechanisms by which fuels degrade under these conditions are not fully understood. Several mechanisms have been proposed for the thermo-oxidative degradation of middle distillates (*20*,*21*,*22*) and some model compounds of FAME (*23*,*24*,*25*,*26*). Studies on FAME/petroleum diesel blends have, however, not been reported.

Increasingly stringent diesel exhaust emissions limits have led to the use of high pressure fuel injection systems which ensure more complete combustion by improving fuel atomisation and mixing (*25*). This increase in pressure has increased the temperature of the fuel in common rail systems to about 150°C. At this temperature, thermo-oxidative degradation may occur. Studies are required to understand what happens in the fuel injection system so that solutions to the problems caused by thermo-oxidative degradation, if any, may be found.

The focus of this project is the analysis of thermo-oxidative products formed during stressing of FAME/petroleum diesel model compound blends. This involves monitoring of both soluble and insoluble species formed during the thermo-oxidative stressing so that a mechanism for the decomposition of FAMEs in the presence of diesel model compounds may be developed. This has been achieved by stressing the fuel under thermo-oxidative conditions in open glass and closed steel reactors. Regular aliquots were removed for compositional analysis by gas chromatography-mass spectrometry (GC-MS) and gas chromatography-flame ionisation detection (GC-FID) and functional group analysis by

Fourier transform infrared (FTIR) spectroscopy and ultra violet-visible (UV-Vis) light spectroscopy.

A quartz crystal microbalance (QCM) was used to monitor the formation of deposits. The procedure, as defined in the standard test method, ASTM D7739-11, was used to monitor the oxygen consumption as well as deposit formation when FAME/petroleum diesel model compound blends were stressed under thermo-oxidative conditions (*27*). The QCM methodology allows deposit formation to be monitored continuously at temperatures that approximate fuel system conditions (*28*).

Solvency refers to the ability of the solvent to dissolve other components present. Biodiesel can dissolve deposits in the fuel system and release deposits accumulated from previous petroleum diesel use (*29*). Biodiesel is a better solvent for polar deposits than diesel. As a result, deposit formation has been seen to increase in blends with low concentrations of FAME compared to neat petroleum diesel but has been seen to decrease at higher FAME concentrations (*25*). The influence of solvency was investigated by doping insoluble deposit precursors into FAME/petroleum diesel model compound blends in order to understand why deposits form in such blends.

1.2 Motivation and objectives of the study

Very little has been reported on the mechanism of deposit formation in biodiesel/petroleum diesel blends. It is possible that the mechanisms for the degradation of the FAME and petroleum diesel components are the same as the neat fuels or that cross-reactions take place between the intermediates formed during the stressing of the blends. Because petroleum diesel is often stable on its own (*10*), the question arises as to the extent that the stability of petroleum diesel changes when blended with biodiesel.

This study was initiated as part of a greater study to investigate effects of fuel composition on deposit formation. An important technique that has not previously been applied to the study of FAME degradation is the use of a QCM. An important component of this study was thus to investigate the appropriateness of using a QCM to measure deposit formation from FAME and FAME/petroleum diesel blends. This was evaluated against accelerated testing in open glass flasks.

The investigation of possible cross-reactions between intermediates formed during the thermo-oxidative degradation of FAMEs and petroleum diesel model compounds formed an important part of this study.

A mechanism for the formation of deposits in jet fuel and by extension diesel involves the formation of soluble macromolecular oxidatively reactive species (*20*,*21*,*22*,*30*). The mechanism by which these are proposed to form involve quinones as key reactive intermediates. Quinones are capable of undergoing Diels-Alder reactions (*31*). It is possible that the conjugated dienes, formed when bis-allylic FAME molecules are heated (*23*,*32*), can combine with the SMORS quinones via Diels-Alder reactions. An example reaction is illustrated in Figure 1.1. Such reaction products have not been reported as far as this author is aware.

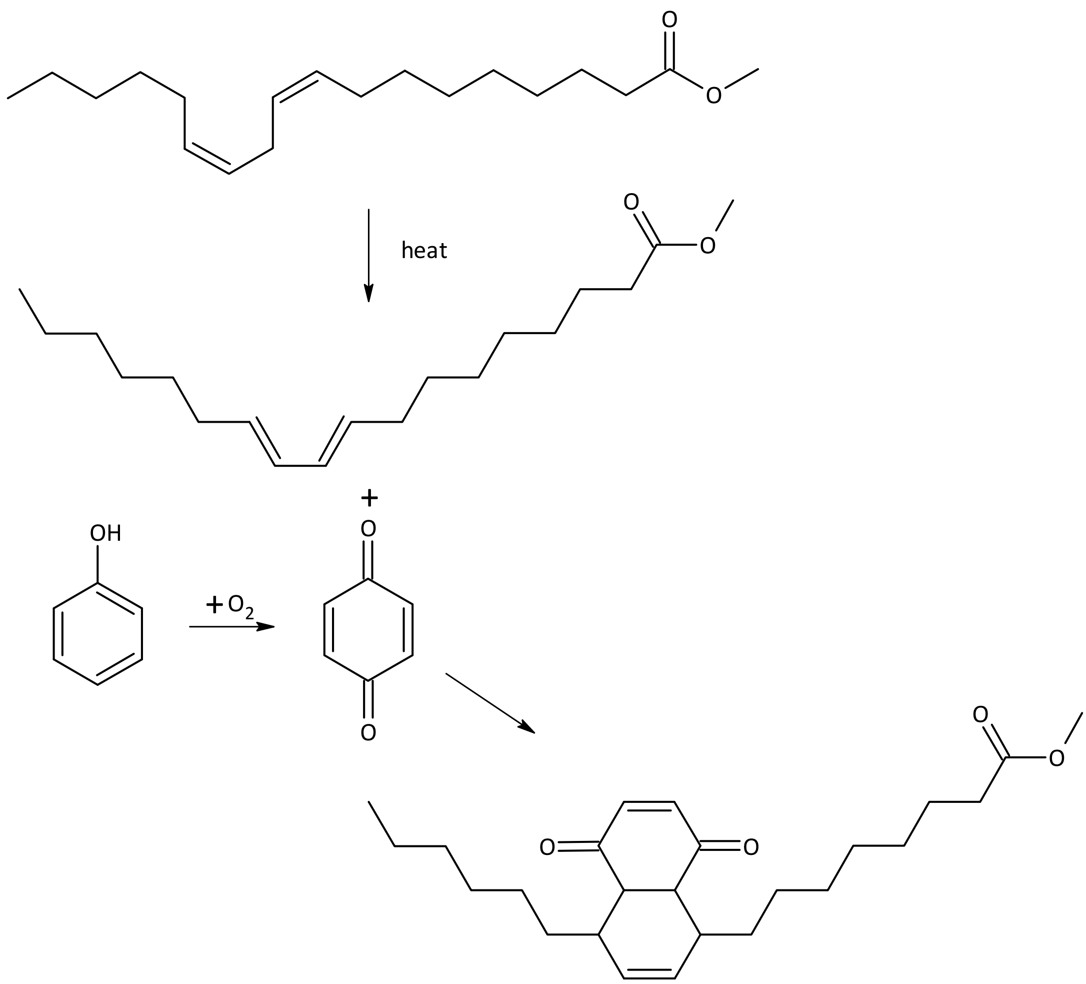

Figure 1.1: Possible Diels-Alder reaction between thermo-oxidative degradation products of petroleum diesel and a fatty acid methyl ester (methyl linoleate)

Acids have been identified as products of FAME degradation (*13*,*23*). A second possible cross-reaction is via acid catalysis of petroleum diesel degradation. Hydrocarbon autoxidation in acidic solution tends to proceed beyond the ketone-alcohol stage to yield carboxylic acids as major products (*33*). The formation of high molecular weight species during the thermo-oxidative degradation has been proposed to involve electrophilic aromatic substitution (*21*,*20*). Electrophilic aromatic substitution can be acid catalysed (*34*). It is thus possible that the formation of weak acids during the degradation of FAME may catalyse the reactions of heteroatom-containing compounds in petroleum diesel. This, too, has not been reported on.

The main objective of this research was to track both soluble and insoluble species formed during the thermo-oxidative degradation of a mixture of diesel model compounds and FAME model compounds in order to investigate the processes of degradation. The data obtained was used to extend mechanisms for petroleum and biodiesel degradation, and any effects observed in blends that may not have been accounted for.

1.3 Limitations in scope of the study

This study was limited to the investigation of diesel model compounds and biodiesel model compounds. Single model compounds were selected from the classes: aromatics, *n*-paraffins and cycloparaffins. The compounds selected were tetralin, *n*-hexadecane and decalin (mixture of isomers) for petroleum diesel. The effect of other aromatics such has naphthalene or the influence of iso *vs* n-paraffins was deemed beyond the scope of this study. Full boiling range petroleum diesels were not studied. It was felt that the use of the latter would complicate gas chromatography (GC) analysis and was thus deemed beyond the scope of this study.

Methyl oleate, methyl linoleate and methyl linolenate for biodiesel were used as FAME model compounds. Where biodiesel was used, this was limited to the single biodiesel rapeseed methyl ester. Investigations of other biodiesels, such as soybean methyl ester, were deemed beyond the scope of this study.

Thermo-oxidative stability studies can be performed across a wide temperature range (110-300^{o}C). In this study, however, experiments were, with a few exceptions, restricted to a temperature of 140^{o}C. Air was continuously introduced in an open flask reactor during the experiment while in QCM experiments only dissolved and head space air was present during the experiment. Studies in an oxygen-free environment were not performed. Other stability tests such as those using the Petroxy^{TM} (*35*) instrument or the Rancimat test (*36*) were not considered because these did not address the formation of deposits directly, but rather the consumption or formation of gaseous/dissolved components.

The influence of only two phenolic species, butylated hydroxyl toluene (BHT) and phenol, were investigated. Furthermore these were added only at a level of 200 ppm. An extensive study of the effect of concentration of such species was deemed beyond the scope of this study. Similarly investigation of other heteroatom-containing compounds in petroleum diesel such as carbazoles was also deemed outside the scope.

The influence of acidic species was investigated by adding *n*-hexanoic acid. Other acids were not considered. Furthermore, only high concentrations of acid were investigated.

Gas chromatography with mass spectrometric detection (GC-MS) and, to a lesser extent, electrospray ionisation-mass spectrometry (ESI-MS) was used for the identification of the oxidation products formed during the experiment. Other identification techniques, such as nuclear magnetic resonance (NMR) spectroscopy and high performance liquid chromatography (HPLC), were not used, nor were separation techniques such as gel permeation chromatography (GPC).

2. Literature review

2.1 Petroleum diesel

Petroleum diesel is a crude oil-derived liquid fuel that is used to power diesel engines (also known as compression-ignition engines) (*37*). Diesel engines are the most efficient among commercial types of internal combustion engines, mainly due to their relatively high compression ratios (*37*,*38*). As a result, in some countries in Europe, 55% of all new vehicle registrations are for vehicles manufactured use diesel engines (*39*). In South Africa, a steady increase in diesel fuel consumption has been observed since 2000 with a high percentage (51%) used in transportation (*40*). Diesel is widely used, including in private and public motor vehicles, boats and machinery. (*41*). Today diesel plays a crucial role worldwide as a source of energy for transportation, manufacturing, power generation, construction, farming, *etc*.

2.1.1 Environmental issues associated with diesel

Conventional compression-ignition (CI) diesel engines have relatively high emissions of mono-nitrogen oxides (NOx) and particulate matter (PM) (*42*). According to the New Hampshire Department of Environmental Services (*43*), diesel fuel emissions contribute to numerous air pollution problems, including a contribution to global warming. Crucial emissions such as PM and NOx adversely affect the environment by inhibiting plant growth and damaging soil structure as well as creating low levels of ozone leading to smog, acid rain and nitrate particulates (*44*). Even though these emissions have been noticeably reduced in recent years, further reductions are required to meet very stringent regulations. One of many solutions to meet current and future emission regulations for diesel engines required the development of advanced compression-ignition engines with common rail diesel fuel injection technology (*45*) (see Figure 2.4).

2.1.2 Diesel specifications

Table 2.1 depicts current diesel specifications used in South Africa. Current diesel specifications in South Africa are compatible with Euro 2 emission standards (*40*). The rapid growth in the number of vehicles in South Africa has led to an increase in total fuel consumption and consequently an increase in total emissions (*40*). This issue is frequently raised in discussions about environmental problems relating to road transport and vehicle emissions.

Table 2.1: Diesel fuel specifications in SA (40)

Property	**Units**	**Limit**	**SANS 342-2006**
Density @ 20°C	kg/ℓ	min	0.8000
Ash content	% m/m	max	0.01
Cetane number		min	45
Carbon residue, Ramsbottom (on 10% residue)	% m/m	max	0.2
CFPP – winter	°C	max	-4
CFPP – summer	°C	max	1
Corrosion, copper strip, 3h @ 100°C		max	1
Distillation, 90% volume recovery	°C	max	362
Sulfur content	mg/kg	max	500
Flash point, PMCC	°C	min	55
Kinematic viscosity @ 40°C	cSt	min max	2.2 5.3
Water content, Karl Fischer	ppm (v/v)	max	500
Total contamination	mg/kg	max	24
Lubricity wear scar diameter	µm	max	460
Oxidation stability	mg/100mℓ	max	2.0
Fatty acid methyl ester (FAME) content	vol %	max	5

2.1.3 Source and composition of petroleum diesel

Petroleum diesel is produced from the fractional distillation of crude oil between 160°C and 360°C (*46*). Petroleum diesel consists of paraffinic, olefinic, naphthenic and aromatic (including benzene and polycyclic aromatic) hydrocarbons, containing 10 to 22 carbon atoms (*41*). Typical hydrocarbons that are found in petroleum diesel are shown Figure 2.1.

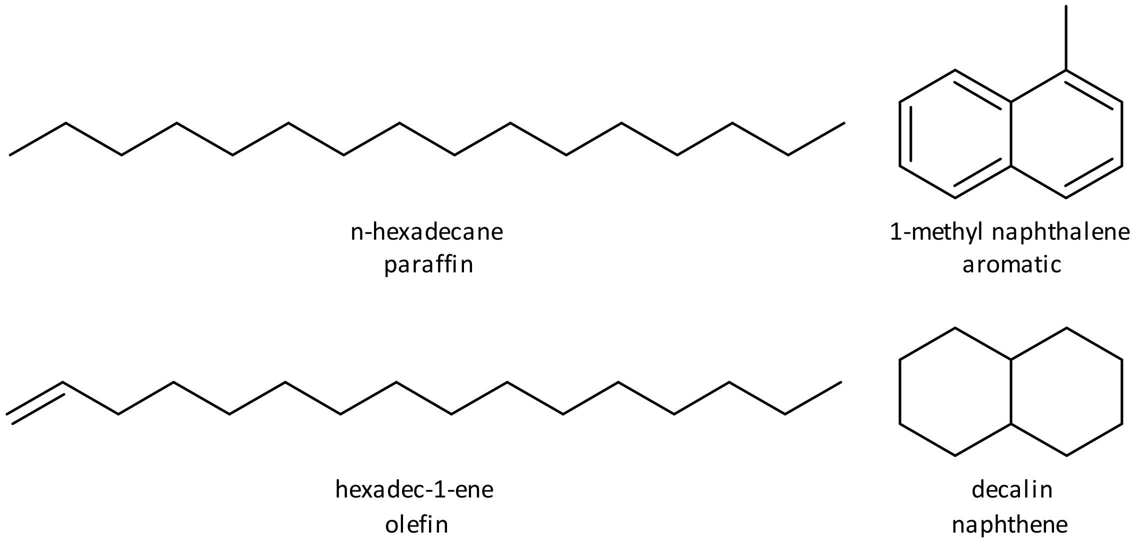

*Figure 2.1 Typical diesel hydrocarbons found in petroleum diesel (*41*)*

Figure 2.2 illustrates a typical carbon number distribution of the hydrocarbons in petroleum diesel. The distribution usually peaks between carbon number 15 and 17.

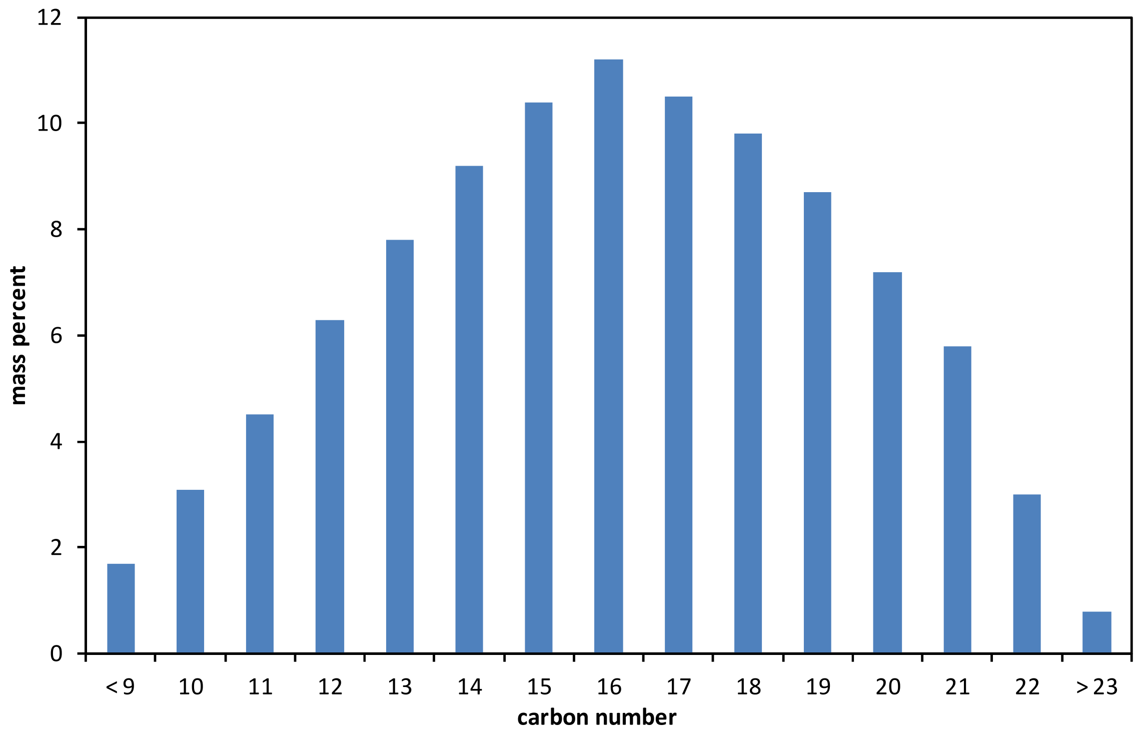

*Figure 2.2 Typical carbon number distribution of petroleum diesel (adapted from (*41*))*

Petroleum diesel also contains trace amounts of compounds containing heteroatoms such as sulfur, oxygen and nitrogen as illustrated in Figure 2.3.

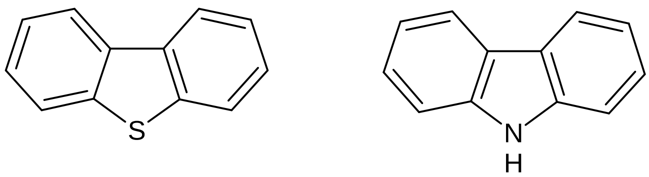

dibenzo[*b*,*d*]thiophene   9*H*-carbazole

*Figure 2.3: Example compounds found in petroleum diesel which contain heteroatoms (*41*)*

2.2 Common rail diesel fuel injection technology

Common rail systems are vehicular fuel injection equipment. Common rail fuel injection systems have significant effects on diesel engine performance and have become widely used in diesel engines (*47*). The common rail diesel fuel system consists of a low pressure supply circuit, a high pressure delivery circuit and a return circuit as illustrated in Figure 2.4 below.

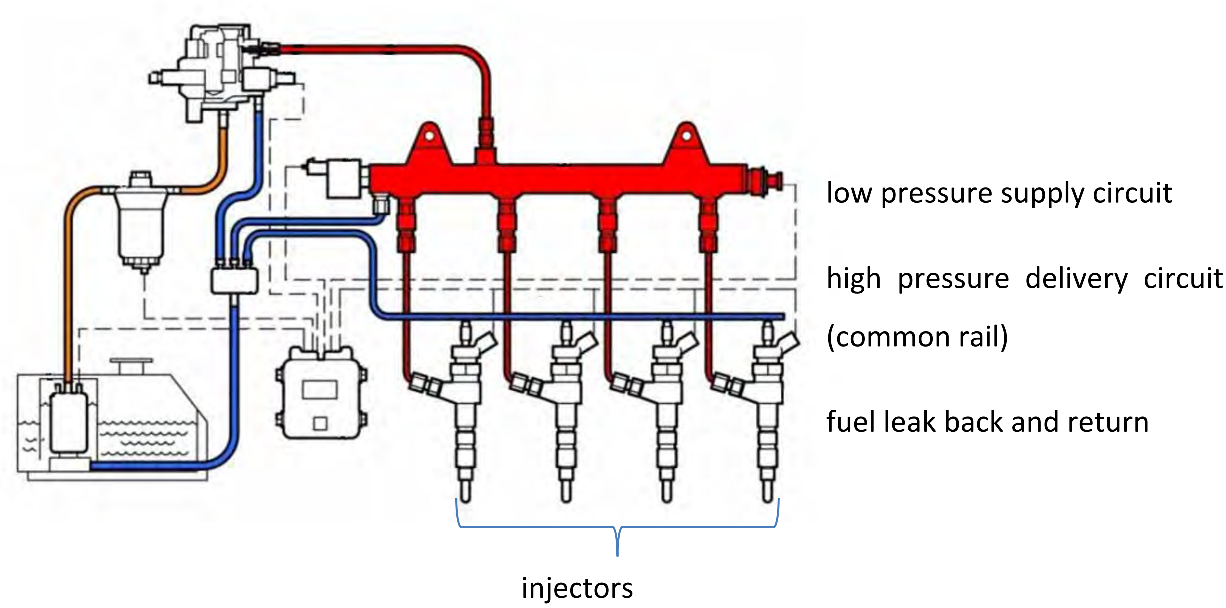

*Figure 2.4: Common rail diesel fuel injection system (reproduced from (*48*))*

The common rail supplies high pressure fuel to the injectors which inject the fuel into the combustion chamber where it is mixed with air (*45*). A high injection pressure is required for the fine atomisation of the fuel and efficient mixing of air and fuel. This results in high power output and reduced soot (*47*).

Fuel in the common rail is often exposed to high temperatures which might promote thermo-oxidative degradation since a large amount of heat is generated when highly-pressurised fuel is released into the fuel return circuit.

Omori *et al*. (*25*) calculated the relationship between injection pressure and temperature of the fuel returned from the injector to the fuel tank. A linear relationship between pressure and temperature was obtained. It was predicted that at an injection pressure of 200 MPa, the fuel would encounter a temperature in excess of 150^{o}C in the rail/returning fuel line.

Common rail systems are made of high precision components with nozzle diameters below 200 μm (*49,50,51*). Small changes in fuel stability can eventually lead to the formation of deposits which would, therefore, affect the injection performance and thus overall engine performance.

The use of biodiesel in diesel engines raises further technical problems. Fuel filters are placed in the fuel line where they play an important role by removing foreign particles from the fuel supplied to an internal combustion engine which may potentially cause problems in the fuel pump and injectors. Biodiesel can cause problems such as the clogging of fuel filters due to the formation of sludge (*52*) or the loosening of existing deposits in a fuel tank (*53*). Sludge typically refers to the materials that settle at the bottom of the fuel as a result of oxidation at high temperatures. Biodiesel sludge is thought to consist of degradation products such as short-chain organic acids and oligomer compounds such as dimers, trimers and tetramers formed from the original esters (*54*).

2.3 Biodiesel

Biodiesel is a renewable fuel intended as a substitute for diesel fuel. Biodiesel has the potential to be a greener alternative fuel for diesel engines because it lowers greenhouse gas emissions compared to diesel from fossil fuels. Biodiesel is biodegradable and produces reduced soot emissions compared with petroleum diesel (*19*). Moreover, its use reduces the dependence on fossil fuels which are likely to decrease in availability and affordability (*2*).

2.3.1 Environmental issues associated with biodiesel fuel

Biodiesel is a cleaner fuel than petroleum diesel, with significantly lower emissions. The use of biodiesel causes reduced emissions of particulate matter, hydrocarbons, carbon monoxide, sulphurous oxides and cancer-causing air toxins. NOx emissions and that of smog-forming compounds are, however, increased (*8*).

Table 2.2 shows the content of tailpipe emissions for the testing of biodiesel, diesel, and a biodiesel/diesel blend. Unlike diesel, biodiesels do not contain sulfur. As a result, blending with biodiesel lowers tailpipe sulfur oxide emissions.

*Table 2.2: Effect of biodiesel on tailpipe emissions (g/bhp-h) (*55*)*

Emission	**Diesel fuel baseline**	**20% biodiesel blend**	**100% neat biodiesel**
Carbon dioxide (fossil)	633.28	534.10	136.45
Carbon dioxide (biomass)	0	108.70	543.34
Carbon monoxide	1.2	1.089	0.6452
Hydrocarbons	0.1	0.09265	0.06327
Particulate matter (PM10)	0.08	0.0691	0.02554
Sulfur oxides (as SO_2)	0.17	0.14	0
Nitrogen oxides (as NO_2)	4.8	4.885	5.227

2.3.2 Biodiesel specifications

One of the key means of ensuring satisfactory in-use biodiesel fuel quality is the establishment of a set of fuel specifications, such as ASTM D6751-14 (in the USA) (*56*) and EN 14214 (in the European Union) (*57*). A detailed summary showing different biodiesel standards is presented in Table 2.3. Several standards are country specific but most specifications are based on ASTM D6751 and EN 14214.

Table 2.3: The standard values of some of the fuel parameters of biodiesel as per ASTM D6751/EN 14214 (56,57,58)

Property	Biodiesel test method	Units	Biodiesel EN 14214/ASTM D 6751
Fatty acid methyl ester (FAME) content	EN 14103	% m/m	96.5 min
Mono-glycerides	EN 14105	% m/m	0.80
Di-glycerides	EN 14105	% m/m	0.20
Tri-glycerides	EN 14105	% m/m	0.20
Linolenic acid methyl ester	EN 14103	% m/m	12
Free glycerine	D 6584	% m/m	0.020
Total glycerine	D 6584	% m/m	0.250
Phosphorus content	D 4951	% m/m	0.001 max
Metal I (Na + K)	EN 14538	ppm	5 max
Metal II (Ca + Mg)	EN 14538	ppm	5 max
Flash point	D 93	^{o}C	93.0 min
Water and sediment	D 2709	vol %	0.050 max
Kinematic viscosity, 40^{o}C	D 445	mm^{2}/s	1.9-6.90
Sulfated ash	D 874	% m/m	0.020 max
Sulfur	EN ISO 20884	Mg/kg	10 max
Copper strip corrosion	D 130	3	3
Cetane number	D 613	-	47 min
Cloud point	D 2500	^{o}C	-3 to 12
Carbon residue	D 4530	% m/m	0.050 max
Acid number	D 664	mg KOH/g	0.50 max
Distillation temperature (T90)	D 1160	^{o}C	360 max
Oxidation stability	EN 15751	hours	3 min
Cold soak filterability	D 7501	seconds	360 max
Methanol content	EN 14110	vol %	0.2 max
Lower heating value		Btu/gal	~118,170
Total contamination	D 5452	mg/kg	24 max
Organic matter (10%)	EN ISO 10370	% m/m	0.3 max
Specific gravity @ 60^{o}C	EN ISO 12185	kg/ℓ	0.88
Iodine value	EN 14111	mg/100g	120 max
Pour point	ISO 3016	^{o}C	-15 to 10

2.3.3 Source and composition of biodiesel

Biodiesel comprises fatty acid methyl esters (FAMEs), derived from the trans-esterification of vegetable oils and animal fats with an alcohol (typically methanol) in the presence of an alkali catalyst (*59*), and small quantities of free fatty acids.

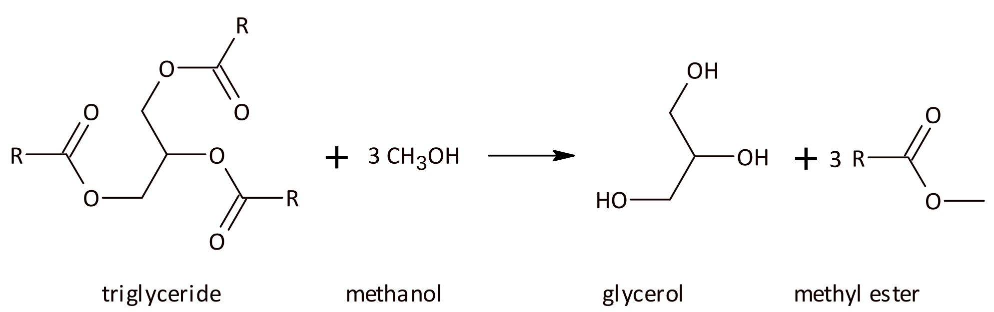

Figure 2.5: Trans-esterification reaction used to produce FAME and glycerol as a by-product (3,6)

Figure 2.5 illustrates a trans-esterification (conversion of one ester into another) reaction of vegetable oil with methanol. Typically methanol is used as the alcohol, for economic reasons, although ethanol is sometimes used commercially (*3*,*60*).

The most commonly used oils for biodiesel production are rapeseed, soybean, sunflower, jatropha, palm oil, tallow and waste cooking oil (*3*,*6*,*7*,*8*). Biodiesel, from rapeseed and soybean feedstock, comprises five main FAMEs, as indicated in Figure 2.6 (*61*). The unsaturated FAMEs in biodiesel, such as RME, typically have *cis* double bonds, although some authors, *e.g.,* Hakka *et al.* (*62*), mistakenly present them as all *trans* forms, replacing methyl oleate with methyl elaidate and methyl linoleate with methyl linoleaidate.

methyl palmitate ($C_{17}H_{34}O_2$)

methyl stearate ($C_{19}H_{36}O_2$)

methyl oleate ($C_{19}H_{34}O_2$)

methyl linoleate ($C_{19}H_{32}O_2$)

methyl linolenate ($C_{19}H_{30}O_2$)

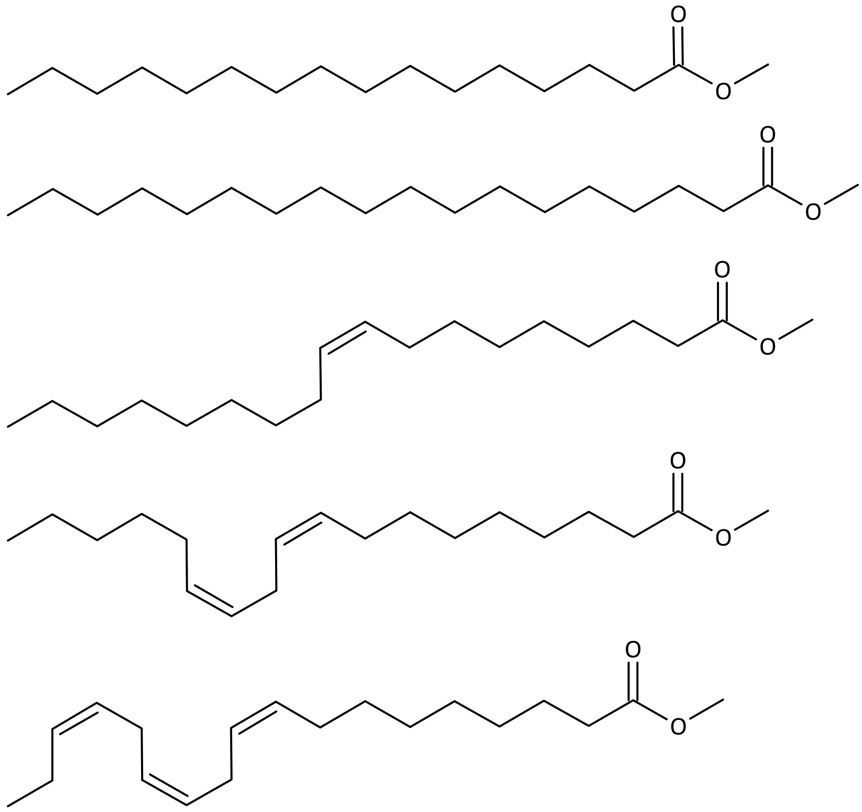

*Figure 2.6: Most common fatty acid methyl esters found in biodiesel, made from rapeseed and soybean feedstock (*61*)*

2.4 Petroleum diesel/biodiesel blends

Petroleum diesel is blended with biodiesel to reduce greenhouse gas emissions (*3*,*4*). Furthermore, neat biodiesel is generally associated with a loss in engine power (*63*). As a result, biodiesel is blended with diesel rather than used on its own to obtain the power levels that are within the levels observed from diesel fuel. Some properties, *e.g.,* stability, are negatively affected in some blend proportions (*25*).

Blends with petroleum diesel are commercially available as substitutes for neat petroleum diesel in diesel engines (*18*). In Europe 7% (% v/v) FAME in diesel is already sold in several major markets (*64*). In South Africa, the government has mandated the blending of biofuels with petroleum diesel from 2015 at a minimum level of 5% (*65*).

In the United States, B20 is commercial available and currently dominates the market for diesel/biodiesel blends. B20 is dominant as it represents a balance of emissions, cold-weather performance and ability to act as a solvent. The use of blends escapes the problems associated with 100% biodiesel such as poor cold-weather performance and material compatibility (*6*).

2.5 Fuel stability

A fuel's stability refers to its resistance to degradation. Color changes and the formation of solid deposits are some indicators of instability (*66*). Fuel degradation leads to the formation of undesirable products. Three types of stability are described in literature, *viz.* oxidation stability, storage stability and thermal stability. The degradation of fuel can occur via different mechanisms, depending on whether the fuel is exposed to storage, thermo-oxidative stressing or pyrolytic conditions. Fuel instability results in increased maintenance costs, equipment vulnerability and decreased reliability (*10*).

2.5.1 Storage oxidation reaction regime (< 100°C)

Storage stability refers to the ability of a fuel to remain in storage under ambient conditions over extended periods of time without significant deterioration. It usually refers to the tendency of a fuel to resist reactions with oxygen near ambient temperatures to form hydroperoxides (*67*). Storage instabilities may manifest in the following ways: colour changes, gum development, sedimentation, change in physical properties, change in chemical properties, or change in combustion properties (*68*).

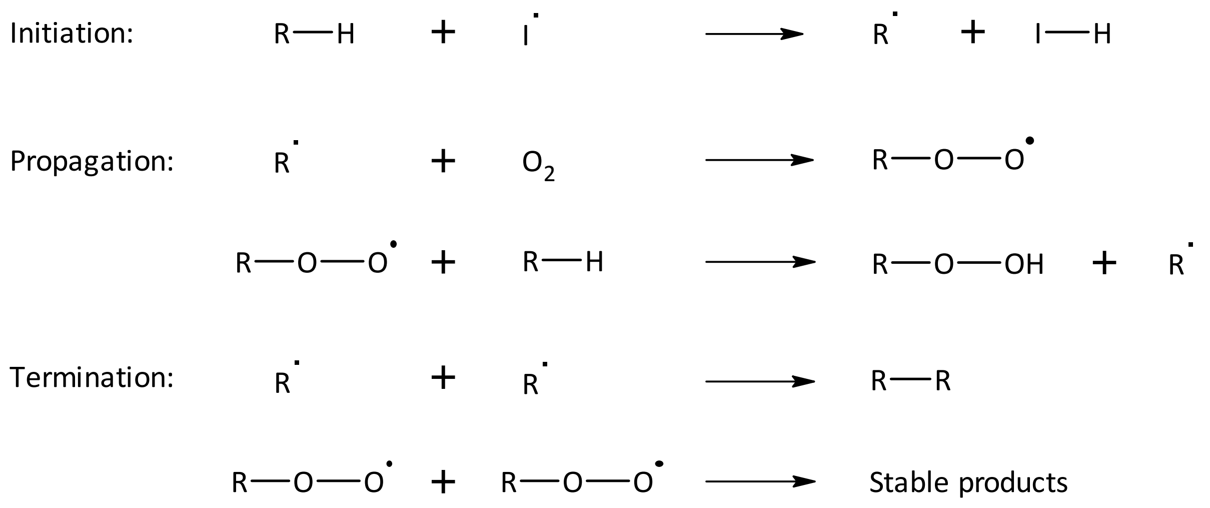

*Figure 2.7: Primary oxidation scheme (adapted from (*17*))*

The scheme, presented in Figure 2.7, involves radical reactions. The scheme is initiated by a radical initiator which abstracts a hydrogen atom from fuel molecules to form a radical. The radicals formed react with available oxygen to form peroxy radicals during the propagation step. The process is terminated by the reaction of radicals with radicals, forming stable products which may be gums and higher molecular species.

2.5.2 Thermo-oxidative reaction regime (110-300°C)

Thermo-oxidative stability refers to the ability of the fuel to resist high temperature stress in the presence of oxygen for a reasonable period without noticeable deterioration. Decomposition occurs by autoxidation reactions and increases with increasing fuel temperature. The temperature range of this regime largely depends on fuel properties (*69*).

2.5.3 Transition regime (300–500°C)

Both autoxidation and pyrolysis reactions contribute to decomposition. The rate of decomposition decreases with increase in fuel temperature, possibly due to the transition from the liquid phase to the supercritical phase which enhances the ability of the solvent to keep species in solution or due to depletion of hydroperoxides (*69*).

2.5.4 Thermal/pyrolysis reaction regime (≥500°C)

Thermal stability refers to a fuel's ability to resist changes that occur due to elevated temperature. Pyrolysis proceeds through a free-radical chain reaction process yielding many products. These free radicals are produced by the breaking of carbon-carbon bonds. Pyrolysis dominates and decomposition is enhanced as fuel temperature increases (*69*).

2.6 Thermo-oxidative stability of petroleum diesel

Diesel stability can refer to storage stability at ambient conditions for extended periods or to thermal stability at high temperatures for a short period. Diesel degradation can lead to the formation of soluble gums and insoluble organic particulates. The stability of diesel is affected by several factors such as the fuel's composition and storage conditions. Stability decreases in the order paraffins > naphthenes > aromatics > olefins. Petroleum diesel is more stable under storage and thermo-oxidative conditions than biodiesel because biodiesel contains a greater amount of molecules with double bonds (*10*).

The presence of trace heteroatom-containing species can decrease the thermal stability of middle distillates (*70*).

The formation of deposits from petroleum-derived middle distillates has been proposed to involve the reaction of low-molecular-weight heteroatomic molecules, such as phenols, indoles, carbazoles, pyrroles, anisoles, to form higher molecular weight structures (*20*,*21*,*22*,*30*). Phenols are known to influence both the rate of oxygen consumption and deposit formation (*71*). Condensation reactions between phenols and other heteroatomic species have been suggested as a key step in the formation of petroleum diesel deposits (*20*,*72*).

The concentration of the phenolic species present affects the amount of deposition. Sobkowiak *et al.* (*20*) noted increased deposition during jet fuel oxidation as the phenol content rose.

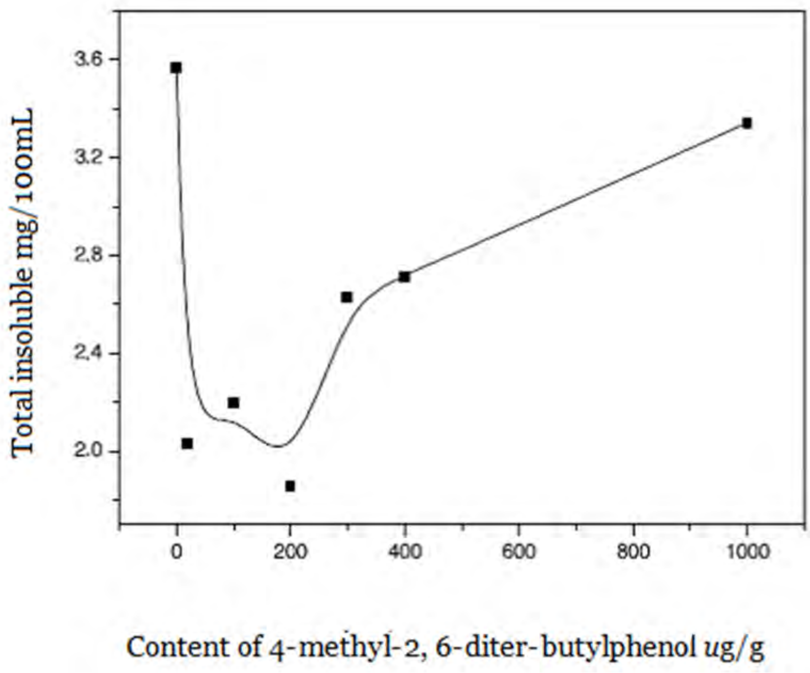

*Figure 2.8: Effect of different amounts of BHT on stability of diesel (reproduced from (*72*))*

The concentration of the phenolic antioxidant, butylated hydroxytoluene (BHT), was demonstrated to have a complex effect on the stability of diesel. Figure 2.8 shows that at low concentrations BHT had an antioxidant effect, indicated by a decrease in the total insoluble material with increasing BHT, but at higher concentrations more deposits were formed.

Species with molecular weights in the range 500-900 g/mol have been extracted from thermo-oxidatively stressed middle distillates using methanol and subsequent precipitation with pentane (*73*). Hardy and Wechter (*73*) coined the term soluble macromolecular oxidatively reactive species (SMORS) to describe these species.

In order to explain the presence of these intermediates, a mechanism has been developed (*20*,*21*,*22*,*30*). These intermediates are species formed when low molecular-weight heteroatomic molecules react to form larger molecular-weight heteroatomic species which usually incorporate oxygen (*21*,*20*). Species, heavier than 900 g/mol, which form from further reaction, precipitate out as deposits (*73*).

An example reaction, showing the formation of a SMORS molecule, is illustrated in Figure 2.9. A compound, often found in petroleum middle distillates, phenol, reacts with oxygen and a hydroperoxide to form 1,4-benzoquinone which subsequently reacts with an electron-rich aromatic compound, *e.g.,* trimethylcarbazole, to yield a low molecular weight SMORS. It is important to note that the reaction scheme shown in Figure 2.9 and, indeed, the SMORS mechanism, itself is meant to be generic and is applicable to a variety of other compounds in addition to the ones shown in Figure 2.9 such as pyrroles, anisoles, indoles, and carbazoles (*30*). Subsequent electrophilic aromatic substitution of the low molecular weight intermediates produces higher molecular weight species.

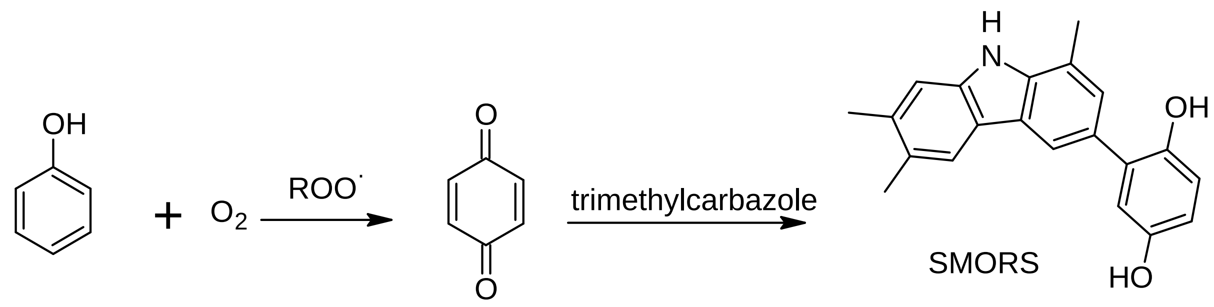

Figure 2.9: Scheme by which SMORS may be formed (*20*,*22*)

Recently Kerkering *et al.* (*74*) have reported on the influence of phenols on the stability of heating/oil FAME blends. They, however, did not use actual deposition as a measure of stability but rather oxygen uptake as measured by Petroxy™ (*35*). All phenols increased the induction time for oxygen uptake although the effect was minimal for pure phenol. Alkylating in the *ortho* and *para* positions, particularly with bulky groups, improved the antioxidant behaviour.

DeWitt *et al.* (*11*) have explored the influence of aromatics on synthetic paraffinic kerosene (SPK) stability. This study did not use model aromatic compounds, as in the current study, but different commercial aromatic solvents with different amounts of monoaromatic compounds, tetralins and indanes, and naphthalenes. They observed that the addition of a monoaromatic species-containing solvent had a small effect on the extent of mass of deposit accumulated. An increase in the rate of oxygen uptake was noted which they ascribed to dilution of the synthetic antioxidant in the neat SPK. It is, however, possible that the faster uptake may be due to the presence of benzylic hydrogen atoms on the monoaromatic species. Benzylic hydrogen atoms are easily abstracted to form radicals which can react with oxygen to form hydroperoxides. DeWitt *et al.* (*11*) suggested that the deposition mechanism may involve the formation of benzofuranones which may react with themselves or other aromatics species to form higher molecular weight species. These authors suggested that higher molecular weight aromatic compounds (*e.g.,* diaromatic species) require fewer steps to grow into insoluble deposit precursors. Diaromatic species may require as few as 2-3 steps to form these precursors. This results in a greater deposition propensity for diaromatic compounds.

On-going studies at the Sasol Advanced Fuels Laboratory at the University of Cape Town are exploring the effect of different types of aromatics on middle distillate stability using flask reactor (*75*) and QCM (*76*) methodologies. Classes include monoaromatic compounds (*e.g.,* cumene), hydroaromatics (*e.g.,* tetralin) and bicyclic aromatics (*e.g.,* naphthalene).

2.7 Formation of deposits from FAME

Fuel stability refers to the resistance of a fuel to degradation processes that alter fuel properties and form undesirable products. In the case of FAMES these include polymers, aldehydes and acids (*13*). The stability of methyl esters with same carbon number and different degrees of unsaturation decreases in the order oleate > linoleate > linolenate (*77*,*78*).

FAME exhibits lower stability compared to petroleum diesel (*24*,*79*,*80*,*81*,*82*,*83*). Because biodiesel contains significant concentrations of polyunsaturated fatty acid esters, storage stability is often a great concern. The storage stability of FAME is affected by several factors such as the nature of the feedstock, fuel additives and impurities, storage and handling conditions.

Extensive studies have been done on storage stability of biofuels, and the mechanism for oxidation is thought to be well understood. Oxidation, as indicated earlier, involves initiation, propagation and termination steps. The initial step of oxidation is illustrated in Figure 2.10. A hydrogen atom, attached to a methylene carbon, allylic and bis-allylic to the double bond is abstracted by a radical initiator (I). The radicals formed react with oxygen to form peroxy radicals which further react in the propagation step. During propagation, these peroxy radicals abstract further hydrogen atoms to form more radicals and a hydroperoxide

(*84*). The reaction continues until termination by radical-radical reactions. Alternately, hydroperoxides decompose to form aldehydes, ketones, acids and esters.

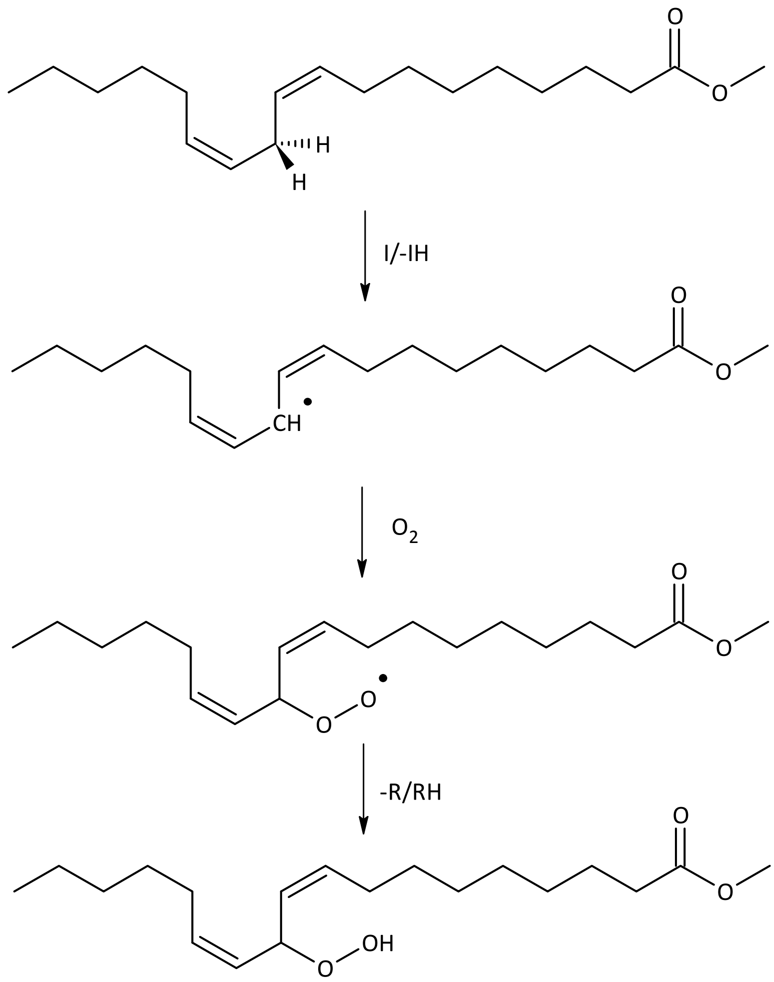

*Figure 2.10: Mechanism for the autoxidation of methyl linoleate, leading to the formation of its hydroperoxides (*58*)*

Homolytic scission of the hydroperoxide gives rise to an alkoxy and a hydroxyl radical (*84*). Further bond scission gives rise to the low molecular weight products mentioned.

Storage stability can be improved by addition of antioxidants (*19,30*). These antioxidants contain highly labile hydrogen atoms that are more easily abstracted by hydroperoxy radicals than hydrogen atoms in the FAME molecules (*2*).

At higher temperatures in the presence of oxygen it is likely that similar processes to those observed for lipids such as cooking oil (fatty acid trigyclerol esters) occur. The main classes are thermolytic cracking, hydrolysis (formation of acids) and the formation of oxygenated products (*85*,*86*,*84*,*87*). Cracking is favoured under conditions of low oxygen.

The oxidation of FAMEs is known to cause the formation of both lower and higher molecular weight species. The mechanism for the formation of smaller carboxylic acids is well established but the details for the formation of oligomers and polymers are less certain. It is the latter that gives rise to the necessary precursors for gums and sludges (*23*). Fang and McCormick (*26*) used Fourier transform infrared (FTIR) and nuclear magnetic resonance (NMR) spectroscopy to investigate FAME degradation. They proposed several high molecular weight structures. Kulkarni and Dalai noted the high molecular weight species formed from lipid oxidation to be dehydrodimers, saturated dimers, polycyclic compounds and polymeric acids (*85*).

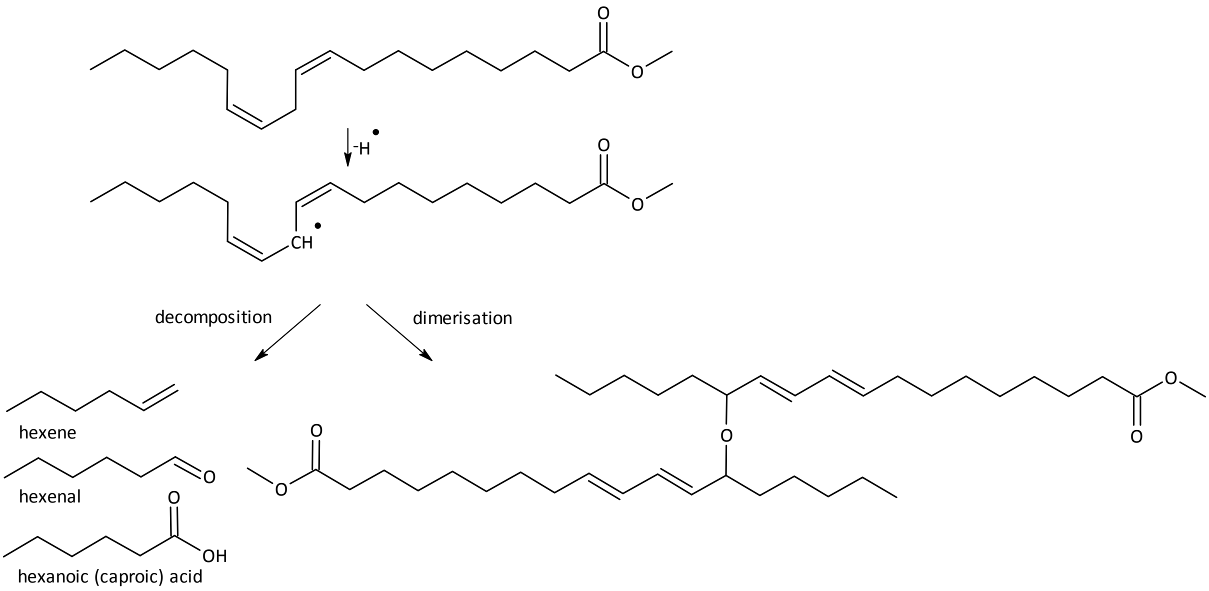

*Figure 2.11: Proposed reaction scheme for the thermo-oxidative degradation of methyl linoleate (adapted from (*23*))*

The reaction scheme in Figure 2.11 was proposed for the thermo-oxidative reactivity of a FAME component, methyl linoleate. It was proposed that monounsaturated compounds are oxidised at allylic carbon atoms while doubly unsaturated species such as methyl linoleate are oxidised at *bis*-allylic carbon atoms (*23*). These *bis*-allylic atoms are more reactive than allylic carbons. The acids formed cause local corrosion of the base metals in fuel systems which results in the formation of iron carboxylate salts onto which the polymers adhere to create a deposit (*25*). The dimers may result from the reaction of alkoxy radicals (see earlier) with alkyl radicals of other FAME molecules. The formation of dimers is favoured by excess oxygen conditions (*87*). Similar crosslinking processes occur in varnishes based on linseed oil where intermolecular coupling of radicals arise from the decomposition of relatively unstable hydroperoxide groups (*88*).

Maccichè *et al.* used ^{1}H-NMR to confirm the presence of increased conjugation, the formation of hydroperoxides and ether linkages upon oxidation of ethyl linoleate (*32*). Oxidation of linoleic esters produces almost exclusively 9- and 13-hydroperoxides which are called outer hydroperoxides (*78*). The pathway proposed in Figure 2.11 involves reaction via 13-hydroperoxides.

Not all authors agree with the scheme in Figure 2.11. Muizebelt *et al.* (*89*) suggested that while species derived from hydroperoxides of unconjugated species favoured radical recombination reactions to form dimers, conjugated hydroperoxides led to radical addition to the double bonds. It should be noted that elsewhere in their paper, Ogawa *et al.* (*23*) presented structures which imply possible addition to double bonds.

An alternative route for the formation of oligomers is via Diels-Alder reactions. At elevated temperatures, *bis*-allylic polyunsaturated FAMEs rearrange to more stable E,E conjugated structures. These conjugated dienes are then capable of reaction with other olefins to form cyclic structures, as indicated in Figure 2.12 (*17,90*).

The lower stability of biodiesel leads to the formation of soluble products such as epoxides, ketones, formic acid, alcohols, saturated aldehydes, unsaturated trans-aldehydes and oligomers, the last of which are insoluble in blends of biodiesel with petroleum diesel (*14*). These precipitates can cause operational problems in diesel fuel pumps and fuel injectors.

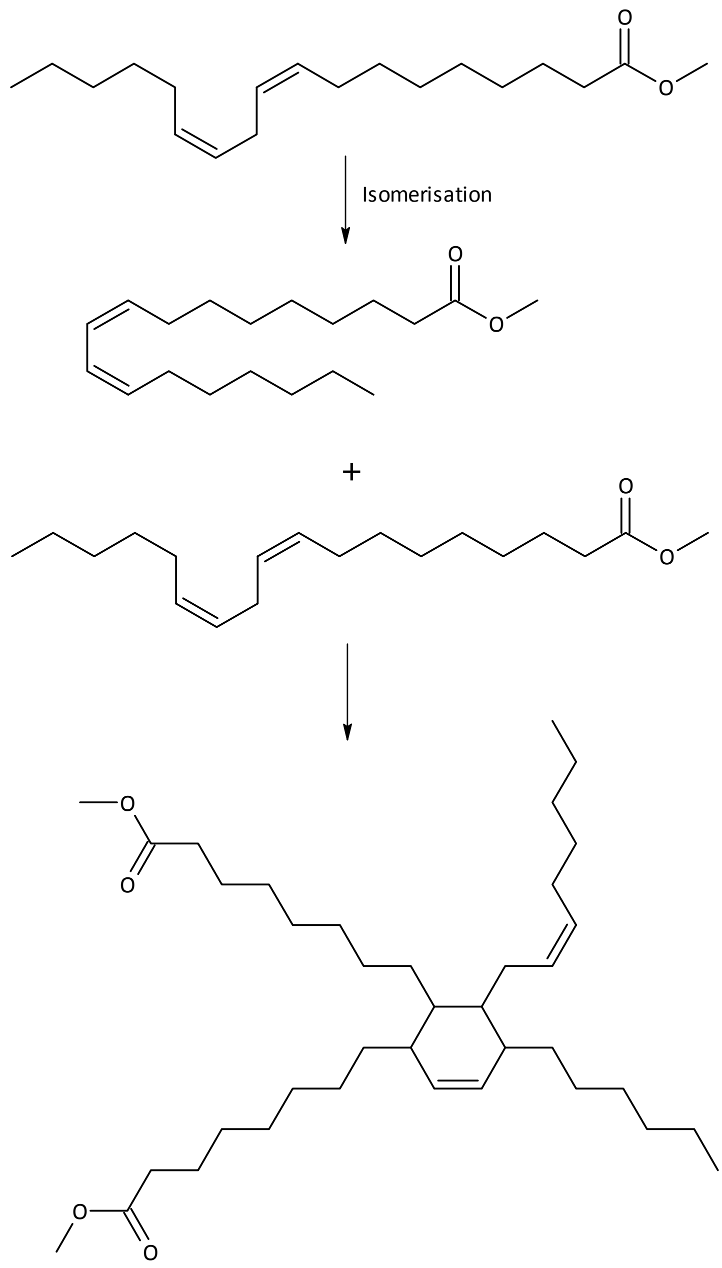

Figure 2.12: Example of a possible Diels-Alder reaction of methyl linoleate-derived compounds

2.8 Oxidation of petroleum diesel constituents

Hydrocarbon hydrogen transfer reactions during thermo-oxidative degradation are important as they play a role in preventing deposit formation and, as a result, increase the stability of the fuel. Therefore, it is also important to evaluate the effect of individual diesel components on deposit formation and, consequently, the effect of composition of the final blends.

Tetralin (1, 2, 3, 4-tetrahydronaphthalene) is a hydrogen donor and can be reversibly hydrogenated-dehydrogenated in a reacting mixture (*91*,*92*). Alemán-Vázquez *et al* (*92*), studied the effect of tetralin, decalin and naphthalene as hydrogen donors in the thermal cracking of a Mexican heavy crude oil. They observed that when tetralin was added as a hydrogen donor, there was 80-90 % conversion to naphthalene. It should, however, be noted that this was in a very low oxidation environment. Figure 2.13 illustrates the conversion of tetralin to naphthalene.

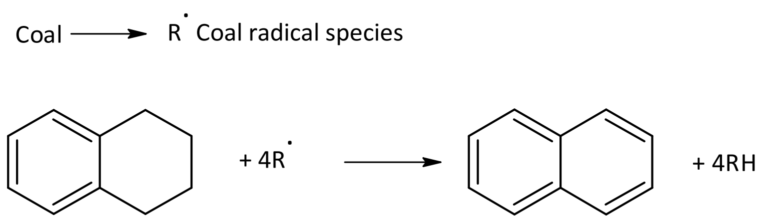

*Figure 2.13: H-transfer from a donor solvent tetralin to coal during coal liquefaction (*91*)*

On the other hand, in the presence of oxygen, tetralin undergoes direct oxidation as shown in the Figure 2.14. Figure 2.14 is the autoxidation mechanism of tetralin. The primary product of tetralin oxidation is a tetralin hydroperoxide (*93*), which then oxidises further to form oxygenated products such as ketones and alcohols (*94*). Robertson and Waters suggested tetralone was formed directly from the hydroperoxide because no further oxygen uptake was noted after hydroperoxide formation (*93*).

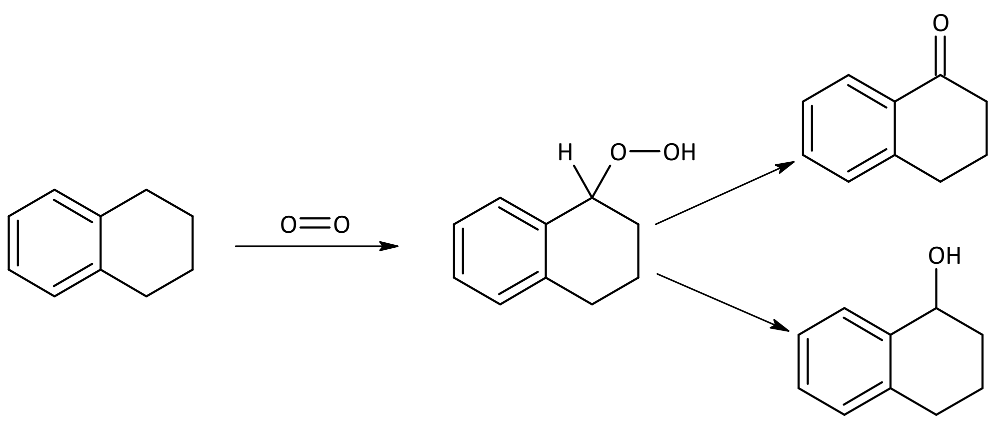

*Figure 2.14: Tetralin autoxidation mechanism (*93*)*

Decalin (decahydronaphthalene) occurs in both *cis* and *trans* isomers, of which the *trans* is energetically more stable due to fewer steric interactions (*95*). Decalin has an attractive feature as a potential hydrogen donor which inhibits deposit formation (*96*). It has the ability to donate hydrogen atoms to the radicals formed by thermal decomposition of fuel, thereby preventing the formation of deposits (*97*). In the presence of oxygen, oxidative attack in decalin isomers occurs in all positions with major products at the ternary position indicated in Figure 2.15 (*98*) which leads to the formation of octahydronaphthalen-4a(2H)-ol.

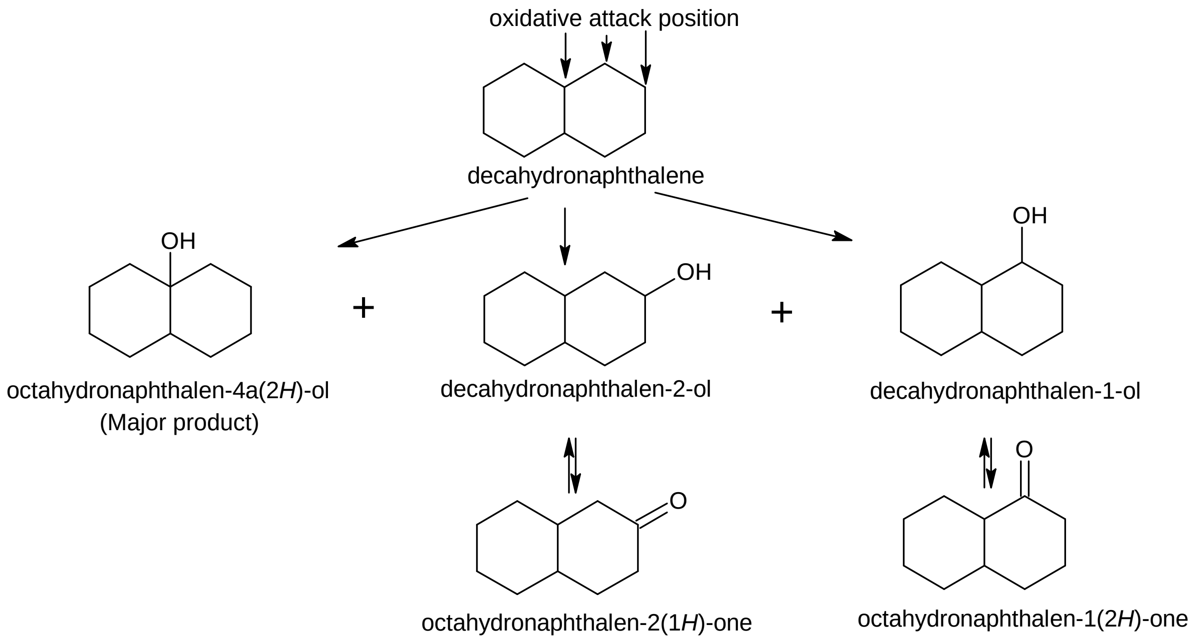

Figure 2.15: Shows positions for oxidation attack on a decalin molecule and the resultant oxidation products

2.9 Investigations of middle distillate stability using a quartz crystal microbalance

When fuel is exposed to high temperatures and oxygen, oxidised soluble and insoluble products are formed. A quartz crystal microbalance (QCM) has the ability to perform real-time measurements of the deposition of these. The technique was developed by Klavetter *et al* (*99*).

Oxygen is limited to that present in the air saturated fuel and the head space above. Choosing an appropriate temperature and limiting the oxygen availability closely approximates that of flowing tests and real fuel system conditions (*28*).

The thermal stability of fuels can be measured using a QCM in the temperature range 120-200^{o}C. An example setup is shown in Figure 2.16. In the current work, the QCM procedure as set out in the standard test method, ASTM D7739-11 (*27*), was used to investigate the thermal stability of biodiesel, petroleum diesel model compounds and blends thereof.

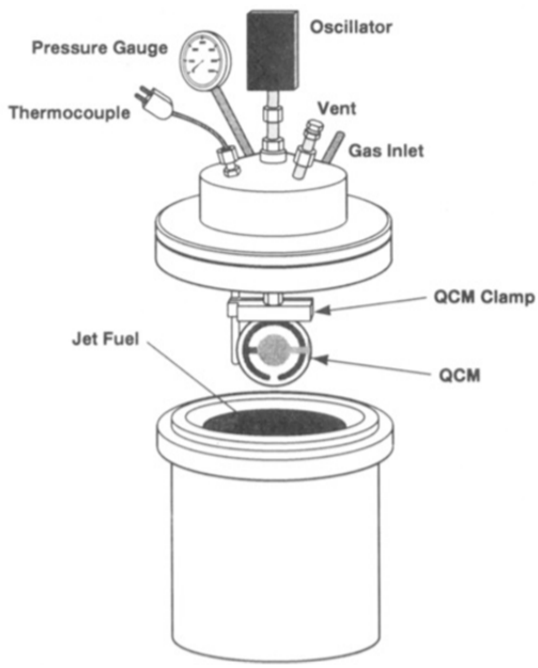

*Figure 2.16: Parr bomb/QCM assembly (reproduced from (*99*))*

A QCM is highly sensitive to surface deposits and is able to readily resolve surface deposits of about 0.1-0.2 µg/cm^2 (*28*). It determines the mass per area of deposit formed by measuring the change in frequency of a quartz crystal resonator. The resonance frequency is disturbed by the addition of a small mass due to film deposition on the surface of an acoustic resonator. The change in frequency may be used to determine the amount of deposit formed. Furthermore the QCM is fitted with a pressure sensor and an oxygen sensor (not illustrated in Figure 2.16). Not only can the deposit formation be monitored with time but also the consumption of oxygen.

Figure 2.17 shows the application of the QCM for a comparative study of the deposit forming potential of four diesels. It should be note that the commercial diesel in Figure 2.17 contained a deposit control additive which may explain why it had low mass accumulation. Kaminuza (*100*) showed that under QCM conditions, the addition of biodiesel to petroleum diesel increased mass accumulation. The extent of deposition from SME was greater than RME which was ascribed to the higher presence of polyunsaturated esters in SME.

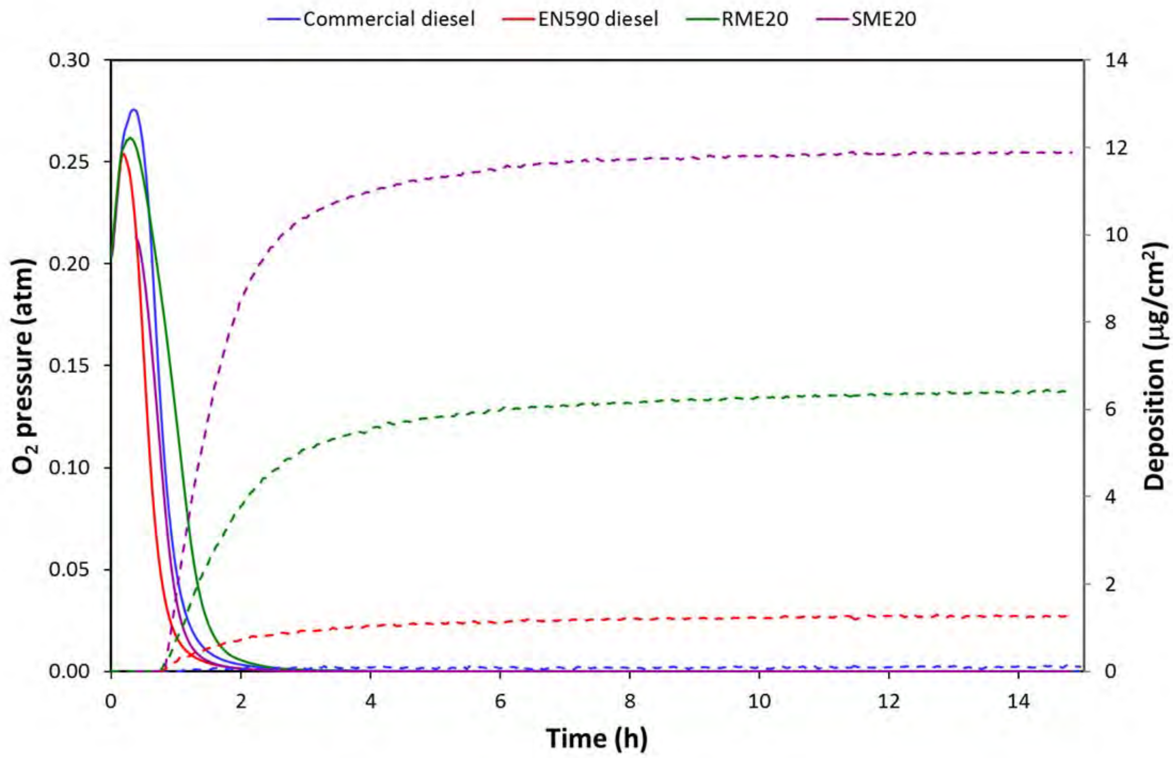

*Figure 2.17: QCM traces of four diesel fuels (a commercial diesel, an EN 590 reference diesel and two 80:20 (v/v) blends of EN 590 diesel with RME and SME) which were exposed to reactor conditions of 140°C and 1 bar of synthetic air for 15 h. The plots indicate mass (deposit) accumulation (dashed lines) and oxygen consumption (solid lines) (reproduced from (*100*))*

The QCM is typically used to study jet fuel (*11,28,99*). As far as could be ascertained, no studies have been reported on the thermo-oxidative stressing of middle distillate model compounds in a QCM. Furthermore, very few studies have been reported for petroleum diesel and no studies for neat biodiesel, FAME model compound or blends of biodiesel and petroleum diesel with the exception of the work of Kaminuza (*100*). He, however, only performed 4 experiments as he was interested in assessing the deposit forming potential of four specific fuels. He performed no mechanistic studies.

2.10 Electrospray ionisation-mass spectrometry (ESI-MS) studies of middle distillates

In electrospray ionisation, ions are produced by applying a high voltage to create a charged aerosol (*101*). As the solvent evaporates the charge is transferred to molecules in the aerosol droplets. ESI is a soft ionisation technique with little or no fragmentation (*101*). By coupling the ionisation with a mass spectrometric detector information can be obtained about the molecular masses of species in solution.

Although ESI-MS has been widely used for analysis of proteins and high molecular mass polymers, it has been sparingly used for liquid hydrocarbon fuels analysis (*12*). This is because fuels such as petroleum diesel are composed primarily of non-polar hydrocarbon species. ESI-MS is more useful for polar species which can be easily protonated or depronated (*102*).

ESI-MS has, however, found niche applications in fuel studies. The high selectivity towards polar species was exploited by Rostad *et al.* (*103*) who used the technique to differentiate between different fuel types based on their polar components. Hughey *et al.* (*104*) used ESI-MS to identify polar species in diesel fuel. Adams *et al.* (*70*) have used HPLC coupled with ESI-MS detection to identify heteroatom-containing species in jet fuel. Because the components of biodiesel are inherently polar, ESI-MS is much more widely used for the study of such fuels than petroleum diesel (*23*,*105*,*106*).

Thermo-oxidative degradation of hydrocarbon fuel leads to the formation of a variety of species containing heteroatoms such as oxygen. Commodo *et al.* (*12*) used positive ESI-MS to identify polar compounds in neat unstressed jet fuel (Jet A-1) and polar species that formed when the fuel was thermally stressed in the presence of oxygen. ESI-MS allowed Commodo *et al.* (*12*) to postulate a mechanism for jet fuel degradation. It was argued that soluble polar species in the m/z 250-400 range were deposit precursors which aggregated, polymerised and/or clustered to form insoluble precursors leading to the precipitation of solid deposits.

The use of ESI-MS for the monitoring of oxidation products has found more use for the study of biodiesel than petroleum diesel because of the easy ionisation of FAME molecules. Catharino *et al.* (*105*) used the technique to characterise biodiesel. Catharino *et al.* (*105*) performed ESI-MS on biodiesel in both positive and negative modes. In negative mode, ESI-MS oxidation products (mainly oxidised fatty acids) formed as a result of thermo-oxidative degradation (120°C, 8 h in excess air) of biodiesel were identified.

Ogawa *et al*. (*23*) also used ESI-MS to track the oxidation of a number of FAME model compounds. The formation of dimers which contained ketone functionalities was noted (Figure 2.18).

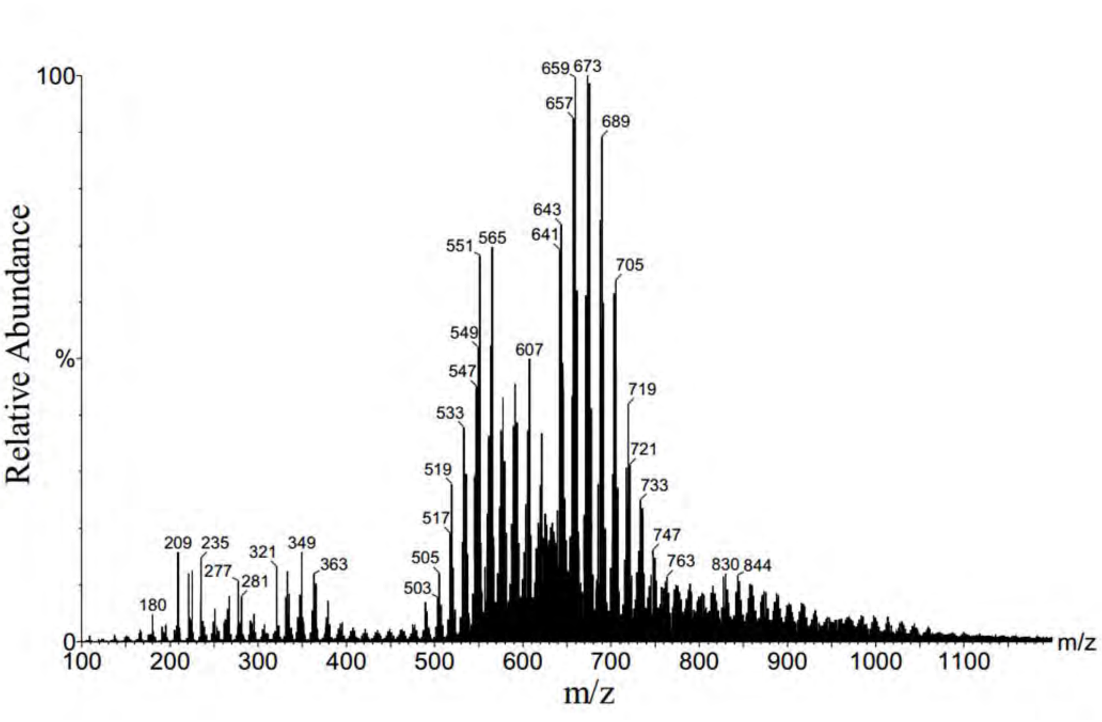

*Figure 2.18. ESI-MS of high molecular fraction, fractioned from oxidised waste cooking oil methyl esters (reproduced from (*23*)). Species are $[M+Na]^+$*

Tarvainen *et al*. (*107*) investigated the species formed during the oxidation (heating in a convection oven at 100°C for 48h) of fatty acid triglycerides as well as the fatty acids, linoleic and linolenic acid. ESI-MS was used to show that linoleic acid which has two double bonds is able to form dihydroperoxides while linolenic acid which has three double bonds, formed both di- and trihydroperoxides.

Recently, Kaminuza (*100*) used positive ESI-MS to investigate the relative stability of blends of petroleum diesel with rapeseed and soybean biodiesels. Figure 2.19 illustrates the ESI-MS(+) spectrum of a stressed soybean biodiesel. Biodiesel consists primarily of FAMEs having molecular masses between 290 and 300 amu (*61*). Kaminuza identified not only the addition of oxygen which increased m/z, but also the dimerization reactions taking place between the esters. This can be identified by the presence of ions in the m/z range (580-700). Similar dimerization was seen with RME although the extent of dimerization was smaller.

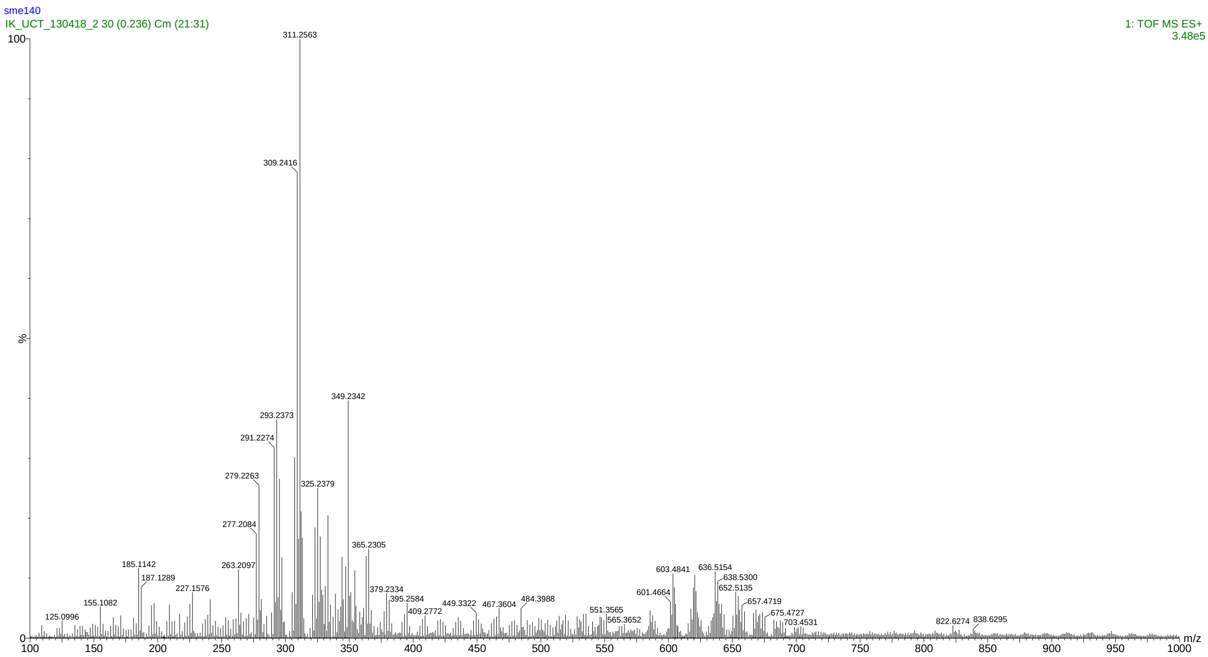

Figure 2.19: ESI-MS(+) spectrum (m/z range 100-1000) of SME, stressed in flowing air at 140^{o}C for 15h (adapted from (100)*)*

2.11 The effect of solvency on the formation of diesel deposits

The ability of a solvent to keep a solute in solution is called its solvency and is typically applied to the ability of a hydrocarbon solvent to keep polar solutes in solution (*108*).

Thermo-oxidative degradation products that form from petroleum diesel are known to be highly polar (*20,21*). Those formed from FAME are also polar in nature because of the inclusion of oxygen-containing functional groups (*23*). The precipitation of compounds from solution is dependent on both their molecular mass and their similarity to the solvent, *e.g.,* in polarity (*109*,*110*). The ester group (-$COOCH_3$) on FAME molecules makes biodiesel an excellent solvent for polar compounds while the non-polar nature of paraffins, present in petroleum diesel, makes them less suitable. Aromatic compounds display stronger interactions between molecules than saturated paraffins because of the uneven distribution of partial charges around the aromatic ring (*110*,*111*).

The solvency of the fuels is likely to play a significant role in the formation of deposits. Oxygen-containing deposits would be expected to dissolve more readily in a solvent with higher polarity. The solvency effect is important when blending FAMEs with petroleum diesel fuel because of the differences in polarity of the fuels (*112*). Omori *et al*. observed that the time to precipitate deposits is lower for blends of 10-20% FAME with petroleum–derived diesel than for the neat FAME and neat petroleum diesel (*25*).

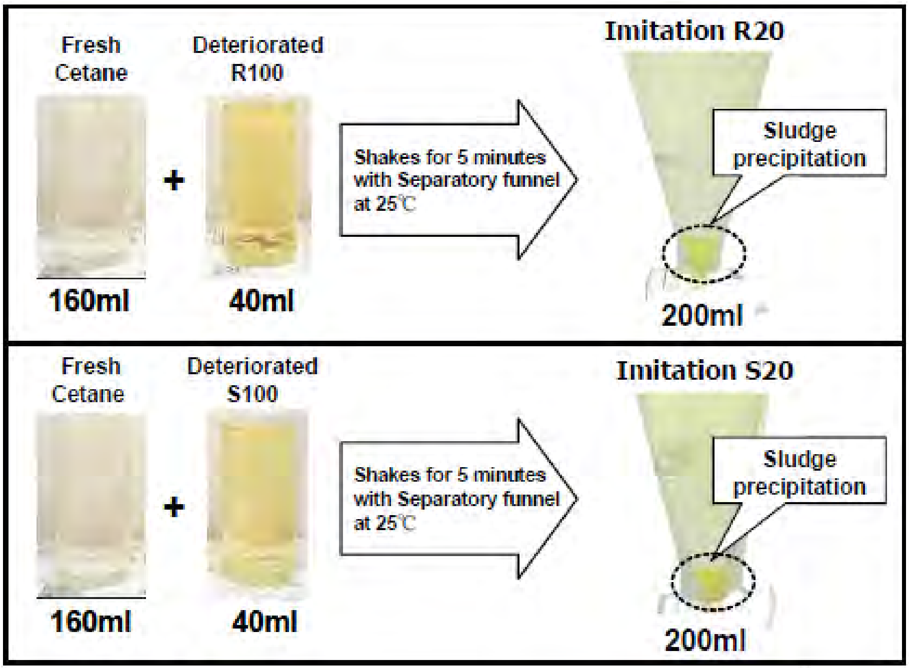

*Figure 2.20: Deposits precipitation caused by the mixing of a fresh petroleum diesel model compound, n-hexadecane, and deteriorated biodiesel (reproduced from (*113*))*

Osawa *et al.* (*113*) blended deteriorated rapeseed methyl esters (RME) and deteriorated soybean methyl esters (SME) with *n*-hexadecane, a model compound for fresh petroleum diesel. The FAMEs had previously been heated for 16h at 115°C. A colour change was observed in the FAMEs but no precipitate. After mixing with the petroleum diesel, precipitates were observed (Figure 2.20). This suggested that the reduction in solvency after the addition of cetane led to deposit precipitation (*113*).

The composition of the diesel with which FAME is blended has been found to be important. Significant quantities of gravimetric solids were observed when SME was blended with Fischer-Tropsch diesel but not when SME was blended with petroleum diesel. The latter contained 60% aromatic compounds while the former contained none. Mushrush *et al.* (*114*) ascribed this trend to lower solvency of the Fischer-Tropsch diesel and/or to the formation of a more stable hydroperoxide species by Fischer-Tropsch components, mainly alkanes (straight and branched (2- and 3-methyl isomers)).

Mitsuri *et al.* (*54*) conducted accelerated thermal oxidation on RME and SME blends with a petroleum diesel, containing 20% aromatic species. A viscous sludge was formed to the greatest extent in the blend ratio (20 to 40 vol%) biodiesel. They found that as the aromatic content decreased in the petroleum diesel, sludge formation increased.

Low phenolic-content petroleum diesel has relatively high thermo-oxidative stability compared to biodiesel. When high volumes of petroleum diesel are added to stressed biodiesel, a significant quantity of insoluble deposits have been observed to form. This leaves a question as to whether deposit formation increases as a result of reduced solvency of the blends, which causes soluble material in the biodiesel portion to become insoluble and drop out of solution or whether it is a consequence of the reactivity of the specific fuel components. Furthermore, the question exists as to whether the same behaviour would be observed if petroleum-derived diesel were blended with biodiesel and the blends were then thermo-oxidatively stressed.

3. Experimental methods

3.1 Materials used

3.1.1 Solvents

All solvents used in this study such as *n*-hexane, acetone, toluene and methanol had minimum purity of 99 % and were purchased from KIMIX (Cape Town, South Africa).

3.1.2 Gases

All the gases used in GC analyses and flask studies were supplied by Air Products SA (Cape Town, South Africa). To avoid contamination during separation by GC, high purity carrier gas, helium 5.0 (Purity ≥ 99.999% with a built-in-purifier GC grade) was used. Hydrogen 5.0 (Purity ≥ 99.999%) was used as a fuel gas in the GC-FID system.

Biodiesel has a high polarity due to the presence of ester groups and hence a higher affinity towards water than diesel fuel. Water or moisture increases the acidity of the fuel as a result of thermo-oxidative instability (*115*). Hence high purity synthetic air, instrumental grade (moisture content below 25 ppm), was used in QCM and flask studies.

3.1.3 Fuels

Model compounds were used in this study to reduce the complexity of the reaction systems. This made identification of reaction intermediates and products by gas chromatography (GC) easier which facilitated interpretation of the results.

Rapeseed methyl ester (RME) is the most commonly used biodiesel in Europe (*61*). RME was selected for this study because it is more thermo-oxidatively stable than soybean methyl ester (SME) and FAMES from other feedstocks (*116*,*117*). The primary unsaturated constituents of RME were used as model compounds in this study and are listed in Table 3.1 along with the paraffinic, cycloparaffinic, aromatic compounds and trace levels of different phenols which were used as model compounds for petroleum diesel. All model compounds were supplied by Sigma Aldrich (Saint Louis, MO, USA) unless otherwise stated. Table 3.1 also includes a number of intermediates which were used for GC analysis.

Table 3.1: Chemicals used

Compound class	Compound	Purity (%)
Full boiling point range fuels	EN 590 reference diesel[1]	-
	Rapeseed methyl ester[1]	-
Petroleum diesel model compounds	Decalin, mixture of *cis* and *trans* isomers (naphthenic)	98%
	n-Hexadecane (paraffinic)	99%
	Tetralin (aromatic)	99%
Biodiesel model compounds	Methyl oleate (18:1)[4]	70%
	Methyl linoleate (18:2)[4]	≥99%
	Methyl linolenate (18:3)[4]	70-80%
Phenolic compounds	Butylated hydroxy toluene (BHT, antioxidant)	90%
	Phenol	≥99.5%
GC reference materials	1-Decalol (mixture of isomers)	97%
	2-Decalol (mixture of isomers)	97%
	1-Decalone (mixture of isomers))	97%
	2-Decalone	97%
	n-Decane	99%
	5,8-Dihydro-1-naphthol	98%
	n-Dodecane	99%
	FAME[2,3,4]	-
	1-Hexadecanol	99%
	2-Hexadecanol	99%
	2-Hexadecanone	98%
	3-Hexadecanone	98%
	1-Hexanoic acid	≥99.5%
	1-Nonanal	95%
	1-Octadecanol	99%
	2-Octadecanone	97%
	3-Octadecanone	97%
	Octahydronaphthalen-4a(2*H*)-ol	95%
	n-Pentane	99%
	n-Tetradecane	99%
	1-Tetradecene	>99.5%
	1-Tetralol	97%
	1-Tetralone	97%
	2-Tridecanone	97%

1. Supplied by Sasol Technology (Johannesburg, South Africa)
2. Supplied by Supelco (Bellefonte, PA, USA)

3. Reference material containing C16-C22 methyl esters: methyl myristate (14:0), methyl palmitate (16:0), methyl stearate (18:0), methyl oleate (18:1), methyl elaidate (18:1), methyl linoleate (18:2), methyl linoleaidate (18:2), methyl linolenate (18:3), methyl arachidate (20:0), methyl behenate (22:0)
4. The first number, in the brackets after the FAME names, indicates the number of carbons in the carboxylic acid from which ester is derived while the second number is the number of double bonds along the carbon backbone

The structures of the fuel model compounds used may be found in Figure 2.1 and Figure 2.6.

3.2 Test matrix

Thermo-oxidative stressing took place in two reactor systems: a QCM and open glass flasks open to the atmosphere. Open glass flasks have been widely in studies, and are reported in the open literature (*17*,*20*,*21*,*118*); hence, experiments in open glass flasks would provide data for comparison. Because fuel in real fuel systems is often oxygen limited, QCM experiments were also performed (*28*).

Diesel fuels contain a mixture of hydrocarbons, which include approximately 65–85% saturates (primarily paraffins including *n*-, *iso*-, and cycloparaffins), 5–30% aromatics (including naphthalenes and alkylbenzenes), and 0–5% olefins (*119*). The percentages vary with manufacturers, crude oil source, the refining processes and sulfur content.

Unless otherwise specified all percentage compositions of blends that were made up are volume per volume (% v/v). 80% *n*-hexadecane/20% tetralin (system DMC-A) was selected as the simplest model system for petroleum diesel. *n*-Hexadecane was chosen because the number of carbons lies at the midpoint of the typical carbon-number range of petroleum diesel (*41*). It has also previously been used as a model compound (*113*). Tetralin is a typical aromatic compound found in middle distillates such as diesel (*11*,*41*).

It has been proposed that decalin has the ability to inhibit deposit formation (*97*). For this reason, it was included as a representative diesel boiling range cycloparaffin. It was included by replacing some of the *n*-hexadecane (System DMC-B). A further model system was produced in which the amount of tetralin was halved (System DMC-C). The ratio of *n*-hexadecane to tetralin was kept constant.

Table 3.2 contains the compositions of the three petroleum diesel model systems.

Table 3.2: Petroleum diesel model compound system compositions (v/v)

Diesel model system	Tetralin (%)	*n*-Hexadecane (%)	Decalin (%)
DMC-A	20	80	0
DMC-B	20	49	31
DMC-C	10	55	35

Methyl oleate, methyl linoleate and methyl linolenate are major components found in RME. These components are found in ratios of 7:3:1 respectively (*120*).

To explore the effect of phenolic compounds, model systems were doped with phenol and the antioxidant, BHT, at the level of 200 ppm. The influence of acids on deposit formation was investigated by adding the acid, *n*-hexanoic acid, at 5%. *n*-Hexanoic acid was chosen because it has been identified as a FAME degradation product (*23*).

3.3 Stabiliser identification

As-received compounds are often supplied in stabilised forms which contain antioxidants. Because antioxidants may affect deposit formation (*72*), it is important that such antioxidants be removed for proper control of the composition of the starting materials for model compound studies.

Procedure

GC-MS (described in Section 3.7.1) was performed to confirm the presence of stabilisers. Stabilisers were not detected in any model compounds used. Consequently, no purification steps were required.

3.4 Quartz crystal microbalance (QCM) thermo-oxidative stressing

This procedure was used to evaluate the thermo-oxidative stability of various fuel blends. Experimental conditions are listed in Table 3.3. The test method was based on the standard test method ASTM D7739-11 (*27*). The system was charged first with air at time zero and the experiment run for 24h. Some fuels tested were also repeated with 200 ppm phenolic compounds (phenol or BHT). Experiments were performed in duplicate with the exception of neat diesel model compound systems which were performed in triplicate and blends containing FAME model compounds which were performed once. Measurements were made of temperature, total pressure, oxygen pressure and mass deposited.

Table 3.3: Fuels tested and QCM test conditions

Fuel		
Diesel model compounds	**Biodiesel compounds**	**Diesel - biodiesel blends**
1. DMC-A	1. RME	1. 80% DMC-A/20% RME
2. DMC-B	2. RME + 200 ppm BHT	2. 80% DMC-A/20% RME + 200 ppm BHT
3. DMC-C		3. 80% DMC-A/20% RME + 200 ppm phenol
		4. 90% DMC-A/10% RME
		5. 70% DMC-A/30% RME
		6. 35% DMC-A/65% RME
		7. 80% DMC-A/20% methyl linoleate (ML)
		8. 80% DMC-A/20% methyl linolenate (MLN)
		9. 80% DMC-A-/20% RMEMC[1,2]
		10. 80% DMC-A/20% RMEMC[1] + 200 ppm BHT*
		11. 80% DMC-A/20% RMEMC[1] + 200 ppm phenol
		12. 75% DMC-A/20% methyl linoleate (ML/5% hexanoic acid
Test conditions		
Temperature (^{o}C)	140	
Time (h)	24	
Pressure (psi)	22 ($\pm$ 1.5 bar)	

1. RMEMC-Rapeseed methyl esters model compound mixture = 64% MO/27% ML/9% MLN
2. Experiment was repeated at 100^{o}C

At the end of the experiment, the stressed fuel was analysed using GC, ESI-MS, UV-Vis spectroscopy and FTIR spectroscopy to assess the extent of degradation.

3.5 Flask oxidation

In these experiments, which are similar to those reported in literature (*17*,*21*,*20*,*118*), fuel was oxidised at 140°C under flowing air and sampled using a syringe at hourly intervals for six hours. This temperature was selected because it allowed for comparison with QCM results. The purpose of these tests was to evaluate thermo-oxidative stability of fuel over time. Tests were performed under flowing synthetic air. The experimental set-up is indicated in Figure 3.1. Analysis of the withdrawn aliquots by GC-MS, GC-FID and ESI-MS allowed the formation and consumption of degradation products to be monitored. Experiments were performed in duplicate.

Procedure

1. 60 mℓ of model fuel blend were placed in a 100 mℓ three-neck round bottom flask equipped with a reflux condenser, thermocouples and gas delivery pipette. In the case of biodiesel model compounds, a 30 mℓ sample was placed in 50 mℓ three-neck round bottom flask. This was done because of the small quantities of these model compounds that were available.
2. The heating mantle was switched on, the gas line was opened and the flow of gas was adjusted to 50 mℓ min^{-1}.
3. The temperature was then allowed to stabilise at 140°C.
4. The test fuel was stressed for 24 hours.
5. 1.5 mℓ aliquots were sampled every hour for 6 hours, and then after 24 hours.
6. After 24h, the remaining sample (49 ± 1 mℓ) was cooled to near 50°C and transferred to 50 mℓ centrifuge tubes which were stored in a fridge at 4°C.
7. Regular sampling provided aliquots for analysis by GC-MS, GC-FID, ESI-MS, UV-Vis and FTIR spectroscopy.
8. The remaining samples were separated into two layers by centrifugation.

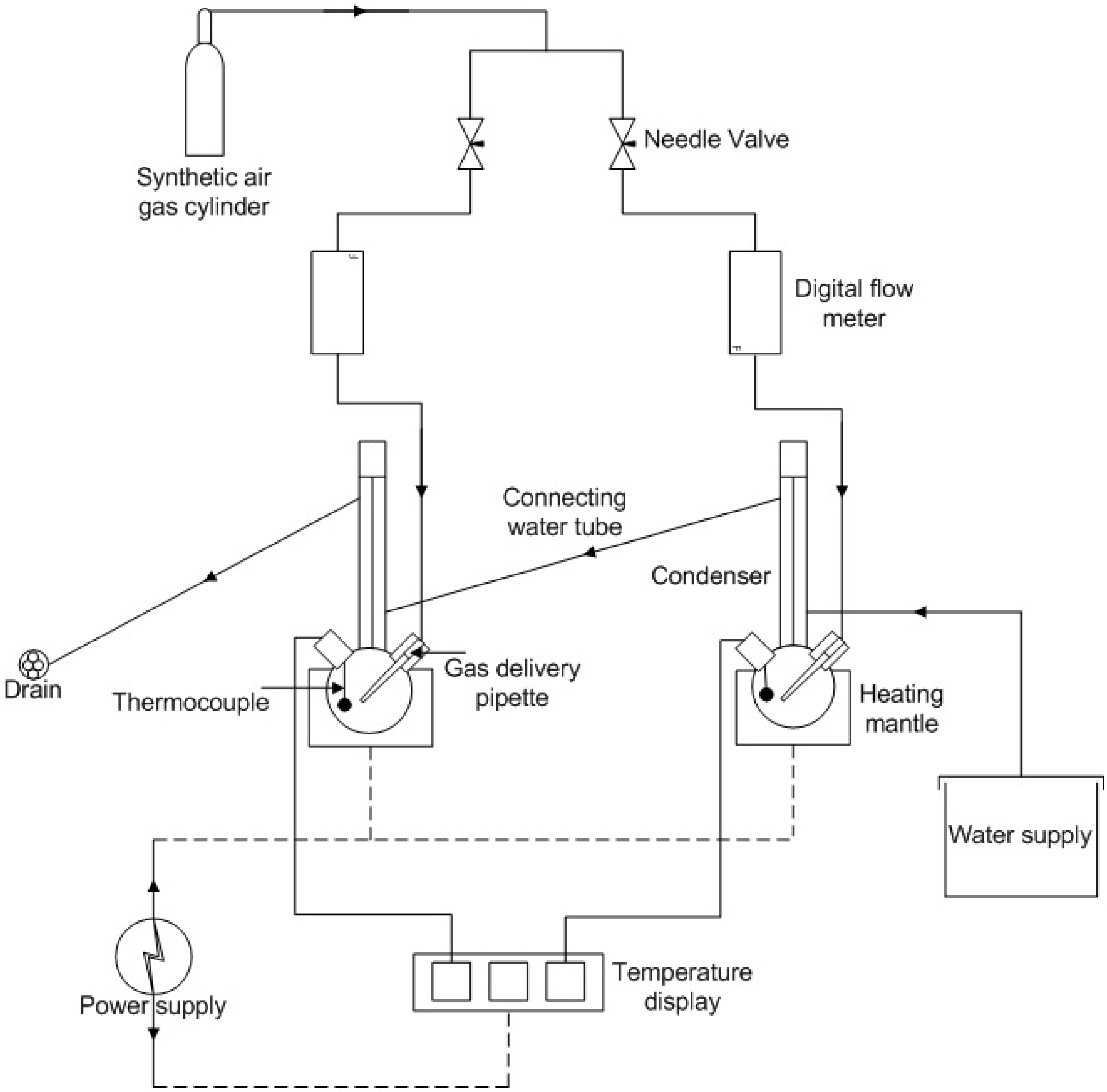

Figure 3.1: Flask reactor experimental setup

3.6 Layer separation by centrifuge

A centrifuge uses centrifugal force to isolate suspended particles from their fluid matrix (*121*). Generally, if a solution of relatively large particles is left to stand, particles will tend to sediment under the influence of gravity. The centrifugation separation technique increases the rate of particle sedimentation by exerting a larger force than earth's gravitational force (*121*).

The two layers formed during thermo-oxidative degradation were separated using a U-320 BOECO centrifuge at the Centre for Bioprocess Engineering Research (CeBER) at the University of Cape Town. Table 3.4 shows the centrifuge test conditions.

Table 3.4: Centrifuge test conditions

Centrifuge	Boeco U-320
Revolutions per minute (rpm)	4000
Time (minutes)	10

Procedure

1. 50 mℓ centrifuge tubes containing stressed fuel were measured to that each tube + fuel had the same mass.
2. The centrifuge tubes were placed in the centrifuge.
3. rpm and time were set as presented in Table 3.4.
4. After centrifugation, the lower layer from stressed fuel matrix was isolated using a pipette.
5. Centrifuge tubes were weighed to obtain the mass of the separated layer.
6. The layers were analysed by GC-MS, GC-FID, ESI-MS, UV-Vis and FTIR spectroscopy.

3.7 Other analytical techniques

3.7.1 Gas chromatography-mass spectrometry (GC-MS)

A Shimadzu GCMS-QP2010 Plus coupled with a high performance quadrupole mass spectrometer and an Agilent GCFID-7890A with flame ionisation detector were used for analysis in this study.

GC was used to track the consumption of model compounds as well as the formation of thermo-oxidative degradation products. Thermo-oxidative degradation products were analysed by GC-MS using the parameters in Table 3.5. The optimisation of these parameters is discussed in Section 10.1 of the Appendix.

Table 3.5: GC and MS parameters

Instrument	Shimadzu QP 2010 Plus GC-MS			
Column	BPX5 - 25m x 0.32 mm ID X 0.25μm film: non-polar column with a maximum temperature of 360°C			
Gas	Helium			
GC injection program				
Injection temperature	270°C			
Injection mode	Splitless			
Injection volume	1 μℓ			
GC pressure program				
Flow control mode	Linear velocity			
Purge flow	3.0 mℓ/min			
Column oven temperature program				
Rate (°C/minute)	Final temperature (°C)	Hold time (min)		
-	50	1		
20	270	5.5		
MS program				
Starttime (min)	End time (min)	Acquisition mode	Start m/z	End m/z
2.5	17.50	Scan	50	450
MS parameters				
Ion source temperature (°C)	Interface temperature (°C)	Solvent cut off time (min)		
260	280	2		

The solvent delay time was set at 2.5 minutes. This was done to protect the MS detector from high concentrations of solvent, TAM (toluene/acetone/methanol), used in the analysis. Analysis of several chromatograms showed the solvent delay fell just prior to the elution of *n*-pentane.

GC was used to track the consumption of the model compounds as well as track the formation of new oxidation products. Products formed during thermo-oxidative stressing on the QCM and flask reactors were analysed by GC-MS and GC-FID. GC-MS allowed for the determination of the composition of stressed fuel whereas GC-FID gave the concentration of both model compounds and some oxidised species.

GC-FID was calibrated using diesel model compounds and their derivatives. Since the major oxidation products were alcohols and ketones, tetralin derivatives (tetralols and tetralones), decalin derivatives (decalols and decalones) and the *n*-hexadecane derivative, 2-hexadecanol were used.

3.7.2 Fourier transform infrared spectroscopy (FTIR)

Stressed fuels were analysed using a Nicolet 6700 FTIR instrument, supplied by Thermo-Scientific. FTIR was used to monitor the formation of oxidised species. In particular changes in the C=C stretches and the formation of C=O stretches were monitored (*23*,*122*,*123*). The experimental parameters are listed in Table 3.6.

Table 3.6: FTIR specifications and experimental parameters

Instrument specifications	
Instrument type	Nicolet 6700 FTIR
Spectral range	7800-350 cm^{-1}
Optical resolution	0.09 cm^{-1}
Wavenumber precision	0.01 cm^{-1}
Experimental parameters	
FTIR mode	Absorbance
Number of sample scans	100
Number of background scans	32.0
Resolution	4.00
Optical velocity	0.63
Aperture	100
Detector	DTGS KBr
Beam splitter	KBr
Source	IR

Samples were placed on the diamond single crystal of a Smart iTR™ attenuated total reflectance (ATR) sampling accessory.

3.7.3 Ultraviolet-visible spectroscopy (UV-Vis)

Stressed fuel was analysed with a T80+ ultraviolet-visible (UV-Vis) spectrometer, supplied by PG Instruments. This was used to monitor colour changes brought about by oxidation (*18*). Because aromatic compounds in petroleum diesel, and biodiesel itself, have a high absorbance in the UV range, three step dilutions were used in this study in order to reduce the absorbance to below 2. In each step, 0.4 mℓ sample was diluted with 9.6 mℓ *n*-hexane.

The viscous lower layer, separated by centrifugation, did not dissolve in *n*-hexane. In these cases, 0.4 mℓ sample was first dissolved in 9.6 mℓ acetone and then filled to 20 mℓ with hexane. A 0.8 mℓ sample was withdrawn and diluted with 9.2 mℓ hexane. In the last step, 0.4 mℓ sample was diluted with 9.6 mℓ *n*-hexane. All samples were analysed in the UV range of 350-200 nm.

3.7.4 Electrospray ionisation/ mass spectrometry (ESI-MS)

Analyses of polar, heavier intermediates were performed using electrospray ionisation–mass spectrometry (ESI-MS) at the Central Analytical Facility of Stellenbosch University. This allowed the formation of high molecular weight species to be detected after 24 hours thermal oxidation. Furthermore species in the sub-ppm range which are not normally amenable to detection by GC-MS may be detected by ESI-MS (*70*).

Both layers (top and bottom) as well as the fuel (after QCM stressing) were analysed where two layers formed.

Samples for ESI-MS analyses were prepared as follows:

1. 5 mℓ of stressed fuel or insoluble layer was mixed with 2 mℓ methanol (fuel: methanol 5:2 by volume) in a separating funnel and the mixture was left for 5 minutes.
2. The methanol layer was collected in GC vials.

The mass spectra of the methanol extract were collected in the range of m/z 100-1500 using parameters indicated in Table 3.7.

Table 3.7: Instrumental parameters used in the acquisition of ESI-MS data

Instrument	Waters Synapt G2
Source	ESI positive/ negative
Cone voltage	15 V
Lock mass (reference)	Leucine enkaphalin (555.6g/ mol)

3.8 Investigations into solvency effects

The influence of solvency on the formation of deposits from petroleum diesel blends with biodiesel has not been widely reported (*23*,*53*,*113*,*124*). Studies have also used stressed biodiesel rather than stressed blends of biodiesel and petroleum diesel (*113*). No studies have been reported for model compound systems, bar the use of *n*-hexadecane (*113*).

In the first set of experiments, RME was stressed for different periods of time in an open glass flask under flowing air. 20% of this stressed RME was then doped into blends of *n*-tetralin with different amounts of tetralin (0%, 20%, 80% and 100%). The addition of 20% stressed RME was chosen because it was used by Osawa *et al.* (*113*). Tetralin was used to represent aromatic compounds in petroleum diesel while *n*-hexadecane represented paraffinic compounds in petroleum diesel.

A second set of experiments was performed to separate the effect of solvency from reactivity effects on thermo-oxidative degradation. Blends of FAME model compounds/*n*-hexadecane/tetralin (polar/non-polar/aromatic) with different polarities were used to investigate the effect of solvency on deposit solubility.

The more dense layers, formed during flask studies, were collected by centrifugation of the blends, stressed at 140^{o}C for 24 hours. These layers were obtained from 80% DMC-A/20% RME.

The solubility of the insoluble layer was assessed using ternary blends of FAME model compounds/*n*-hexadecane/tetralin of different ratios presented in Table 3.8.

Table 3.8: Diesel/biodiesel ternary blends for solvency effect experiments

Blend No.	Amount (%)		
	n-Hexadecane	Tetralin	FAME model compounds (7:3:1 blend)
1.	0	0	100
2.	10	30	60
3.	20	60	20
4.	80	20	0
5.	80	10	10
6.	20	80	0
7.	100	0	0
8.	0	100	0

Procedure

1. 0.8mℓ neat n-hexadecane/tetralin or diesel/biodiesel ternary blends were placed in a 2 mℓ centrifuge tube.
2. 0.2mℓ of the stressed RME/stressed lower layer was added to the centrifuge.
3. The mixtures were shaken for 5 min.
4. The mixture in a centrifuge tube was observed after 5 min and again after 24 h for phase separation.

4. QCM thermal oxidation

A summary of the average masses accumulated, that were measured after 24h, for each experiment may be found in Table 10.2 in the Appendix. Unless otherwise specified, experiments were performed in duplicate.

4.1 Effect of diesel composition on thermo-oxidative stability

Diesel model compound systems (DMC) A, B and C were used in this study to evaluate the effect of composition on thermo-oxidative stability of diesel fuel. All diesel model compounds were evaluated under the same QCM conditions. The results, presented in Figure 4.1, are the average of 3 experiments. They allowed a comparison between the different petroleum diesels compositions to be made.

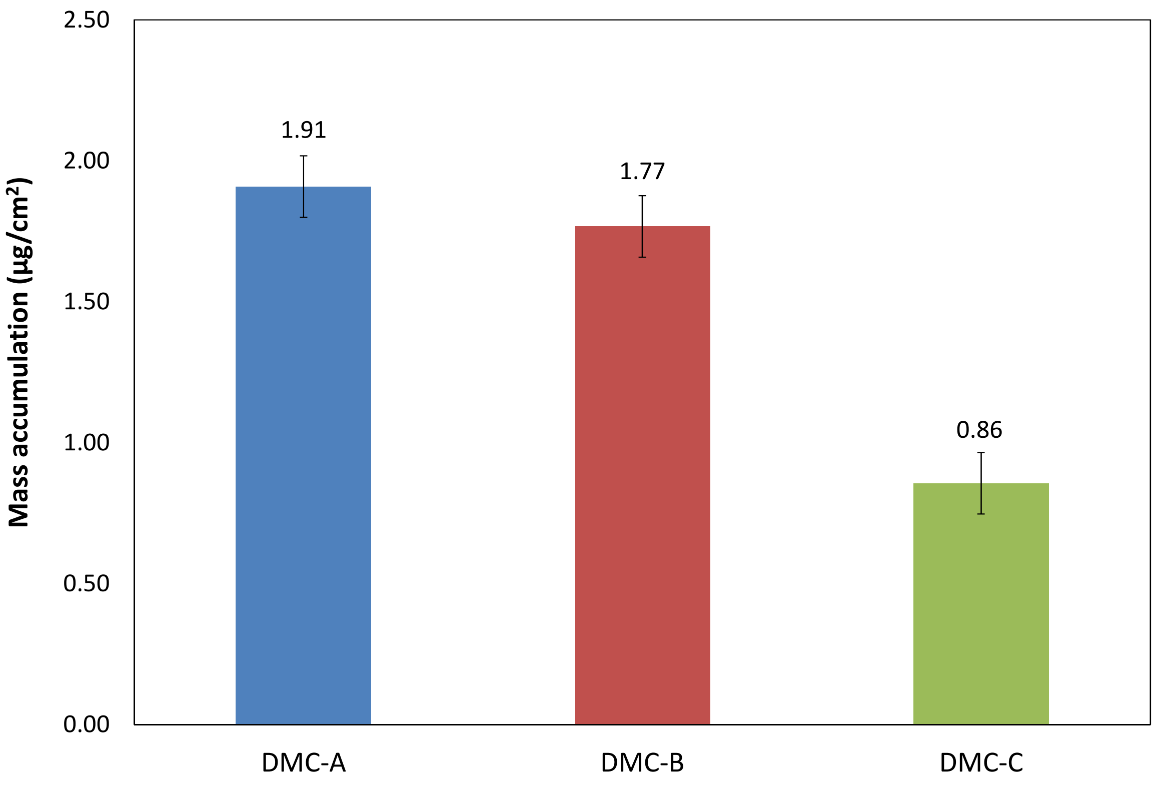

Figure 4.1: Average mass accumulation of different diesel model compound systems after oxidation in a QCM at 140^{o}C for 24h. The error bars represent one standard deviation of the mean either side of the mean.

Diesel model compounds were seen to form significantly less deposits than biodiesel (see Section 4.2) during QCM oxidation with DMC deposits in a range between 0.8 and 2 μg/cm^2. The DMC-A blend which contained 80% *n*-hexadecane and 20% tetralin formed the most deposits. The amount of deposit formed in system DMC-B which contained 20 % tetralin, 49% *n*-hexadecane and 31% decalin was slightly lower but the difference was not statistically significant. The fuel containing the lowest amount of tetralin (10%), DMC-C, formed the lowest quantity of deposits.

4.1.1 Discussion

The stability of diesel is influenced by the presence of oxidatively reactive species. Petroleum diesel, in general, is more stable than biodiesel (*24*,*79*,*80*,*81*,*82*,*83*). The presence of the aromatic, tetralin, in fuel reduced the stability of the fuel and increases the formation of deposits with the amount of deposit formed increasing with increasing tetralin levels. The amount of mass accumulated approximately doubled when the tetralin concentration doubled. The results are consistent with the observation by DeWitt *et al.* (*11*) that deposition increased as the aromatic level increased. The mass accumulations, measured in this study, are within the range measured by DeWitt *et al* (*11*).

It has been suggested that decalin can act as a hydrogen donor in reactions which inhibits oxidation (*92*). Alemán-Vázquez *et al.* (71) suggested that decalin can donate hydrogen to radicals formed during thermo-oxidation inhibiting the formation of deposits. In the current study, however, in the presence of high amounts of tetralin, no statistical improvement could be seen when systems DMC-A and DMC-B were compared. It is suggested that this is because the conditions investigated by Alemán-Vázquez *et al.* (*92*) were near to oxygen free.

In all further QCM experiments, the model compound system, DMC-A, which is a blend of 80% *n*-hexadecane and 20% tetralin was used.

4.2 Thermo-oxidative stability of diesel model compound/biodiesel blends

To investigate the effect of the addition of biodiesel, a diesel model compound (DMC-A, 80%)/FAME (RME, 20%) blend was subjected to QCM oxidation at 140°C for 24 hours. The results are depicted in Figure 4.2 with a comparison with the neat diesel model compound system and neat FAME.

Note that in all figures that follow, the oxygen concentration is reported as a notional % rather than a percentage of the gas in the headspace. It is proportional to the oxygen partial pressure. The value exceeds the 21% in air because the QCM is pressurised to 1.5 bar and is then heated to 140°C increasing the oxygen partial pressure further causing an apparent increase in oxygen percentage. Above 43% apparent oxygen concentration, the detector was saturated.

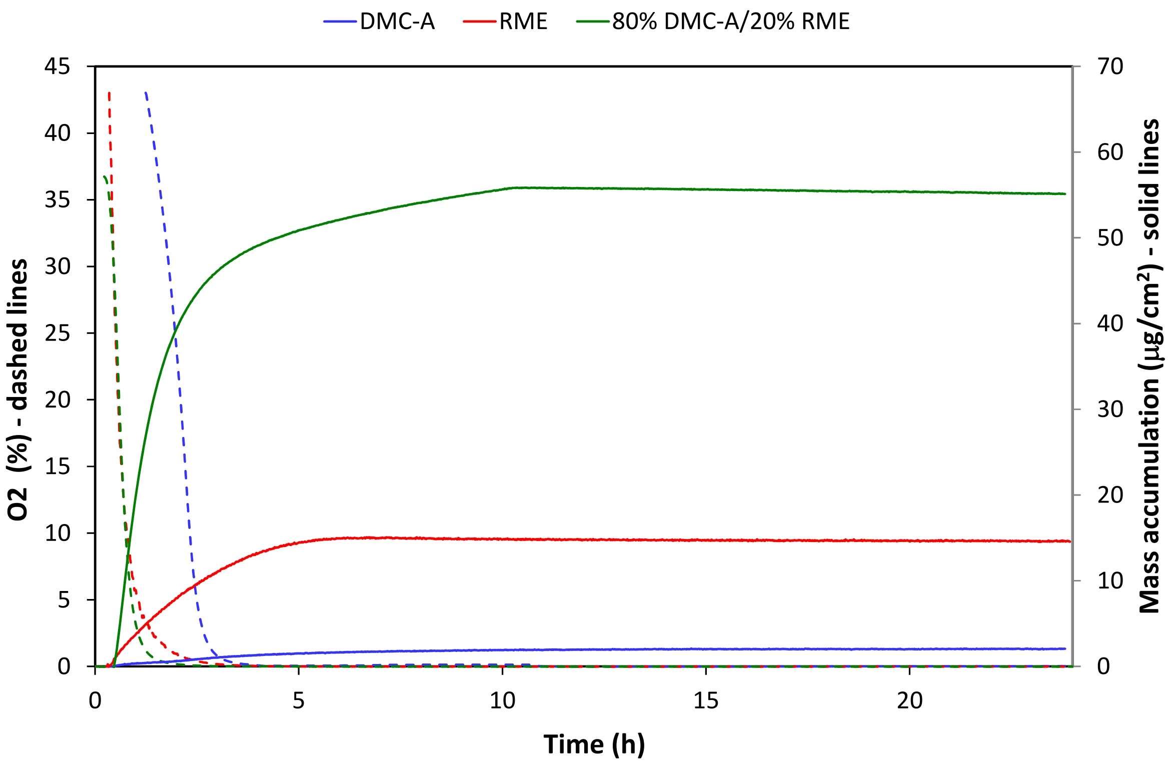

Figure 4.2: Oxygen depletion and mass accumulation for the oxidation of DMC-A, RME and a 80/20 DMC-A/RMA blend in a QCM at 140°C for 24h

The QCM mass accumulation curve indicates that the neat diesel model system is significantly more stable at this temperature. Oxygen consumption was significantly slower than systems which contained RME (both neat and blended). The nominal percentage oxygen present dropped below 5% after 2.5h for DMC-A compared to 1.1h for RME. The respective times taken to reach 0.1% were 3.9h and 3.3h.

Although RME formed more deposits than neat DMC-A at this temperature, the deposit formation increased even further when RME was blended with the diesel model system. Oxygen consumption was even faster (0.9h to reach 5% and 2.9h to reach 0.1%)

4.2.1 Discussion

The QCM methodology is suitable for the investigation of the stability of biodiesel containing systems. The methodology is far more powerful than that contained in ASTM D7545-14 (*35*). The latter test, using a Petroxy™ instrument, measures only oxygen consumption. No estimation of a fuels deposition potential is provided in this method.

In the presence of oxygen, RME is rapidly oxidised. The rapid depletion of oxygen is the result of oxidative attack at allylic and *bis*-allylic carbons on the RME backbone (*58*). Hydrogen atoms at the latter sites are more easily abstracted than those on the constituent molecules of DMC-A.

Significantly, the level of deposits formed increased even further when RME was blended with a diesel model compound system. The amount of mass accumulated is lower than what was observed by Kaminuza (*100*) because he a) charged the QCM with a lower pressure of air, and b) the blend of RME he used contained small quantities of antioxidant.

It is suggested that the deposits which form contain oxygen, making them polar in nature (*23*). Neat RME is more polar than the diesel model system because of the presence of oxygen-containing ester groups. The blending of DMC-A with RME decreases the polarity of the fuel. It is suggested that this in turn reduces the ability of the blend to maintain the deposits in solution. The amount of deposition is lower for the stressing of neat RME than the 80:20 blend because of the similarities in the nature of the products and RME. This is explored further in Section 4.6.

4.3 Effect of degree of FAME unsaturation on thermo-oxidative stability

FAME model compounds with carbon number 19 with different degreeS of unsaturation were used in this study to investigate the effect of degree of FAME unsaturation on thermo-oxidative stability. Methyl linoleate (18:2) and methyl linolenate (18:3) were used. An experiment was performed using methyl oleate (18:1) but due to a data connection fault, data was not logged. Owing to limited quantities of model compounds available, no repeat experiments could be performed using methyl oleate (18:1). These FAME model compounds were blended with diesel model compounds and the results are shown in Figure 4.3.

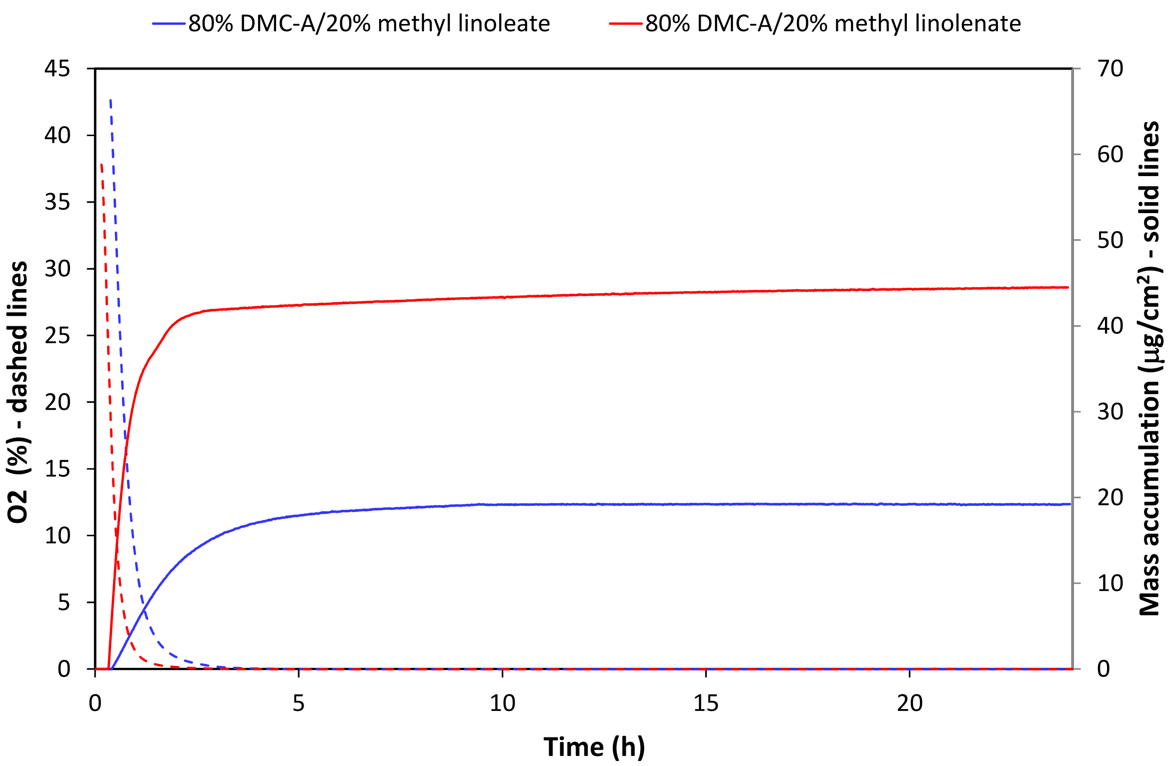

Figure 4.3: Oxygen depletion and mass accumulation for the oxidation of 80% DMC-A blends with individual FAME model compounds with different degrees of unsaturation in a QCM at 140^{o}C for 24h.

The red curve in Figure 4.3 indicates that the blend containing methyl linolenate, which has the most double bonds along the carbon backbone (*62*), produces the most deposits. The amount of deposits formed in all cases is larger than typical middle distillate fuels (*99*,*125*). As can be seen in Figure 4.3, oxygen was consumed rapidly in all model systems. Consumption was however quicker for methyl linolenate (3 double bonds, 5% O_2 reached after 0.7h, 0.1% after 2.2h) than methyl linoleate (2 double bonds, 5% O_2 reached after 1.2h, 0.1% after 3.3h).

4.3.1 Discussion

The resistance of FAME to degradation is affected by the degree of FAME unsaturation (*13*,*77*). Gunstone (*78*) reported that linoleates were 27 times as reactive towards autoxidation as oleates, and linolenates were 77 times more reactive.

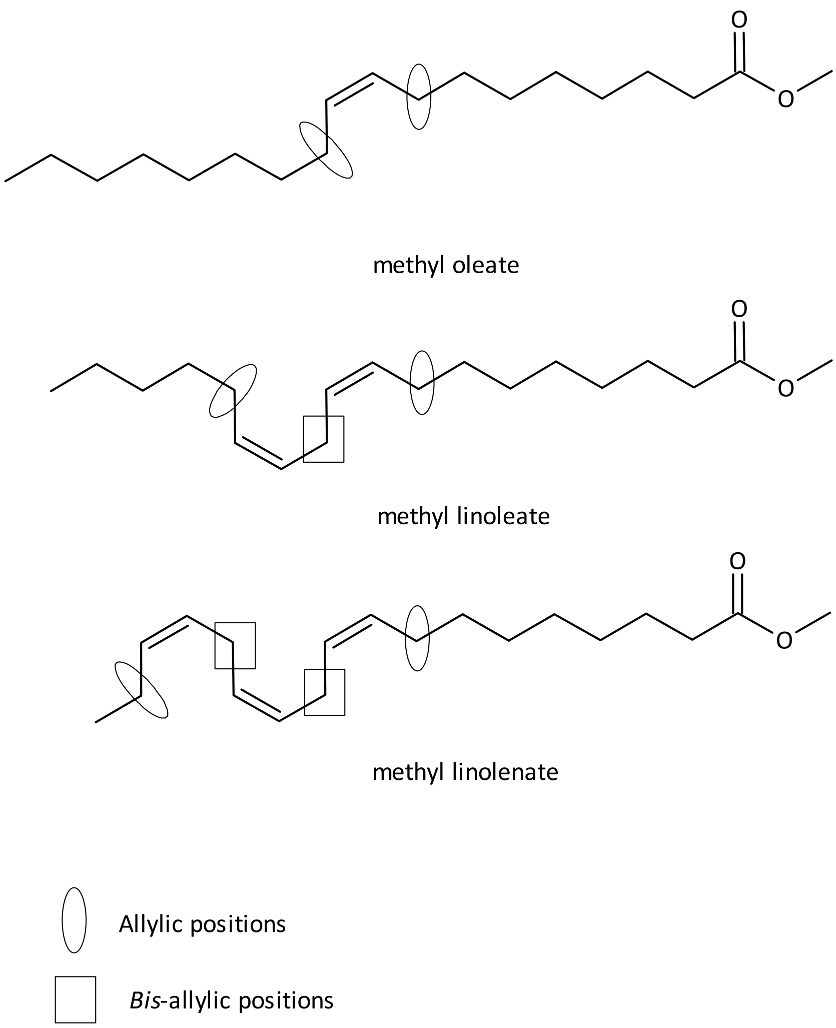

Figure 4.4: The positions in methyl oleate, methyl linoleate and methyl linolenate that are vulnerable to oxidation (adapted from (58)*)*

Oxidation is initiated at the allylic and most specifically at the reactive *bis*-allylic carbon atoms highlighted by circles in Figure 4.4. All unsaturated C19 FAMEs have 2 allylic carbons but differ in the number of *bis*-allylic carbon atoms. FAMEs with a high degree of unsaturation are more prone to oxidation due to an increase in the number of *bis*-allylic carbon atoms. This is consistent with the fact that Kaminuza (*100*) observed greater deposits from diesel blends containing SME rather than RME. SME contains more unsaturated molecules, including methyl linolenate (*126*).

Methyl linolenate has two highly reactive *bis*-allylic carbon atoms; hence, when blended with diesel model compounds, it produced a relatively higher amount of deposits than the other FAMEs with one and two double bonds. This increases the number of pathways to form conjugated dienes. In turn, the statistical likelihood of forming links between FAME esters, leading to higher molecular weight compounds, is increased. The higher number of *bis*-allylic carbon atoms also accounts for the higher rate of oxygen consumption.

4.4 Effect of phenols on thermo-oxidative stability

BHT and phenol were used to investigate the effect of phenolic compounds on thermo-oxidative stability. 200 ppm BHT and phenol were doped into 80% DMC-A blends with 20% RME. The mass accumulation and oxygen accumulation were monitored over time for 24h and the results are depicted in Figure 4.5.

Figure 4.5 indicates that adding BHT to a highly depositing fuel reduced the formation of deposits. BHT reduced the mass accumulation by approximately 25%. Phenol on the other hand increased the extent of deposition. The addition of BHT was also observed to reduce the amount of deposit formed when neat RME (not illustrated) was stressed from 14.9 to 12.4 $\mu g/cm^2$ after 24h. Adding BHT reduced the rate of consumption of oxygen. The blend, without BHT, took 0.9h to reach 5% and 2.9h to reach 0.1% compared to 1.4h and 4.1h for the blend containing BHT. This is typical behaviour for an antioxidant (*74*). A delay in oxygen consumption was also observed when BHT was added to neat RME.

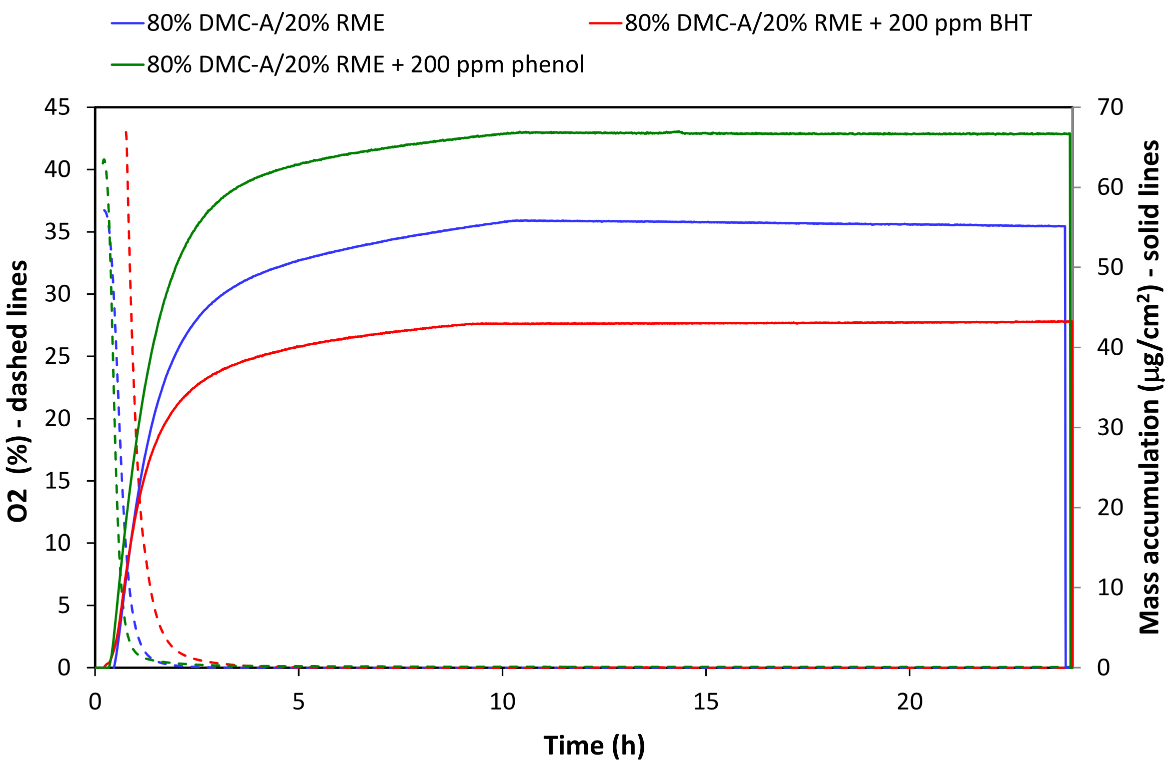

Figure 4.5: The effect of the phenolic compounds (phenol and BHT) on oxygen depletion and mass accumulation during the oxidation of diesel model compound/RME blends in a QCM at 140°C for 24h

Because BHT is a storage antioxidant, the effect of temperature on BHT activity was investigated. The experiment was performed under the same QCM conditions but at 100 °C instead of 140 °C. The results are presented in Figure 4.6.

At 100°C, oxygen consumption was significantly slower. Oxygen was fully consumed after more than 16h. Interestingly the mass accumulation after 24h was 200% more than what was observed at 140°C with no maximum having been reached. Furthermore the shape of the mass accumulation curve appeared to have changed. An S-shaped deposition profile was observed at the lower temperature. Such a profile was also observed in the neat model compound systems, for some systems studied by DeWiitt *et al.* (*11*) as well as those being investigated by Coetzee (*76*).

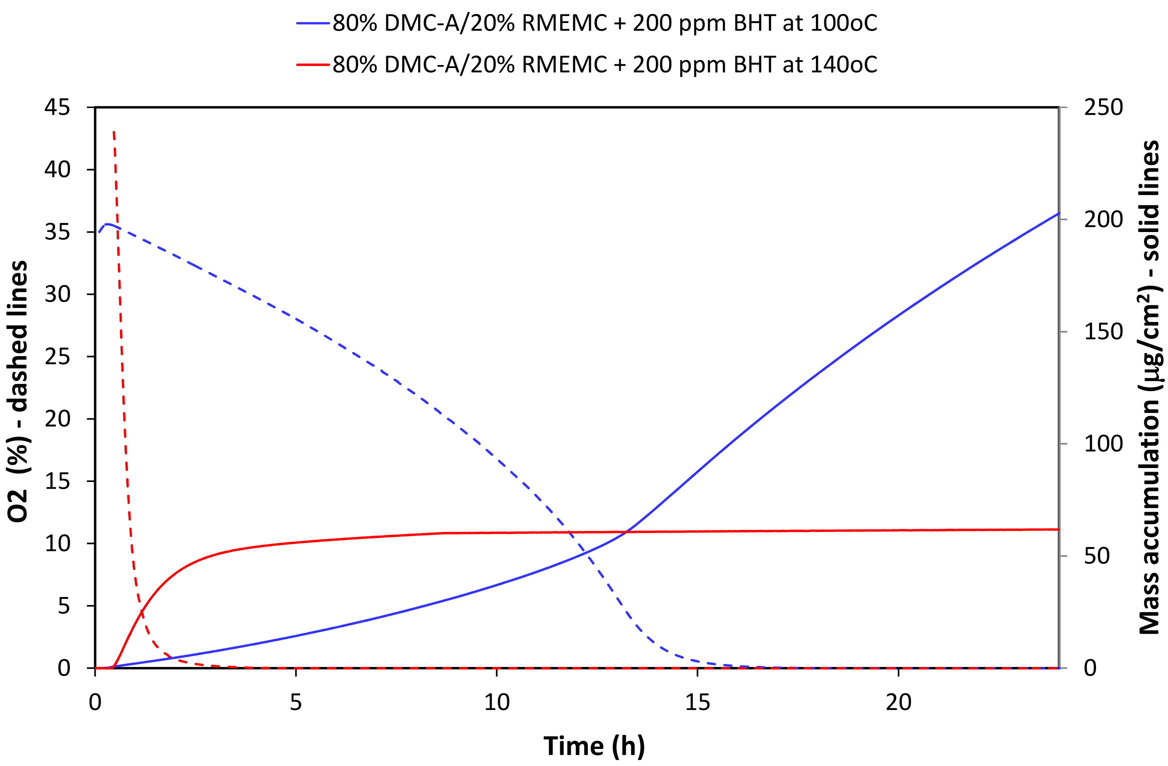

Figure 4.6: Comparison of the effect of BHT on oxygen depletion and mass accumulation during the oxidation of diesel model compound/FAME model compound blends in a QCM at 100°C and 140°C for 24h

4.4.1 Discussion

The antioxidant, BHT, reduces the quantity of deposits formed by donating hydrogen to the radical and hence terminates the reaction. Because the hydrogen in BHT is highly labile, the oxidation occurs more slowly at the *bis*-allylic or allylic carbon atoms along the FAME backbones until the antioxidant is fully consumed. Deposits then quickly form in the presence of oxygen at high temperature. This might be because BHT starts to decompose at temperatures around 120 °C offering the fuel less protection from high temperature (*127*).

In the fuel blend containing phenol, oxygen is fully consumed after an hour but deposition continues until it starts to level off after 4h. Kerkering *et al.* (*74*) have demonstrated very little, if any, antioxidant behaviour by phenol, unlike BHT.

Phenols are known to increase the formation of deposits in certain fuels (*20,22,30*). It is possible that phenol may react with tetralin oxygenates to form deposit precursors via a

SMORS mechanism (*22*). Coetzee, in an unpublished study, has demonstrated that the presence of a variety of phenols increases deposition during QCM oxidation studies in model compounds containing tetralin and other benzylic hydrogen-containing aromatic species (*76*). It should be noted that phenol, which was used here, is unsubstituted. Hence, no investigation of the steric affects in hindered phenols is explicitly addressed. BHT represents the extreme of a completely hindered phenol. A study of the detailed effect of steric hindrance in phenols was beyond the scope of this work

It is possible that these lower molecular species react with other molecules in the fuel matrix via electrophilic substitution to form higher molecular species known as SMORs and which precipitate out. An alternative possibility is that phenol interacts detrimentally with the FAME molecules to form cross-product species. Gas chromatographic and electrospray ionisation–mass spectrometric investigations were performed to investigate this possibility (see Chapter 6).

Under storage conditions, *i.e.* at lower temperatures, oxygen consumption was delayed in the presence of BHT. This might be indicative of effective radical termination by BHT. Once oxygen is fully consumed, the amount of deposits continued to increase. This is likely the result of oligomerisation reactions between FAME molecules to form higher molecular weight species. The shape of the mass accumulation curve in Figure 4.6 changed once the oxygen concentration became low with the slope increasing. This may indicate that at least two oxidation mechanisms are responsible for deposit formation at 100^{o}C. A similar increase in the slope of mass accumulation upon oxygen depletion has been observed by Coetzee (*76*).

It is unclear why the extent of deposition is greater at 100^{o}C than 140^{o}C but this may be due to the inhibition of a deposition mechanism at 140^{o}C that is important at 100^{o}C or increased deposit solubility at 140^{o}C. Further investigations of the effect of temperature were deemed beyond the scope of this study.

4.5 The impact of the addition of acids

Acids are common degradation products of FAME. 75% DMC-A/20% methyl linoleate/5% *n*-hexanoic acid blends were thermo-oxidatively stressed at 140 ^{o}C in a QCM reactor for 24 hours.

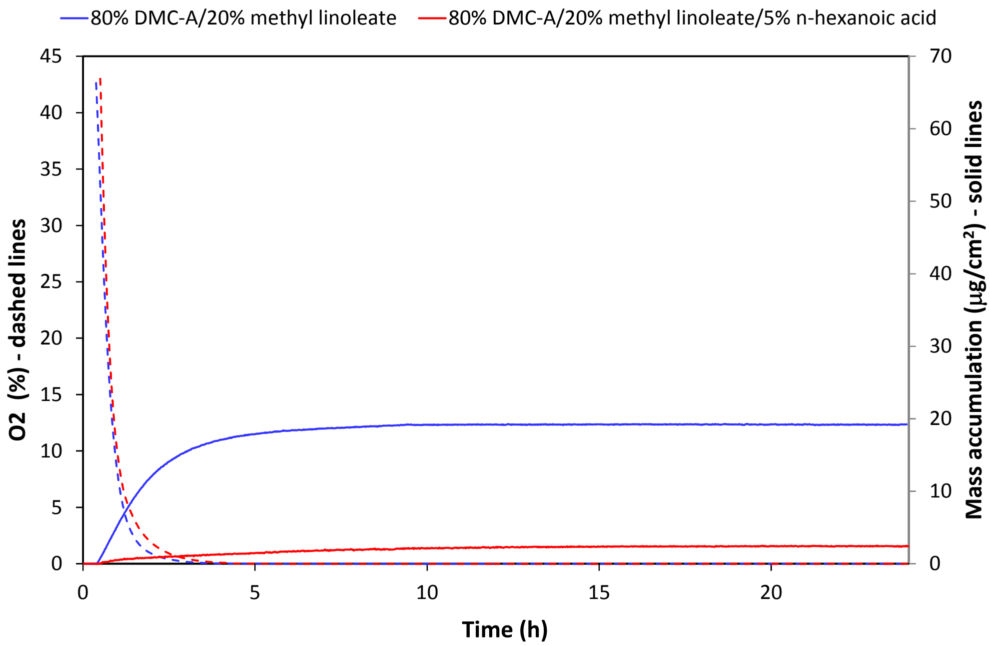

Figure 4.7: The effect of the addition of an acid on oxygen depletion and mass accumulation during the oxidation of diesel model compound/methyl linoleate blends in a QCM at 140^{o}C for 24h

Figure 4.7 shows tha the addition of *n*-hexanoic acid to the DMC-A/methyl linoleate blend significantly decreased the amount of deposits formed during QCM oxidation (by approximately 85%). Very little effect on the rate of oxygen uptake, however, was observed.

4.5.1 Discussion

Low molecular weight acids are often formed during the degradation of FAMEs (*23*). Acids are known to catalyse the hydrolysis of fatty acid methyl esters. However, as is apparent from Figure 4.7, the addition of acid significantly decreases the amount of material deposited. This indicates that degradation is not necessarily synonymous with deposit formation.

It is suggested that, although the acid may cause the formation of lower molecular weight compounds from FAMEs, it has an inhibitory effect on dimerisation reactions. The addition of large quantities of acid would lead to the esterification of hydroperoxides, formed during degradation, preventing dimerisation. It should be stressed that this experiment used high quantities of acid (5%). The impact of lower levels of acid is unclear. The high concentration of acid was chosen to reflect the situation where old, destabilised diesel is blended with neat petroleum diesel. This situation may occur in the field where biodiesel has been stored for some time.

4.6 The effect of solvency on deposit formation during oxidation in a QCM reactor

The effect of fuel solvency was investigated by stressing diesel model compound/biodiesel blends containing different amounts of biodiesel. 10, 20, 30 and 65 % RME were blended with DMC-A. The results are illustrated in Figure 4.8. With the exception of the 20% blend, only single experiments were performed. Figure 4.8 presents a representative for the 20% RME blend which was repeated in triplicate.

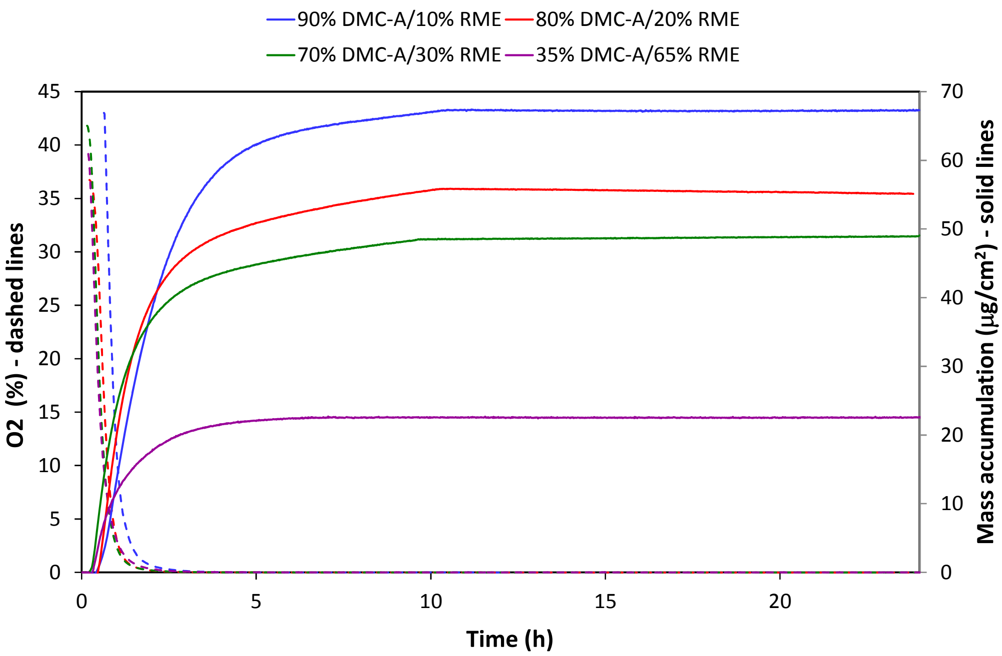

Figure 4.8: Oxygen depletion and mass accumulation for the oxidation of DMC-A/RME blends of varying blend ratios in a QCM at 140°C for 24h

Counterintuitively the mass accumulated increased as the concentration of the primary deposit-forming molecules, the FAMEs, decreased. In all cases the level of deposition was greater than any of the heavy depositing jet fuels, reported by Sobkowiak *et al.* (*20*).

4.6.1 Discussion

Although diesel model compound systems produce very low quantities of deposits, a significant increase in the quantity of deposits was observed once biodiesel was introduced. Figure 4.9 shows mass accumulation as a function of the percentage of RME in the blend. The blend with the lowest polarity (90% DMC-A/10% RME) produced the highest amount of deposits.

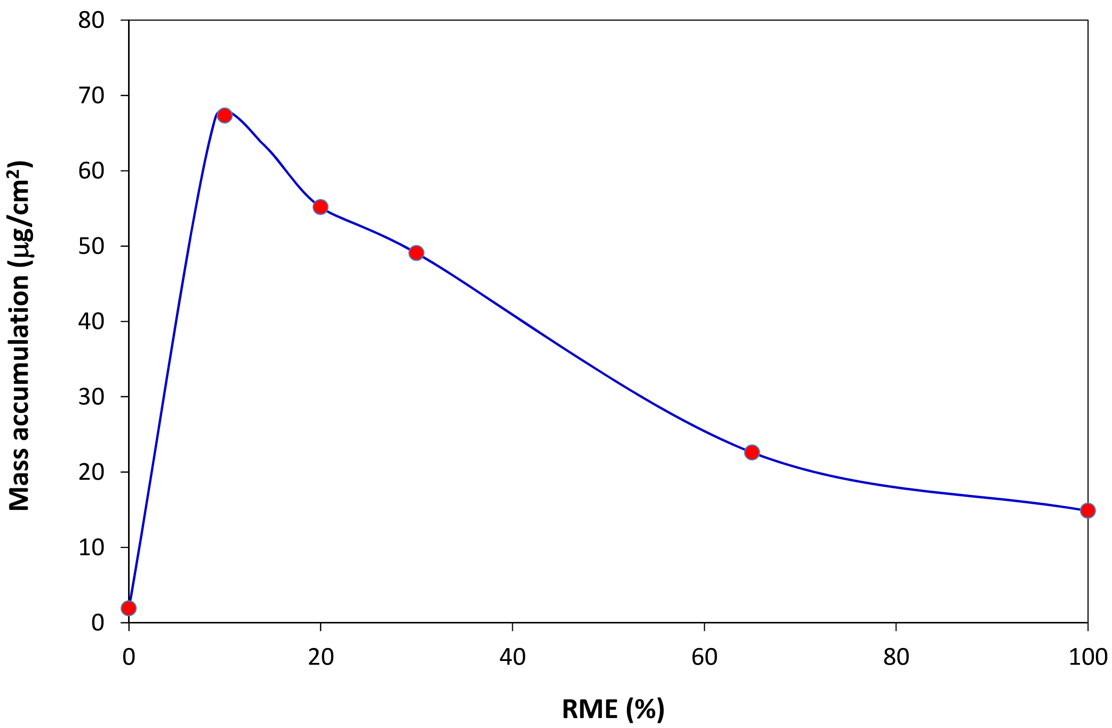

Figure 4.9: Effect of biodiesel content on mass accumulation for biodiesel/diesel model compounds blends

It is clear that the addition of a small quantity of RME to a diesel model compound system greatly increased the extent of deposit/sludge formation. The 10% biodiesel blend formed about 4.5 times more deposit/sludge than 100% biodiesel.

Deposits and deposit precursors are polar in nature and should be more soluble in polar biodiesel (*20*,*21*,*23*). Blending biodiesel with petroleum diesel reduces the polarity of the fuel and hence the fuel's capacity to dissolve the deposits. Since deposit formation/measurement in a fuel matrix depends, among other things, on the fuel's ability to dissolve the deposits and the amount of deposit precursors present, increasing the amount of biodiesel increases the fuel's capacity to dissolve the deposits, forming less insoluble deposits. Hence blends with low biodiesel content formed relatively high levels of deposits. The greater extent of deposit formation in low RME-containing blends suggests that the ability of the fuel to keep deposits in solution is more important than the potential amount of deposit precursor molecules, *i.e.* percentage RME.

Hughey *et al.* (*112*) suggested that the effect of solvency was important when blending FAMEs with petroleum diesel. It was observed that blend composition also had an impact on oxygen consumption, as illustrated in Figure 4.10.

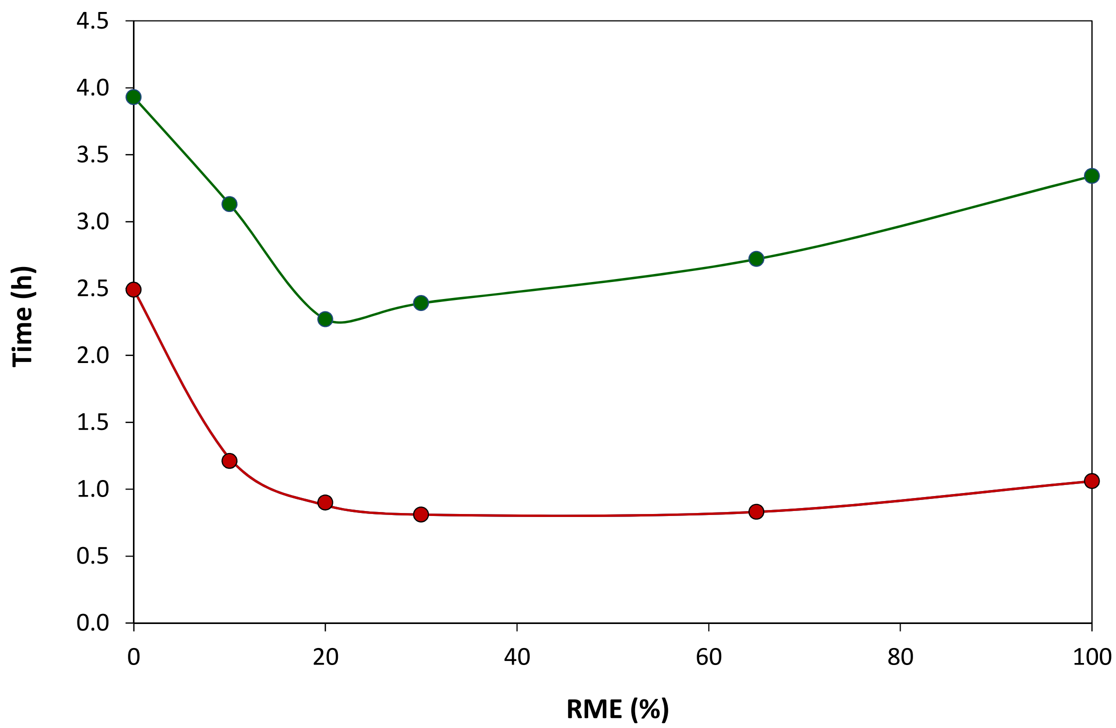

Figure 4.10: Effect of biodiesel content on oxygen consumption for biodiesel/diesel model compounds blends. Time taken to reach 5% O_2 (red curve); time taken to reach 0.1 % O_2 (green curve).

The addition of RME to DMC-A increased oxygen consumption at low levels of RME blending. This suggests that fuel polarity also influences the reactivity of FAMEs towards oxygen. The mechanism underlying this effect is unclear. Mitsuri *et al.* (*54*) observed an increase in sludge formation at a similar blend percentage.

A similar effect to that observed in this study was seen by Osawa *et al.* (*113*) who observed the time till deposition/phase separation, when biodiesel/petroleum diesel blends were stressed in flowing oxygen at 110^{o}C, was lowest in the range of 10-30% biodiesel. They, however, do not provide full details of their experimental method and their grammar is such that it is unclear whether they actually measured time till deposit formation or some other quantity such as time till acid formation by a Rancimat test (*36*).

4.7 Conclusions

The use of a quartz crystal microbalance to investigate the formation of deposits in biodiesel-containing systems has been performed rigorously for the first time. The ability to measure mass accumulation allows the QCM to be far more versatile than other instruments used to investigate biodiesel blend stability such as the Petroxy^{TM} (*35*) which only measures oxygen depletion.

Significantly more deposits/sludge were formed from RME-containing systems than from systems containing petroleum diesel model compounds alone. This can be ascribed to the presence of allylic and, in particular, *bis*-allylic carbons with highly labile hydrogen atoms attached. FAME model compound investigations clearly demonstrated the link between the number of double bonds in the FAME backbone and the extent of mass accumulation. Methyl linolenate, which has a high degree of unsaturation, had the worst thermo-oxidative stability of the C19 olefinic FAMEs tested.

The presence of the aromatic compound, tetralin, led to the formation of increased deposits in diesel model compound systems. It is possible that this followed the formation of deposit precursors such as 1-tetralone and 1,4-naphthoquinone, following a SMORS-like mechanism (*21*,*22*,*30*). This is explored further using compositional analysis in Chapter 6. It was unclear from the data obtained in this study whether decalin improves the stability of diesel fuel, as has been suggested elsewhere (*92*), by inhibiting radical reactions through hydrogen donor reactions. More in-depth investigation of the influence of different petroleum diesel model compounds was beyond the scope of this study but forms part of the on-going investigations of Coetzee (*76*).

Phenol increased mass accumulation when added to diesel model compound/biodiesel blends. This is consistent with the suggestion by Heneghan and Zabarnick (*71*) that phenols influence the rate of oxygen consumption and deposit formation. The exact mechanism for this is unclear but it is possible that phenol may react with tetralin oxygenates to form deposit precursors of increasing molecular mass via a SMORS mechanism (*21*,*22*,*30*).

BHT, on the other hand, reduced the amount of deposits to a small extent in the fuel during thermo-oxidative stressing. The mechanism by which deposits are formed appears to be different under accelerated storage oxidation conditions (100^{o}C) and thermo-oxidative conditions. These preliminary experiments show that a QCM might be useful in evaluating the performance of an antioxidant. This would go further than observing any effect on oxygen consumption but also on actual deposit formation.

The addition of large quantities of acid greatly reduced deposit formation. It is possible that the acid reacts with key intermediates (possibly alcohols), terminating the deposit formation process.

Investigations into the effect of solvency on biodiesel/diesel model system blends using a QCM reactor have never been performed prior to this study. Blending small quantities of biodiesel with diesel increased the amount of deposits that precipitated after the oxidation of the blend components. Oxidation products are likely polar in nature. The solubility of these polar components would be expected to be lower in non-polar hydrocarbons than polar biodiesel. As a result they separate and precipitate out, reducing the stability of the final blends.

5. Open flask oxidation

5.1 Spectroscopic investigations of oxidative stressing

5.1.1 Visual inspection of thermal oxidative degradation of diesel/biodiesel blends

Diesel and biodiesel model compounds were used to investigate the effect of composition on thermal-oxidative stability of the diesel/biodiesel blends. Oxidation was performed under flowing air at 140°C in open glass flasks. Unlike QCM experiments where oxygen in the headspace is reduced to zero during the course of the experiment, the continuous presence of oxygen is likely to lead to continuous oxidative attack of FAME molecules.

While one liquid phase was observed in the flasks at 140°C, phase separation occurred after the stressed fuels were cooled down to room temperature. No such phase separation was observed during QCM stressing. Figure 5.1 contains two examples, illustrating the formation of two layers after open flask oxidation of diesel/biodiesel blends. The lower layers were typically darker and more viscous than the upper layers.

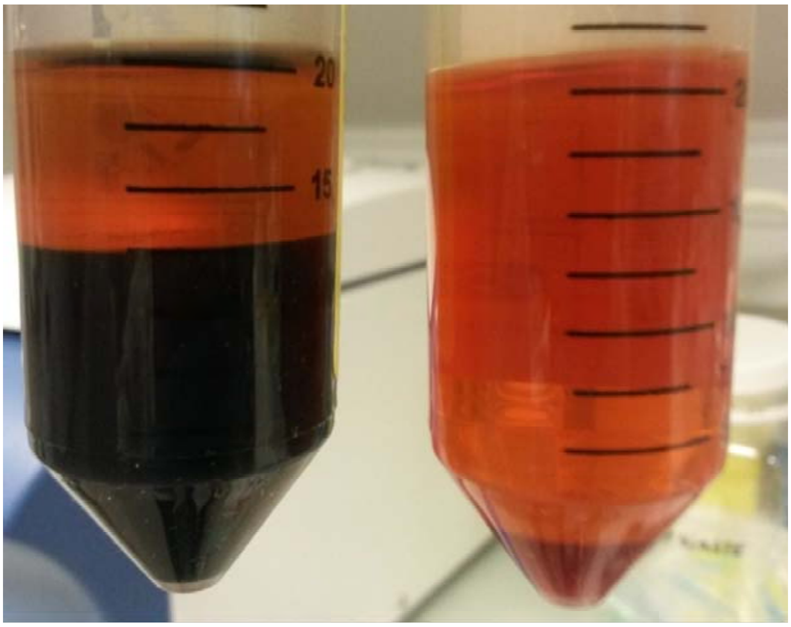

Figure 5.1: The separation of the two layers formed during flask oxidation of diesel/biodiesel blends after oxidative stressing at 140°C for 24h (Left: highly depositing fuel and right: low depositing fuel)

Different biodiesel model compounds were observed to form deposits with different colour intensities. Figure 5.2 shows the colours of the lower layers, formed after stressing blends of diesel model compounds with model biodiesel methyl esters of different degrees of unsaturation. The colour intensity of the deposits increased with increasing unsaturation of the biodiesel model compounds.

Figure 5.2: Lower layers separated after open flask oxidation (at 140^{o}C for 24h) of 80% DMC-A blends with 20% FAME model compounds. Methyl oleate (left), methyl linoleate (centre) and methyl linolenate (right.

After stressing neat RME, no phase separation was observed as was the case for the neat diesel model compound systems and the DMC/biodiesel blends.

Figure 5.3 illustrates the colour change of a diesel model compound system and RME, before and after stressing for 24h in open flask studies. In addition to the formation of separate layers, the colour of the fuel changed from colourless in the case of DMC-A to a deep orange (see Figure 5.3) and from light yellow for diesel/biodiesel blends to a deeper yellow in the case of neat RME. Blends, which contained diesel model compounds, also took on an orange colour on stressing.

Figure 5.3: Diesel model compound system (DMC-A) (A) and neat RME (B) before (left) and after (right) open flask oxidation (24h at 140^{o}C)

5.1.2 FTIR analysis

After open flask oxidation, the layers of the stressed fuel were separated by centrifugation. Each layer was analysed individually by FTIR. An example may be found in Figure 5.5.

It can be inferred from FTIR spectra that oxygen-containing species were formed during oxidative stressing in the open flask under flowing air.

Comparison of the spectrum for the fuel stressed in the QCM in Figure 5.4 and those for *n*-hexadecane and tetralin in the Appendix (Figure 10.7 and Figure 10.10), from NIST Standard Reference Database Number 69 (*128*), reveal very little difference.

Significant new features are, however, present in the spectrum for DMC-A stressed under flowing air. These include a broad absorbance band between 3100 and 3650 cm^{-1}. This band is ascribed to the formation hydroxyl (-OH) groups, likely 1-tetralol (see Section 6.2.1). There are also the formation of a number of bands between 1600 and 1750 cm^{-1} (at 1600, 1690 and 1720 cm^{-1}).

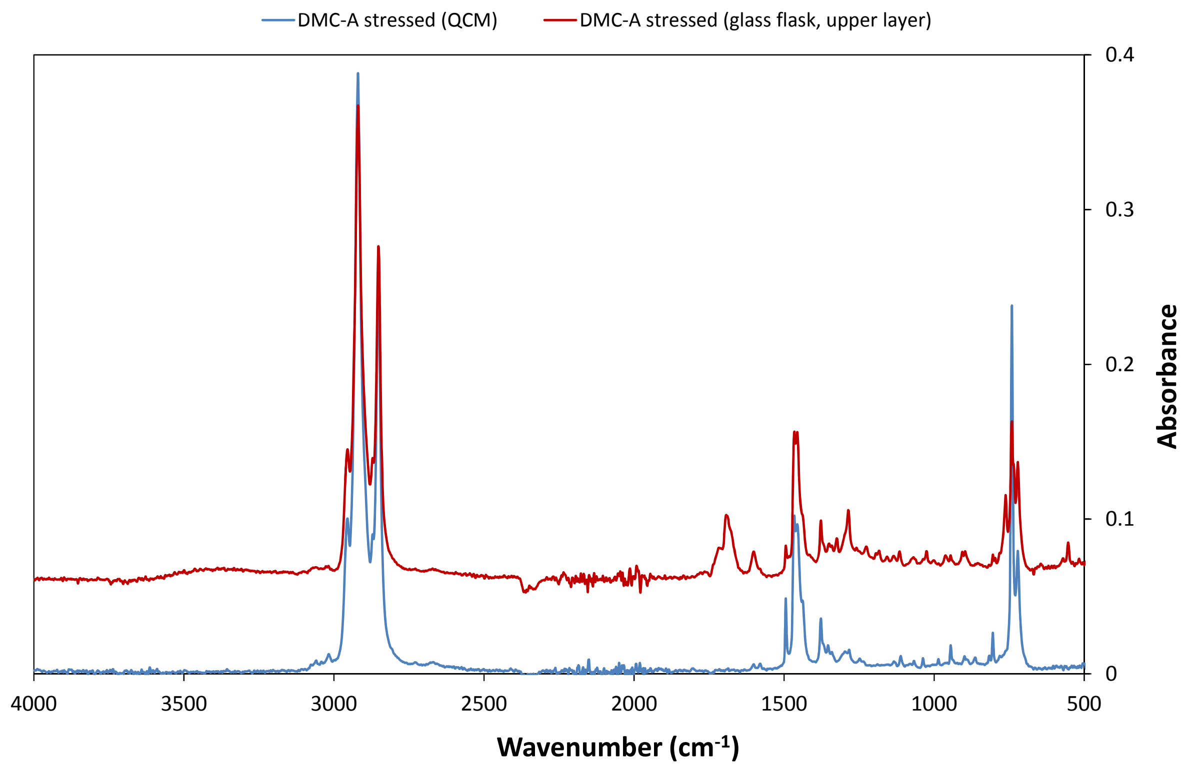

Figure 5.4: Comparison of the FTIR spectra of DMC-A after 24h oxidative stressing at 140^{o}C in a QCM and an open flask. Spectra are offset for clarit.

It is suggested that the band at 1720^{-1} is formed by hexadecanones (saturated ketones) while that at 1690 cm^{-1} is caused by ketones, derived from tetralin, such as 1-tetralone, 2,3-dihydronaphthalene-1,4-dione and 1,4-naphthoquinone (structures may be found later in Figure 6.29). The band is at a lower frequency than those of hexadecanone because of conjugation of the C=O with aromatic C=C bonds in the tetralin derivatives. The band at 1600 cm^{-1} is actually part of a doublet with the second band at 1580 cm^{-1}. These are due to one of the modes of aromatic C=C stretches. This may be clearly seen in the spectra from DCM-A, stressed in the QCM. The band at 1600 cm^{-1} swamps the 1580 cm^{-1} absorbance in the reference spectrum for 1-tetralone (see Figure 10.12). This is further evidence of the formation of tetralin oxidation products.

Figure 5.5 illustrates the effect that stressing has on the FTIR spectra of 80% DMC-A/20% RME blends. A comparison is that the blue and red curves have very little difference despite the formation of deposits in the QCM. The spectra for the neat components in RME may be found in Figure 10.16. This is because all of the model compounds contain similar functional groups which are not conjugated.

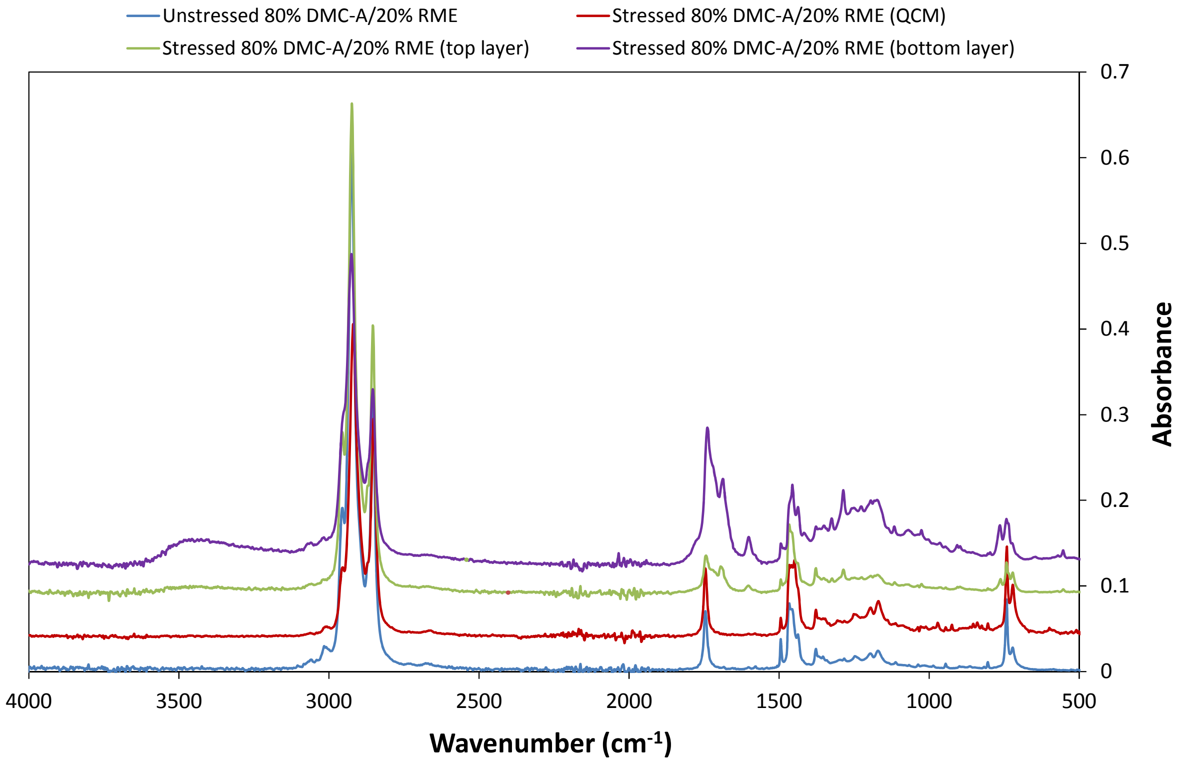

Figure 5.5: Comparison of the FTIR spectra of unstressed 80% DMC-A/20% RME blends, QCM-stressed and the two layers formed after 24h oxidative stressing of this blend at 140^{o}C in an open flask. Spectra are offset for clarity

The green curve in Figure 5.5 shows a pronounced absorption of infrared radiation in a broad band near between 3100 and 3650 cm^{-1}. This can be ascribed to the formation of hydroxyl (-OH) groups during oxidation. This would be present in alcohols and carboxylic acids. It can be seen that no such groups were present in the unstressed blend (blue curve). The extent of absorption in this region is smaller for fuel from the upper stressed layer (red curve). Part of this absorbance may also be due to water formed during the coupling of FAME molecules. The band at 1745 cm^{-1} in the unstressed fuel is due to the presence of C=O stretch of fatty acid ester molecules.

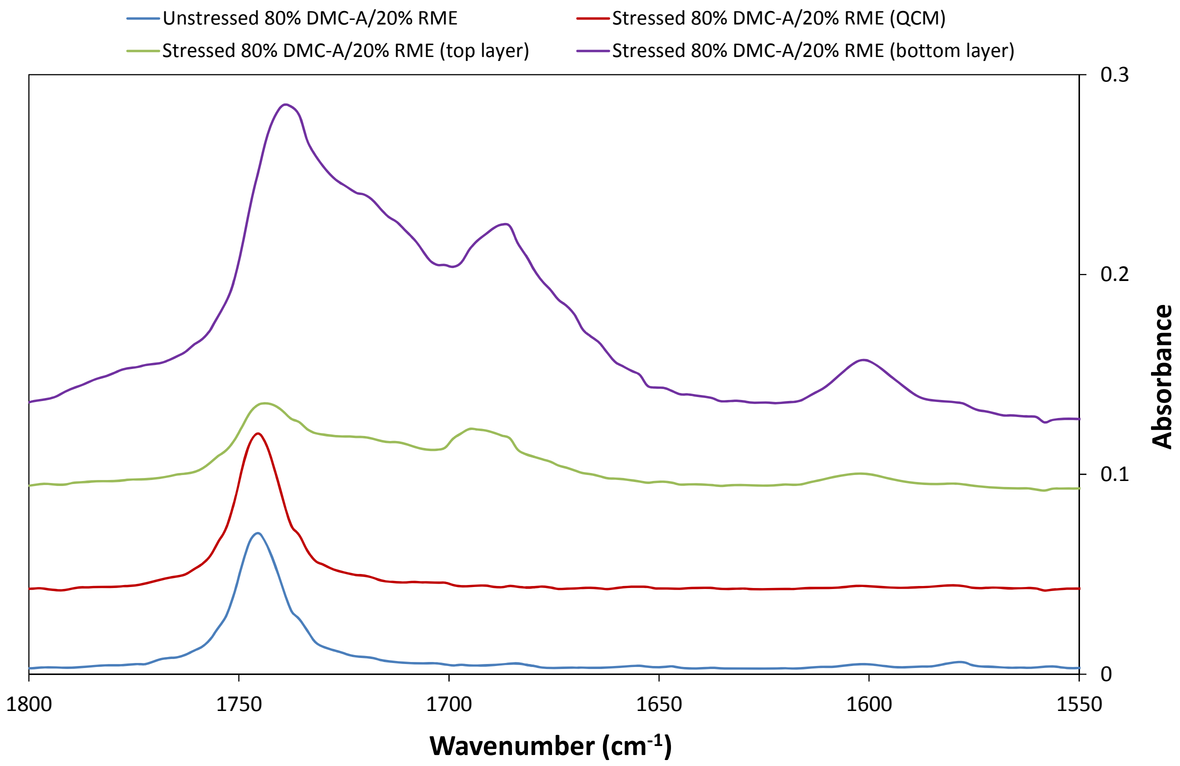

Figure 5.6: Magnification of the region 1800-1550 cm^{-1} of unstressed 80% DMC-A/20% RME blends, QCM-stressed and the two layers formed after 24h oxidative stressing of this blend at 140^{o}C in an open flask. Spectra are offset for clarity

The region 1550-1800cm^{-1} (Figure 5.6) contains absorbance bands due to carbonyl and double bond stretches. The methyl ester C=O stretch can be seen at 1745 cm^{-1} in the unstressed sample's spectrum. This close-up reveals that stressing in the QCM made very little change. However, extended stressing in flowing air caused significant changes. A band starts to appear at 1690 cm^{-1}. This is ascribed to the formation of tetralin ketones, and conjugated ketones and aldehydes. A shoulder starts to develop at 1720 cm^{-1}, ascribed by Muik et al. (*123*) to aldehyde C=O, and the peak at 1745 cm^{-1} shifts to 1740 cm^{-1} and grows in size when the lower layer is analysed. The shoulder at 1720 cm^{-1} is also in the upper layer. Using difference spectra, Ogawa *et al.* (*23*) also noted the formation of the band at 1720 cm^{-1} when FAME, derived from waste cooking oil, was heated in flowing air at 120^{o}C for 20-35h. The shoulder that forms near 1770 cm^{-1} is likely due to unsaturated carboxylic acids that form on decomposition. The band at 1601 cm^{-1} results from tetralin oxidation and possibly from double bonds conjugated with ketones/aldehydes from FAME decomposition.

A comparison of the FTIR absorbance of the two layers formed when stressed 80% blends of DMC-A with 20% FAME model compound can be found in Figure 5.7 and Figure 5.8.

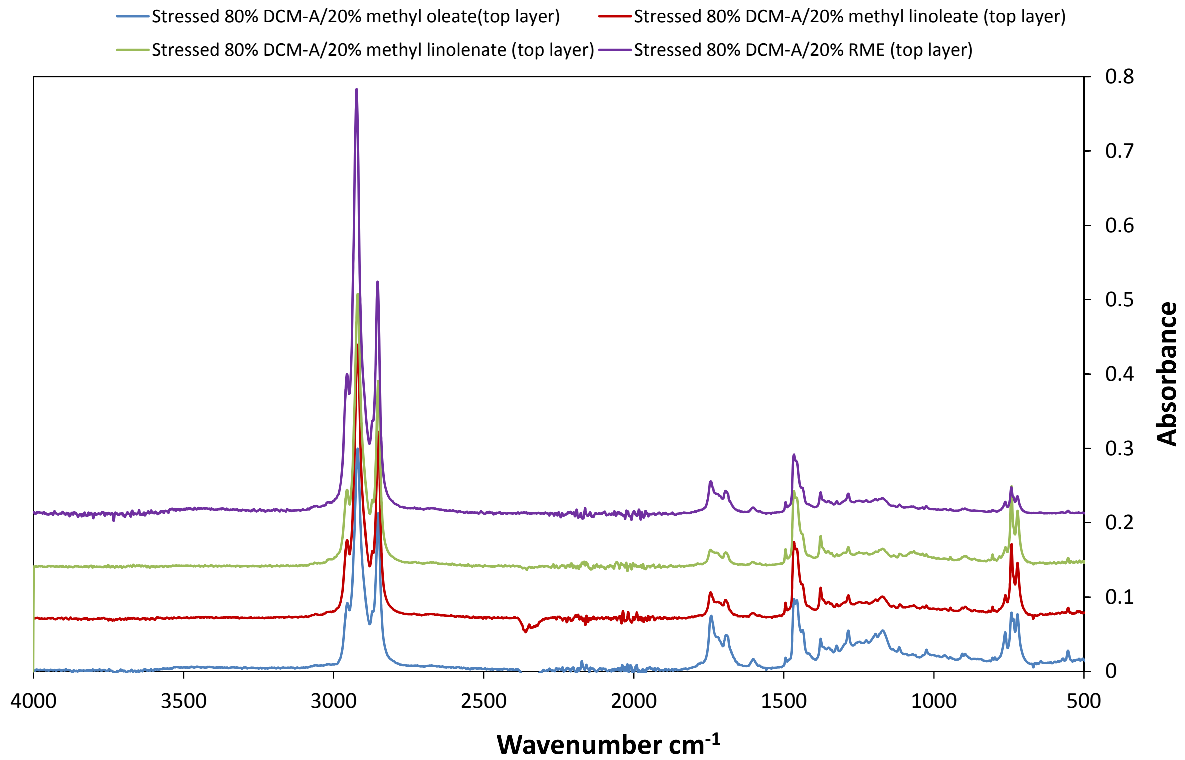

Figure 5.7: Comparison of the FTIR spectra of the upper layer, obtained by stressing 80% DMC-A/FAME model compound blends in an open flask at 140^{o}C for 24h

What can be seen is that the usual features, described for the top layer of RME, are for the most part present here. Interestingly the –OH stretch is absent in the case of the layers from blends containing methyl linoleate and methyl linolenate. Furthermore, although C=O stretches are present, they are less strong for the more unsaturated FAME, *i.e* methyl linolenate. In Figure 5.8, it can be seen that all samples have the –OH band but here the C=O stretch follows an opposite trend and becomes more significant as the degree of unsaturation increases.

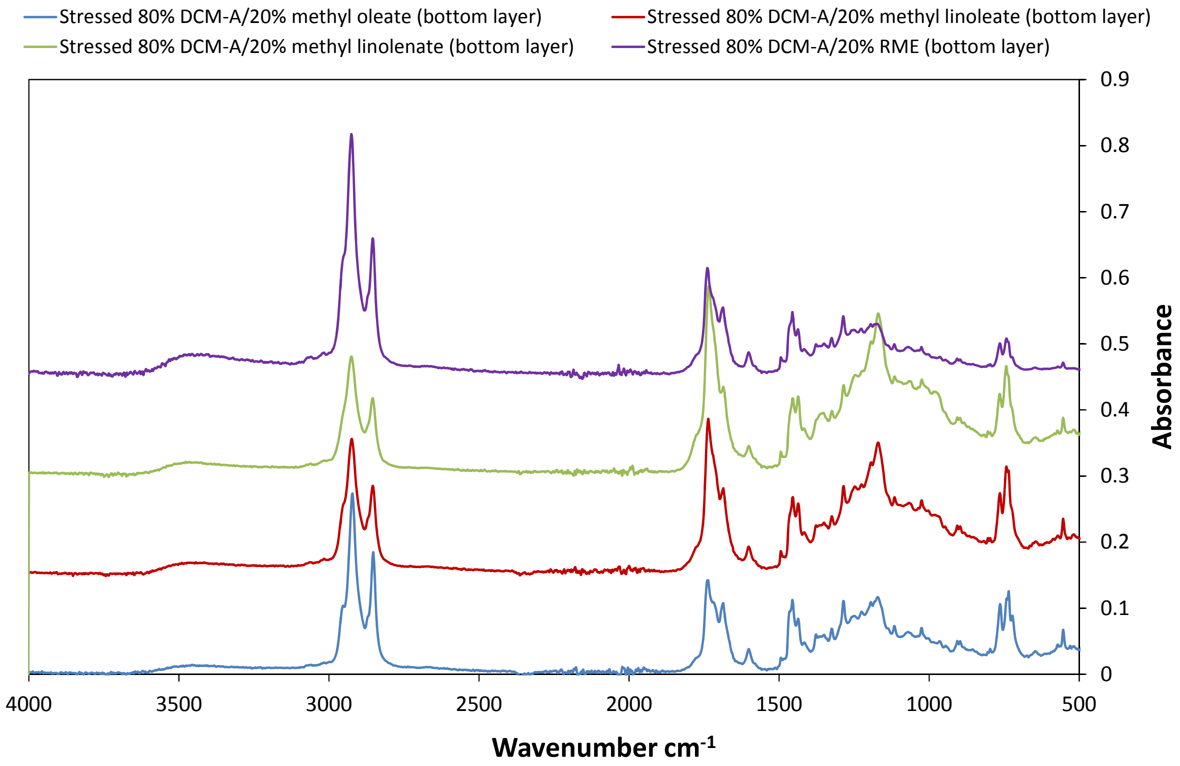

Figure 5.8: Comparison of the FTIR spectra of the lower layer, obtained by stressing 80% DMC-A/FAME model compound blends in an open flask at 140^{o}C for 24h

5.1.3 UV-Vis analysis

UV-Vis spectra were used to analyse the layers formed during flask oxidation. As was the case with FTIR spectra, no significant differences could be discerned between the unstressed fuels and those that had been stressed in the QCM for 24h.

The spectra in Figure 5.9 indicate that the absorption by the denser, lower layer is much greater than the absorption by the top layer. Similar spectra to those presented in Figure 5.9 were observed for blends of 80% DMC-A with 20% FAME model compounds. These are presented in the Appendix (Figure 10.24, Figure 10.25 and Figure 10.26). It can seen in Figure 5.9 that the highest peak intensity in the QCM spectrum (and the unstressed fuel) is greater than that observed in the upper layer of the fuel, stressed under flowing air in an open flask. The same effect was observed for DMC-A blends with methyl oleate and linoleate. It should, however, be noted that the area under the entire absorbance band is greater for the stressed upper layer than for the QCM-stressed fuel.

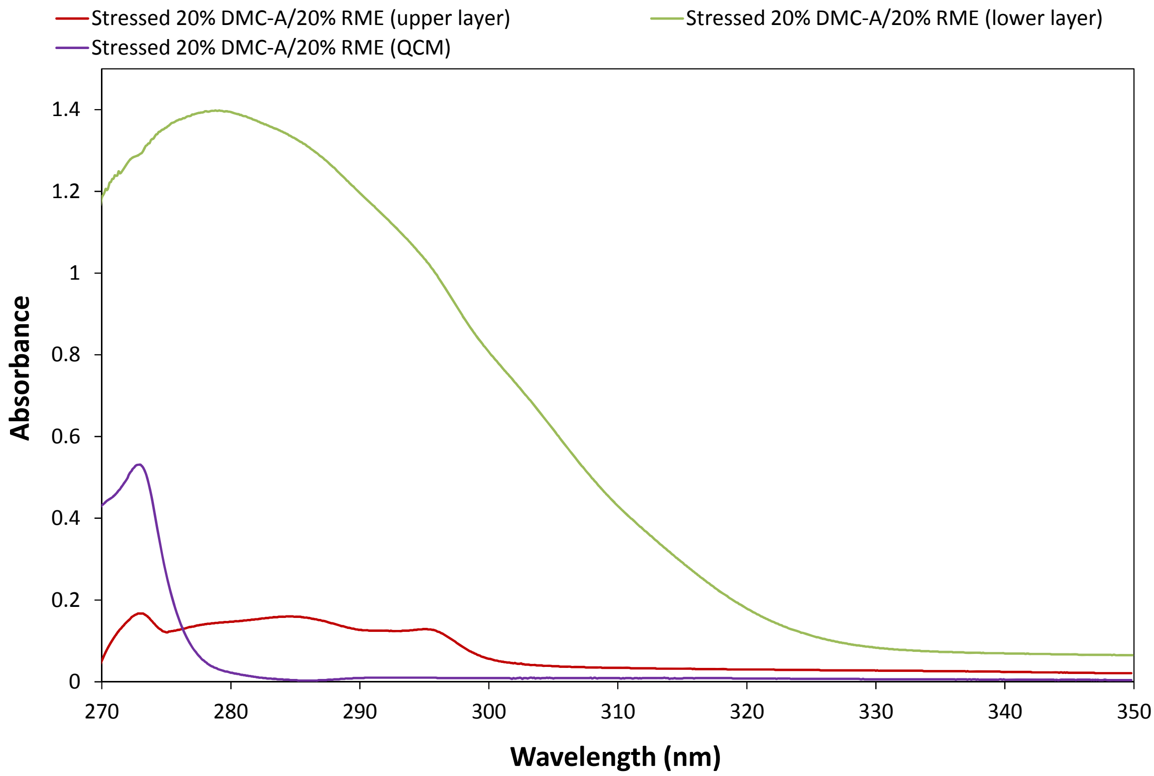

Figure 5.9: UV absorbance spectra of stressed 80% DMC-A/20% RME after oxidative stressing at 140°C for 24h in a QCM and in an open flask

The effect of the degree of unsaturation in the FAME backbone was investigated by analysing the stressed fuels, produced upon stressing blends of 80% DMC-A and 20% FAME model compounds. The absorption spectra for the upper layer of fuel stressed in an open flask are presented in Figure 5.10. It can be seen that absorption increases with increasing degree of unsaturation in order of: methyl linolenate (three double bonds) > methyl linoleate (two double bonds) > methyl oleate (one double bond). That of the RME blend is very similar in shape to a combination of the methyl oleate and methyl linoleate. This is not surprising given that these two compounds are the major components of RME (*126*). It can be seen that all spectra (except the unstressed fuel) consist of at least three bands. Similar behaviour is seen in stressed DMC-A. Stressed RME has only two primary bands with that centred on 296 nm absent (see Figure 5.13).

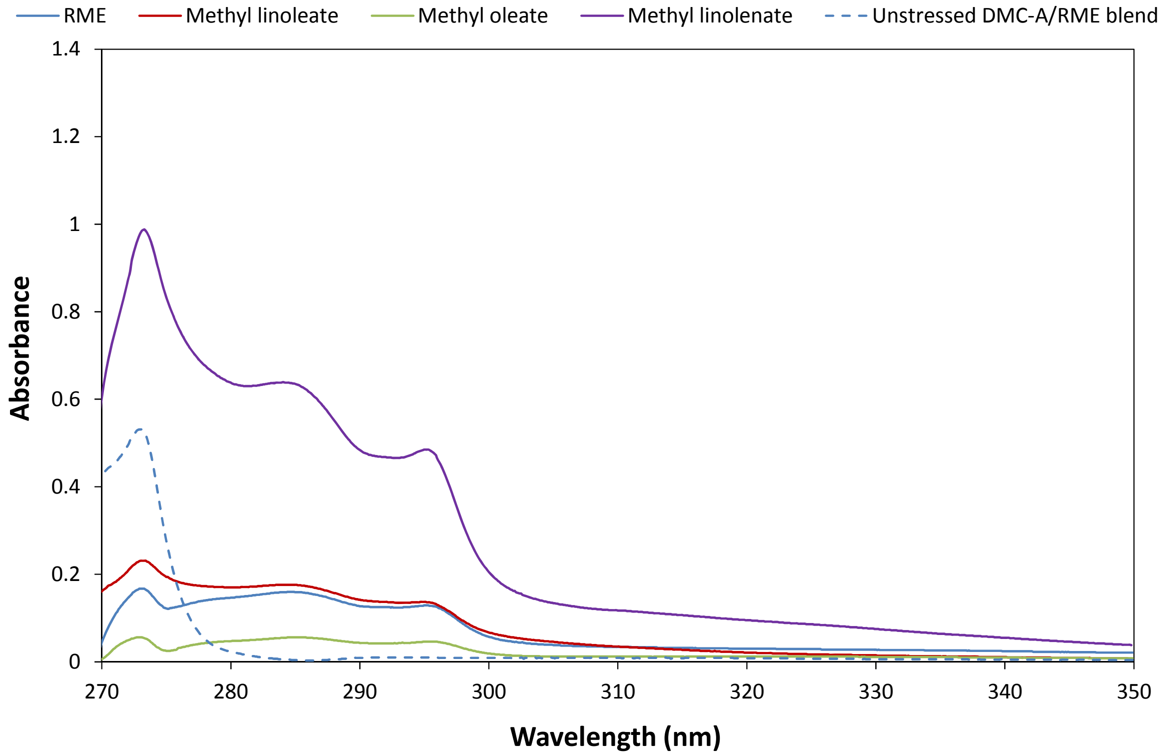

Figure 5.10: UV absorbance spectra of the upper layer for 80% DMC-A/20% blends with RME and compound blends after oxidative stressing at 140^oC for 24h in an open flask. The curve for 80% unstressed and 80% DMC-A/20% RME blend is provided for comparison

Similar trends can be seen for absorption by the lower layer of open flask-stressed fuel (see Figure 5.11). Increasing unsaturation leads to increasing absorption of UV radiation. The three absorbance bands in the upper layer (see Figure 5.10) are again present but there is an extra shoulder centred on 305 nm. It is unclear, however, why absorbance by the RME blend is greater than that of all FAME model compound blends.

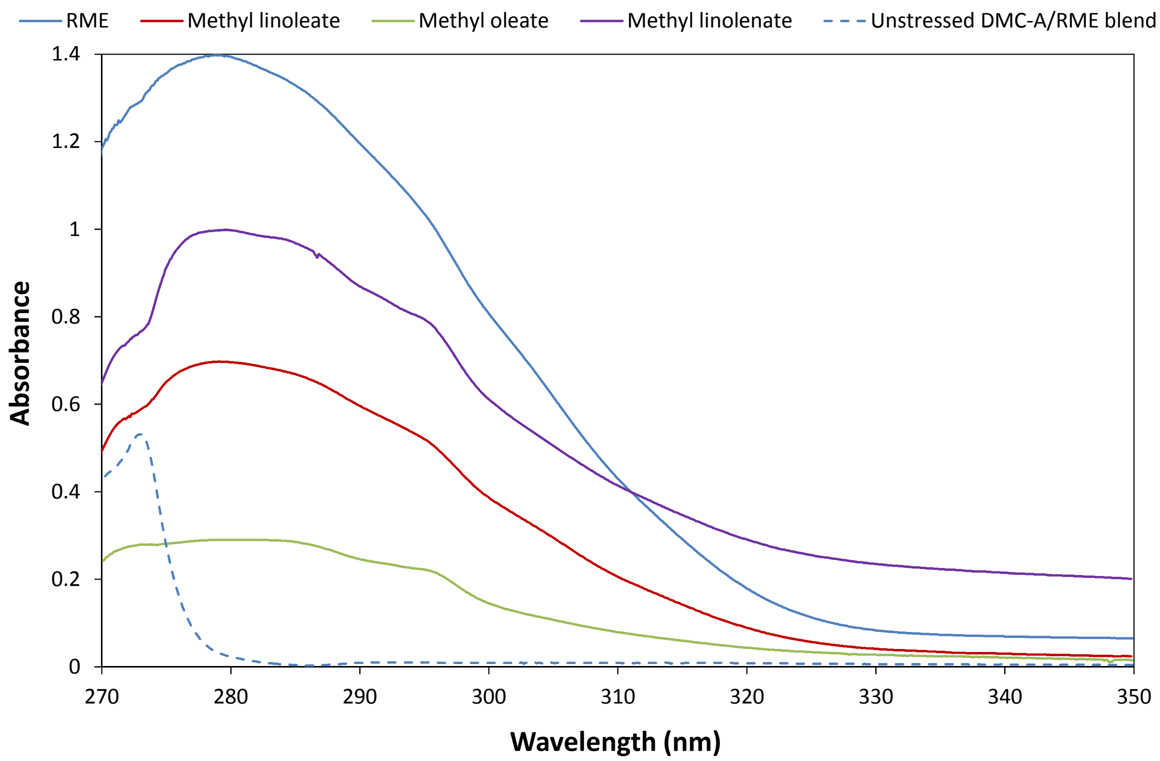

Figure 5.11: UV absorbance spectra of the lower layer for 80% DMC-A/20% blends with RME and compound blends after oxidative stressing at 140^{o}C for 24h in an open flask. The curve for and 80% unstressed 80% DMC-A/20% RME blend is provided for comparison

5.1.4 Discussion

After open flask stressing at 140^{o}C for 24h, phase separation was observed for all systems except neat RME. Unlike the case with QCM oxidation where no separation occurred, the formation of an insoluble layer can be ascribed to the greater extent of oxidation brought about by the continuous presence of oxygen during flask stressing. It is suggested that phase separation is the result of the formation of molecules of increased polarity, as a result of the incorporation of more oxygen-containing functional groups (see Figure 5.5) and molecular weight with extended oxidation. As molecular weight increases, solubility is known to decrease for statistical thermodynamic reasons (*129*). The higher molecular weight of molecules in the lower layers would also increase their viscosity. Only one phase was observed when RME was stressed because the polarity of RME is sufficiently high to keep the lower (sludge) layer in solution.

Oxidation leads to the formation of conjugation (*23*) which is suggested was responsible for the deepening of the yellow colour after thermo-oxidative stressing of RME. The formation of an orange colour by systems containing the DMC-A model compound is likely due to the formation of 1-tetralone and 1-tetralol which are yellow in colour and 1,4-naphthoquinone which is a dark orange/brown. These species were identified by GC in significant quantities (see Chapter 6). The lighter colour of the upper layers is indicative of the presence of fewer and less oxidised species than the lower layer.

The more vulnerable the FAME was to oxidation, *i.e.* the greater the degree of unsaturation, the more intense (darker) the colour was of the insoluble layer. Methyl linolenate which has three double bonds is able to form longer conjugated systems than other FAME isomers.

FTIR spectra indicate the presence of oxygen-containing species, over and above the original FAME esters. These are likely alcohols, esters, acids and ketones. These are the products common in literature (*13*,*18*,*33*). Kaminuza (*100*) observed the formation of these bands at 3500-3000, 1776, 1705 cm $^{-1}$ and suggested that the bands were characteristic of thermo-oxidative products. Spectra for the lower layers suggest that these contained species with greater amounts of oxygen. Absorption intensities for -OH and C=O stretches were much greater for the lower layer.

Table 5.1: Comparison of the ratio of the intensity of the carbonyl stretch (at maximum between 1735 and 1750 cm^{-1}) and stretch due to tetralin at 1466 cm^{-1}

Fuel blend	QCM	Flask (top layer)	Flask (bottom layer)
80% DMC-A/20% methyl oleate	0.33[1]	0.77	1.60
80% DMC-A/20% methyl linoleate	0.72	0.35	2.67
80% DMC-A/20% methyl linolenate	0.74	0.23	3.30
80% DMC-A/20% RME	0.95	0.28	2.14

1. Carbonyl stretch was anomalously weak in this spectrum. The value should be treated with caution.

Table 5.1 presents a comparison of the intensity of absorbance, as measured by the peak height, of the carbonyl stretch near 1745 cm^{-1} and the band at 1466 cm^{-1}. The band at 1466 cm^{-1} is due to tetralin and appears fairly impervious to oxidation. A similar analysis could have been performed by normalising the carbonyl stretch against the primary CH stretch.

However, because oxidation introduces conjugation and more -CH_3 end groups this is a poorer reference to use.

Two opposite trends can be seen: the ratio of carbonyl stretch in the top layer decreases as unsaturation increases while the ratio increases in the lower layer. This suggests that highly oxygenated species (those with significant carbonyl stretches) such as ketones and carboxylic acids move into the lower layer while fewer remain in the top layer. As more oxygenates are concentrated in the lower layer, less of these species remains in the upper layer hence the trend is reversed. Methyl linolenate which has three double bonds is the most reactive of the FAME model compounds. RME which contains all three lies in between. Further evidence for the concentration effect is that the ratio for the bottom layer is greater than the ratio for the QCM experiments while the ratio for the top layer is lower. The spectra for the fuel, after QCM stressing, is very similar to that of the unstressed fuel. In the case of methyl oleate the ratio in the top layer is very similar to the unstressed fuel. It should be noted that an alternative explanation is that tetralin is avoiding the lower layer and the real explanation may be a combination of the two effects.

As is shown in Section 6.3.2 oxidation of methyl linolenate and methyl linoleate-containing blends leads to the formation of large quantities of ketones and carboxylic acids. By contrast, isomerisation (double bond migration to form conjugated systems) is not available to methyl oleate and these ketones are not formed. The primary oxygenated species (other than esters) that was seen in stressed methyl oleate-containing fuels were epoxides. Because this is a blend, some ketones and quinones do form from tetralin.

It is suggested that as the lower layer forms, highly polar ketones and carboxylic acids separate from the less polar blend. These form the lower layer into which macromolecular oxygenates dissolve. By contrast less of the lower layer (see Section 5.2) is formed by stressing methyl oleate-containing fuels because far fewer ketones and acids are formed. The high polarity of the lower layer in the cases of methyl linolenate and methyl linoleate explains why the lower layer for these compounds contain an –OH stretch absorbance band but methyl oleate does not. By contrast the –OH stretch can be seen in the upper layer of the stressed methyl oleate-containing blend but not for the polyunsaturated FAMEs. RME, which contains all three types of FAMEs, has an –OH absorbance in both layers.

The oxygenated species are also likely responsible for increased UV absorption with the extent of absorption being a function of the degree of oxidation. A noticeable bathochromic shift with the formation of new bands can be seen. Greater oxidation of the species present explains the greater absorption of the lower layers and an increase in absorption with increasing unsaturation. Methyl linolenate and methyl linoleate are capable of double bond migration which gives rise to these conjugated species.

5.2 Layer separation by centrifugation

After 24h of open flask oxidation, the fuel was placed in 50 mℓ centrifuge tubes and centrifuged. The lower layer was separated from the rest of the stressed fuel and weighed. Duplicate stressing experiments were performed. The average masses of the lower layers, measured in duplicate experiments, are presented in Table 5.2.

Table 5.2: Amount of insoluble (lower) layer formed after 24h of thermo-oxidative stressing (140^{o}C, open flasks) of various diesel and biodiesel model compounds and their blends

Fuel system	Mass of lower layer(g)		
	No phenols (g)	**+BHT (g)**	**+phenol (g)**
DMC A (60 mℓ)	4.65	3.10	3.41
DMC B (60 mℓ)	5.86	5.23	
DMC C (60 mℓ)	2.61	1.35	1.79
RME (60 mℓ)	n/a	n/a	
80% DMC A/20% RME (60 mℓ)	5.84	5.14	5.43
80% DMC C/20% RME (60 mℓ)	3.94	2.57	2.81
80% DMC A/20% MO (30 mℓ)	3.52[5]		
80% DMC A/20% ML (30 mℓ)	13.25[5]		
80% DMC A/20% MLN (30 mℓ)	13.94[5]		
80% DMC A/20% RMEMC (30 mℓ)	12.72[5]	12.19[5]	

1. MO = methyl oleate, ML = methyl linolenate and MLN = methyl linolenate
2. RMEMC refers to a 7:3:1 (v/v) blend of methyl oleate:methyl linoleate:methyl linolenate
3. n/a – only 1 phase formed
4. Missing values – experiments not performed

5. Smaller volumes were used in these experiments because of limited quantities of FAME model compounds available. The reports 2.4 times the measured masses for these since approximately 21 mℓ, rather than 51 mℓ remained after stressing in these experiments

Different model compounds formed different amounts of the dense layer, depending on the composition. DMC-C and DMC-B both contain decalin, *n*-hexadecane and tetralin. DMC-A and DMC-B which contained twice as much tetralin as DMC-C formed more of the lower layer. When the diesel model compound system, which contained the least tetralin, was blended with RME, the quantity of the denser layer was reduced.

RME on its own does not form a separate layer. Blending with diesel model compounds, however, leads to the formation of a separate layer in the fuel matrix. The amount of the lower layer formed in diesel/biodiesel model compound blends was slightly higher than the amount formed in diesel model systems on its own although not to the same extent as seen with QCM experiments.

Methyl oleate formed the lowest amount of the dense layer during flask oxidation. Methyl linoleate, unexpectedly, formed very similar amounts of the lower layer.

Doping both phenolic compounds decreased the quantity of the lower layer in both neat diesel model compound systems and blends with RME. The greatest reduction was seen when BHT was added. These trends were seen with both neat diesel model compound systems and blends with RME. When DMC-A was stressed, the quantity of the insoluble layer formed was reduced by approximately 35 % upon addition of BHT. A reduction of 12 % was seen when BHT was added to 80% DMC-A/20% RME. Similar results were observed when DMC-C was stressed. The reduction in insoluble layer formation was approximately 50% for the neat system and 35% for the blend with RME.

5.2.1 Discussion

Phase separation occurs when a) components of the fuel reach too high a molecular mass to remain in solution and/or b) become too polar to remain in solution.

Tetralin oxidises easily in the presence of oxygen, at lower temperatures than decalin and *n*-hexadecane (*93*). The extent of oxidative products increases as the amount of tetralin present increases. Consequently, model compound systems containing higher quantities of tetralin could be expected to show enhanced formation of phase separation. These results are consistent with the observation made during QCM stressing (see Figure 4.1).

Biodiesel is a good solvent and will dissolve polar species in the fuel matrix. The polar products that form during flask oxidation have high affinity for biodiesel. Therefore, no separate layers were observed when neat RME was stressed. Adding diesel model compounds to biodiesel causes phase separation, likely due to reduced solvency (see section 5.3). Interestingly the quantity of the lower layer was not significantly greater than the neat diesel model compound systems. This is in contrast to QCM results (see Figure 4.2). It should be noted that the extent of oxidation is significantly greater in the open flask experiments than the QCM experiments. The unlimited supply of oxygen in open flask experiments likely causes significant hydrocarbon oxidation and the formation of more high molecular weight species which is not the case with QCM experiments. The fact that the amount of the dense layer formed from DMC/RME blends depends on the DMC composition suggests that tetralin oxygenates also contribute to high molecular weight species under these conditions. The increase in viscosity is similar to that when cooking oil (fatty acid triglyceride esters) is heated above 160^{o}C in open air (*85*).

Model systems containing FAME model compounds with *bis*-allylic carbon atoms (methyl linoleate and methyl linolenate) formed quantities of the denser layer (up to 25% of the total original fuel). These compounds have a higher likelihood of oligomerisation because of the presence of such carbon atoms. It is unclear why the phase separation was so much greater for the systems containing a blend of FAME model compounds than those containing RME.

Phenolic compounds decreased the extent of phase separation during open flask oxidation. GC analysis revealed that there was no BHT present after 24h of stressing. The lower level of phase separation may be the result of less oxidation or less oligomerisation leading to higher molecular masses. While the effect of adding BHT was consistent with QCM experiments (compare the data in Table 5.2 with Figure 4.5), the effect of phenol was in contrast.

5.3 The effect of solvency and solubility on phase separation

The effect of solvency was seen to be important during QCM stressing. As a result, an investigation was conducted in order to understand whether deposit formation increases as a result of reduced solvency of fuels of different composition (varying polarity).

5.3.1 Effect of degree of oxidation on phase separation

Solvency effects were investigated by blending fresh diesel model compounds with RME which had been stressed in an open flask for 19, 24 and 48h at 140^{o}C. No phase separation occurred in the polar biodiesel after 48h of stressing despite extensive oxidation but a colour change was observed. 20% (% v/v) of stressed biodiesel was then mixed with 80% unstressed diesel model compounds (DMC-A). This is illustrated in Figure 5.12.

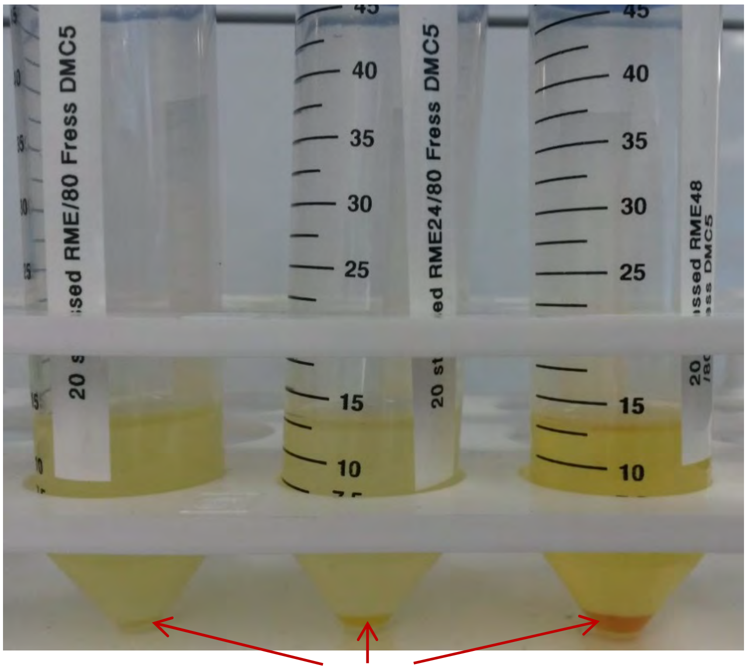

Figure 5.12: Phase separation in fresh DMC-A blended with RME, stressed for 19 (left), 24 (centre) and 48 h (right)

Rapid phase (< 5 min) separation was observed after blending stressed rapeseed biodiesel with fresh diesel model compounds. The extent of phase separation increased with the extent of stressing of the RME.

UV-Vis analysis

UV-Vis spectroscopy was used to analyse what effect the stressing time had on the stressed RME, obtained from the aforementioned experiments.

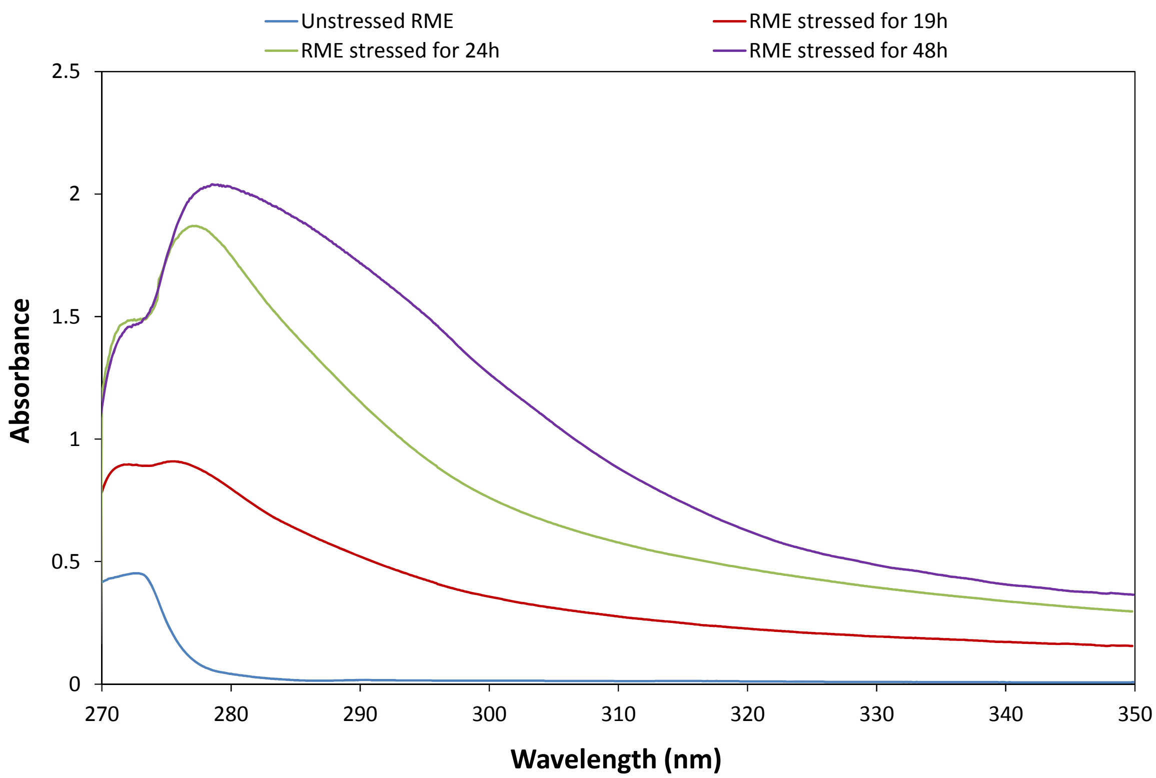

Figure 5.13: UV absorbance spectra of RME, stressed for 19, 24 and 48h at 140^{o}C in an open flask

Figure 5.13 shows that the rapeseed biodiesel, stressed for 48h, had the highest absorbance.

5.3.2 Influence of aromatic content on phase separation

n-Hexadecane/tetralin blends were used to investigate the influence of aromatic compounds on the solubility of deposit precursors in diesel model compounds. An 80% DMC-A/20% RME blend was stressed for 24h at 140^{o}C in an open flask. The lower layer, formed during stressing, was then added to unstressed blends of *n*-hexadecane and tetralin. Figure 5.14 shows the influence of the concentration of tetralin on the solubility of deposit precursors in diesel model compounds.

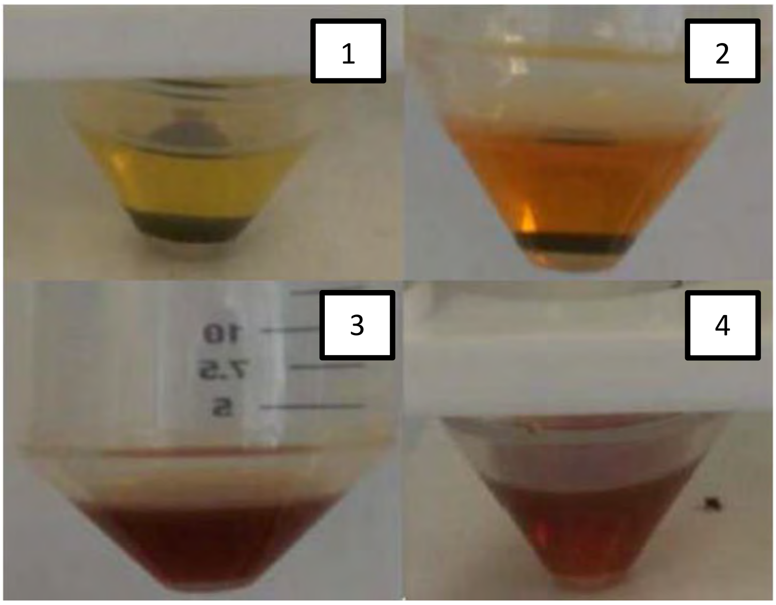

Figure 5.14: Effect of aromatic content on the solubility in diesel model compounds [1-0% tetralin, 2-20% tetralin, 3-80% tetralin and 4-100% tetralin]

The highly stressed fuel was completely soluble in 100% tetralin and insoluble at 0% tetralin. Solubility of the stressed fuel was observed to increase with increasing tetralin concentration in the blend. The colour of the unstressed (upper) fuel layer darkened until no phase separation could be observed.

UV-Vis analysis of the top layer of the phase-separated blends in Figure 5.14 was performed. It was observed that UV absorbance in the range 270-320 nm decreased as the aromatic content decreased. The highest absorbance was observed for non-phase-separated blends.

5.3.3 Effect of the ternary blend composition on phase separation

Ternary blends of biodiesel (RME), a paraffin (*n*-hexadecane) and an aromatic compound (tetralin) were used for these investigations. 20% of the lower layer, derived from the stressing of an 80% DMC-A/20% RME blend at 140^{o}C for 24h in an open flask, were added to 80% of different unstressed ternary blends. Figure 5.15 illustrates the solubilisation of the stressed layer in different ternary blends.

1 2 3 4 5 6

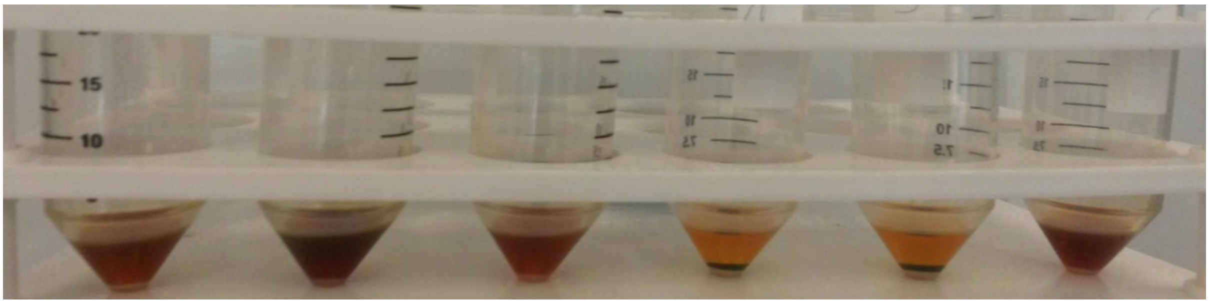

Figure 5.15: Effects of biodiesel/diesel ternary model compound blend composition upon stressed fuel solubilisation [1 (100% biodiesel), 2 (10% n-hexadecane/30% tetralin/60% RME), 3 (20% n-hexadecane/60% tetralin/20% RME), 4 (80% n-hexadecane/20% tetralin/0% RME), 5 (80% n-hexadecane/10% tetralin/10% RME) and 6 (20 % n-hexadecane/80% tetralin/0% RME)]

Stressed fuel that was insoluble in stressed biodiesel/diesel model compounds blends was observed to completely dissolve in ternary blends with high tetralin or high RME or combined RME and aromatic content. A dark orange colour was observed in other ternary blends where the stressed fuel completely dissolved. Samples 4 and 5 in Figure 5.15 formed separate layers within 5 minutes, however.

5.3.4 Discussion

The amount of oxidised RME molecules increased as the stressing period increased as indicated by the UV absorbance increase. The solubility of these stressed fuels in a model diesel/biodiesel blend decreased as the extent of stressing increased. This is ascribed to the increased polar nature and/or molecular weight of the stressed fuel components that phase separate. This has the implication that where oxidised (aged) biodiesel is added to unstressed fuel, phase separation and the formation of sludge which could clog fuel filters might be expected. This is consistent with the observations made by Osawa *et al*. (*113*) who observed the separation of stressed biodiesel when mixed with fresh *n*-hexadecane. These authors suggested that the sludge precipitated due to reduced polarity of the fuel.

Tetralin (a model aromatic compound) in the fuel blend improved the ability of unstressed fuel to dissolve highly oxidised fuel. It is suggested that the electron-rich π system of an aromatic molecule interacts more strongly with oxygenated stressed fuel components than *n*-hexadecane. Consequently, all deposit precursors were fully dissolved in 100% tetralin. This was not the case when adding the stressed fuel to *n*-hexadecane since it does not contain any electron-rich π system. This is consistent with the results of Mitsuri *et al.* (*54*) who observed that increasing aromatic content in petroleum diesel decreased sludge formation in blends with biodiesel.

Highly stressed fuel/sludge has been demonstrated to absorb in the UV range (see Section 5.1.3). As the amount of deposits/deposit precursors increase in unstressed fuel, the UV-Vis absorbance increases and the colour darkens. It is suggested that this indicates the solubilisation of greater quantities of deposit precursors and precursors that are more polar. The presence of RME in ternary blends was observed to solubilise stressed fuel. This is consistent with RME-containing fuels dislodging/solubilising tank sludges/deposits (*53*).

5.4 Conclusion

Biodiesel/diesel model compound blends do not only form sludge during thermo-oxidative stressing but also form soluble deposit precursors. Unlike QCM experiments, phase separation was observed occurred after open flask stressing. This is ascribed to the greater extent of oxidation in the flask experiments where oxygen is not limited, leading to greater quantities of more oxygenated and high molecular weight fuel species.

The colour change, observed during stressing, is mostly likely the result of the formation conjugated compounds and, in the case of systems containing tetralin, the formation of 1,4-naphthoquinone.

The quantity of tetralin in the original fuel determined the extent of phase separation as a result of high molecular weight tetralin-containing oxygenates being formed. However, the presence of tetralin in unstressed fuel was observed to increase the solubility of stressed fuel components, derived from diesel model components and biodiesel. This is likely the result of interactions between the electron-rich π system of tetralin and polar components of stressed fuel.

FAMEs with high degree of unsaturation were observed to oxidise to a greater extent than mono-unsaturated FAMEs, as evidenced by FTIR and UV spectra. This leads to greater phase separation. This is consistent with the lower stability of soybean methyl ester (SME) compared to rapeseed methyl ester (RME) observed by other authors (*100*). The former has a higher concentration of polyunsaturated FAME molecules (*126*).

BHT reduced the amount of phase separation seen which is ascribed to a reduction in the extent of formation of oxidation products in the fuel matrix.

Phase separation was demonstrated to be a function of fuel composition when stressed fuels were mixed with unstressed fuels. Increasing the oxidation of the stressed fuel reduced solubility (more phase separation was observed) while increasing the polarity of the unstressed fuel (either by the inclusion of RME or more aromatic species) increased the solubility of stressed fuel components. Phase separation might be expected in storage tanks when stressed fuel is added to fuels of lower polarity, *i.e.* those that are more paraffinic. The observations made here are consistent with the loosening of deposits by biodiesel (*53*). It would be expected that similar effects may be seen with fuels with higher aromatic contents.

6. Compositional analysis of stressed diesel/biodiesel blends

6.1 QCM thermal oxidation

QCM samples were analysed on completion of 24h of thermo-oxidative stressing.

6.1.1 Diesel model compounds

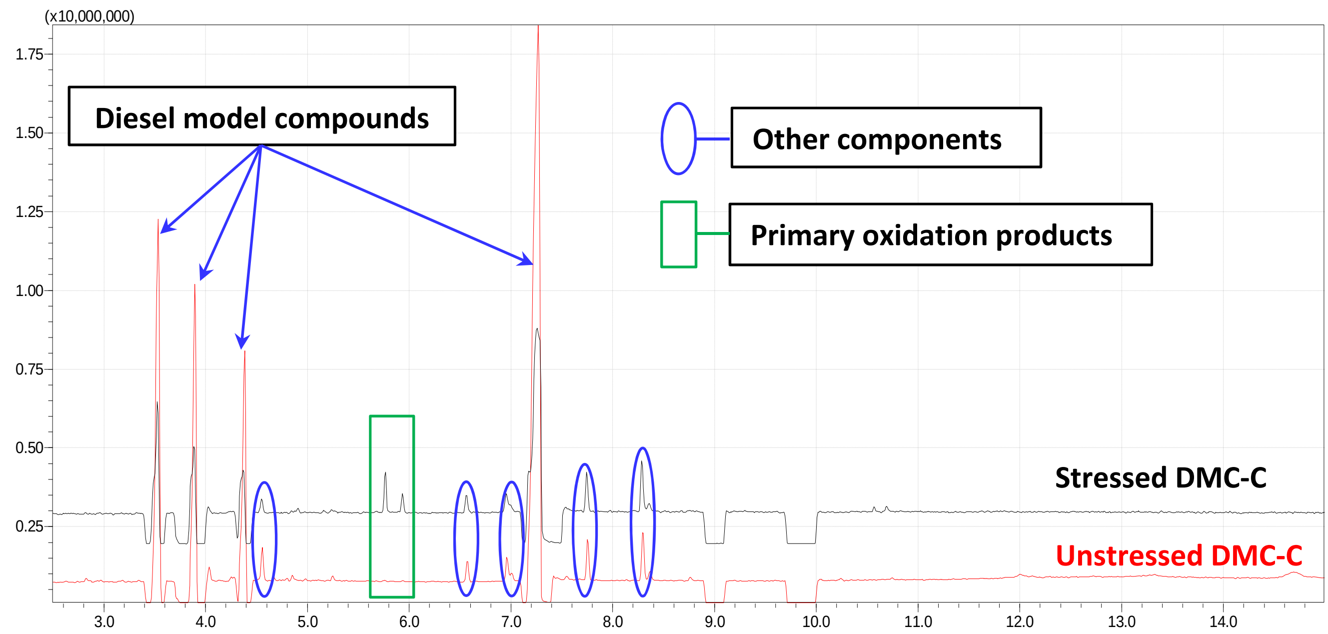

Figure 6.1: GC chromatograms of unstressed and stressed diesel model system (DMC-C), after QCM oxidation at 140^{o}C for 24h

Although DMC-C was made up of 3 solvents, 4 peaks were observed because the decalin used was a mixture of isomers. *Trans*-decalin eluted after 3.53 min, *cis*-decalin at 3.88 min, tetralin at 4.37 min and *n*-hexadecane after 7.26 min. The GC-MS chromatogram of unstressed diesel model systems indicated that model systems contain small quantities of other components (highlighted in blue). These were identified as a contaminant of tetralin, naphthalene, at 6.56 min and paraffins *n*-tetradecane (C14, 6.56 min), *2*-methyl tridecane (C14, 6.96 min), *n*-octadecane (C18, 7.74 min) and *n*-isocane (C20, 8.32 min). The *n*-alkanes were present at low levels in the *n*-hexadecane. The negative steps in the chromatograms are where the detector voltage was reduced to prevent detector saturation. This was performed at the elution times when the model compounds, which were present in high concentrations, eluted.

Differences can be observed between stressed and unstressed diesel model systems. The primary oxidation products, identified as 1-tetralol (5.77 min) and 1-tetralone (5.94 min) (highlighted in green in Figure 6.1), were observed when all diesel model systems were stressed. The amount of these tetralin oxygenates increased with higher concentrations of tetralin in the original model systems.

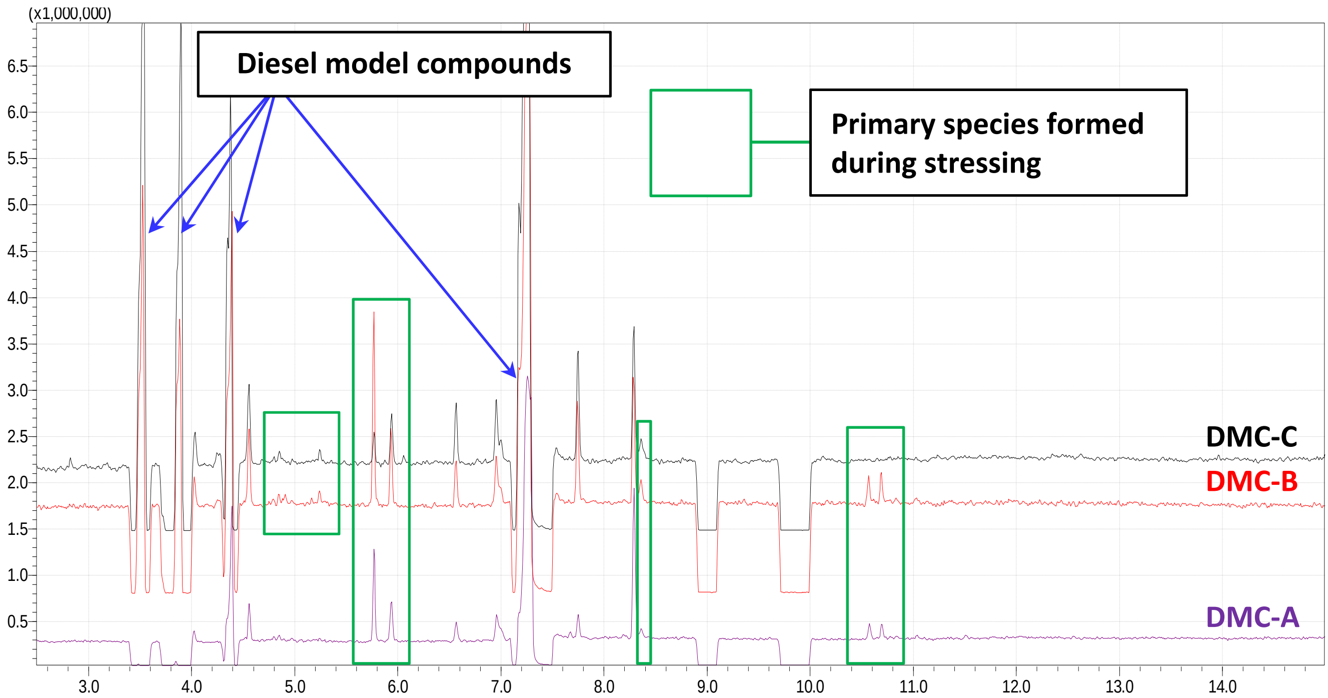

Figure 6.2: GC-MS chromatograms of diesel model systems after QCM oxidation at 140^{o}C for 24h

Additional hydrocarbons and cross-products (products that formed as a result of the reactions between degradation products) were also formed. Naphthalene was detected in all model systems after 24h at levels in excess of its initial concentration. An oxidised species of *n*-hexadecane, 2-hexadecanol, eluted after 8.36 min. Additional hydrocarbons (both normal and 1-methyl) were observed. The highlighted species, eluting after 10 min, were alkyl tetralins, 1-ethyl-tetralin (10.58 min) and 1-propyl-tetralin (10.70 min). Small quantities of a variety of decalin alcohols were observed to elute between 4.7 and 5.6 min in systems that contained decalin (DMC-B and DMC-C) (see *Figure 6.2*). Further information may be found in Table 10.3, Table 10.4 and Table 10.5 in the Appendix.

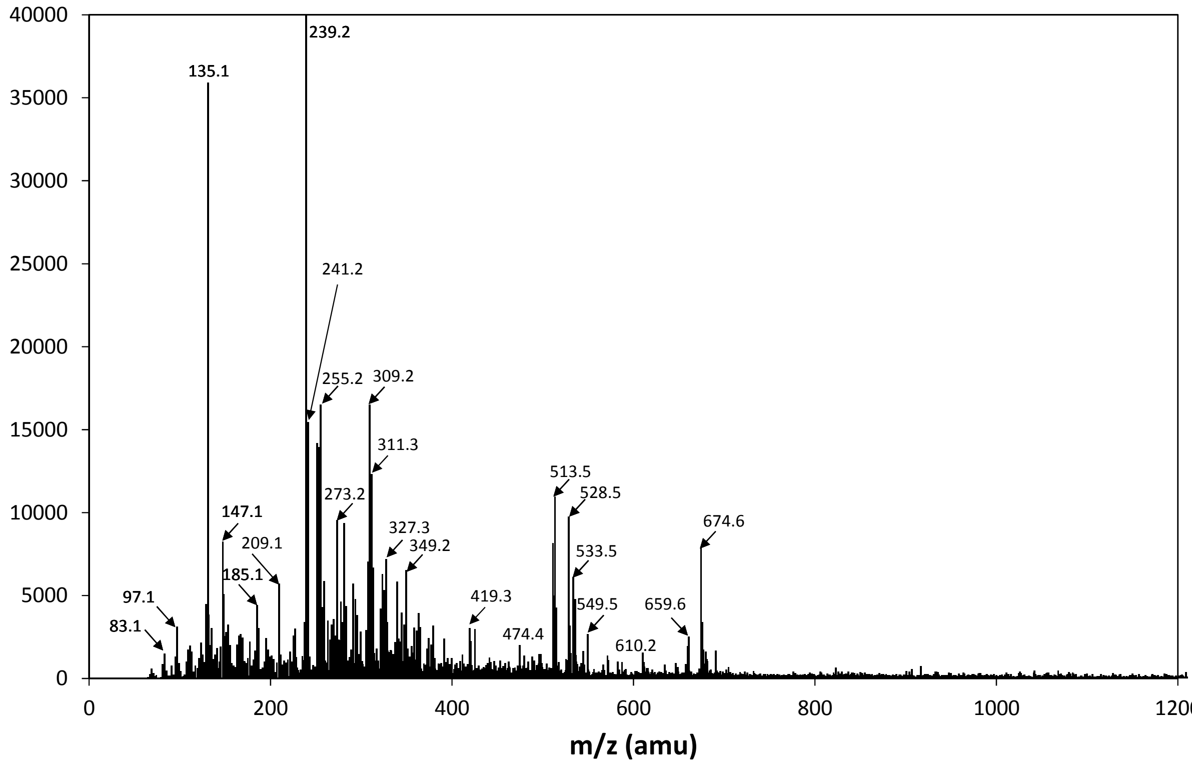

Figure 6.3: ESI-MS(+) spectrum for DMC-A after oxidation at 140°C in a QCM for 24h (0-1200 amu)

Figure 6.3 presents the positive ESI spectrum for the DMC-A model compound system which had been stressed in the QCM. The mass numbers, reported in the figure, are for the $[M+H]^+$ ions. Some key ions with tentative assignments are 131 (tetralol), 147 (tetralone), 239 (hexadecenone/hexadecenal) and 241 (hexadecanone/hexadecenol). The peak at 255 might be heptadecanal/one. The acid hexedecenoic acid is not likely as ESI-MS(+) is not suited to species that are easily negatively charged.

What can also be seen are a number of higher molecular weight species centred on 309, 513 and 674. Figure 10.27 and Figure 10.28 in the Appendix present the data in more detailed form. Figure 10.29 contains the negative ESI-MS spectrum for stressed DMC-A.

The ESI-MS(+) for DMC-B, which contained decalin, was very similar but had an important additional peak at 153, ascribed to decalone (see Figure 10.30 in the Appendix).

6.1.2 RME

Figure 6.4 contains chromatograms of the unstressed RME used for DMC/blends and a fresh sample, obtained towards the end of this study. The latter RME was not used for oxidation experiments because of its late arrival. The compositions of the old and fresh biodiesel are slightly different. The older biodiesel, which was used, contained low molecular species, consistent with partial oxidation of this fuel during storage. The common antioxidant, BHT (6.64 min), could not be observed in the older RME used although it was present in the newer RME. Peaks highlighted were identified as oxidation products. These were short chain olefinic aldehydes such as 2,4-E,E-nonadienal (5.20 min), 2,4-E,E-decadienal (5.48 min) and the aldehydic ester, methyl 9-oxononoate (6.24 min). These species were present in much lower concentrations in the newer sample.

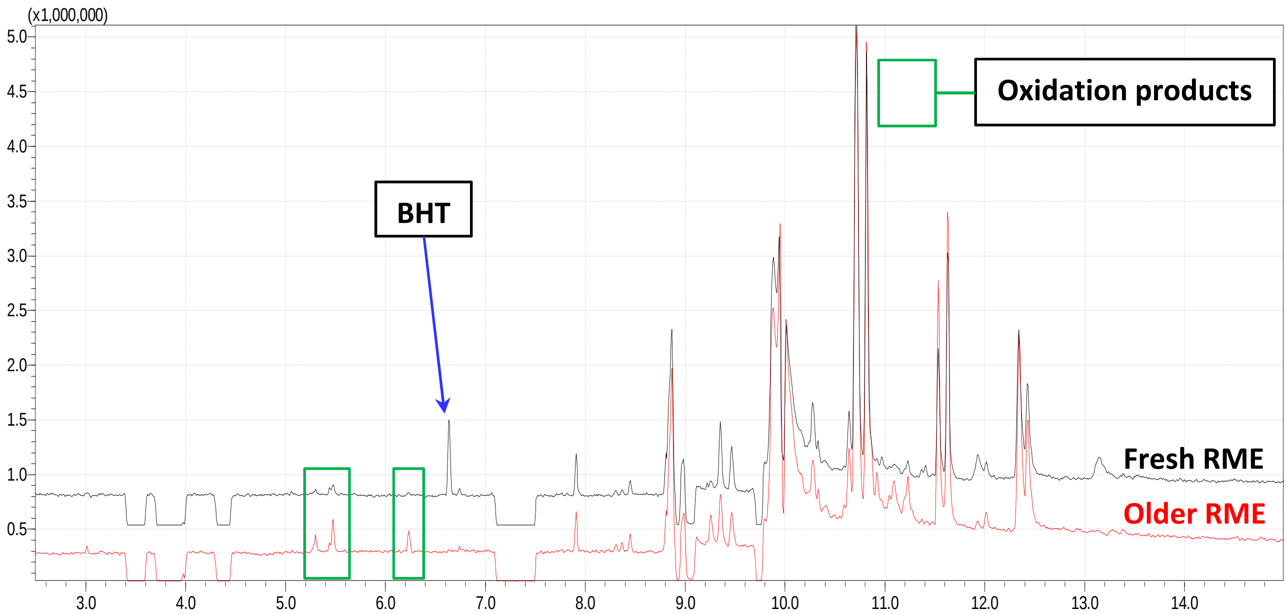

Figure 6.4: GC-MS chromatograms of RME, used in this study, and fresh RME, containing BHT, indicating the presence of oxidised species in aged biodiesel

Oxidation of RME led to an increase in the concentration of the species mentioned above as well as the formation of aldehydes such as *cis*-5-dodecenal (8.31 min) and *cis*-9-octadecenal (9.95 min), an alcohol of methyl oleate (methyl ricinoleate (10.69 min)) and the epoxide of methyl oleate, methyl *cis*-3-pentyloxiraneundecanoate (10.72 min). Further details may be found in Table 10.6 in the Appendix.

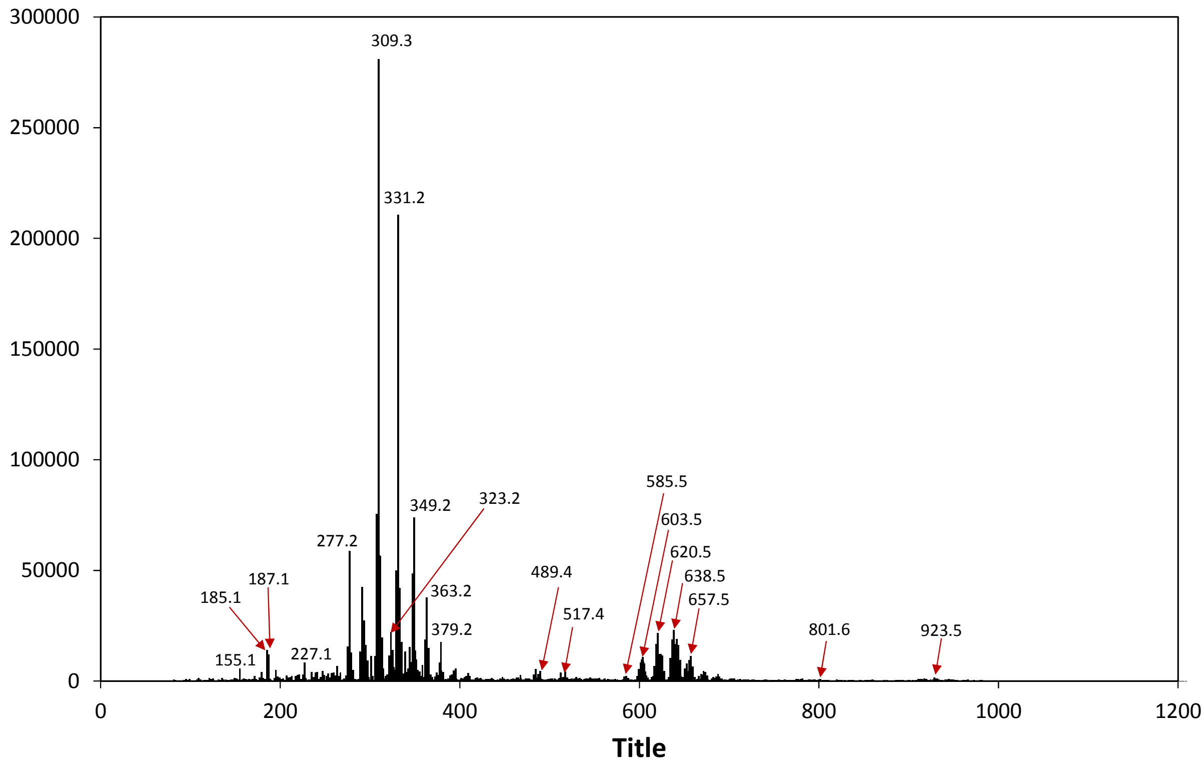

Figure 6.5: ESI-MS(+) spectrum for RME after oxidation at 140°C in a QCM for 24h (0-1200 amu)

Oxidation of RME leads to the formation of species in the range 600-680. These are likely oxo-ethers of the esters in the original biodiesel. Each set of peaks above 600 represents the inclusion of one additional ketone/or alcohol species. A small set of products could be observed in the ESI-MS around 900-950. These are consistent with ethers in which three ethers are combined. The species in the region 300-380 are oxidised forms of the original esters. It is unclear what gives rise to the species between 490 and 517 but these may be longer chain esters formed from alcohol decomposition products of FAME. The ESI-MS(+) spectrum is similar to that obtained by Ogawa *et al*. (*23*) if one accounts for the fact that they represent $[M+Na]^+$ adducts. They did observe more species with m/z > 800 amu but this was because they pre-concentrated their samples by GPC first.

The ESI-MS(-) revealed that oxidised fatty acids were formed as well as the fatty acids of the original esters, the largest of which is oleic acid ($[M-H]^-$ = 281). Refer to Figure 10.31 through Figure 10.34 in the Appendix.

6.1.3 RME/diesel model compound blends

Blending diesel model systems with biodiesel further deteriorated thermo-oxidative stability of the final blends. Increased quantities of 1-tetralol and 1-tetralone were formed compared to the neat diesel model compound systems. More products are revealed in Figure 6.6. The products formed are a combination of compounds formed by diesel model compounds and biodiesel or FAMEs. No obvious products resulting from the reaction of tetralin derivatives and FAME decomposition products could be identified.

The use of model compounds simplifies the analysis of the chromatography. Rapeseed biodiesels contain even higher esters, saturated and single unsaturated, which are not present in FAME model compounds as illustrated in Figure 6.6.

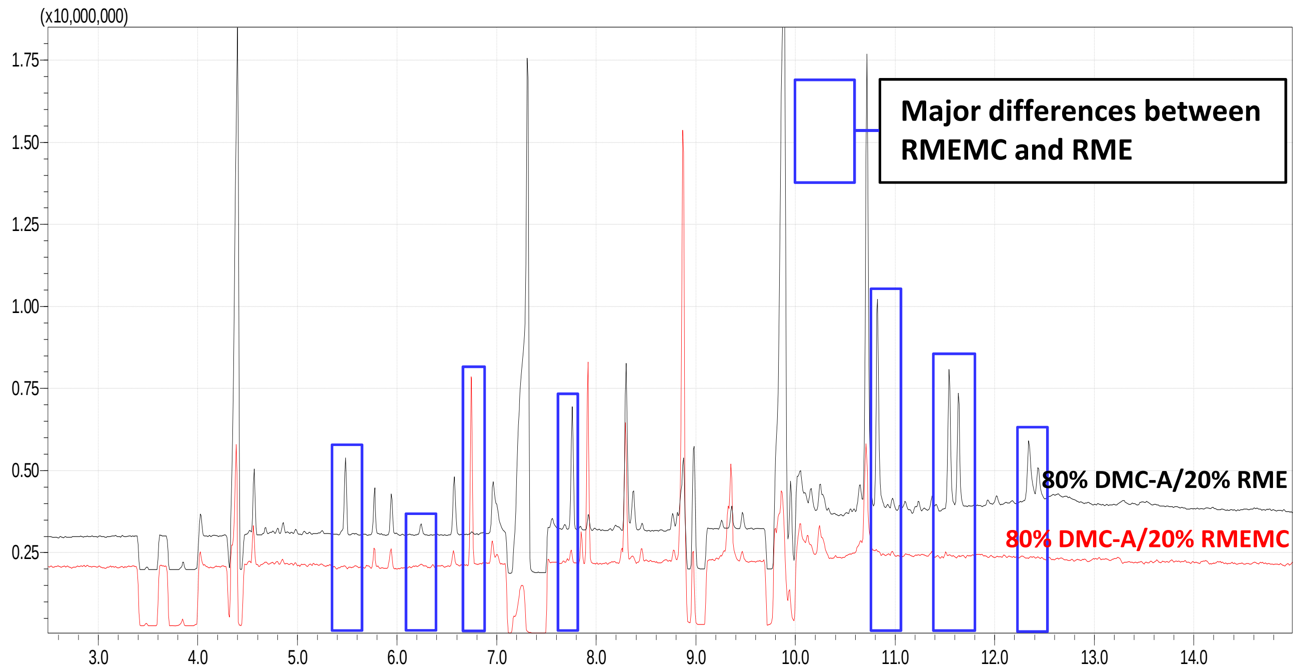

Figure 6.6: GC-MS chromatograms of 20% RME and RMEMC (7:3:1 methyl oleate:methyl linoleate:methyl linolenate) blends with DMC-A after 24 hour QCM oxidation at 140°C

The behaviour of blends with specific FAME model compounds is dealt with in the next section. The ESI-MS spectra (See Figure 10.35 through Figure 10.38 in the Appendix) are comprised of many of the same peaks that are present in the oxidation of RME and DMC-A on their own. There are a few differences, however. The tetralol (131) and tetralone (147) peaks are much less significant. Important new peaks are evident at 159 in the ESI-MS (+) spectrum and at 165 in the ESI-MS(-) spectrum.

6.1.4 Diesel model compound/biodiesel model compound blends

Methyl esters derived from C18 fatty acids and different degrees of unsaturation formed different products during QCM oxidation. Figure 6.7 shows a GC-MS chromatogram of 80% diesel model system/20% FAME blends of different degrees of FAME unsaturation after 24h of QCM oxidation. Model compounds and likely oxidation products of methyl oleate, methyl linoleate and methyl linolenate/diesel model system blends are presented in Table 10.7, Table 10.8, and Table 10.9 in the Appendix.

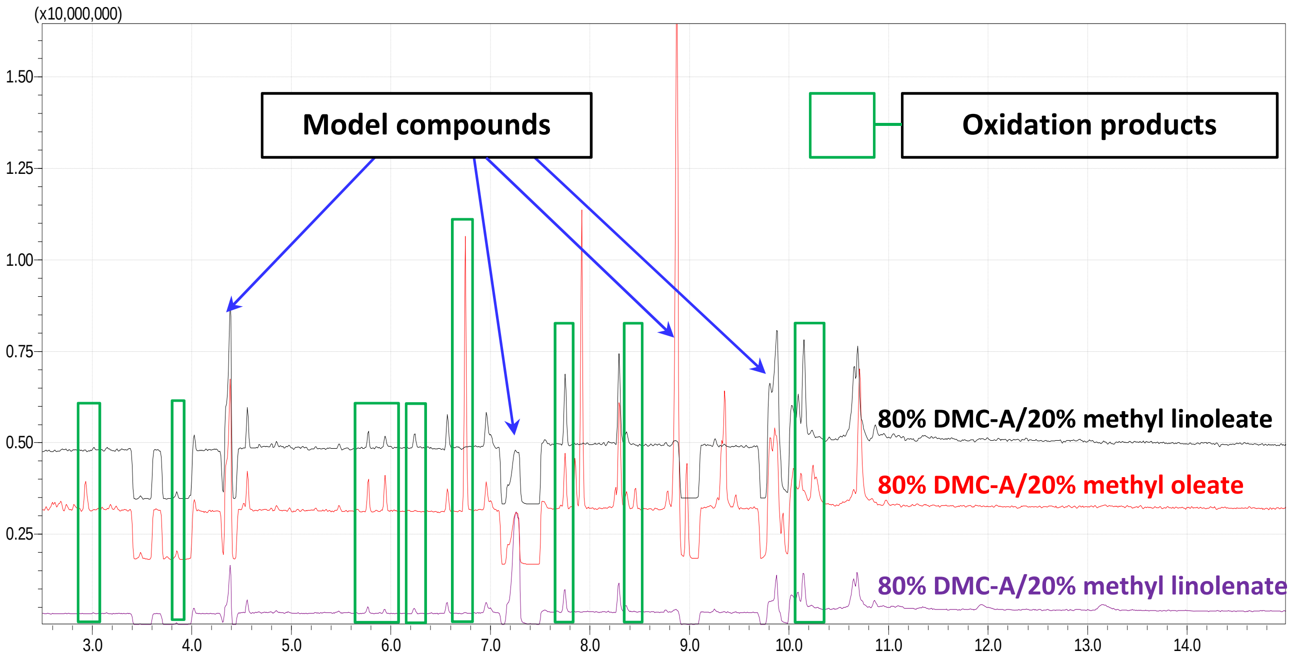

Figure 6.7: GC-MS chromatograms of 80% diesel model compounds and 20% FAME model compounds after 24 hour QCM oxidation at 140^{o}C

A number of acidic species were observed. These included pentanoic acid (2.95 min) and hexanoic acid (3.72 min). Oxidation products observed included shorter chain esters and hydroxyl esters such as methyl ricinoleate (10.68 min). An interesting species, found in large quantities after methyl oleate oxidation, was the epoxide of methyl oleate, methyl *cis*-3-pentyloxiraneundecanoate (10.71 min).

The methyl linoleate and methyl linolenate blends also formed a product which was an aldehydic derivative of the esters, methyl 9-oxononoate (6.24 min). This was not observed in the methyl oleate blends

Because these are blends with DMC-A, similar compounds to those found during the oxidation of neat DMC-A were found. Peaks, not highlighted or referred to, were present before methyl oleate/diesel model system blends were stressed. This is because lower purity methyl oleate which contained other monounsaturated esters, such as methyl palmitoleate (7.92 min), was used. It can be seen that the tetralol and tetralone concentrations were greatest for the blend containing methyl oleate. This FAME compound is the least reactive of the three model compounds (*78*). It is suggested that the other FAMES (methyl linoleate and methyl linolenate) are more likely to have a hydrogen atom abstracted than tetralin, thereby slowing down tetralin oxidation.

When looking at the ESI-MS spectra for 80% DMC-A/20% FAME model compound blends (see Figure 10.39 through Figure 10.50 in the Appendix), the tetralol (131) and tetralone (147) peaks are much less significant than in neat DMC-A systems. This is consistent with GC-MS data and the competition of FAME molecules with tetralin for oxygen molecules. Important new peaks are again evident at 159 in the ESI-MS (+) spectrum and at 165 in the ESI-MS(-) spectrum. A comparison with the spectra for the stressed neat RME reveals that in the case of methyl oleate the major peak for each set of oxidised species is at m/z that is +2 greater (279/277, 311/309, 325/323, 333/331, 365/363). Furthermore the species at 333 and 349 are more significant relative to the other peaks than both neat RME and 80% DMC-A/20% RME. Responses at 179 and 193 which are significant in the ESI-MS(-) were absent in that of stressed 100% RME. As discussed later these may be aromatic carboxylic acids.

The spectra for the oxidation of methyl linoleate blends were very similar to that of methyl oleate blends. However, certain peaks such as the 309/311 pair seen in methyl oleate was shifted by -2 to 307/309. This is consistent with the molecular mass of methyl linoleate being two less than that of methyl oleate. The spectrum in the region 600-650 was very similar to that of stressed 100% RME. That of the ESI-MS(-) also resembled the 100% RME and 80% DMC-A/20% RME far more than the methyl oleate blend. As mentioned, the peaks of the oxidised species associated with oxidised methyl linoleate shifted -2 units on average.

In the case of the species in the range 600-720 the shift was -4 units. This is consistent with the latter arising from dimers. These would contain 2 linoleate groups, each of which would reduce m/z by 2. Similar behaviour was seen with the ESI-MS spectra of methyl linolenate. The major peak in the dimerisation range was at 653/655 compared to 638 for blends with the other 2 esters and RME. This indicates that the methyl linolenate dimer has on average one more ketone group. This is consistent with the greater reactivity of methyl linolenate as a result of it having more *bis*-allylic carbons.

6.2 Flask oxidation

Aliquots, withdrawn during flask oxidation after each of the first six hours, were used to track compositional changes during flask oxidation. Measurements were also made after 24h. In these cases analysis revealed much greater degradation than was observed in QCM experiments. Where chromatograms are presented for 24h oxidation, these are for the upper layer formed. For the first 1-6h of oxidation only one layer was present in all experiments.

6.2.1 Diesel model compounds

Different model compounds formed different oxidation products. The GC-MS chromatograms of DMC-A and DMC-B are presented in Figure 6.8 and Figure 6.10.

As with QCM oxidation, the oxidation of tetralin to 1-tetralol and 1-tetralone was observed. This was observed as soon as 1h into the stressing procedure and the concentrations of these species were observed to increase with time. At 24h, however, significant quantities of the quinone, derived from tetralin, 1,4-naphthoquinone (6.23 min), was present. Trace quantities of this species were noted after 1h of oxidation. Smaller quantities of monohydroquinone, in which one of the ketone groups is replaced by a hydroxyl group, were observed at 7.10 min. At 24h, the presence of benzene-1,2-dicarboxylic acid (5.53 min) could be observed. Small quantities of 2-tetralol and 2-tetralone were also present. The amount of tetralin present was greatly reduced after 24h.

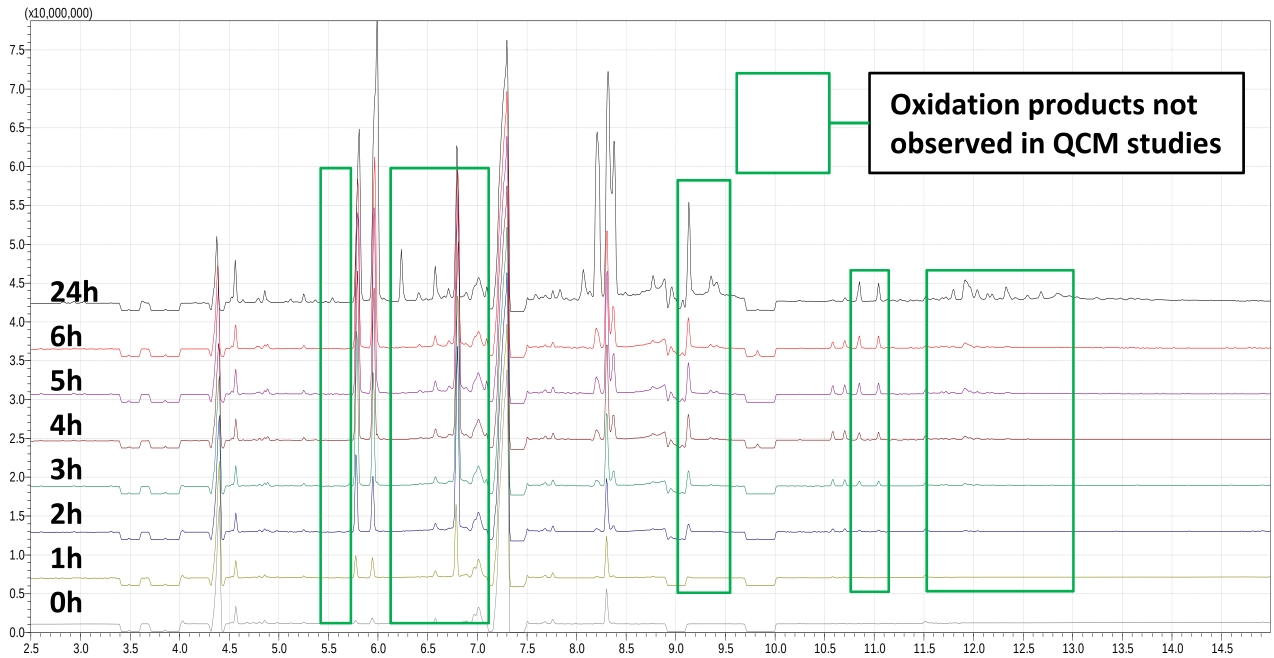

Figure 6.8: GC-MS chromatograms of DMC-A over 24h thermo-oxidative stressing at 140^{o}C in an open flask reactor. Sampling period, indicated on the left.

After 1h, the alkyl tetralins, 1-ethyl tetralin and 1-propyl tetralin started to appear. Their concentrations increased till 24h. The formation of longer chain tetralins, such as 1-octyltetralin could also be observed. The oxidation products such as 1,4-naphthoquinone and longer-chain alkyl tetralins highlighted in Figure 6.8 were not observed when DMC-A was subjected to thermo-oxidative stressing in the QCM. This is evidence of more extensive oxidation under conditions of flowing oxygen as expected.

As time progressed, more shorter chain and branched alkanes were observed. Not only were hexadecanols observed (seen in QCM oxidation spectra), but also more oxidised species such as hexadecanones (*e.g.,* at 8.18 min) and alkyl esters (9.12 min) were observed. An interesting product was the epoxide, hexadecyl oxirane (9.33 min) which was observable after 24h. Short chain acids were detected at 3.84 min (pentanoic acid), 3.62 min (hexanoic acid), 5.15 min (heptanoic acid) and 6.39 min (nonanoic acid).

Stressed fuel was analysed by GC-FID to investigate the consumption of model compounds and the formation of new products. Figure 6.9 illustrates the concentration of new oxidation products formed from diesel model compound oxidation. Initially, the concentration of 1-tetralol was very close to that of 1-tetralone. However, after 24h, the latter had exceeded the alcohol concentration, indicative of oxidation having progressed further. Interestingly, after 24h, *cis*-and *trans*-decalin were present although they were not observed at 6h. This corresponded to 2.1% of the original tetralin. 2.7% of tetralin had converted to naphthalene.

64% of the tetralin had been converted to other compounds after 24h. *n*-Hexadecane was more resistant to oxidation with 13% having been converted.

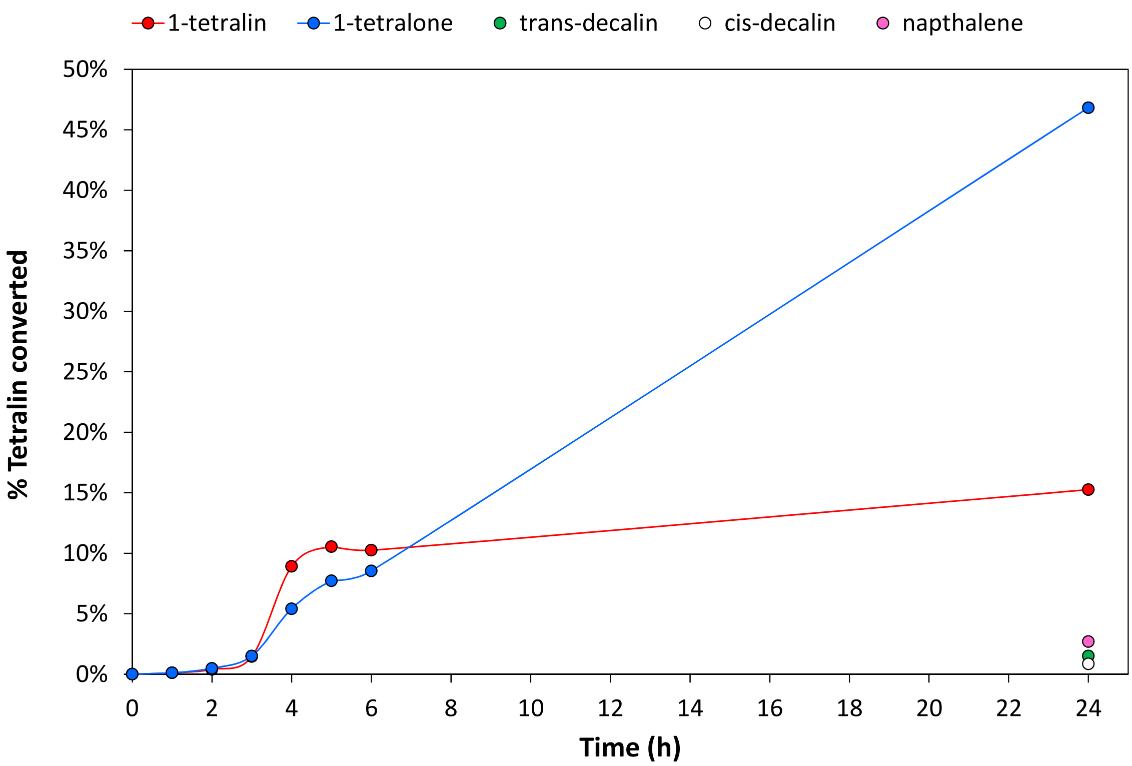

Figure 6.9: GC-FID: Conversion of tetralin in DMC-A over 24h thermo-oxidation in an open flask reactor at 140°C

Again, oxidation products could be detected by GC-MS after just 1 hour. These included 1-tetralol and 1-tetralone but also naphthalene at increased levels. Like DMC-A, benzene-1,2-dicarboxylic acid, 2,3-dihydronaphthalene-1,4-dione and 1,4-naphthoquinone were present after 24h. Products common to QCM reactions are highlighted in Figure 6.10.

Decalin was observed to oxidise more slowly than tetralin. Oxidation products began to appear after 4h. The species with the highest MS detector response was *trans*-octahydronaphthalen-4a(2*H*)-ol (4.91 min). After five hours the *cis*-isomer (5.17 min) was observed. The lower concentration of the *cis*-isomer is consistent with less *cis*-decalin being present in the unstressed DMC-B than *trans*-decalin as well as the *trans*-isomer being more stable (*95*).

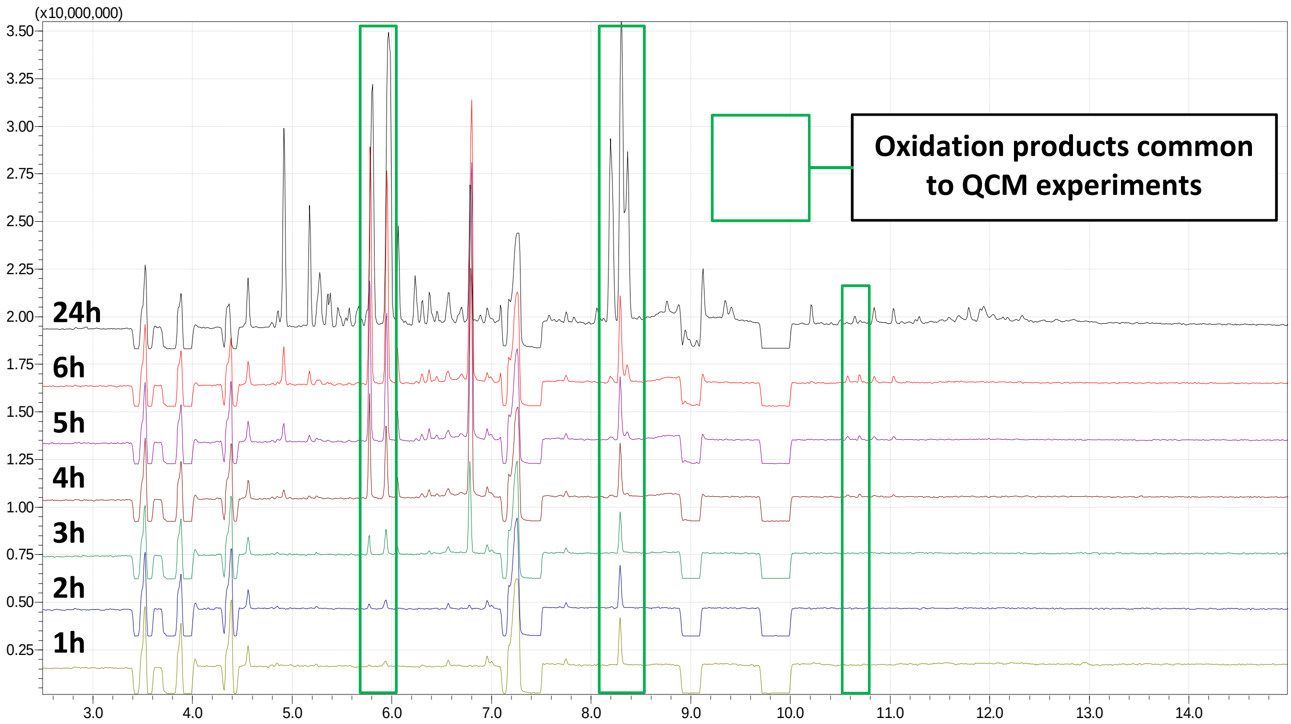

Figure 6.10: GC-MS chromatograms of DMC-B over 24h thermo-oxidative stressing at 140^{o}C in an open flask reactor. Sampling period, indicated on the left.

As time progressed, more and different oxidation products were formed. This can be seen in the 24h chromatogram where many species can be observed to have eluted between 5.4 and 5.7 min after *trans*-octahydronaphthalen-4a(2*H*)-ol and between 6 and 7 min after 1-tetralone. These included 1-decalol (5.27 min) and 2-decalol (isomers at 5.57 and 5.65 min). The 1-decalol isomers were observed earlier (after 4h) than the 2-decalol isomers and in greater concentrations. Isomers of 1-decalone were observed after 5h by GC-MS (*trans* at 5.34 min and *cis* at 5.45 min) in very small quantities where after their concentration increased. Small quantities of the decalin-derived dione, octahydronaphthalene-1,4-dione, and the dicarboxylic acid, cyclohexane-1,2-dicarboxylic acid, could be identified after 24h of stressing. A variety of alkyl decalins could also be identified.

Stressed fuel was analysed by GC-FID to investigate the consumption of model compounds and the formation of new products. Figure 6.11 illustrates the concentration of new oxidation products formed from diesel model compound oxidation. As with DMC-A, the concentration f 1-tetralol was initially similar to that of 1-tetralone but was significantly lower after 24h. By contrast, at 24h the concentration of decalones was lower than the decalols, consistent with the greater oxidative stability of decalin.

61% of the tetralin had been converted to other compounds after 24h. *n*-Hexadecane was more resistant to oxidation with 11% having been converted. The overall conversion of decalin after 24h was approximately 20%.

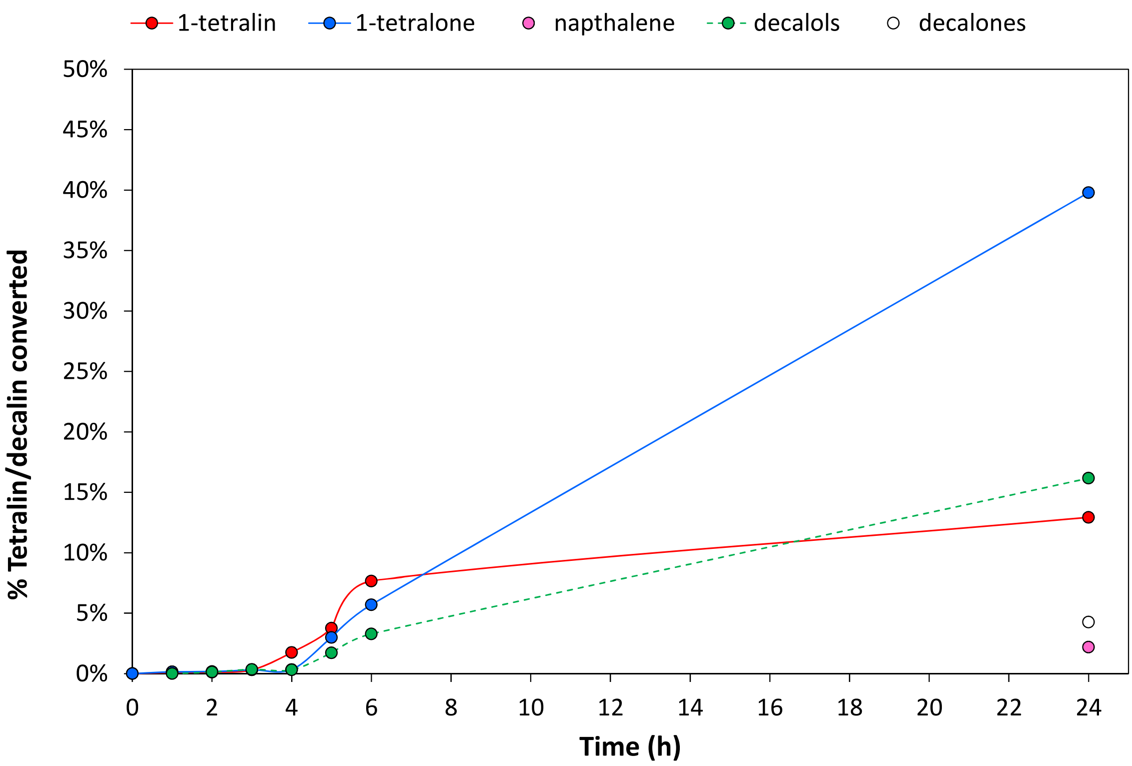

Figure 6.11: GC-FID: Conversion of tetralin and decalin in DMC-B over 24h thermo-oxidation in an open flask reactor at 140^{o}C

DMC-B and DMC-C formed similar products with different concentrations. DMC-B had relatively more tetralin and less decalin. Hence, more decalin oxygenates were observed between 4.8 and 7 minutes when DMC-C was stressed. Proportionately fewer tetralin derivatives were observed for the oxidation of DMC-C. The more model compounds used to make the diesel model system, the more complex the GC-MS chromatograms were. Overlapping peaks became an issue. Hence for further flask oxidation studies the simpler DMC-A system was used.

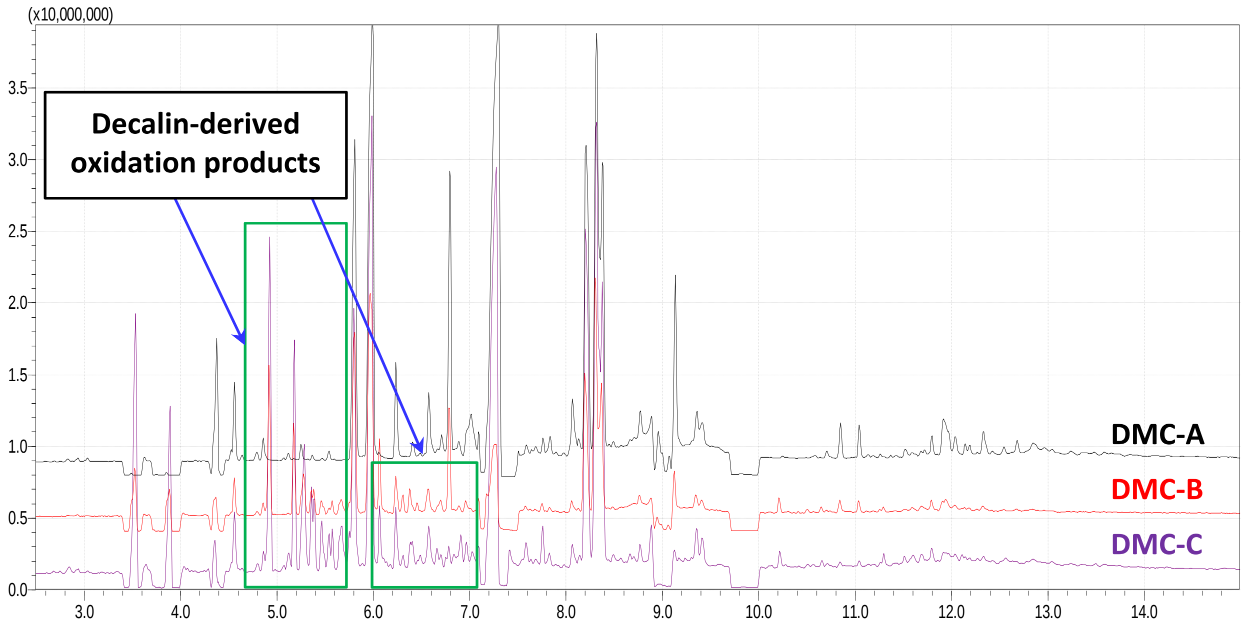

Figure 6.12: GC-MS chromatograms of different diesel model compound systems after 24h thermo-oxidative stressing at 140^{o}C in an open flask reactor

The ESI-MS(+) of the lower layer revealed far more species than were observed when DCM-A was stressed in a QCM. Figure 6.13 illustrates a narrow band of low molecular weight m/z. The peaks associated with tetralone (147) and tetralol (131) have disappeared and been replaced by napthalene-1,4-dione $[M+H]^+$ ion at m/z = 159.

As before the peak at 239 is ascribed to hexadecenone/hexadecenal (an unsaturated ketone/aldehyde.).

The series 185, 199, 213 all differ by 14. A possible homologous series would be odecanone/dodecanal (or oxirane), tridecanonal/-one and tetradecanonal/-one. Careful examination reveals that 115, 129, 143, 157, 171 are also present, potentially extending the series down to heptanal/heptanone. Although these peaks are weak they are significantly higher than their neighbouring peaks.

Care should be taken when interpreting ESI-MS spectra. The response of the ESI-MS instrument can vary widely for different classes of compounds and even within classes (*70*). Among other things, the intensity of an ESI-MS(+) peak depends on the original concentration of the species, and it's likelihood of being ionised (including the stability of the ion formed and its volatility). Low molecular weight peaks are more likely to evaporate with the solvent causing such peaks in the same series to have lower intensities for the same original concentration.

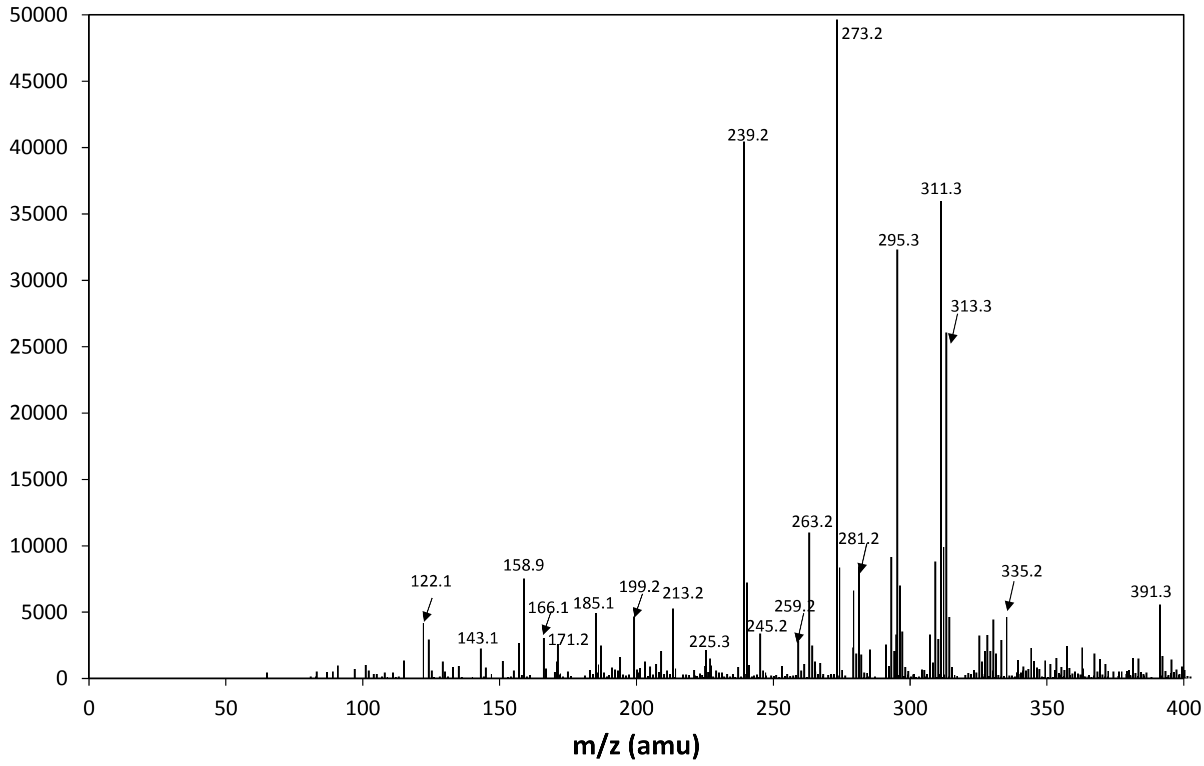

Figure 6.13: ESI-MS(+) spectrum for the lower layer from DMC-A after oxidation at 140^{o}C in a QCM for 24h (0-400 amu)

One of the objectives of this study was to try identify SMORS species. Benzoquinones and naphthoquinones are electrophiles, capable of undergoing electrophilic aromatic substitution (*22*). While 1,4-naphthoquinone could be identified by GC-MS, SMORS could not. The small peak at 291 might be a SMORS species resulting from the electrophilic aromatic substitution of tetralin and naphthalene-1,4-dione (*22*). The peak height, however, is too small for this to be conclusive. With the exception of 291, none of the other species in the region 250-350 were consistent with electrophilic aromatic addition. It is more likely that these are hexadecane-derived species, *e.g.,* the series 279, 295, 311 is consistent with higher dienals – nonadecadienal, icosadienal etc. The species at 281, 297 and 313 could be the associated oxirane or alcohol. It is possible that the species at 259 and 273 arise from addition of hexanal/epoxy hexane to heptenal/epoxy heptane to naphthalene-1,4-dione. Botha (*75*) has noted that while electrophilic aromatic substitution products were observed when tetralin was stressed on its own, these were not present when stressing took place in dodecane. No consistent homologous series could be identified in the range 250-350. These could be keto species derived from hexadecane, esters or the products of tetralin derivatives with hexadecane degradation products.

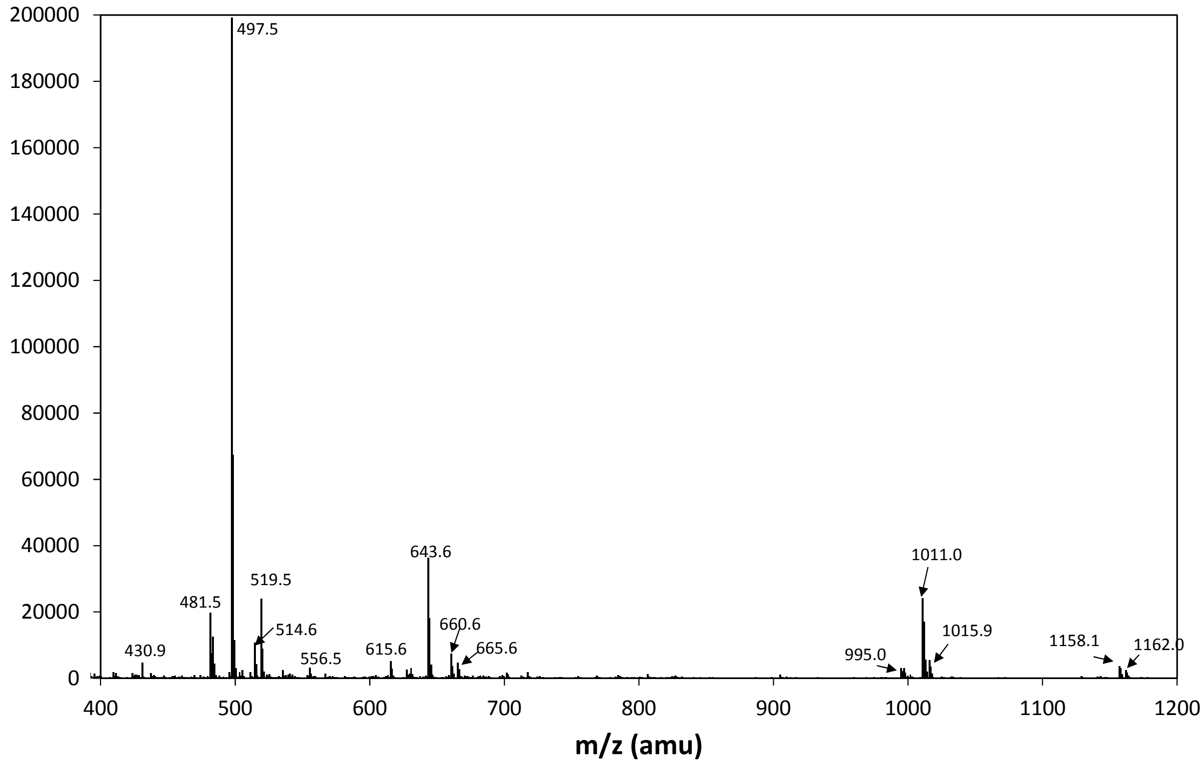

Figure 6.14: ESI-MS(+) spectrum for the lower layer from DMC-A after oxidation at 140^{o}C in a QCM for 24h (400-1200 amu)

Figure 6.14 illustrates that higher molecular weight oligomers are formed, centred on m/z 499, 643, 1012 and 1158. Interestingly the difference between last two peaks is 146 and that between 643 and 499 is 144. The addition of tetralol might be responsible for the former and tetralone for the latter. These high molecular weight species are different to those formed in the QCM. The ESI-MS(+) spectra for the upper and lower layers were similar in terms of the peaks observed, although the peaks associated with tetralin/tetralone were observed in the upper layer. However, the high molecular weight species (m/z > 1000 amu) were present in relatively low amounts. The molecular weights of the high molecular weight species are different to those observed in ESI-MS of the QCM stressed DMC-A.

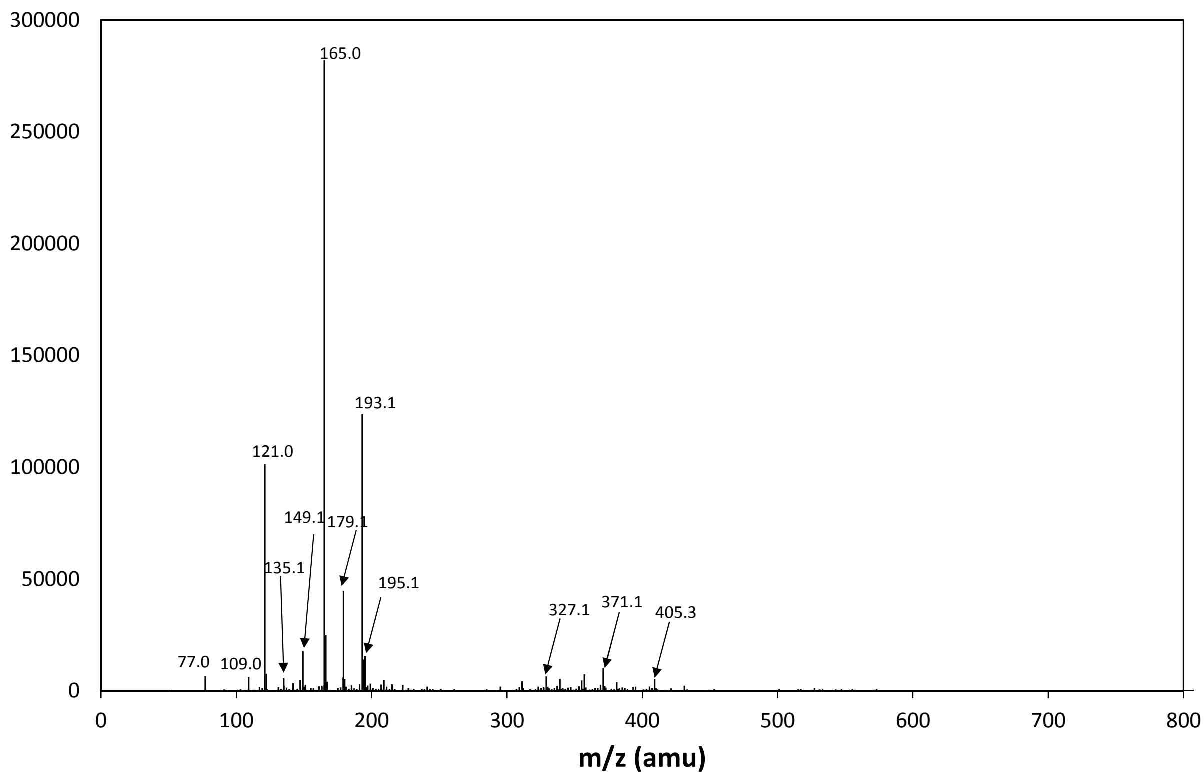

Figure 6.15: ESI-MS(-) spectrum for the lower layer from DMC-A after oxidation at 140°C in a QCM for 24h (400-1200 amu)

The ESI-MS(-) spectrum has a large peak at 165. This is likely o-phthalic acid. This is separated by 14 from 179 and another 14 from 193 suggesting a series of methylene groups between the phenyl ring and the carboxylate group. More of the higher molecular weight acids were present in the upper layer. It should be noted that ESI-MS(-) does not only identify carboxylic acids but other species which can deprotonate such as phenols (*70*). However, none of the major peaks were consistent with aromatic phenols such as naphthol. Refer to Figure 10.51 through Figure 10.53 in the Appendix for the ESI-MS spectra of the upper layer.

6.2.2 Effect of phenols on thermo-oxidative stability of diesel model compound systems

The addition of the antioxidant, BHT, prevented the formation of oxidised species such as 1-tetralol and 1-tetralone during the first six hours of oxidative stressing of the diesel model compound system, DMC-A (compare Figure 6.8 with Figure 6.16). GC-FID analysis revealed that after 24h as nearly as much 1-tetralol had formed as when BHT was not present and 92% of the 1-tetralone. In contrast, hexadecane oxidation to hexadecanol and hexadecanone was reduced. BHT, however, did provide oxidative stability during the 1st 6 hours. Cross-product species such as ethyl and propyl tetralin were not evident in the first 6 hours but did form after 24h.

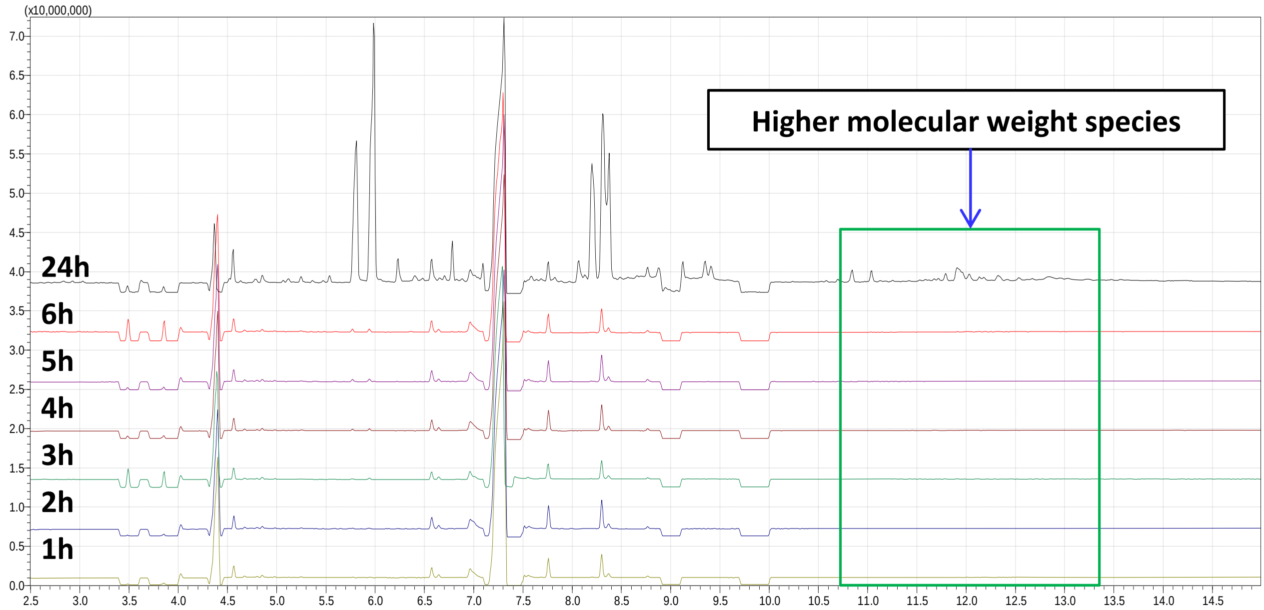

Figure 6.16: GC-MS chromatograms DMC-A, doped with 200 ppm BHT, over 24h thermo-oxidative stressing at 140^{o}C in an open flask reactor. Sampling period, indicated on the left

The addition of phenol did not prevent the oxidation of DMC-A. The formation of 1-tetralol and 1-tetralone are clearly evident after 1h. Alkyl tetralin and other high molecular weight species were detected by GC-MS after the second hour in DMC-A doped with phenol (see Figure 6.17). 1,4-Naphthoquinone (6.23 min) and benzene-1,2-dicarboxylic acid (5.53 min) could be observed after 24h. No new oxidation products could be observed, compared to neat DMC-A. Differences between DMC-A, with and without phenol, were slight in both the GC-MS and GC-FID chromatograms. This was unlike the observation of Robertson and Waters (*93*) who observed that phenol slowed oxidation by 30%. However, they did add phenol at 1% (10 000 ppm) which is much greater than that used in this study. These results are more in line with those of Kerkering *et al.* (*74*).

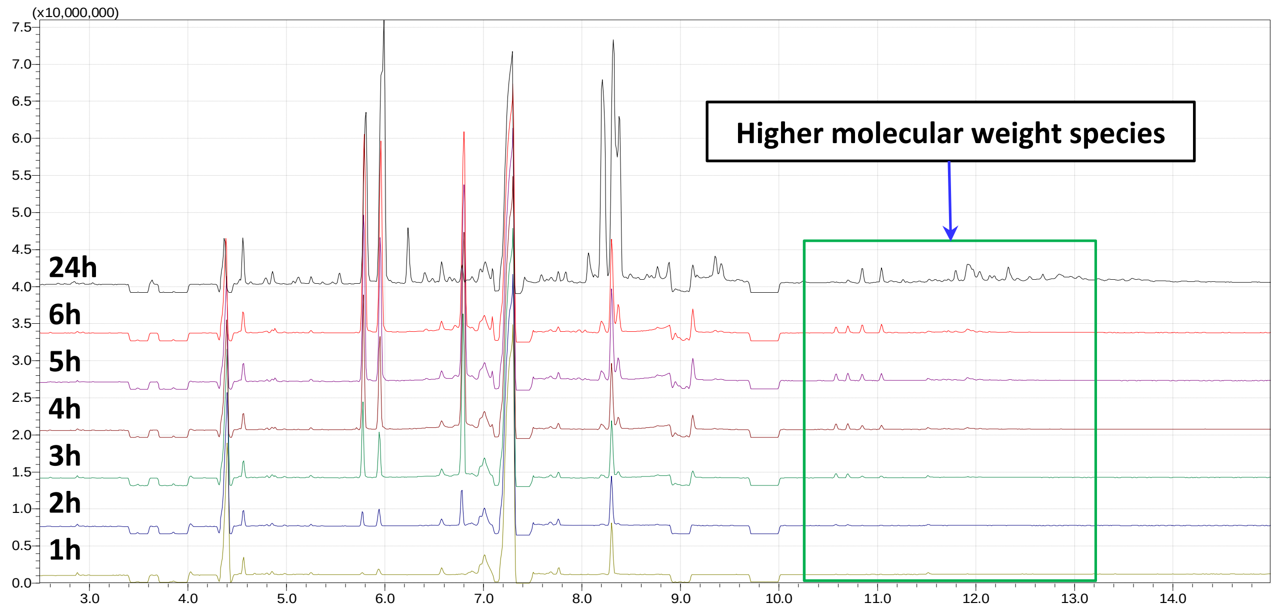

Figure 6.17: GC-MS chromatograms of DMC-A, doped with 200 ppm phenol, over 24h thermo-oxidative stressing at 140°C in an open flask reactor. Sampling period, indicated on the left

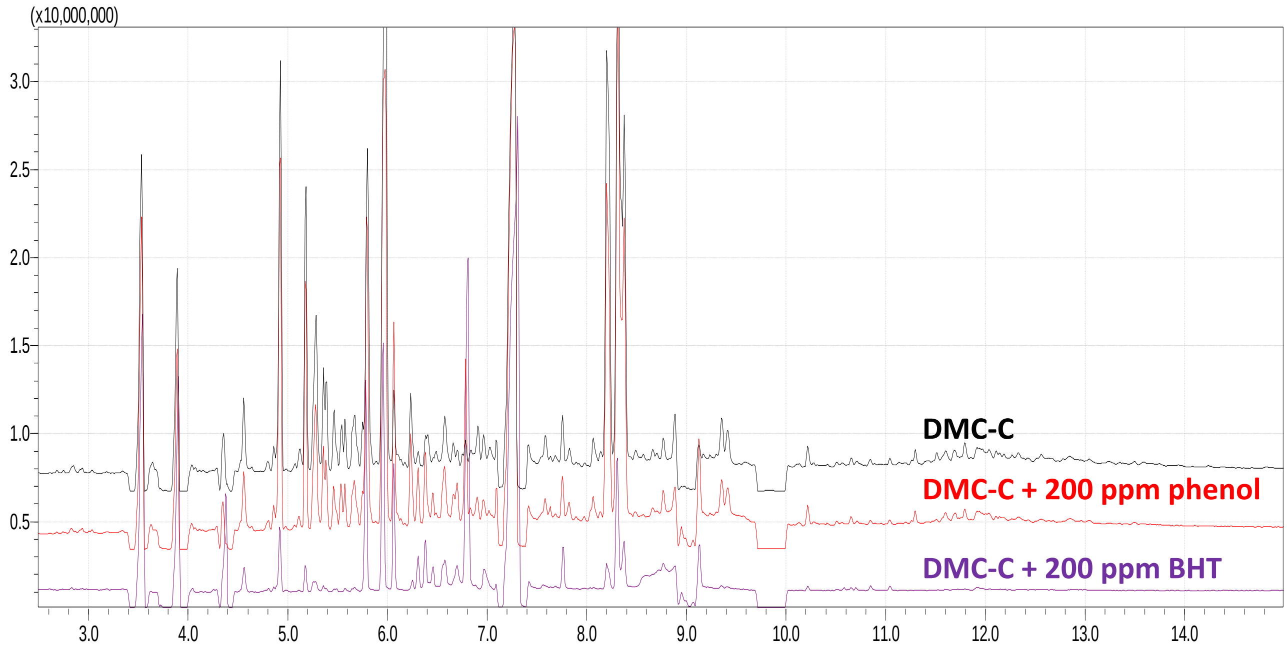

Figure 6.18: GC-MS chromatograms comparing the effect of different phenolic compounds on DMC-C after 24h thermo-oxidative stressing at 140°C in an open flask reactor

BHT reduced the amount of the lower layer formed during flask oxidation. The number of peaks and the quantity of oxidation products formed in DMC-C + BHT (indicated by the purple curve in Figure 6.18) were lower than those formed during the stressing of neat DMC-C and DMC-C, doped with phenol. While little impact on the tetralin derivatives was noted, significantly fewer decalin oxygenates (eluting between 5.2 and 5.8 min) were formed. Alkyl decalins (eluting between 6.2 and 6.8 min) were still present.

6.2.3 Diesel model compound/FAME blends

When methyl oleate, methyl linoleate and methyl linoleate were blended in a 7:3:1 ratio to simulate RME and then blended with DMC-A, a mixture of the oxidation products of those formed from the individual FAME molecule were seen after 24h. Figure 6.19 shows oxidation products of diesel/methyl ester blends over time during flask oxidation.

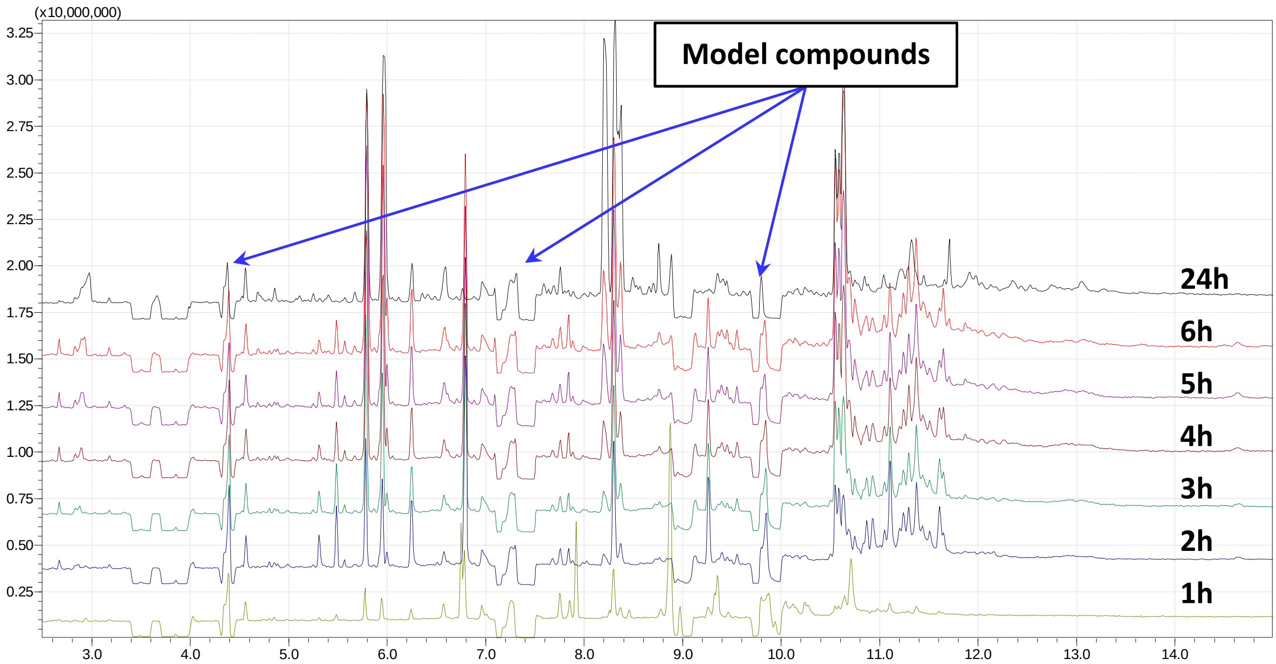

Figure 6.19: GC-MS chromatogram of 20% RME model system/80% DMC-A over 24h thermo-oxidative stressing at 140°C in an open flask reactor. Sampling period, indicated on the right

It can be seen that significant quantities of species elute after 11 min after 2h stressing. These species were a range of epoxides and long chain esters and ethers.

When DMC-A was blended with the FAME model compound mixture, it was observed that 1-tetralol and 1-tetralone, which were observed after two hours during flask oxidation of the neat DMC-A, were detected after the first hour of the experiment. They were also present in greater quantities after 6h. It can be seen that methyl 9-oxononanoate (6.21 min) was already observed after 1h of stressing. As with DMC-A, the *n*-hexadecane oxygenates (various hexadecanones and 1/2-hexadecanol) were observed. Greater quantities of acid were noted. Butanoic and pentanoic acid can clearly be seen eluting before 3.50 min together with hexenal. At 5.32 min is (E,E) 2,4-nonadienal and at 5.50 min is (E,E) 2,4-decadienal. These species can be seen to increase in concentration between 2 and 6h and then disappear almost completely by 24h. This is suggestive of them being oxidized to carboxylic acids at longer oxidation time. Similar behaviour is seen for (E,E) 2,4-dodecadienal at 9.30 min.

The Appendix contains chromatograms for the stressing of diesel model compound blends with RME doped with phenolic compounds (see Figure 10.20).

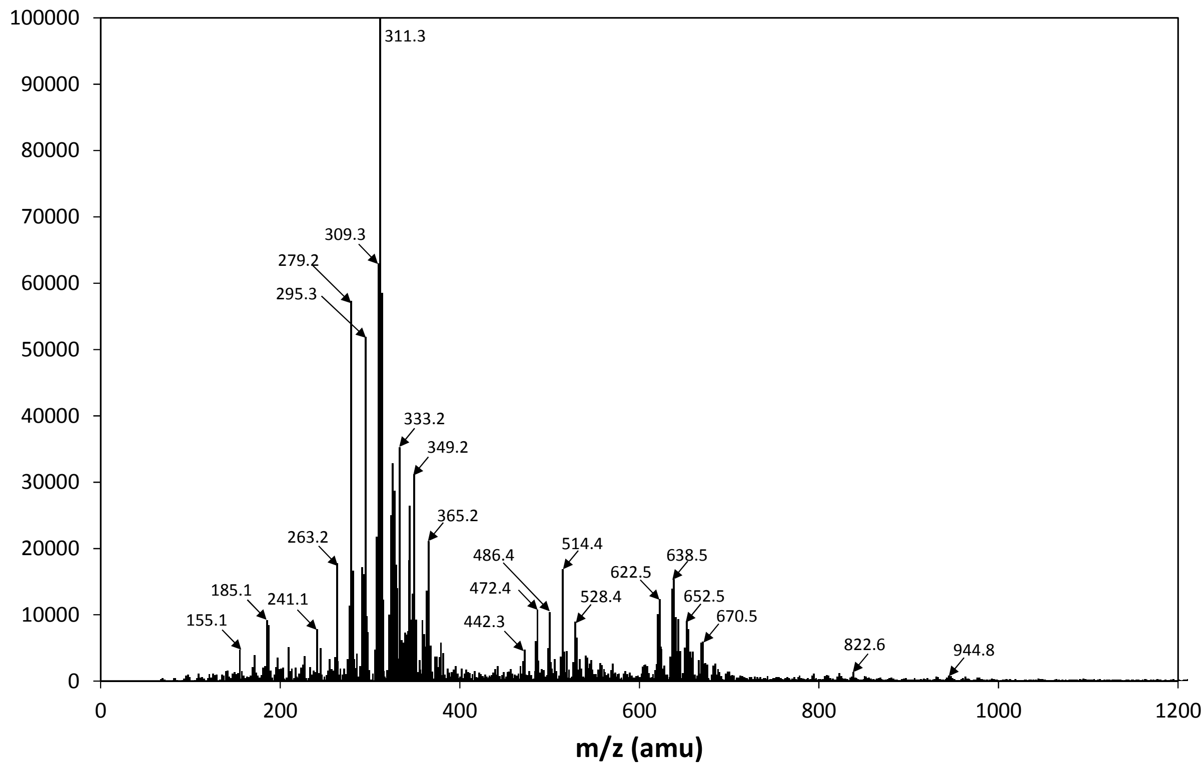

Figure 6.20. ESI-MS(+) spectrum for RME after oxidation in an open flask for 48h

If one compares Figure 6.5 with Figure 6.20 one can see that the oxidation products below m/z = 400 amu are very similar. Furthermore the species in the region 600-680 are similar. However, what has changed is the emergence of oxidised species with m/z in the range 420-

560 amu. Furthermore the relative amount of species with m/z > 800 amu has also increased. There are also significantly more high molecular weight acids in the ESI-MS(-) spectrum. This spectrum and further details of the ESI-MS(+) spectra may be found in Figure 10.54 through Figure 10.56 in the Appendix.

ESI-MS spectra are contained in Figure 10.57 through Figure 10.62 in the Appendix for the upper and lower layers of 80% DMC-A/20 % RME. The ESI-MS(+) spectra are a combination of the species in the layers for stressed DMC-A and stressed RME. The layers do differ in the average molecular mass of the species present with lighter species in the upper layer. The amount of oxygenated species in the range 420-560 amu is greater than that in the range 600-680 amu while in the lower layer the latter is more significant. Furthermore there are significantly more high molecular weight acids in the lower layer as can be seen in the ESI-MS(-) spectrum.

6.2.4 Diesel/biodiesel model compound blends

As was seen in the QCM experiments, biodiesel model compounds with different degrees of FAME unsaturation formed different oxidation products during flask oxidation. Since oxygen is unlimited during flask oxidation, the quantity and concentration of products that formed were greater than those formed during QCM oxidation as can be seen in Figure 6.21. In particular many oxygenated species were observed. Many shorter chain compounds (alkanes, alcohols, acids and ketones) were present. The species eluting before 3.4 min are short acids. A number of higher molecular weight species with elution times greater than 11 min were observed. These products together provide evidence of methyl ester decomposition. It was apparent that the number and quantity of species formed increased as the degree of unsaturation increased. A number of furanones such as 3-dodecyl-2,5-furandione were observed at low concentrations in oxidised blends of DMC-A with linoleic and linolenic acid.

Significant quantities of the aldehydic ester, methyl 9-oxononanoate (6.21 min), were observed when systems containing methyl linoleate and methyl linolenate were stressed. Methyl 9-oxononanoate was not found when 80% DMC-A/20% methyl oleate was stressed. After the stressing of methyl oleate, epoxides (oxiranes) were observed after 1h and 9,10 diols were observed after 3h. Epoxides and diols were also observed in the linoleate and linolenate blends.

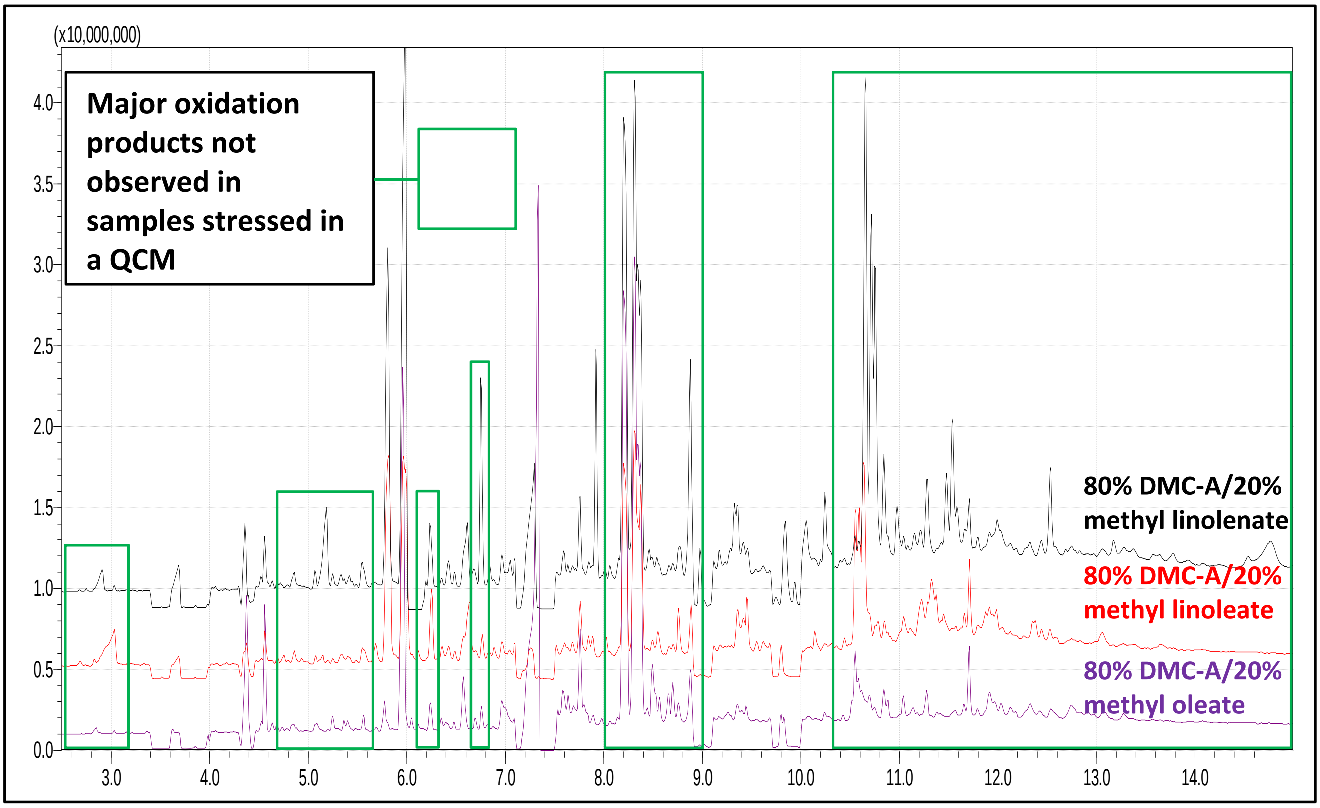

Figure 6.21: GC-MS chromatograms of DMC-A/model FAME compound blends after 24h thermo-oxidative stressing at 140°C in an open flask reactor

The ESI-MS spectra of the model compounds, in particular those of methyl linolenate and methyl linoleate, resembled those of RME. This is not surprising given that these are the more reactive esters in RME (*78*). The ESI-MS spectra for diesel model compound/individual FAME model compound blends can be found in Figure 10.62 through Figure 10.77 in the Appendix.

6.3 Discussion

6.3.1 QCM oxidation

Diesel model compound systems

Additional hydrocarbons formed were a result of *n*-hexadecane degradation. Figure 6.22 illustrates how shorter chain alkanes can be formed. Because of their volatility, ethylene and propylene could not be detected. Indirect evidence of their formation is that the alkyl tetralins, 1-ethyl tetralin and 1-propyl naphthalene, were formed.

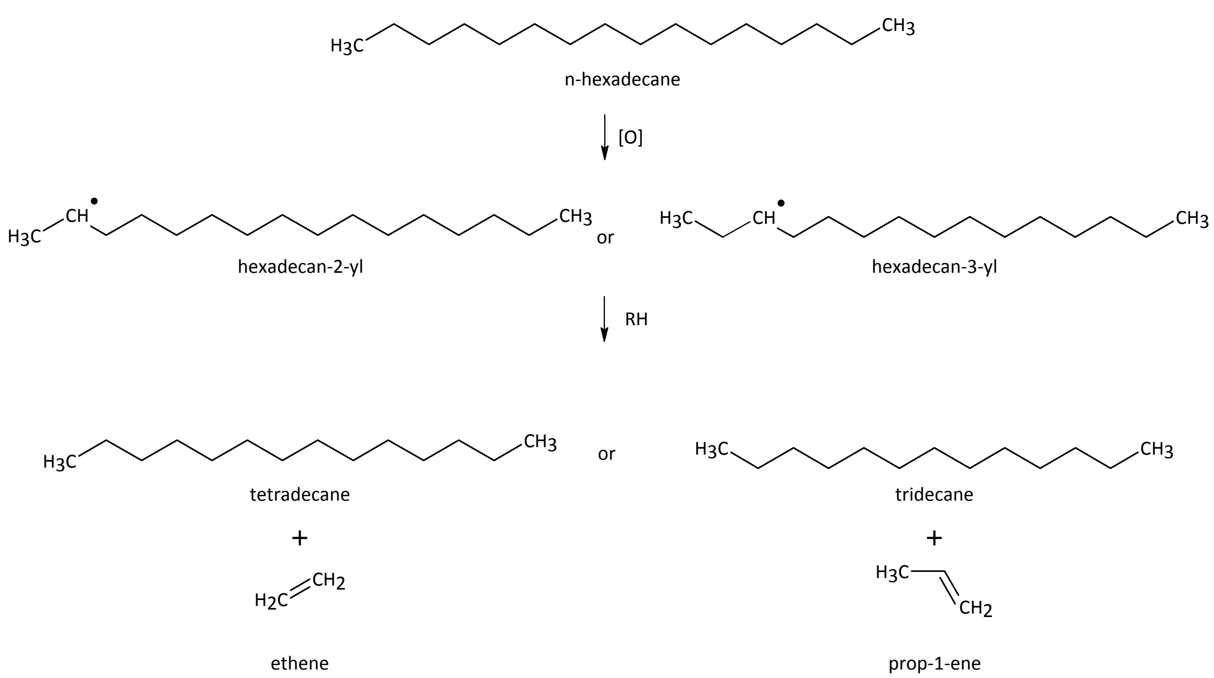

Figure 6.22: n-Hexadecane degradation: Example reaction pathway for the formation of lower alkanes

In the presence of oxygen and heat, it is suggested that tetralin likely undergoes direct oxidation initiated by radicals to form tetralin-1-hydroperoxide. The peroxide is formed at this position because of the presence of the labile benzylic hydrogen.

Tsang and Cui calculated bond energies for tetralin (*113*). As can be seen in Table 6.1 it is far easier to break and thus abstract a proton from the α (1) position. This explains why 1-tetralol and 1-tetralone are more prevalent than 2-tetralol and 2-tetralone. No 5-hydroxytoluene was observed.

*Table 6.1. Activation energies to break C-C and C-H bonds in tetralin (reproduced from (*130*))*

	C-H (kcal/mol)		C-C (kcal/mol)	
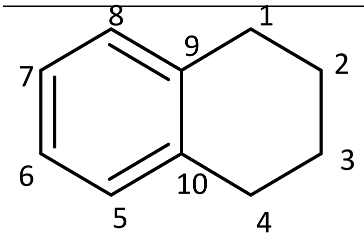	C-1	87	C1-C9	101
	C-2	96	C1-C2	73.3
	C-6	108	C2-C3	84.4

The hydroperoxide decomposes to 1-tetralol and 1-tetralone. Robertson and Waters proposed that tetralin-1-hydroperoxide was unstable and formed 1-tetralol and 1-tetralone (*93*). The fact that the initial concentrations are similar is consistent with Robertson and Waters suggestion that they form simultaneously from two hydroperoxide molecules. However, the extreme oxidative conditions used here means that tetralol does actually oxidise to tetralone. Unfortunately the GC-MS program used did not allow the detection of hydroperoxides which have been reported elsewhere (*75*).

ESI-MS is extremely useful in identifying patterns of compounds formation. Because compounds are a) extracted into methanol and b) need to be easily ionised by a soft source, it is not suitable for hydrocarbons like tetralin and n-hexadecane but is useful for identifying polar species. Because oxidation experiments were performed in this study, they would likely contain oxygen. ESI-MS (+) revealed a strong response at m/z = 147. This is consistent with tetralone (M_w = 146 g mol^{-1}).

One would expect tetralol at 149 but it is absent. However, there is a peak at 131 which is consistent with tetralol. Although ESI-MS is considered a soft technique it can cause molecular breakdown, especially with alcohols (*131*). This is illustrated in Figure 6.23. The 1-tetralyl radical is reported to be relatively stable (*132*).

The ESI-MS(+) spectrum for DCM-B which contained decalin was very similar except for peaks at 155 and 153 which are consistent with decalone and decalin. They were much smaller than those for the tetralin species, suggesting the latter is more readily oxidised.

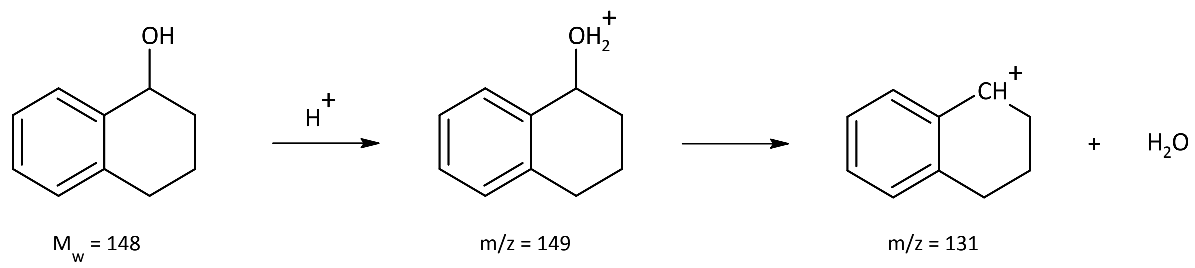

Figure 6.23: Formation of m/z= 131 in tetralol ESI-MS (+)

The peak at 165 is possibly tetralin-diol (M_w = 164 g mol^{-1}). Such species were identified in small quantities by GC-MS. Centred around 240 are the hexadecane oxygenates. 2-Hexadecanone was identified by GC-MS. This species is consistent with the peak at 241. ESI-MS (+) does not allow conclusive identification of species. 241 could also be from hexadecenol or hexadecanyl oxirane. It is suggested that the peak at 239 is hexedecenone. 2-Hexadecanol which was observed by GC-MS could not be seen at 243 but there is a small cluster centred on 225 which would be consistent with the loss of water as in Figure 6.23. The peak at 185 could be dodecanal (or possibly dodecanone). *n*-Dodecane is a small impurity in the *n*-hexadecane but it could also be formed by cracking of *n*-hexadecane, followed by oxygenation. It is unclear how the high molecular weight species are formed although the ones between 240 and 320 may be esters of short acids with hexadecanol.

An important peak in the ESI-MS(+) spectrum (Figure 6.11) of the lower layer from flask stressing of DMC-A indicated that tetralone had been consumed but that an important species, 1,4-naphthoquinone, might have been formed $[M+H^+]$ = 159. This is a potential intermediate for SMORS formation. Peaks for the potential parent intermediates for 1,4-naphthoquinone, naphthalene-1,4-diol or tetralin-1,4-dione (both M_w = 160) could not be observed. Present in the $[M-H]^-$ was a large peak at 165 which is consistent with o-phthalic acid. The species at 179 and 183 could possibly form a homologous series with $–CH_2$- inserted between the COOH and the aromatic ring. Species at low molecular masses such as 83 and 97 are consistent with pentenal and hexenal, observed by GC-MS.

Although ESI-MS(+) (Figure 6.11) of highly stressed DMC-A does contain a peak at 291 the evidence for such a SMORS species being formed is inconclusive at best.

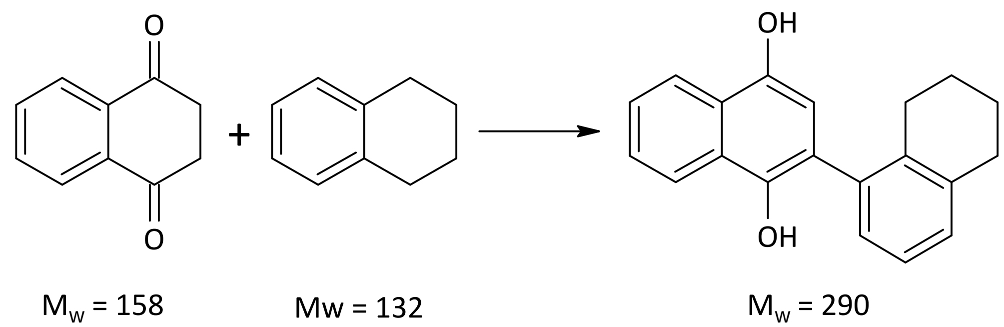

Figure 6.24: Possible electrophilic aromatic substitution between tetralin and naphthalene-1,4-dione to form species of M_w = 290.

High oxidation of *n*-hexadecane leads to cracking and oxidation. This is illustrated by the heptadecanal to tetradecanal series. These imply the loss of ethene, 1-propene and 1-butene (for tetradecanal to dodecanal, the peaks in this series with the highest response) during cracking.

There is indirect evidence from ESI-MS spectra that tetralin species are combining with high molecular weight oligomers. There is a peak in the ESI-MS(+) of the stessed sample at m/z = 481. 481 is consistent with a dimer of hexadecane which is a keto ether. An alternative and probably more likely possibility is the formation of hexadecyl hexadecanoate from the oxidation products, hexadecanol and hexadecanoic acid (both of which were seen by GC-MS).

The ESI-MS(+) spectra for both the upper and lower layers are similar. However, the presence of peaks > 1000 amu in the ESI-MS(+) of DMC-A suggests that the average molecular weight of the oligomers in the upper layer is less than that in the lower layer. This may be because solvency causes oligomers with M_w > 1000 g mol^{-1} to precipitate. There were also fewer of the cracked ketones in the upper layer. In addition to 1,4-naphthoquinone, evidence for tetralol existed.

It is suggested that naphthalene is formed via the dehydrogenation of tetralin. Alemán-Vázquez *et al.* report that tetralin may convert to naphthalene via hydrogen transfer reactions when crude oil is refined (*92*).

It is suggested that 1-ethyl tetralin and 1-propyl tetralin are formed from the reaction of ethene and 1-propene, produced by the degradation of *n*-hexadecane (see Figure 6.22), with 1-tetralin radicals or tetralin-1-hydroperoxide. Burklé-Vitzthum and Michels (*133*) suggest that 1-ethyl tetralin is obtained from the addition of ethylene to a 1-tetralyl radical. Longer chain alkyl tetralins that were observed after 24h in flask reactions would form in a similar manner but with higher molecular weight alkenes which would result from hexadecane and/or FAME cracking (*132*).

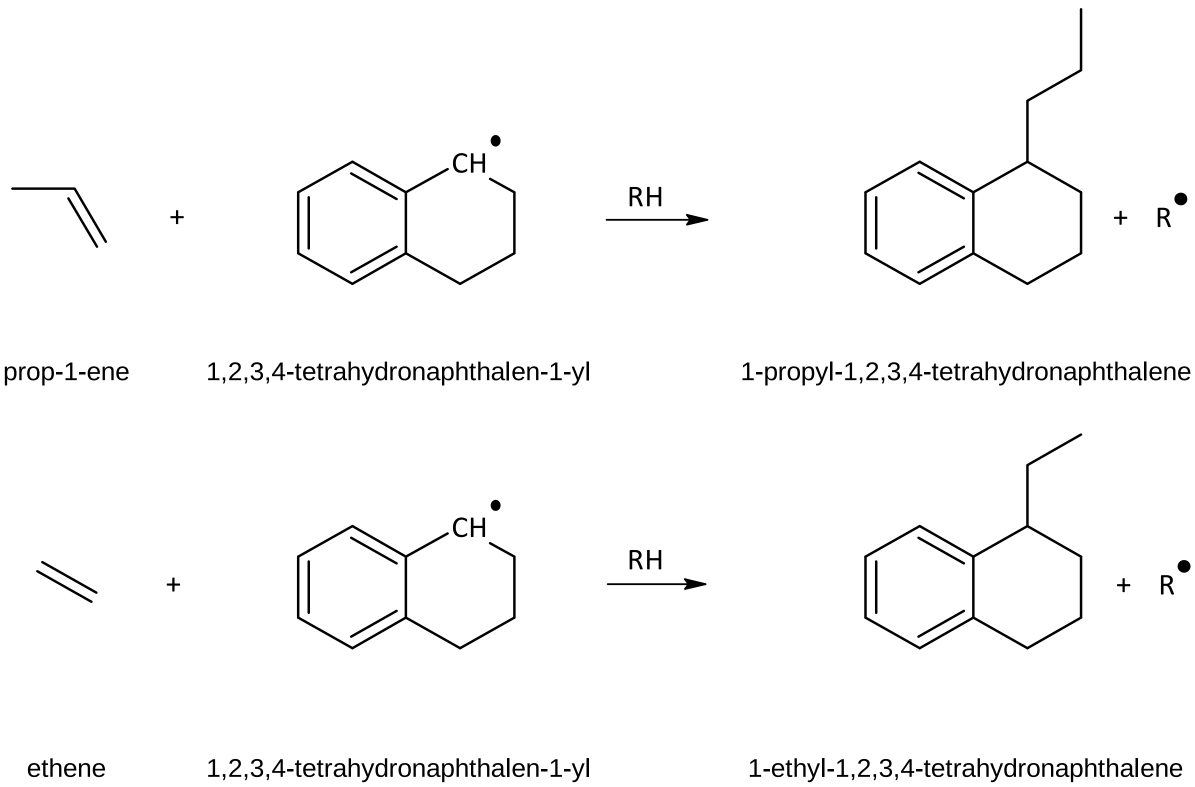

Figure 6.25: Pathway for the formation of alkyl tetralins

RME

GC-MS analysis revealed the presence of oxidised species that had formed during the storage of RME. Two examples are illustrated in Figure 6.26. A newer sample that contained BHT did not contain these species. These species are likely to have formed during storage after β-scission of the olefinic esters in RME.

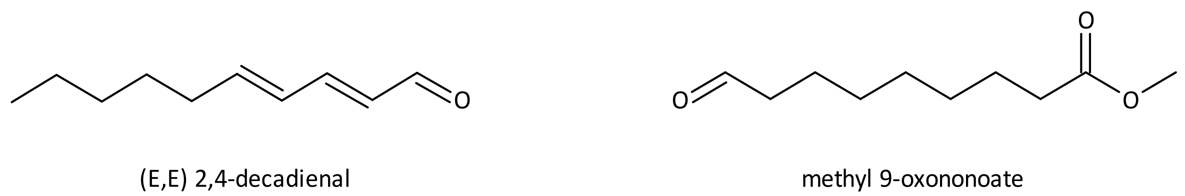

Figure 6.26: The oxygenates (E,E) 2,4-decadienal and methyl 9-oxononoate found in the RME used in this study

QCM oxidation of RME led to the formation of other oxygenates as illustrated in Figure 6.27:

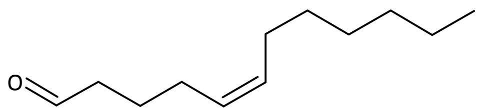

cis-5-dodecenal

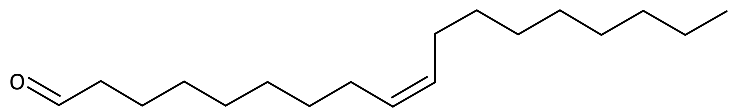

cis-9-octadecenal

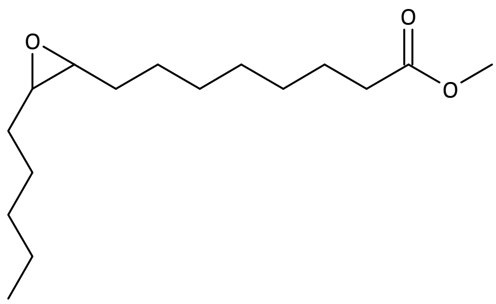

methyl *cis*-3-pentyloxiraneundecanoate

Figure 6.27: Oxygenates observed after the oxidation of RME in a QCM for 24h at 140^{o}C

Methyl *cis*-3-pentyloxiraneundecanoate is the epoxide of methyl oleate, otherwise known as methyl *cis*-9-octadecenoate. *cis*-9-Octadecenal is also derived from methyl oleate. Compare its structure (Figure 6.27) with that of methyl oleate (Figure 2.6). It is the aldehyde formed when the methyl group is removed from methyl oleate.

Diesel model compound/biodiesel model compound blends

FAMEs of carbon number 19 and different degrees of unsaturation formed different products during QCM oxidation. Methyl 9-oxononoate (illustrated in Figure 6.26) is formed from the oxidation of polyunsaturated methyl linoleate and methyl linolenate, but not methyl oleate. A scheme for its formation is discussed later (see Figure 6.32). Large quantities of methyl *cis*-3-pentyloxiraneundecanoate were formed from the oxidation of methyl oleate.

No species, derived from reactions between FAME model compounds and tetralin derivatives, could be identified.

RME/diesel model compound blends

The effect of FAME on diesel model compound oxidation was indirect. Increased quantities of 1-tetralol and 1-tetralone were formed when RME was stressed with diesel model compounds than when the diesel model compounds were stressed alone. It is possible that the acidic degradation products of FAME are capable of catalysing tetralin oxidation. As with the model biodiesel compounds, no obvious products derived from the reaction of diesel model compound derivatives with FAME decomposition products could be identified.

Various aldehydic esters and ester epoxides were again seen as well as the hydroxy oleate, methyl ricinoleate. This is similar to methyl oleate except it has a hydroxyl group attached to carbon atom number 12 in the main chain. It is illustrated in Figure 6.28.

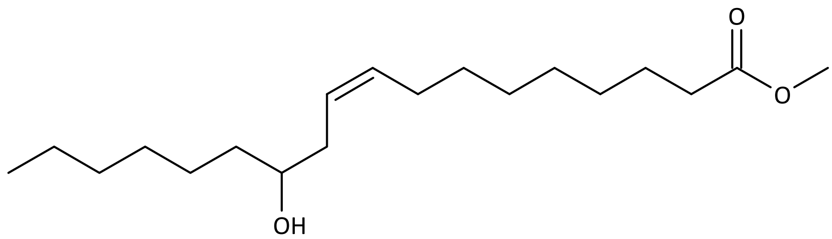

methyl ricinoleate

Figure 6.28: Structure of methyl ricinoleate

6.3.2 Flask oxidation

Greater quantities of oxidised species and more highly oxidised species were observed after stressing in flask reactors for 24h than in QCM experiments. This can be ascribed to the presence of unlimited oxygen in the flask experiments.

Diesel model compound systems

As with QCM oxidation, oxidation of tetralin to 1-tetralol and 1-tetralone was observed. These were present after 1h. Oxidation is likely sequential with 1-tetralol forming before 1-tetralone. Evidence for this is the fact that in the initial stages 1-tetralol concentrations exceeded those of 1-tetralone slightly but after 24h the situation was reversed.

Unlike the GC-MS analysis of QCM-stressed model compound systems, 4-hydroxy-1-tetralone, 2,3-dihydronaphthalene-1,4-dione and the quinone (1,4-naphthoquinone) were detected after 24h as well as benzene-1,2-dicarboxylic acid.

GC-FID concentration reasults revealed that tetralin was the most reactive of the diesel model compound components investigated. Far greater quantities of tetralin were converted than decalin and *n*-hexadecane.

A tetralin oxidation pathway is proposed which is presented in Figure 6.29. Tetralin oxidation is initiated at the alpha position to the aromatic ring. In the presence of limited oxygen, oxidation stops after the formation of 1-tetralone. The QCM results were very similar to what Woodward *et al.* observed during tetralin oxidation (*94*). During flask oxidation, however, more oxidised species, such 4-hydroxy-1-tetralone, 2,3-dihydronapthalene-1,4-dione and 1,4-naphthoquinone, were observed. As a result, the amount of tetralin after open flask oxidation was greatly reduced. While the formation of 2,3-dihydronaphthalene-1,4-dione has been reported when tetralin oxidation has been studied, the presence of benzene-1,2-dicarboxylic acid has not. It is suggested that this is the ultimate product of tetralin oxidation resulting from ring opening. It is unclear whether this first requires the formation of 1,4-naphthoquinone or can form directly from 2,3-dihydronapthalene-1,4-dione.

The quantities of 1-tetralol and 1-tetralone were much higher than those of 2-tetralol and 2-tetralone. This can be ascribed to the easier formation of the 1-tetralyl radical than the 2-tetralyl radical (*130*). Hydrogen atoms, alpha to aromatic rings, are far more easily abstracted than those in beta positions.

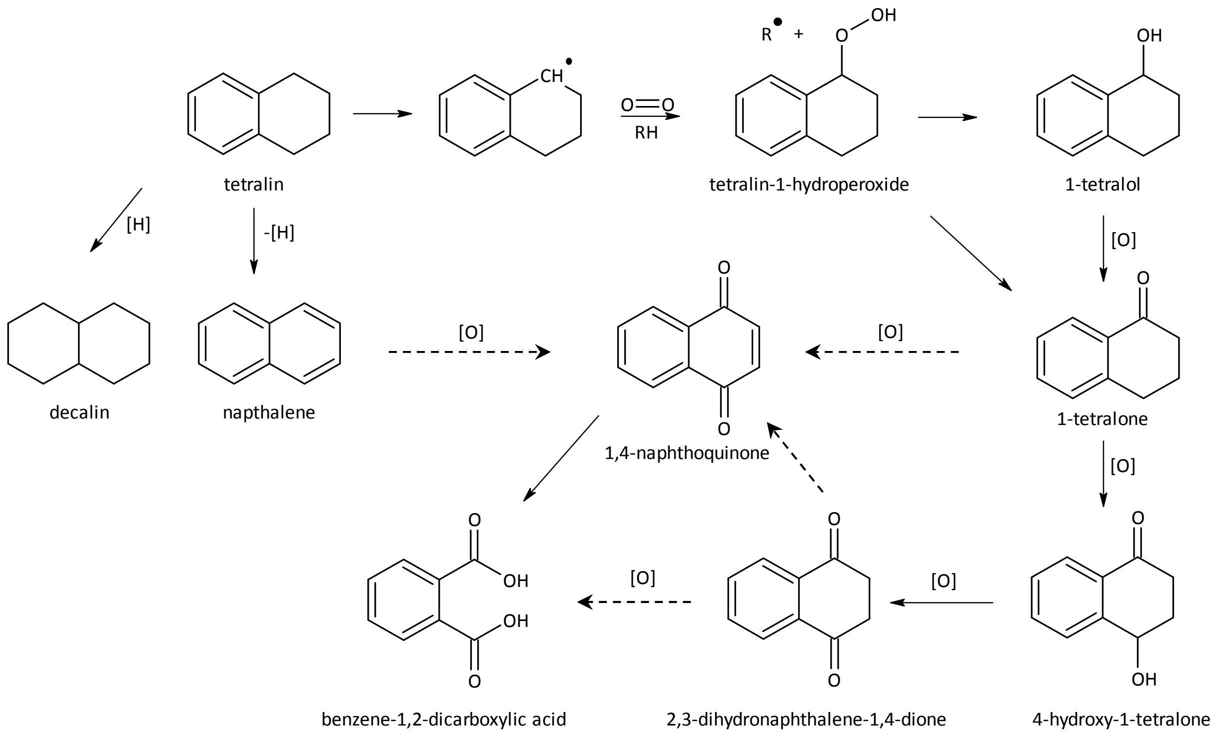

Figure 6.29: Suggested major reaction pathway for the oxidation of tetralin

For clarity other species such as 3,4-dihydronapthalene-1,2-dione have been omitted. All species in the above diagram were observed by GC, although some only in small quantities. Early on 1-tetralol and 1-tetralone were observed while after 24h additional naphthalene, benzene-1,2-carboxylic acid and 1,4-napthoquinone were present in significant quantities. The increase of the concentration of the latter preceded formation of excess naphthalene. The dashed arrows show possible pathways while those with solid arrows have been confirmed. 1,4-Naphthoquinone converts to 2,3-benzenedicarboxylic acid (o-phthalic acid) with the loss of CO, ring opening and subsequent oxidation (*134*). It is known that 1,4-naphthoquinone can be formed by the hydroxylation of naphthalene to 1,4-naphthol which can in turn be converted to 1,4-naphthoquinone. The oxidative conversion of 4-hydroxy-1-tetralone to o-phthalic acid has been observed as a viable pathway in bacteria (*135*). Peaks consistent with all of the oxygenates in Figure 6.29 have been observed in the ESI-MS spectra, in particular those for 1,4-naphthoquinone and o-phthalic acid. A peak at 149 was observed in the ESI-MS(+) which is consistent with phthalic anhydride which has been observed when pure tetralin is oxidised. It was, however, not observed in GC analysis in the current study. The initial stages of tetralin oxidation have been updated to include the observation that tetralol does oxidise directly to tetralone as shown by the higher tetralone concentration in 24h flowing air stress tests.

It is suggested that naphthalene is formed by the dehydrogenation of tetralin. Tetralin, decalin and naphthalene are known to be involved in hydrogen transfer reactions (*92*).

The formation of alkyl tetralins, 1-ethyl tetralin and 1-propyl tetralin, was slower than the tetralin oxygenates, 1-tetralol and 1-tetralone, as these were detected only after 3h. After 24h, longer chain alkyl tetralins, which were not seen in QCM experiments, could also be observed. It is suggested that these form via the reaction of tetralin radicals with longer chain alkenes, similar to the pathway set out in Figure 6.25.

Shorter and longer chain as well branched alkanes were observed to form with time and at greater concentrations than in QCM experiments. The formation of shorter alkanes and alkenes can be ascribed to greater radical initiated cracking of *n*-hexadecane in an unlimited oxygen-containing atmosphere. Longer and branched alkanes would be formed by the reaction of alkenes, such as ethene and 1-propene, with alkyl radicals.

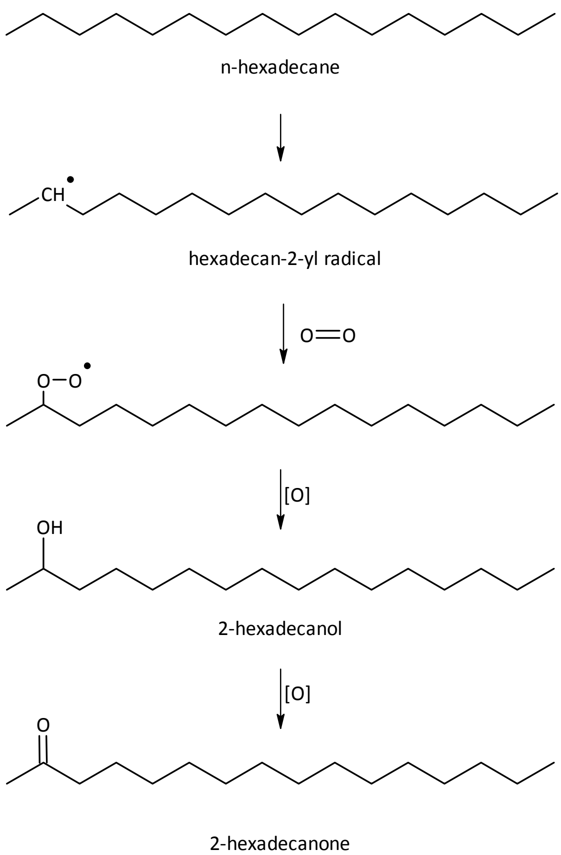

Figure 6.30: Suggested pathway for the formation of C16 oxygenates.

Further evidence of the greater extent of oxidation is the presence of hexadecanones, acids and esters, over and above hexadecanols which were observed in systems stressed in the QCM. These oxygenates were primarily the result of oxidation at the 2-position as illustrated in Figure 6.30. Where oxygen was limited (QCM experiments), oxygenation did not proceed to the formation of hexadecanone.

The epoxide, hexadecyl oxirane, which was observed after 24h stressing is suggested to form from the reaction of oxygen with hexadecanyl radicals.

Interestingly, in systems that did not contain decalin (DMC-A), decalin was identified after 24h. The exact mechanism of decalin formation is unclear but it may be via tetralin disproportionation to naphthalene and decalin (*93*).

Decalin oxidised more slowly than tetralin. Alcohols were observed after 4-5h. The formation of the octahydronaphthalen-4a(2*H*)-ols before 1-decalol and 2-decalol suggests that the hydrogen atoms attached to the carbon atoms where the cyclohexane rings meet are more labile. Jaffe *et al.* (*98*) also observed oxidative attack on decalin at all positions. They too found octahydronaphthalen-4a(2*H*)-ol to constitute the largest fraction of decalin alcohols formed.

A pathway which explains the formation of decalin oxygenates is provided in Figure 6.31. The pathway bears strong similarities to that of tetralin (Figure 6.29).

2-Decalone has been omitted because it forms in very small quantities. Further oxidation leads to the formation of decalones, octahydronapthalene-4-hydroxy-1-one (omitted above for clarity), diones and ultimately to benzene-1,2-dicarboxylic acid after ring opening of the cyclic 1,4-dione. The presence of benzene-1,2-dicarboxylic acid has not been reported in decalin oxidation schemes before. Such species could be identified in the ESI-MS spectra of DMC-B after flask oxidation for 24h.

In oxygen-limited systems such as in the QCM, oxidation did not proceed as far as the formation of decalones which were not observed.

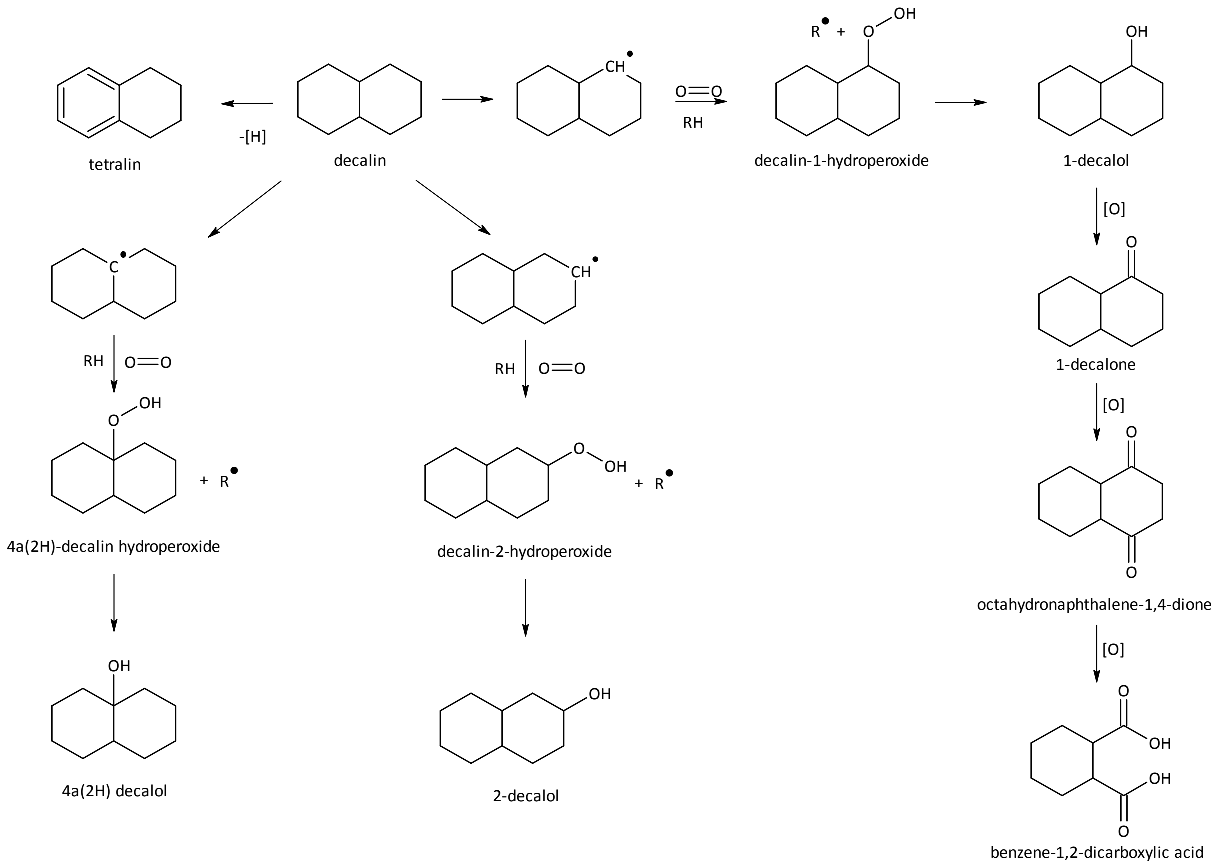

Figure 6.31: Suggested reaction pathway for the oxidation of decalin

Effect of phenols on the thermo-oxidative stability of diesel model compound systems

Oxidation of tetralin by BHT was observed to be inhibited after 6h. After 24h, BHT was no longer present and similar species were found as when BHT was not present.

Phenol did not display any antioxidant behaviour. Phenol did appear, however, to promote the formation of larger quantities of 1-tetralol and 1-tetralone. It can be speculated that the earlier formation of alkyl tetralins may suggest that phenol promotes the formation of tetralin radicals. Investigations of why this might be so were deemed beyond the scope of this study.

Diesel/biodiesel model compounds

The presence of unlimited oxygen led to the formation of far more degradation products than was observed in QCM experiments. These were both of lower and higher molecular weight than the esters present before oxidation. A variety of acids, ketones, aldehydes and epoxides were observed.

Large quantities of the aldehydic ester, methyl 9-oxononanoate, were observed, particularly after the stressing of systems containing methyl linoleate and methyl linolenate. After the stressing of methyl oleate, epoxides (oxiranes) and 9,10 diols could be seen.

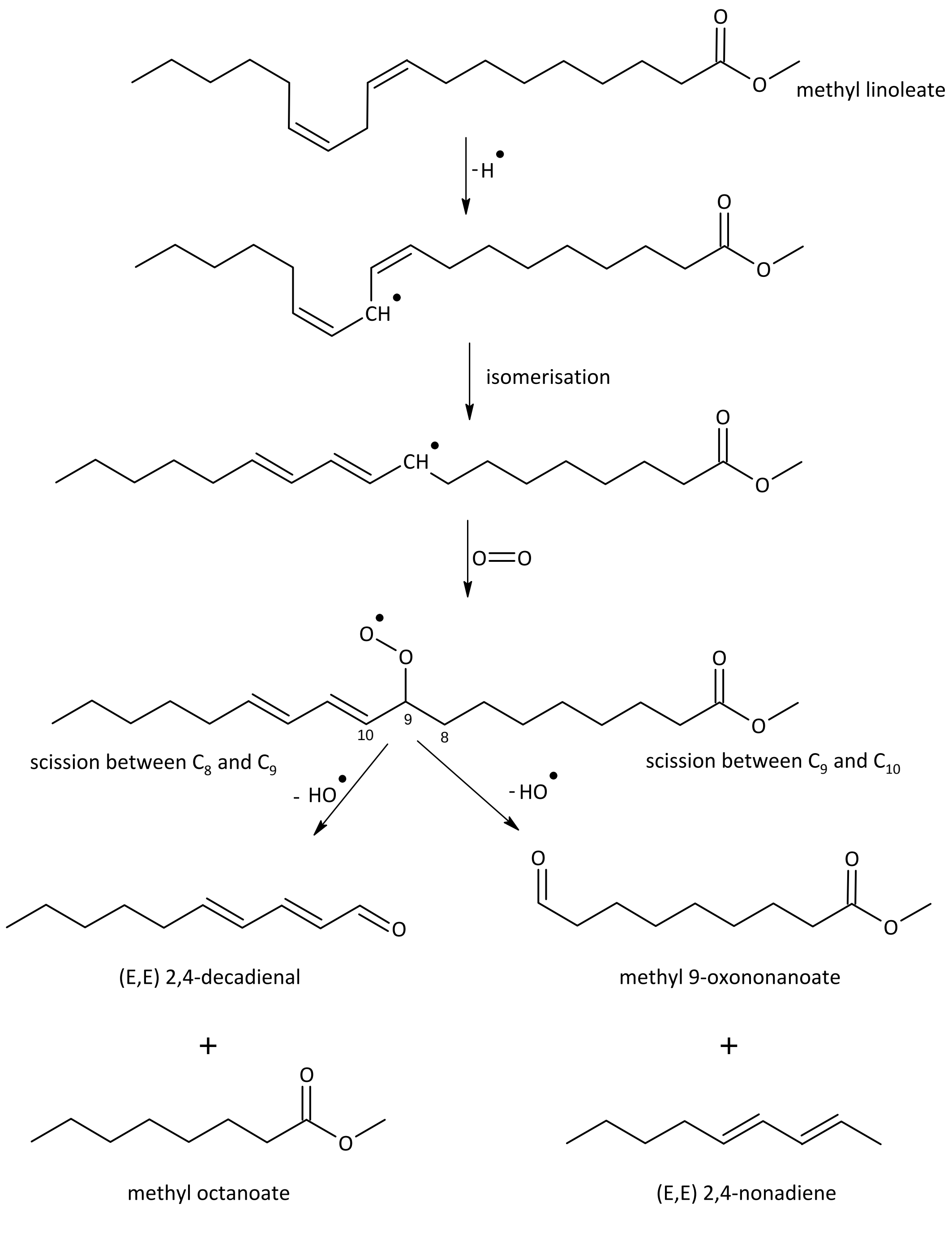

Figure 6.32: Oxidation of methyl linoleate: Suggested reaction pathway

A pathway for the degradation of methyl linoleate is suggested in Figure 6.32. This pathway explains the formation of methyl 9-oxononanoate. It also allows for the formation of (E,E) 2,4-decadienal which was observed in pre-stressed RME as well as stressed methyl linoleate blends. It should be noted that methyl linoleate has a *cis* orientation at the double bonds while the double bonds are *trans* in (E,E) 2,4-decadienal. This is consistent with the isomerisation step that has been proposed (*23*).

An analogous pathway can be developed for the oxidation of methyl linolenate.

C8-C12 aliphatic esters were observed in small quantities which is consistent with the left hand pathway. C5-C9 dienes were also observed after extended oxidation, consistent with the right hand pathway. Methyl 9-oxononanoate could not be formed from methyl oleate since it cannot undergo the isomerisation step in Figure 6.32.

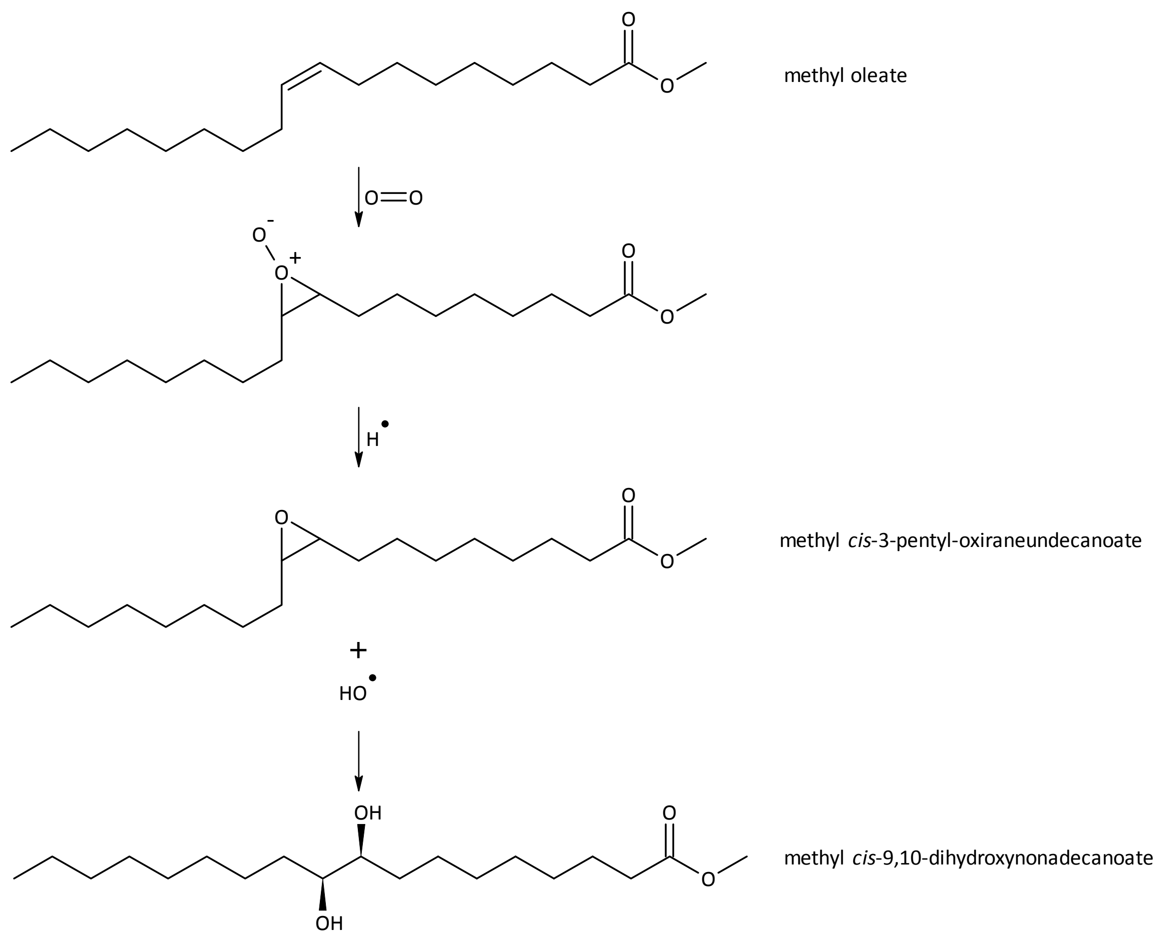

Figure 6.33: Suggested pathway for the formation of epoxides and diols from methyl oleate

These species were also observed in QCM stressing experiments, indicating yet again that polyunsaturated methyl esters are easily oxidised. A similar mechanism can be developed for the attachment of the hydroperoxide at C13. A similar process can be applied to methyl linolenate.

Not only was methyl oleate observed to break down into smaller molecules but significant quantities of methyl *cis*-3-pentyloxiraneundecanoate were also observed after extended stressing of systems containing methyl oleate. Methyl *cis*-9,10-dihydroxynonadecanoate was also observed. The pathway in Figure 6.33 illustrates this oxidation pathway.

A few interesting products were observed such as (Z,Z) 9-hexadecenyl 9-hexadecenoate acid. 9-Hexadecenoic acid is palmitoleic acid which is a C16 analogue of oleic acid. This suggests that ester hydrolysis and reformation is occurring.

When biodiesel model compounds were added to diesel model compounds, the thermo-oxidative stability of the final blends deteriorated. Diesel model compound products that were only detected after three or five hours in the absence of FAME were detected after one hour in blends. Examples include 1, 4-naphthoquinone and 2-hexadecanol which were detected after the first hour. Some products such as decalin oxygenates that were not formed in the diesel model system (DMC-A) were detected after blend flask oxidation. This indicates blending can affect the kinetics of the formation of degradation products.

Significant amounts of FAME-derived aldehydes were detected in the first 6h but not after 24h. Because the quantity of acidic species (particular C9 and C10 acids) increased with time, it is suggested that these aldehydes were oxidised to acids.

Diesel model compound/FAME blends

Significant quantities of epoxides and long chain methyl esters (> 20 carbon atoms) were detected as soon as 2h after stressing had begun. 1-Tetralol and 1-tetralone were observed after 1h, rather than after 2h in the absence of FAME. They were also formed in greater quantities in the early stage of oxidation. The mechanism underlying this is unclear but may be because acidic decomposition products of FAME catalyse tetralin oxidation.

Oxidation of various blends (model compounds and RME) suggest that the processes: a) thermolytic cracking, b) hydrolysis (formation of acids) and c) the formation of oxygenated products which are proposed to occur in lipid oxidation occur here too (*85*,*86*,*84*,*87*). Evidence is provided by a) the presence of fatty acids b) the presence of a variety of acids including those derived from the FAME model compounds, and c) the variety of aldehydes and oxiranes mentioned previously.

ESI-MS spectra revealed that dimers of methyl esters were formed during QCM oxidation. Most of these dimers contained ketone functional groups. The ESI-MS(+) spectra suggested that RME, methyl oleate and methyl linoleate contained, on average, 3 ketone groups. The oxidation of methyl linolenate produces, on average, four such groups. This is consistent with the higher reactivity of methyl linolenate (*78*). These species are likely precursors of deposits.

Severe oxidation in an open flask under flowing air at 140^{o}C produced a further set of high molecular weight compounds between m/z 450 and 600. The structures of these are unknown at this stage but it is possible that they are long chain esters of FAME molecules. For instance, 9-(Z)-hexadecenyl-9-(Z)-hexadecenoate, which has a molecular weight of 476.8 g mol^{-1}, was observed by GC-MS. This species is formed from palmitoleic alcohol and palmitoleic acid. Palmitoleic acid is the C16 analogue of methyl oleate. 9-(Z)-Octadecenyl-9-(Z)-octadecenoate which could be formed from methyl oleate has a molecular mass of 532.8 g mol^{-1} which is in the range of these other high molecular weight species formed. Oxidation will provide shorter chain fatty acids which may provide the necessary species. ESI-MS(-) spectra of oxidised RME reveal significant quantities of fatty acids which could allow for the formation of such species.

Furanones have been postulated as contributors to deposit formation (*11*). These were observed in some DMC-A/biodiesel model compound systems. Their concentrations, however, were small. Investigations into their effect was deemed outside the scope of this investigation.

Revelation of these structures will require further research which was beyond the scope of this study. One approach to tackle this would be to use tandem ESI-MS-MS where the parent ion is broken down into fragment ions in the second step which can be used for identification.

6.4 Conclusions

6.4.1 QCM oxidation

In experiments involving diesel model compounds, oxidation products included ketones, aldehyde, acids, and alcohols.

In all diesel model compounds, autoxidation followed the initial formation radicals and the hydroperoxides. Products formed in addition to acids, ketones and alcohols were lower and higher molecular weight alkane/alkene esters as well as cross products formed by reactions of acids and alcohols. Lower alkanes/alkenes products were formed by the cracking of hexadecyl radicals while higher alkene/ alkane products were addition products. Alkyl tetralins are suggested to form from 1-tetralyl radicals, and small olefins formed by the cracking of hexadecane.

Blending biodiesel with diesel model compounds deteriorates the stability of the final blends. More oxidation products were formed in blends than diesel model compounds or biodiesel individually. Oxidation products that formed were dependent on the initial amount of the starting components.

6.4.2 Flask oxidation

Oxidation brought on compositional changes over time. The oxidation products formed were distinctive to the specific model compounds used. DMC-C and DMC-B had the same model compounds hence similar products, albeit that species derived from tetralin, were lower in concentration for DMC-C because DMC-C contained less tetralin to start with.

Oxidation started immediately after the experiment was initiated. Primary products were similar to those formed during QCM oxidation but greater amounts and more types of oxygenates were detected due to unlimited oxygen supply during flask oxidation. Tetralin and *n*-hexadecane were more vulnerable to oxidation than decalin and naphthalene.

Compared to tetralin which was reactive in two positions (α abd β), decalin was reactive in all positions hence a variety of isomers was observed. However, the rate of reaction was much lower.

ESI-MS(+) of highly stressed fuel containing tetralin indicated the primacy of the species 1,4-naphthalenedione. Furthermore cracked ketones could be identified as well as possible hexadecanyl esters. Compounds in the upper and lower layers are very similar with the exception that very high molecular weight species are absent from the upper layer.

BHT protected fresh biodiesel against extensive oxidation when thermo-oxidative experiments were performed at 100^{o}C. However, BHT did not offer complete protection from oxidation at 140^{o}C due to thermal decomposition and consumption of the antioxidant at this temperature.

BHT showed a positive effect (inhibition) on stability during flask oxidation. Phenol instead showed a negative effect (promotion of fuel instability) on stability during flask oxidation. It is possible that phenols caused instabilities in the fuel by forming SMORS (*22*). These results were consistent with the results observed with fuel doped with phenol. Although phase separations in stressed blends were slightly reduced in blends with phenol, oxidation was initiated earlier than in blends without phenols.

In biodiesel/diesel model compound blends, higher molecular mass cross products form in addition to cross products observed in diesel model compounds alone. These were formed through acid-alcohol reaction and alcohol condensation reactions. Blending deteriorated the thermo-oxidative stability even further. Products that were not observed in diesel or biodiesel were present in diesel/biodiesel blends. Aldehyde products formed during flask oxidation were involved in other reactions to form secondary products or cross products.

The mechanistic steps proposed are very similar to mechanisms proposed in literature. However, several mechanisms needed to be extended or have different aspects combined. Due to unlimited air supply during flask oxidation, oxidation in biodiesel/diesel model compounds led to much more highly oxidised species than QCM oxidation. As an example, tetralin was oxidised further to form a dicarboxylic acid and naphthoquinone which were not observed during QCM oxidation.

7. Conclusions

With the exception of four exploratory experiments by Kaminuza (*100*), this study represents the first rigorous application of the QCM methodology to the thermo-oxidative degradation of FAMEs and blends containing FAMEs. The quantity of mass accumulated (deposits formed) exceeded what is typical for middle distillates (*11*,*20*,*28*,*99*). The QCM could be used to elucidate effects such as that of the degree of FAME saturation and diesel composition.

Of the compounds, present in diesel and those tested, tetralin appeared to be the most significant for deposit formation. A variety of oxidised species were detected by GC/MS for both QCM and open flask oxidation experiments. It is possible that these species, in particular 1,4-naphthoquinone, may go on to form deposits via a SMORS mechanism (*22*). ESI-MS spectra did not reveal any definitive proof of SMORS precursor species. Furthermore, no conclusive evidence was observed for reactions between FAME and diesel model compound degradation products. It was not possible to identify Diels-Alder products which suggest that this route to deposits is minor. The interaction between these two fuel systems was indirect with FAME breakdown products appearing to promote the oxidation of tetralin.

The model compound approach greatly simplifies product analysis but it must be stressed that other factors such as the effect of olefins and naphthalenes in diesel have not been explored. Furthermore, the effect on deposition of blocking the α position in tetralin would be worthy of further study. The effect of FAME (poly)unsaturation on deposit formation was demonstrated in oxygen limited environments, *i.e.* in the QCM. The trends were, however, consistent with previous observations in open systems and those performed here.

Preliminary experiments have demonstrated that the QCM has the potential to evaluate the efficacy of antioxidants. Not only does the test provide information such as oxygen consumption like the Petroxy^{TM} (*35*), and hence FAME degradation, but it also provides information on actual deposit formation and whether antioxidants have an effect here, too.

It was apparent that the extent of oxidation in accelerated tests performed under flowing air far exceeded that in the QCM. In particular, FTIR and UV-Vis spectroscopy demonstrated very slight changes to the fuel composition during oxidation in the QCM, yet deposits were noted. This was despite highly oxidised species not been identifiable by GC-MS for QCM oxidised fuels although mono-oxidised species, such as 1-tetralone, were observed in both QCM and open flask systems. This, again, points to the use of a QCM being more representative of real-life situations, in particular those that occur in diesel fuel injectors. After extended periods of exposure, fuels exposed to flowing air at high temperatures were prone to phase separate.

It was demonstrated that fuel composition and its effect on solvency are very important. Importantly the addition of unstressed FAME and aromatics solubilised deposits that had already formed by increasing fuel polarity. Deposits are polar in nature as a result of the incorporation of oxygen. Evidence for this was provided by FTIR spectroscopy. This has implications for the dissolution/loosening of tank deposits which has been observed after the addition of FAME in the commercial market. However, it needs to be stressed that the addition of these components increased deposits when they themselves were stressed. The solvency experiments also suggest that the blending of small quantities of FAME may lead to increased deposits when the blended fuel is oxidised. This is primarily the effect of lower solvency because of lower fuel polarity but oxygen uptake in the QCM and the faster formation of oxygenated products (seen in GC analyses) suggest that increased reactivity must also play a role. ESI-MS(+) provided evidence that high molecular weight species phase separated into a lower layer in the case of flask stressed diesel model compounds.

Existing mechanisms for fuel components have been confirmed and in some cases extended. In particular it has been observed that both tetralin and decalin are able to be oxidised to 1,2-dicarboxylic acids. In the former case, this is likely via the formation of 1,4-naphthoquinone. Evidence was provided for the isomerisation of polyunsaturated FAMEs. While the FAME constituents have *cis* double bonds, conjugated *trans* (E,E) decomposition products were observed. Cleavage of FAME molecules occurred adjacent to the double bonds as the result of initial attack at allylic and *bis*-allylic carbons. Evidence from GC and ESI-MS, in particular, indicated the formation of dimers and trimers. It is this increase in molecular weight that gives rise to deposits. A different set of high molecular weight species to the dimers was identified by ESI-MS(+) of FAME blends stressed at 140^{o}C under flowing air. Their structure remains unknown at this stage.

Experiments in the QCM with the addition of acids does suggest that the uptake of oxygen is not synonymous with deposit formation and caution needs to be taken with oxygen uptake measurements, where FAME is present, when predicting ultimate quantity of deposits formed.

8. Recommendations

Because of the limited scope of this study and based on findings reported in this dissertation, a number of recommendations are made for future investigations. These are:

- The diesel model compounds used were restricted to decalin, *n*-hexadecane and tetralin. A broader range of compounds, including aromatic species, could be explored. This would shed light on the observations made by DeWitt *et al.* (*11*). These should include naphthalene which may be responsible for the formation of the possible SMORS precursor, 1,4-naphthoquinone. The use of 1,4-dialkyl tetralins could shed light on whether tetralin is more important than naphthalene as a SMORS/deposit precursor. The use of 100% paraffin (including blends containing cycloparaffins) should be investigated. Olefinic diesel would be of interest because of the presence of double bonds. In particular investigations of the presence of conjugated dienes could be explored. Results should ultimately be compared to experiments using full boiling point range diesels of different compositions. This can readily be performed using a QCM.
- In order to investigate mechanistic effects further, key intermediates such as 1-tetralone and 1,4-naphthoquinone could be added to systems that don't contain tetralin. Their effect on deposition in QCM experiments would be of interest. A range of concentrations should be investigated. Furthermore their oxidation might be explored on their own.
- Different model FAME compounds could be used in future to expand the investigation into thermo-oxidative stabilities. Saturated FAMEs, such as methyl palmitate (16:0), can be used in biodiesel model compounds to represent unsaturated groups in biodiesel. A pertinent question is whether the presence of an ester group influences deposition as the alkyl chain part of methyl palmitate is very similar to *n*-hexadecane. A wide range of different model compounds would provide comprehensive information about the reactions taking place in the actual fuel.
- In this study, only neat RME was study in the QCM. Other FAMEs such as SME should be considered for investigation.

- Interesting effects were seen when BHT and phenol were added and the doped fuels explored by QCM. Other precursors, which have been implicated in SMORS formation, such as carbazoles, pyrroles, anisoles, thiols and thiophenes could be tested in the QCM to test the SMORS mechanism as well as their effect on blends containing FAME. In the same vein, the effect of other antioxidants of different classes, such as phosphites and quinolones, could be investigated.
- The influence of acids was explored in a cursory fashion in this study because a detailed study was deemed out of scope. The addition of acid was observed to reduce deposits from FAME blends. This, though, was at a high concentration of acid. A more detailed investigation of acids, including acid molecular weight, structure (including conjugated acids such as maleic acid) and their concentration could reveal insights into the quantity of deposit formation, and the effect on reactions of hydro-peroxides. Importantly this investigation should look at acid effects in combination with different FAME model compounds.
- QCM experiments were oxygen-limited. Oxygen concentrations could be varied. Of interest would be experiments on FAME systems in which the head space was solely nitrogen. A comparison of a system in which the fuel was oxygenated and deoxygenated when compared with the results seen here would be of interest. The decomposition of FAMEs is strongly tied to the presence of oxygen. However, it is possible that double bond isomerisation can occur under the application of heat only. The effect of this on deposit formation would be of interest. Oxygen concentration experiments with tetralin-containing systems would also be of interest. This could investigate whether tetralin, as well as decalin and naphthalene, prevent radical formation and thus lower deposition.
- High molecular weight compounds, formed in the QCM and in flask studies, should be isolated by gel permeation chromatography (GPC). Modern GPC columns have resolution in the 100-1000 amu range. It would be interesting to see what effect different compositions and oxygen concentrations have on the molecular weight of deposit precursors. After separation these precursors should be characterised by ^{1}H-NMR and ^{13}C-NMR. This would be novel in the case of diesel model compound systems and would complement ESI-MS data obtained in this study. The application

of other techniques such as matrix-assisted laser desorption/ionisation-mass spectrometry (MALDI-MS) to deposits formed on the QCM crystals could be considered.

- The use of tandem techniques should be considered. These could be ESI-MS-MS in which a higher voltage ionisation is used to fragment ions formed during the first step. By use of an MS spectral library, this could provide more information about molecular structure. HPLC-MS could be used to better separate species so as to simplify individual ESI-MS spectra. This would reduce matrix effects which are reported to be significant for phenolic species (*131*).
- A broader range of solvency experiments should be considered, especially in the QCM. These would look at the combination of FAMEs with diesel model compounds of different composition, *e.g.,* highly paraffinic systems. The influence of cycloparaffins on solvency would also be of interest. All results should be compared to commercial petroleum diesel, with and without deposit control additives.
- The unexpectedly high mass accumulation seen for BHT-containing systems, tested at 100^{o}C in the QCM should be more fully explored. This could be done with a broader range of temperatures and antioxidant concentrations.
- Specific investigations of fuel viscosity were beyond the scope of this dissertation. It is recommended that changes, brought upon by fuel deterioration, be investigated. They should be compared and, where possible, correlated with fuel deposition.
- A study of the initiation processes was beyond the scope of this dissertation. These have been studied in detail in flask oxidation studies. All QCM experiments were analysed at the completion of each run (24h). It is recommended that a series of QCM experiments be performed on system DCM-A (neat) and a DCM-A/methyl linoleate blend for shorter time periods. These time periods should include the stage in which the mechanism of deposit formation appears to change, as evidenced by a change in slope in the mass accumulation curve. Analysis by ESI-MS in particular would reveal whether polymerisation reactions occur while peroxy radicals are still present or require the absence of peroxy radicals after oxygen has been completely depleted.

- Initiation of autooxidative processes by peroxy radicals has been well studied. However, the formation of these species in QCM reactions could be further studied by stopping QCM reactions after shorter time periods when oxygen would still be present.
- This study was the first study of its kind to investigate FAME oxidation in a QCM. It clearly demonstrates the potential for this technique. To relate QCM experiments to real world diesel injectors, it is recommended that QCM data be compared to deposit formation in a fuel flow rig.
- Now that the suitability of the QCM has been established, it is recommended that its potential for the used of the study of antioxidants at a range of concentrations and temperatures be made.

9. References

1. Çengel, Y. A.; Boles, M. A. *Thermodynamics: an engineering approach,* 5th ed.; McGraw-Hill: New York, NY, 2011.

2. Deligianis, A.; Anastasakos, A.; Anastopoulos, G.; Dodos, G. S.; Zannikos, F. Effectiveness of various phenolic compounds (commercial and non-commercial) on biodiesel oxidation stability. *SAE Technical Paper Series* **2013**, *2013-01-1128*.

3. Tan, K. T.; Lee, K. T. Biodiesel production in supercritical fluids. In *Biofuels: alternative feedstocks and conversion processes;* Pandey, A., Larroche, C., Ricke, S. C., Dussap, C. G., Gnansounou, E., Eds.; Academic Press: Oxford, UK, 2011; pp 339-352.

4. Basha, S. A.; Gopal, R.; Jebaraj, S. A review on biodiesel production, combustion, emissions and performance. *Renew. Sustain. Energy Rev.* **2009**, *13*, 1628-1634.

5. Chen, Y.-F.; Wu, Q. Production of biodiesel from algal biomass: current perspectives and future. In *Biofuels: alternative feedstocks and conversion processes;* Pandey, A., Larroche, C., Ricke, S. C., Dussap, C. G., Gnansounou, E., Eds.; Academic Press: Oxford, UK, 2011; pp 399-413.

6. Lam, M. K.; Lee, K. T. Production of biodiesel using palm oil. In *Biofuels" alternative feedstocks and conversion processes;* Pandey, A., Larroche, C., Ricke, S. C., Dussap, C. G., Gnansounou, E., Eds.; Academic Press: Oxford, UK, 2011; pp 353-373.

7. Singh, S. P.; Singh, D. Biodiesel production through the use of different sources and characterization of oils and their esters as the substitute of diesel: A review. *Renew. Sust. Energy Rev.* **2010**, *14*, 200-216.

8. Huynh, L.-H.; Kasim, N. S.; Ju, Y.-H. Biodiesel production from waste oils. In *Biofuels: alternative feedstocks and conversion processes;* Pandey, A., Larroche, C., Ricke, S. C., Dussap, C. G., Gnansounou, E., Eds.; Academic Press: Oxford, UK, 2011; pp 375-396.

9. *ASTM D975-14a: Standard specification for diesel fuel oils;* ASTM International: West Conshohocken, PA, 2014.

10. Batts, B. D.; Fathoni, A. Z. A literature review on fuel stability studies with particular emphasis on diesel oil. *Energy & Fuels* **1991**, 5, 2-21.

11. DeWitt, M. J.; West, Z.; Zabarnick, S.; Shafer, L.; Striebich, R.; Higgins, A.; Edwards, T. Effect of aromatics on the thermal-oxidative stability of synthetic paraffinic kerosene. *Energy & Fuels* **2014**, *28*, 3696-370.

12. Commodo, M.; Fabris, I.; Groth, C. P. T.; Gulder, O. L. Analysis of aviation fuel thermal oxidative stability by electrospray ionization mass spectrometry (ESI-MS). *Energy & Fuels* **2011**, *25*, 2142-2150.

13. Pullen, J.; Saeed, K. An overview of biodiesel oxidation stability. *Renew. Sustain. Energy Rev.* **2012**, *16*, 5924-5950.

14. Baer, F.; Schmidt, L.; Schaper, K.; Fan, Z.; Eskiner, M.; Staufenbiel, J.; Geiser, J.; Schilde, B.; Bornschlegel, B.; Krahl, J. Ageing of biodiesel. *6th International Conference on Biodiesel*, Berlin, 2013.

15. Reddy, K. T. *PhD Thesis: Thermal stability of distillate hydrocarbon fuels;* Drexel University: Philadelphia, PA, 1987.

16. Hartikka, T.; Kiiski, U.; Kuronen, M.; Mikkonen, S. Diesel fuel oxidation stability: A comparative study. *SAE International* **2013**, *2013-01-2678*.

17. Natarajan, E. Stability studies of biodiesel. *Int. J. Energy Sci.* **2012**, 2, 152-155.

18. Chuck, C. J.; Bannister, C. D.; Jenkins, R. W.; Lowe, J. P.; Davidson, M. G. A comparison of analytical techniques and the products formed during the decomposition of biodiesel under accelerated conditions. *Fuel* **2012**, *96*, 426-433.

19. Focke, W. W.; Van der Westhuizen, I.; Grobler, A. B.; Nshoane, K. T.; Reddy, J.; Luyt, A. S. The effect of synthetic antioxidants on the oxidative stability of biodiesel. *Fuel* **2012**, *9*4, 227-233.

20. Sobkowiak, M.; Griffith, J.; Wang, B.; Beaver, B. Insight into the mechanisms of middle distillate fuel oxidative degradation. Part 1: on the role of phenol, indole, and carbazole derivatives in the thermal oxidative stability of Fischer-Tropsch/Petroleum jet fuel blends. *Energy & Fuels* **2009**, *23*, 2041-2046.

21. Kabana, C. G.; Botha, S.; Schmucker, C.; Woolard, C.; Beaver, B. Oxidative stability of middle distillate fuels. Part 1: Exploring the soluble macromolecular oxidatively reactive species (SMORS) mechanism with jet fuels. *Energy & Fuels* **2011**, *25*, 5145-5157.

22. Beaver, B.; Gao, L.; Burgess-Clifford, C.; Sobkowiak, M. On the mechanisms of formation of thermal oxidative deposits in jet fuels. Are unified mechanisms possible for both storage and thermal oxidative deposite formation for middle distillate fuels. *Energy & Fuels* **2005**, *1*9, 1574-1579.

23. Ogawa, T.; Kajiya, S.; Kosaka, S.; Tajima, I.; Yamamoto, M.; Okada, M. Analysis of oxidative deterioration of biodiesel fuel. *SAE Technical Paper Series* **2008**, *2008-01-2502*.

24. Paligová, J.; Joríková, L.; Cvengroš, J. Study of FAME stability. *Energy & Fuels* **2008**, *22*, 1991-1996.

25. Omori, T.; Tanaka, A.; Yamada, K.; Bunne, S. Biodiesel deposit formation mechanism and improvement of fuel injection equipment (FIE). *SAE Technical Paper Series* **2011**, *2011-01-1935*.

26. Fang, H. L.; McCormick, R. L. Spectroscopic study of biodiesel degradation. *SAE Technical Paper Series* **2006**, *2006-01-3300*.

27. *ASTM D7739-11 Standard practice for thermal oxidative stability measurement via quartz crystal microbalance;* ASTM International: West Conshohocken, PA, 2013.

28. Zabarnick, S. Studies of jet fuel thermal stability and oxidation using a quartz crystal microbalance and pressure measurements. *Ind. & Eng. Chem. Res.* **1994**, *33*, 1348-1354.

29. *Biodiesel: handling and use guidelines,* 3rd ed.; US Department of Energy: Oak Ridge, TN, 2006.

30. Aksoy, P.; Gul, O.; Cetiner, R.; Fonseca, D. A.; Sobkowiak, M.; Falcone-Miller, S.; Miller, B. G.; Beaver, a. B. Insight into the mechanisms of middle distillate fuel oxidative degradation. Part 2: On the relationship between jet fuel thermal oxidative deposit, soluble macromolecular oxidatively reactive species, and smoke point. *Energy & Fuels* **2009**, *23*, 2047-2051.

31. Nicolaou, K. C.; Snyder, S. A.; Montagnon, T.; Vassilikogiannakis, G. The Diels–Alder reaction in total synthesis. *Angew. Chem. Int. Ed.* **2002**, *41*, 1668-1698.

32. Miccichè, F.; Van Straten, M. A.; Ming, W.; Oostveen, E.; Van Haveren, J.; Van Der Linde, R. Oxidation and oligomerization of ethyl linoleate under the influence of the combination of ascorbic acid 6-palmitate/iron-2-ethylhexanoate. *Appl. Catal. Gen.* **2006**, *29*7, 174-181.

33. Franck, C. E. *PhD thesis: Hydrocarbon autooxidation;* University of Cincinnati: Cincinnati, OH, 1949.

34. Sykes, P. *A guidebook to mechanism in organic chemistry,* 6th ed.; Longman Scientific & Technical: Harlow, 1986.

35. *ASTM 7545-14: Standard test method for oxidation stability of middle distillate Fuels — rapid small scale oxidation test (RSSOT);* ASTM International: West Conshohocken, 2014.

36. *EN 14112 Fat and oil derivatives—fatty acid methyl esters (FAME)—determination of oxidation stability (accelerated oxidation test);* European Committee for Standardisation: Brussels, Belgium, 2003.

37. Xin, Q. *Diesel engine system design;* Woodhead Publishing: Cambridge, UK, 2011.

38. Dec, J. E. Advanced compression-ignition engines—understanding the in-cylinder processes. *Proc. Comb. Inst.* **2009**, *32*, 2727-2742.

39. *European vehicle market statistics;* International Council on Clean Transportation:

Berlin, Germany, 2013.

40. SAPIA Future Fuels Working Group. *Petrol and diesel in South Africa and the impact on air quality;* SAPIA: Sandton, South Africa, 2008.

41. Bacha, J.; Freel, J.; Gibbs, A.; Gibbs, L. *Diesel fuels technical review;* Chevron: San Ramon, CA, 2007.

42. Simescu, S.; Ulmet, V.; Neely, G.; Khair, |. A novel approach for diesel NOX/PM reduction. *SAE Technical Paper Series* **2010**, *2010-01-0308*.

43. *Diesel vehicles and equipment: Environmental and public health impacts;* New Hampshire Department of Environmental Services: Concord, NH, 2014.

44. US Environmental Protection Agency. National clean diesel campaign. http://www.epa.gov/cleandiesel/basicinfo.htm (accessed Nov 04, 2014).

45. Lai, M.-C. D.; Dingle, P. J. *Diesel common rail and advanced fuel injection systems;* SAE Internationa: Warrendale, PA, 2005.

46. *An introduction to petroleum refining and the production of ultra low sulfur gasoline and diesel fuel;* International Council on Clean Transportation: Washington, DC, 2011.

47. Huhtala, K.; Vilenius, M. Study of a common rail fuel injection system. *SAE Technical Paper Series* **2001**, *2001-01-3184*.

48. Kitchen, T. Common rail diesel fuel systems, 2012. https://personel.omu.edu.tr/docs/ders_dokumanlari/894_52413_1913.pdf (accessed April 12, 2013).

49. Badock, C.; Wirth, R.; Fath, A.; Leipertz, A. Investigation of cavitation in real size diesel injection nozzles. *Int. J. Heat & Fluid Flow* **1999**, *20*, 538-544.

50. Velaers, A.; De Goede, S.; Woolard, C.; Burnham, R. Injector fouling performance and solubility of GTL diesel dosed with zinc. *SAE Int. J. Fuels Lubr.* **2013**, *6*, 276-288.

51. Payri, R.; Salvador, F.; Gimeno, J.; De la Morena, J. Study of cavitation phenomena based on a technique for visualizing bubbles in a liquid pressurized chamber. *Int. J. Heat & Fluid Flow* **2009**, *30*, 768-777.

52. Bannister, C. D.; Chuck, C. J.; Bounds, M.; Hawley, J. G. Oxidative stability of biodiesel fuel. *Proc. Inst. Mech. Eng., D: J. Auto. Eng.* **2011**, *225*, 99-114.

53. Durbin, T. D.; Miller, J. W.; Jiang, S. M. *Biodiesel fleet furability study;* California Air Resources Board: Riverside, CA, 2010.

54. Mitsuri, O.; Ebinuma, Y.; Sasaki, S.; Takashiba, T.; Takaki, Y.; Jetter, J. J.; Reinschmidt, U. Influence of base diesel fuel upon biodiesel sludge formation tendency. *SAE Technical*

Paper Series **2009**, *2009-01-0482*.

55. Sheehan, J.; Camobreco, V.; Duffield, J.; Graboski, M.; Shapouri, H. *An overview of biodiesel and petroleum diesel life cycles;* U.S. Department of Energy's National Renewable Energy Laboratory: Golden (CO), 1998.

56. *ASTM D6751: Standard specification for biodiesel fuel blend stock (B100) for middle distillate fuels;* ASTM International: West Conshohocken, PA, 2014.

57. *EN 14214 - Automotive fuels. Fatty acid methyl esters (FAME) for diesel engines;* European Committee for Standardisation: Brussels, Belgium, 2013.

58. Yaakob, Z.; Narayanan, B. N.; Padikkaparambil, S.; Unni K., S. a. A. P. . M.; Surya, U. K.; Mohamed, A. P. A review on the oxidation stability of biodiesel. *Renew. Sust. Energy Rev.* **2014**, *3*5, 136-153.

59. Freire, D. M. G.; de Sousa, J. S.; Cavalcanti-Oliviera, E. A. Biotechnological methods to produce biodiesel. In *Biofuels: alternative feedstocks and conversion processes;* Pandey, A., Larroche, C., Ricke, S. C., Dussap, C. G., Gnansounou, E., Eds.; Academic Press: Oxford, UK, 2011; pp 315-335.

60. Demirbas, A. Progress and recent trends in biofuels. *Progr. Energy & Comb. Sci.* **2007**, *3*3, 1-18.

61. Hoekman, S. K.; Broch, A.; Robbins, C.; Ceniceros, E.; Natarajan, M. Review of biodiesel composition, properties, and specifications. *Renew. Sust. Energy Rev.* **2012**, *16*, 143-169.

62. Hakka, M. H.; Glaude, P. A.; Herbinet, O.; Battin-Leclerc, F. Experimental study of the oxidation of large surrogates for diesel and biodiesel fuels. *Combustion & Flame* **2009**, *15*6, 2129-2144.

63. Shahid, E. M.; Jamal, Y. A review of biodiesel as vehicular fuel. *Renew. Sust. Energy Rev.* **2008**, *12*, 2484-2494.

64. Caprotti, R.; Bhatti, N.; Balfour, G. Deposit control in modern diesel fuel injection systems. *SAE Technical Paper Series* **2010**, *2010-01-2250*.

65. *Petroleum Products Act (120/1977): Regulations regarding the mandatory blending biofuels with petrol and diesel;* South African Department of Minerals and Energy Affairs: Pretoria, South Africa, 2012; Vol. 566, p 35623.

66. Zhu, Y. *MS Thesis: An experimental study on thermal stability of biodiesel fuel;* Syracuse Univeristy: Syracuse, NY, 2012.

67. Knothe, G. Analysis of oxidized biodiesel by 1H-NMR and effect of contact area with air. *Eur. J. Lipid Sci. Technol.* **2006**, *10*8, 493-500.

68. Berkhous, S. K. *PhD Thesis: Thermal oxidative stability of coal-based JP-900 jet fuel: Impact on selected physical properties;* Pennsylvania State University: State College, PA, 2007.

69. Ronghong, L.; Tavlarides, L. L. Thermal stability and decomposition of diesel fuel under subcritical and supercritical conditions. *J. Supercritical Fluids* **2013**, *75*, 101-111.

70. Adams, R. K.; Zabarnick, S.; West, Z. J.; Striebich, R. C.; Johnson, D. W. Chemical analysis of jet fuel polar, heteroatomic species via high performance liquid chromatography with electrospray ionization–mass spectrometric detection. *Energy & Fuels* **2013**, *27*, 2390-2398.

71. Heneghan, S. P.; Zabarnick, S. Oxidation of jet fuels and the formation of deposit. *Fuel* **1994**, *73*, 35-43.

72. Hui-Peng, L.; Jian, S.; Hua, Z.; Li, Z.; Yu-Tai, Q. Effects of phenols on the stability of FCC diesel fuel. *Petr. Sci. Technol.* **2009**, *27*, 486-497.

73. Hardy, D. R.; Wechter, M. A. Characterization of soluble macromolecular oxidatively reactive species (SMORS) from middle distillate diesel fuels: Their origin and role in instability. *Energy & Fuels* **1994**, *8*, 782-787.

74. Kerkering, S.; Koch, W.; Andersson, J. T. Influence of phenols on the oxidation stability of home Heating oils/FAME blends. *Energy & Fuels* **2015**, *in press*.

75. Botha, S. *PhD thesis: The effect of different aromatic compounds on the thermo-oxidative stability of paraffinic fuels;* University of Cape Town: Cape Town, South Africa, 2015 (ongoing).

76. Coetzee, J. *MSc dissertation: Quartz crystal microbalance investigations into the oxidation of diesel model compound systems;* University of Cape Town: Cape Town, 2015 (on-going).

77. Paligová, J.; Joríková, ; Cvengroš, J. Study of FAME stability. *Energy & Fuels* **2008**, *22*, 1991-1996.

78. Gunstone, F. *Fatty acid and lipid chemistry;* Blackie Academic and Professional: London, UK, 1996.

79. Bouaid, A.; Martinez, M.; Aracil, J. Long storage stability of biodiesel from vegetable and used frying oils. *Fuel* **2007**, *8*7, 2355-2373.

80. Knothe, G.; Dunn, R. O. Dependence of oil stability index of fatty compounds on their structure and concentration and presence of metals. *J. Am. Oil Chem. Soc.* **2003**, *80*, 1021-1026.

81. Dunn, R. O. Effect of antioxidants on the oxidative stability of methyl soyate (biodiesel). *Fuel Process Technol.* **2005**, *86*, 1071-1085.

82. Knothe, G. Some aspects of biodiesel stability. *Fuel Process Technol.* **2007**, *88*, 669-677.

83. Jain, S.; Sharma, M. Prospects of bidiesel from jatropha in India: a review. *Renew. Sust. Energy Rev.* **2010**, *14*, 761-771.

84. Frankel, E. N. Lipid oxidation. *Prof. Lipid Res.* **1980**, *19*, 1-22.

85. Kulkarni, M. G.; Dalai, A. K. Waste cooking oil - an economical source for biodiesel: a review. *Ind. Eng. Chem. Res.* **1996**, *45*, 2901-2913.

86. Cvengros, J. J.; Cvengrosová, Z. Used frying oils and fats and their utilization in the production of methyl esters of higher fatty acids. *Biomass Bioenergy* **2004**, *27*, 173-181.

87. Nawar, W. W. Chemical changes in lipids produced by thermal processing. *J. Chem. Ed.* **1984**, *6*1, 299-302.

88. Lazzari, M.; Chiantore, O. Drying and oxidative degradation of linseed oil. *Polym. Degrad. Stabil.* **1999**, *6*5, 303-313.

89. Muizebelt, W. J.; Hubert, J. C.; Neilen, M. W. F.; Klaasen, R. P.; Zabel, K. H. Crosslink mechanisms of high-solids alkyd resins in the presence of reactive diluents. *Progr. Org. Coating* **2000**, *40*, 121-130.

90. Zuleta, E. C.; Baena, L.; Rios, L. A.; Calderón, J. A. The oxidative stability of biodiesel and its impact on the deterioration of metallic and polymeric materials: a review. *J. Brazil. Chem. Soc.* **2012**, *23*, 2159-2175.

91. Chawla, B.; Keogh, R.; Davis, B. H. Conversion of tetralin to naphthalene during coal liquefaction: A coal rank phenomenon. *ACS Fuel Division*, New Orleans, 1987; pp 342-351.

92. Alemán-Vázquez, L. O.; Cano-Domínguez, J. L.; García-Gutiérrez, J. L. Effect of tetralin, decalin and naphthalene as hydrogen donors in the upgrading of heavy oils. *Procedia Engineering* **2012**, *42*, 532-539.

93. Robertson, A.; Waters, W. A. Some features of the autoxidation of tetralin. *Royal Soc. Chem.* **1945**, *4*2, 201-210.

94. Woodward, A. E.; Mesrobian, R. B. Low temperature autoxidation of hydrocarbons: The kinetics of tetralin oxidation. *J. Am. Chem. Soc.* **1953**, *7*5, 6189-6195.

95. Oehlschlaeger, M. A.; Shen, H. S.; Frassoldati, A.; Pierucci, S.; Ranzi, E. Experimental and kinetic modeling study of the pyrolysis and oxidation of decalin. *Energy & Fuels* **2009**, *23*, 1464-1472.

96. Kyungchan. Chae, A. V. Thermal decomposition of decalin: An ab initio study. *J. Org. Chem.* **2007**, *72*, 3179-3185.

97. Chae, K.; Violi, A. Thermal decomposition of decalin: An ab initio study. *J. Org. Chem.* **2006**, *7*2, 3179-3185.

98. Jaffe, F.; Steadman, T. R.; McKinney, R. W. Primary products of decalin autoxidation. *J. Am. Chem. Soc.* **1963**, *85* (3), 351–353.

99. Klavetter, E. A.; Martin, S. J.; Wessendorf, K. O. Monitoring jet fuel thermal stability using a quartz crystal microbalance. *Energy & Fuels* **1993**, *7*, 582-588.

100. Kaminuza, I. *MSc dissertation: Thermal and chemical analysis of carbonaceous materials: Diesel soot and diesel fuel reactor deposits;* University of Cape Town: Cape Town, 2013.

101. Hofstadler, S. A.; Bakhtiar, R.; Smith, R. D. Electrospray ionisation mass spectrometry. Part 1. Instrumentation and spectral interpretation. *J. Chem. Ed.* **1996**, *73*, 82-88.

102. Kujawinski, E. B.; Freitas, M. A.; Zang, X.; Hatcher, P. G.; Green-Chruch, K. B.; Jones, R. B. The application of electrospray ionization mass spectrometry (ESI MS) to the structural characterization of natural organic matter. *Org. Geochem.* **2002**, *33*, 171-180.

103. Rostad, C. E. Screening of polar components of petroleum products by electrospray ionization mass spectrometry. *Energy & Fuels* **2005**, *19*, 992-997.

104. Hughey, C. A.; Hendrickson, C. L.; Rodgers, R. P.; Marshall, A. G. Elemental composition analysis of processed and unprocessed diesel fuel by electrospray ionization Fourier transform ion cyclotron resonance mass spectrometry. *Energy & Fuels* **2001**, *15*, 1186-1193.

105. Catharino, R. R.; Milagre, H. M. S.; Saraiva, S. A.; Garcia, C. M. Biodiesel typification and quality control by direct infusion electrospray ionization mass spectrometry fingerprinting. *Energy & Fuels* **2007**, *21*, 3698-3701.

106. Cunha, I. B. S.; Fernades, A. M. A. P.; Tega, D. U.; Simas, R. C.; Nascimento, H. L.; de Sa, G. F.; Daroda, R. J.; Eberlin, M. N.; Alberici , R. M. Quantitation and quality control of biodiesel/petrodiesel (Bn) blends by easy ambient sonic-spray ionization mass spectrometry. *Energy 7 Fuels* **2012**, *26*, 7018-7022.

107. Tarvainen, M.; Suomela, J.-P.; Kallio, H. Ultra high performance liquid chromatography–mass spectrometric analysis of oxidized free fatty acids and acylglycerols. *Eur. J. Lipid Sci. Technol.* **2011**, *113*, 409-422.

108. Totten, G. E., Vestbrook, S. R., Shah, R. J., Eds. *Fuels and lubricants handbook: technology, properties, performance and testing;* ASTM International: West Conshohocken, PA, 2003.

109. Piedmont Biofuels. Solvency effects. http://www.biofuels.coop/education/resources/solvency-effects (accessed April 23, 2013).

110. Hansen, C. *Hansen solubility parameters: a user's handbook,* 2nd ed.; CRC Press: Boca Raton, FL, 2007.

111. Hunter, C. R. Arene-arene interactions: electrostatic or charge transfer. *Angew. Chem.* **2003**, *32*, 1584-1586.

112. Hughey, A. Carbon particulate and fuel filter plugging. http://esource.alstribology.com/WB020/eSource_Template/Carbon_Particulate.html (accessed April 12, 2013).

113. Osawa, M.; Eninuma, Y.; Sasaki, S.; Takashiba, T.; Takaki, Y.; Jetter, J. J.; Reinschmidt, Y. Influence of base diesel fuel upon biodiesel sludge formation tendency. *SAE Int. J. Fuels Lubr.* **2009**, *2*, 127-138.

114. Mushrush, G. W.; Willauer, H. D.; Bauserman, J. W.; Williams, F. W. Incompatibility of Fischer-Tropsch diesel with petroleum and soybean biodiesel. *Ind. Eng. Chem. Res.* **2009**, *48*, 7364-7367.

115. Dawar, S. Water contamination in fuel: cause and effect. http://www.afssociety.org/automotive/93-water-contamination-in-fuel-cause-and-effect (accessed January 30, 2014).

116. Jain, S.; Sharma, M. P. Review of different test methods for the evaluation of stability of biodiesel. *Renew. Sust. Energy Rev.* **2010**, *14*, 1937-1947.

117. Demirbas, A. *Biodiesel: a realistic fuel alternative for diesel engines;* Springer: London, 2008.

118. Dinkov, R.; Hristov, G.; Stratiev, D.; Aldayri, V. B. Effect of commercially available antioxidants over biodiesel/diesel blends stability. *Fuel* **2009**, *88*, 732-737.

119. Liang, F.; Lu, M.; Keener, T. C.; Liua, Z.; Khangb, S.-J. The organic composition of diesel particulate matter, diesel fuel and engine oil of a non-road diesel generator. *J. Environ. Monitoring* **2005**, *7*, 983-988.

120. Park, J.-Y.; Kim, D.-K.; Lee, J.-P.; Park, S.-C.; Kim, Y.-J.; Lee, J.-S. Blending effects of biodiesels on oxidation stability and low temperature flow properties. *Biores. Technol.* **2008**, *99* (5), 1196-1203.

121. Wilson, K.; Walker, J. Centrifugation techniques. In *Principles and techniques of practical biochemistry;* Cambridge University Press: Cambridge, UK, 2000; pp 263-273.

122. Coleman, M. M.; Selvaraj, L.; Sobkowiak, M.; Yoon, E. Potential satbilizers for jet fuels subjected to thermal stress above 400 ºC. *Energy & Fuels* **1992**, 535-539.

123. Muik, B.; Lendl, B.; Molina-Diaz, A.; Ayora-Cañada, M. J. Direct monitoring of lipid oxidation in edible oils by Fourier transform Raman spectroscopy. *Chem. Phys. Lipids* **2005**, *134*, 173-182.

124. Purcella, G. *Do it yourself guide to biodiesel: Your alternative fuel solution for saving money, reducing oil dependency, and helping the planet;* Ulysses Press: Berkeley, CA, 2007.

125. Balster, L. M.; Corporan, E.; DeWitt, M. J.; Edwards, J. T.; Ervin, J. S.; Graham, J. L.; Lee, S.-Y.; Pale, S.; Phelps, D. K.; Rudnick, L. R.; Santoro, R. J.; Schobert, H. H.; Scahfer, L. M. Development of an advanced, thermally stable, coal-based jet fuel. *Fuel Proc. Technol.* **2008**, *89*, 364-378.

126. Bamgboye, A. I.; Hansen, A. C. Prediction of cetane number of biodiesel fuel from the fatty acid methyl ester (FAME) composition. *Int. Agrophys.* **2008**, *22*, 21-29.

127. Youssef, R. S. Evaluation of antioxidants stability by thermal analysis and its protective effect in heated edible vegetable oil. *Ciência e Tecnologia de Alimentos* **2011**, *31*, 475-480.

128. Stein, S. E. Infrared spectra in NIST Chemistry WebBook, NIST Standard Reference Database Number 69. http://webbook.nist.gov (accessed Jan 18, 2015).

129. Cowie, J. M. G.; Arrighi, V. *Polymers: chemistry and physics of modern materials,* 3rd ed.; CRC Press: Boca Raton, FL, 2007.

130. Tsang, W.; Cui, J. P. Homogeneous gas-phase decyclization of tetralin and benzocyclobutene. *J. Am. Chem. Soc.* **1990**, *112*, 1665-1671.

131. Alberti-Dér, Á. *PhD dissertation: LC-ESI-MS/MS methods in profiling of flavonoid glycosides and phenolic acids in traditional medicinal plants: Sempervivum tectorum L. and Corylus avellana L.;* Semmelweis University: Budapest, Hungary, 2013.

132. Bounaceur, R.; Scacchi, G.; Marquaire, P.-M.; Dominé, F.; Brévart, O.; Dessort, D.; Pradier, B. Inhibiting effect of tetralin on the pyrolytic decomposition of hexadecane. Comparison with toluene. *Ind. Eng. Chem. Res.* **2002**, *41*, 4689-4701.

133. Burklé-Vitzthum, V.; Michels, R. Experimental study and modeling of the role of hydronaphthalenics on the thermal stability of hydrocarbons under laboratory and geological conditions. *Ind. Eng. Chem. Res.* **2005**, *44*, 8972-8987.

134. Onwudili, J. A.; Williams, P. T. Reaction mechanism for the decomposition of phenanthrene and naphthalene under hydrothermal conditions. *J. Supercritical fluids.* **2007**, *39*, *399-408*.

135. Samanta, S. K.; Chakraborti, A. K.; Jain, R. K. Degradation of phenanthrene by different bacteria: evidence for novel transformation sequences involving the formation of 1-naphthol. *Appl. Microbio. Biotechnol.* **1999**, *53*, 98-107.

10. Appendix

10.1 GC optimisation

Fuel samples were analysed by gas chromatography with either mass spectrometric or flame ionisation detection (GC-MS or GC-FID) before and after thermo-oxidative stressing. GC optimisation experiments were used to obtain the best separation for both model compounds and thermo-oxidative degradation products.

As biodiesel and petroleum diesel fuels are different in nature, an initial investigation was performed to identify the best GC column for separation of the constituents of the model systems. The same columns were used in both the GC-MS and GC-FID systems. Only the GC-FID instrument was used for optimisation.

Biodiesel, which is polar, is different in nature from petroleum diesel (non-polar); hence, columns ranging from a polar column to a non-polar column were assessed. During this stage of the study, other GC parameters such the thermal program to be used were investigated. The optimised method was used for all later GC analysis.

Table 10.1 shows GC parameters used in the optimisation of separation.

Table 10.1: GC parameters for separation optimisation assessment

Instrument	GC-FID	GCFID-7890A Agilent Technologies
Column	[90% cyanopropyl] methyl-polysiloxane (BPX90)	Polar column - 30m x 0.25 mm ID X 0.25µm film, maximum temperature of 260/280°C.
	[5% diphenyl/90%dimethyl] polysiloxane (BPX-5)	BPX5 - 25m x 0.32 mm ID X 0.25µm film: non-polar column with a maximum temperature of 360/370°C.
	Methyl polysiloxane (HP-ULTRA 1)	Bonded methyl polysiloxane non-polar column - 50m x 0.32 mm ID X 0.52µm film with a temperature range from -60°C to 325°C (350°C).
Carrier gas	Helium	

GC injection program	Injection temperature Injection mode Split ratio Injection volume	250^oC Splitless 100:1 $1\mu\ell$
Detector	FID Temperature: 300^oC	
Oven	High heating rate: 50^oC (hold: 1 minute) - 250 (onlyBPX90) / 270^oC (hold: 5 minutes) at 20^oC/minute. Low heating rate: 50^oC (hold: 1 minute) - 250 (only BPX90) / 270^oC (hold: 7 minutes) at 10^oC/minute.	

All GC columns were conditioned prior to analysis at the column maximum temperature (see Table 10.1) for 1 hour. To avoid column bleeding, the maximum oven temperature was programmed to be lower than the maximum column temperature. Two rates of temperature increase, 10^oC/min and 20^oC/min, were investigated. This was done to allow maximum separation of the components while minimising the time for analysis.

10.1.1 BPX90 column

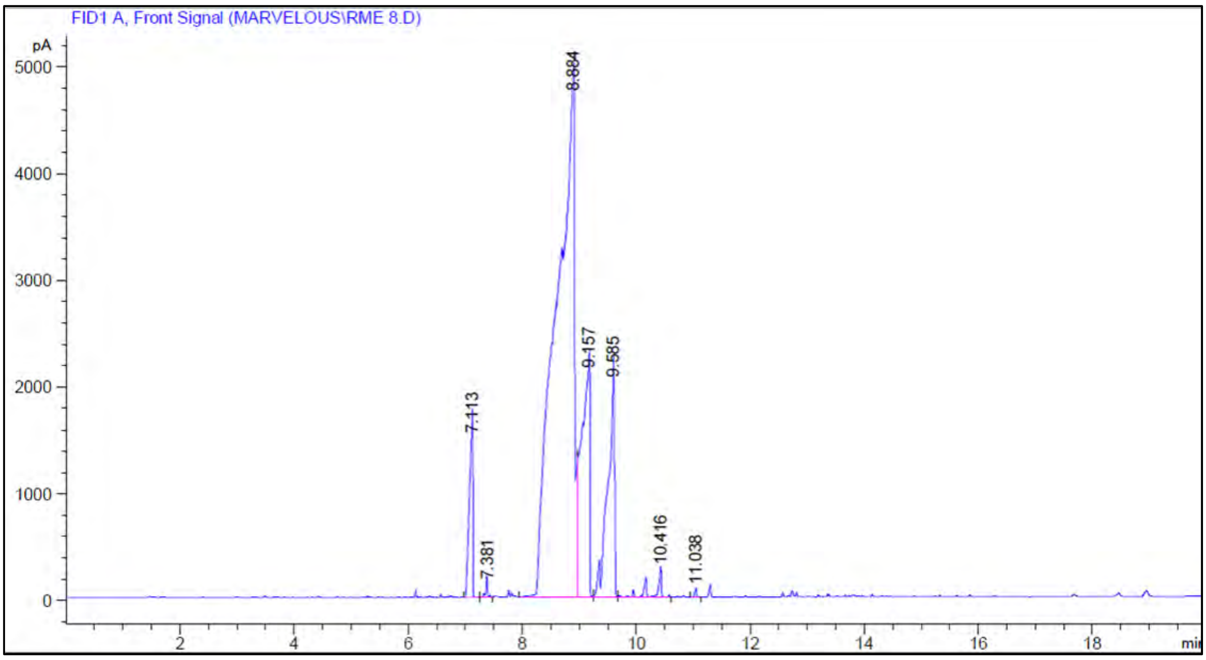

Figure 10.1: GC-FID chromatogram of neat RME. Oven temperature ramped at 20^oC/min

A polar column with cyanopropyl-substituted polysilphenylene-siloxane stationary phase was used to compare the separation of the components with non-polar columns, BPX-5 and HP-ULTRA 1. Separation of RME components is depicted in Figure 10.1.

The GC chromatogram shows the separation of C19 FAMEs with different unsaturation. C19 (3/2) FAMES elute first followed by C19 (1) FAME and last C19 (0) FAME. The number refers to the number of double bonds in the FAME. Extremely poor peak shape was observed. An attempt was made to improve separation by reducing the heating rate.

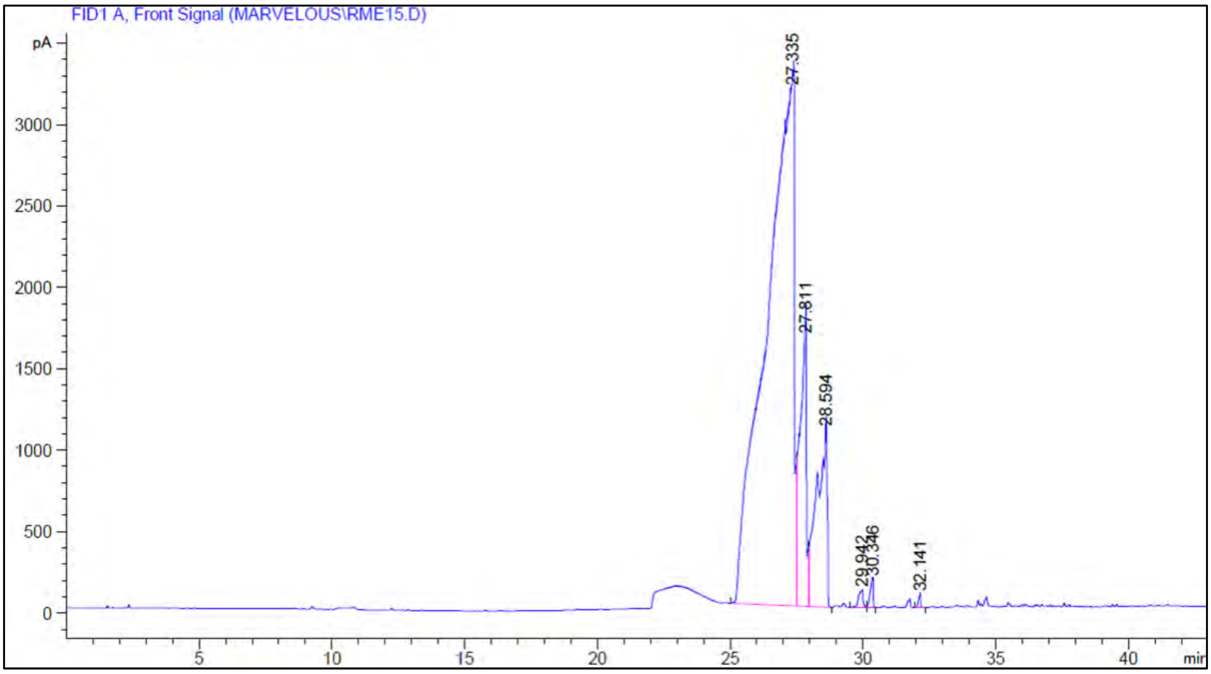

Figure 10.2: GC-FID chromatogram of neat RME. Oven temperature ramped at 10^{o}C/min.

No improvement in peak shape was achieved. The use of the BPX90 column was deemed inappropriate.

10.1.2 BPX-5 column

Neat methyl oleate was analysed using GC-FID and a non-polar BPX-5 (5% diphenyl/90%dimethyl polysiloxane) column at different heating rates (10^{o}C/min and 20^{o}C/min). The results are shown in Figure 10.3 and Figure 10.4.

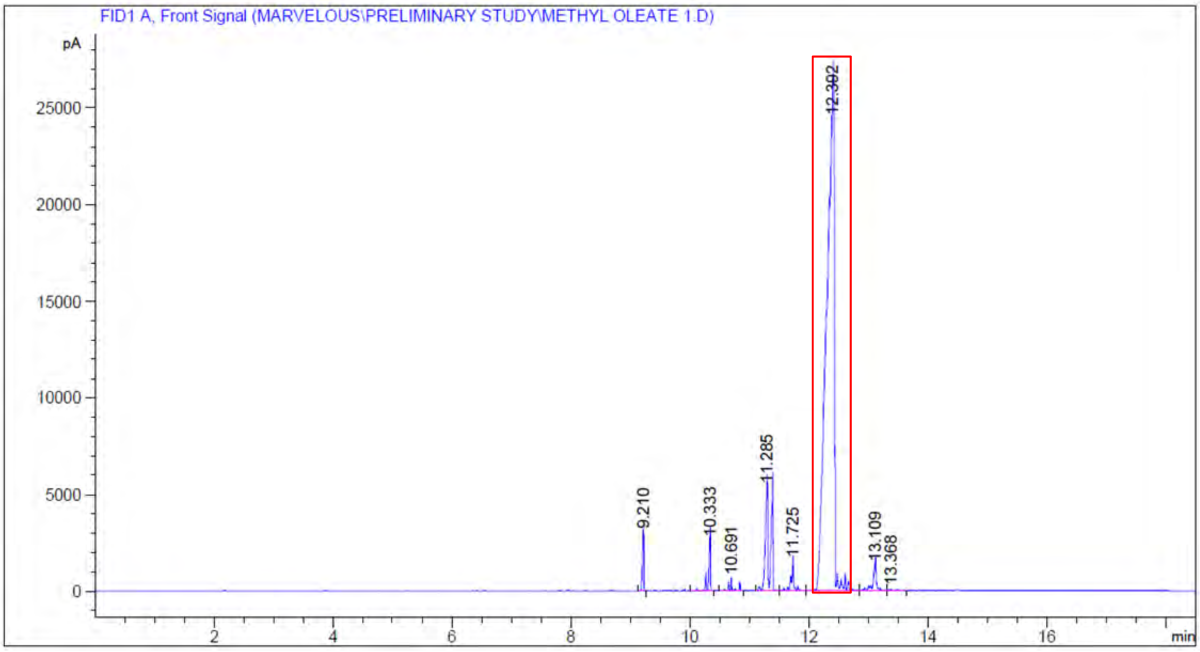

Figure 10.3: GC-FID chromatogram of neat methyl oleate. Oven temperature ramped at 20^{o}C/min.

The results show that the constituents of 70% methyl oleate were well separated using this column. The methyl oleate used contained monounsaturated esters of different chain lengths. The C13 ester eluted at 9.21 min, C15 at 10.33 min, C17 at 11.29 min, C19 at 12.39 min and C21 at 13.11 min.

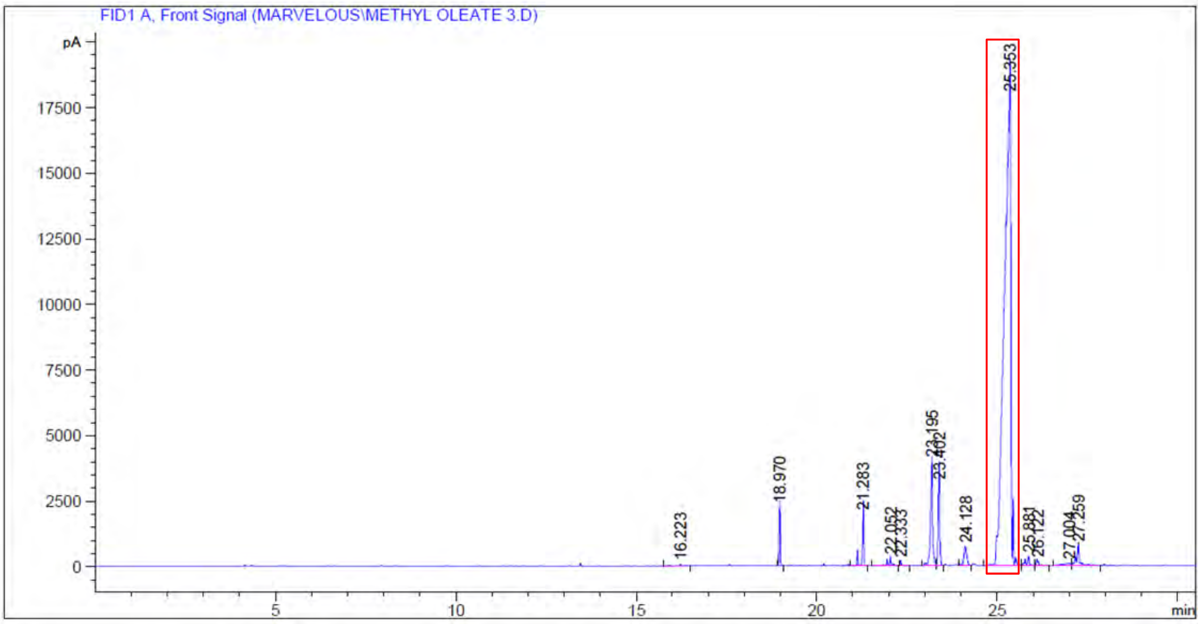

Figure 10.4: GC-FID chromatogram of neat methyl oleate. Oven temperature ramped at 10^{o}C/min.

10.1.3 HP-ULTRA 1 column

The HP-ULTRA1 column has a similar stationary phase to the BPX5 column but is twice as long. The film thickness is also greater. Chromatograms were obtained from running the GC-FID at 20^{o}C/min and 10^{o}C/min heating rates. These are presented in Figure 10.5 and Figure 10.6.

Extremely good separation of components was achieved at 20^{o}C/min for a mixture of RME and an EN590 reference diesel. Extremely narrow peaks were obtained, indicative of the efficiency of the column.

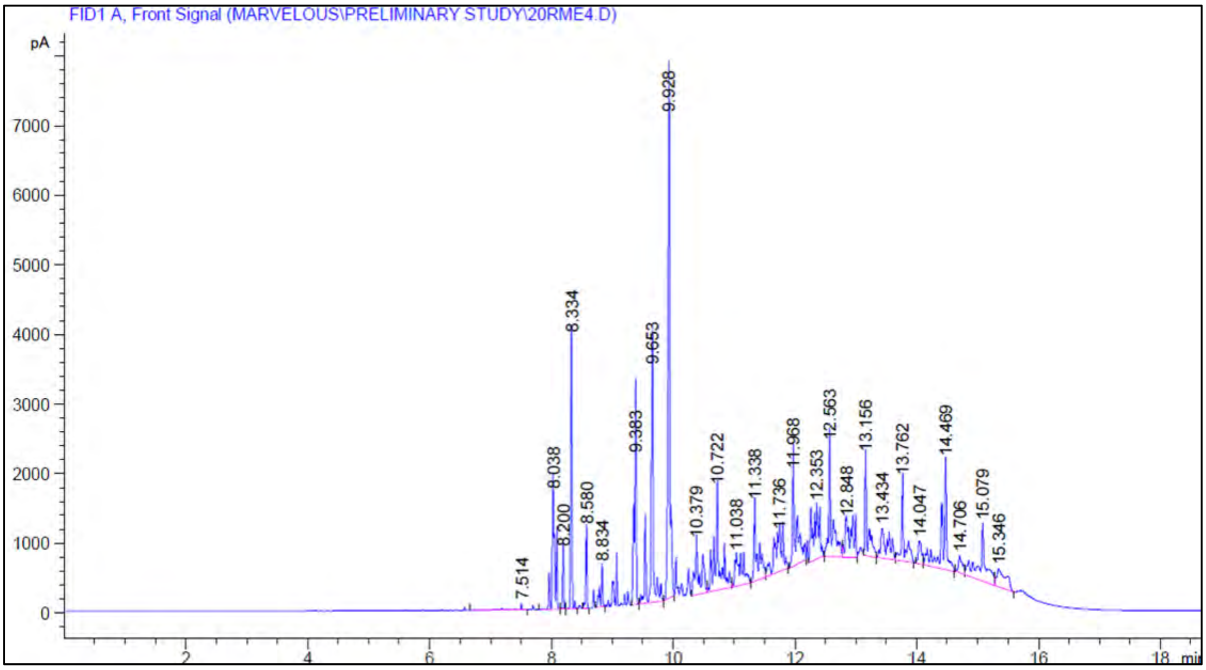

Figure 10.5: GC-FID chromatogram of neat 20% RME/80% EN 590 reference diesel blend. Oven temperature ramped at 20^{o}C/min

At 10^{o}C/min, even better separation was achieved but with an even longer elution time.

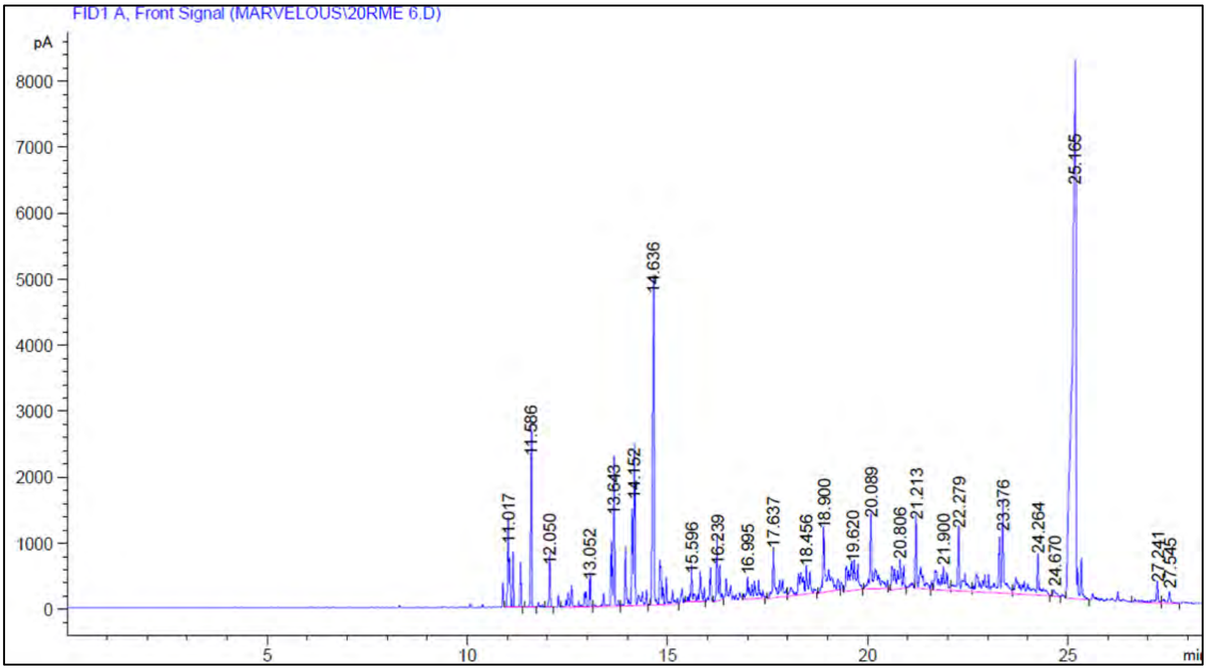

Figure 10.6: GC-FID chromatogram of neat 20% RME/80% EN 590 reference diesel blend. Oven temperature ramped at 10^{o}C/min

10.1.4 Discussion

Poor peak shape meant that the used of the BPX90 column was not deemed acceptable.

Rapid analysis could be achieved using HP-ULTRA 1 column. The column is extremely efficient with peaks being very narrow.

The BPX5 column also provided acceptable peak shape and separation. Because it was a shorter column than the HP-ULTRA 1 column, elution times were reduced although the peaks were not as narrow.

Since simpler diesel model compound systems were to be analysed rather than a full boiling range diesel, fewer species would be expected after stressing. The BP-X5 column was chosen as a column of choice in this study since it provided acceptable separation with the shortest analysis times. This column was also found to be the most robust.

10.2 QCM mass accumulation

Table 10.2: Mass accumulation after 24 h thermo-oxidative stressing at 140^oC in a QCM for different diesel and biodiesel model compound systems and their blends

Fuel system	**Mass accumulation (µg/cm^2)**		
	No – phenols (g)	**+BHT (g)**	**+Phenol (g)**
DMC A	1.91*		
DMC B	1.77*		
DMC C	0.86*		
RME	14.86	12.39	
80% DMC A/20% RME	55.16*	43.21	66.71
90% DMC A/10% RME	67.31**		
70% DMC A/30% RME	49.06**		
35% DMC A/65% RME	22.59**		
80% DMC A/20% ML	19.15		
80% DMC A/20% MLN	40.12		
75% DMC A/20 % ML/5% n-hexanoic acid	2.49**		
80% DMC A/20% RMEMC 140 ^oC	88.13	61.80	111.32
80% DMC A/20% RMEMC 100 ^oC	293.26	193.14	

1. RMEMC = 7:3:1 (v/v) mixture of methyl oleate, methyl linoleate and methyl linolenate
2. MO = methyl oleate, ML = methyl linolenate and MLN = methyl linolenate
3. Blends of DMC-A with methyl oleate could not be investigated owing to limited quantities of methyl oleate available
4. * Triplicate experiment
5. ** Single experiment

10.3 FTIR spectra

This section contains FTIR spectra from the NIST Standard Reference Database Number 69 (NIST Chemistry Webbook) of raw materials and potential intermediates (*108*).

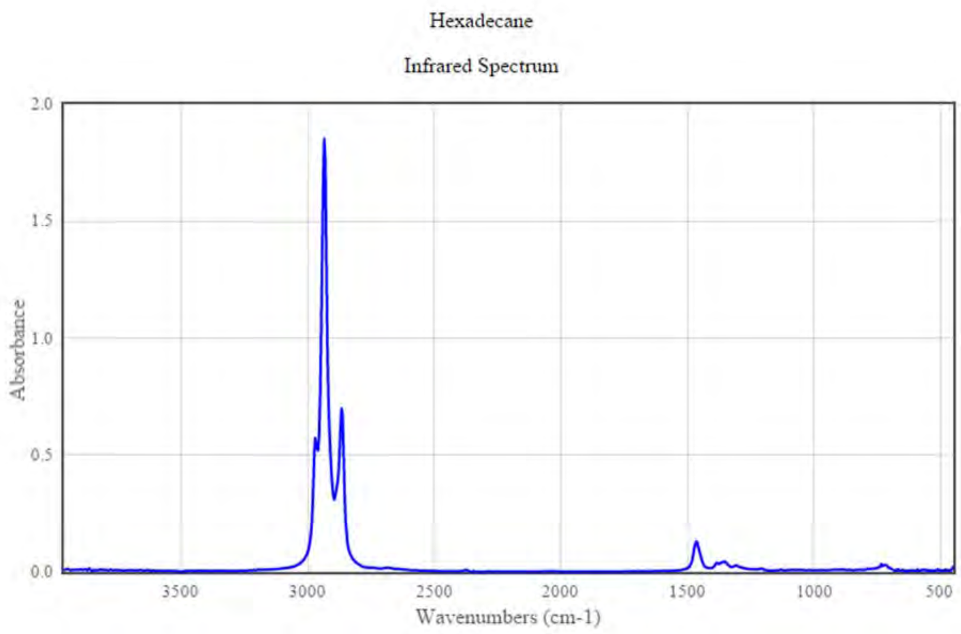

Figure 10.7: Reference FTIR spectrum of n-hexadecane (108)

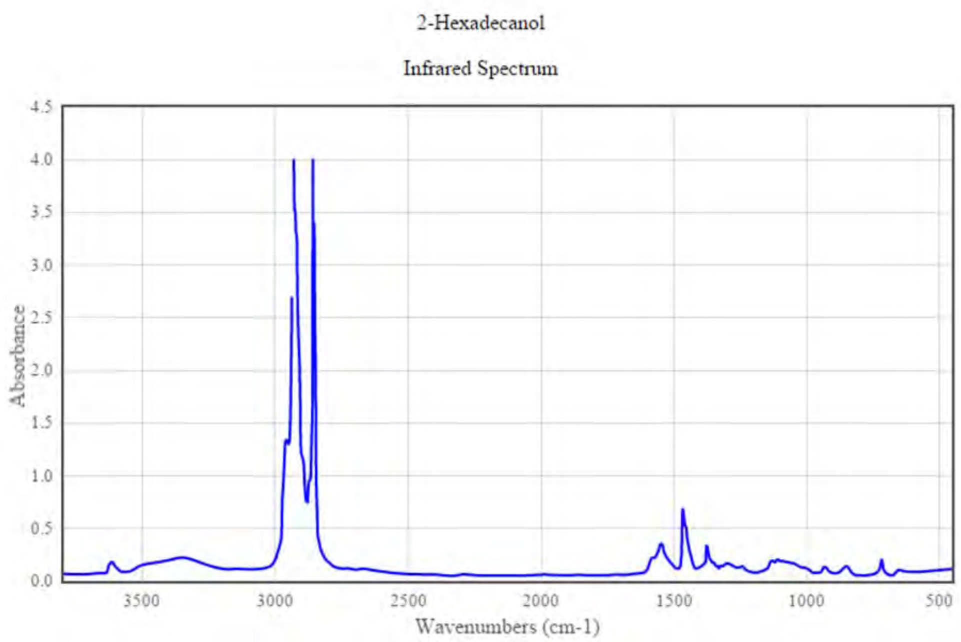

Figure 10.8: Reference FTIR spectrum of 2-hexadecanol (108)

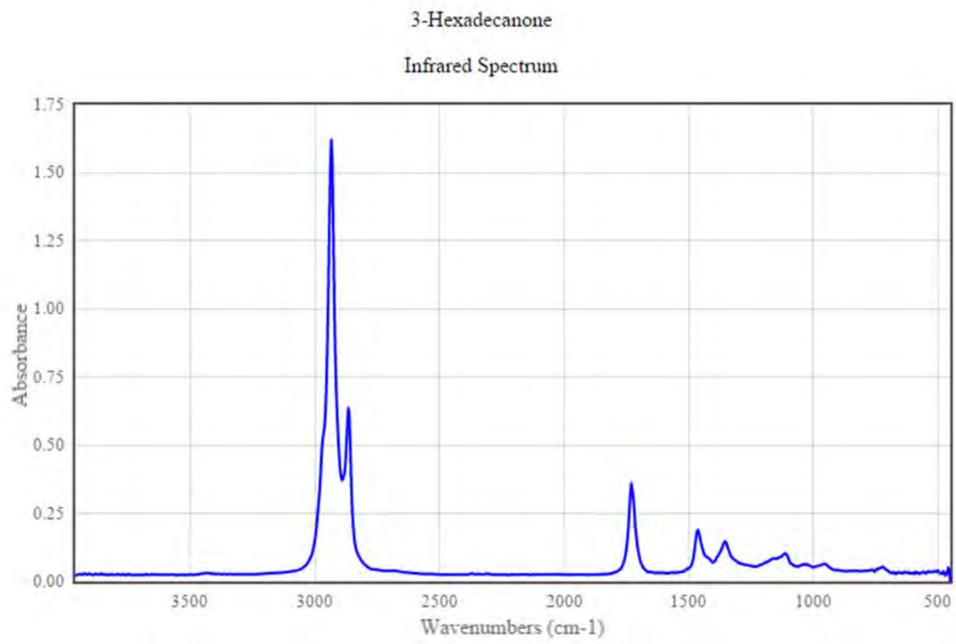

Figure 10.9: Reference FTIR spectrum of 3-hexadecanone (108)

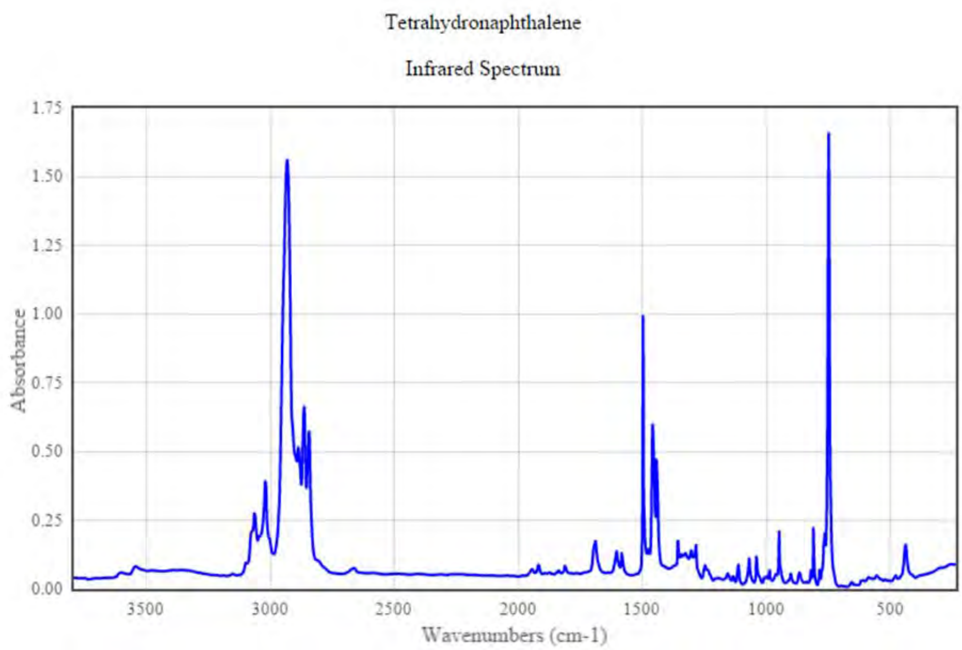

Figure 10.10: Reference FTIR spectrum of tetralin (108)

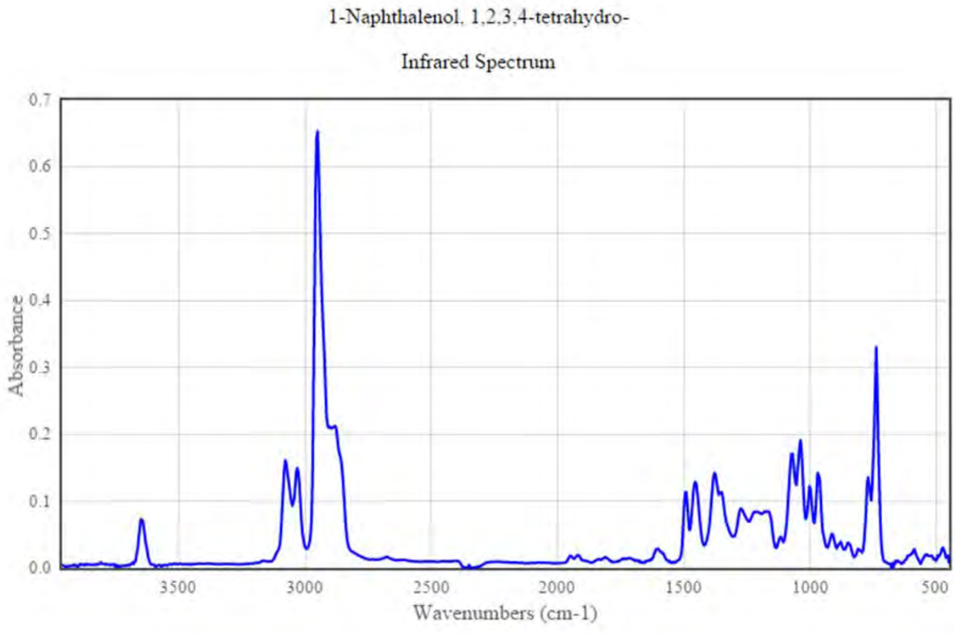

Figure 10.11: Reference FTIR spectrum of 1-tetralol (108)

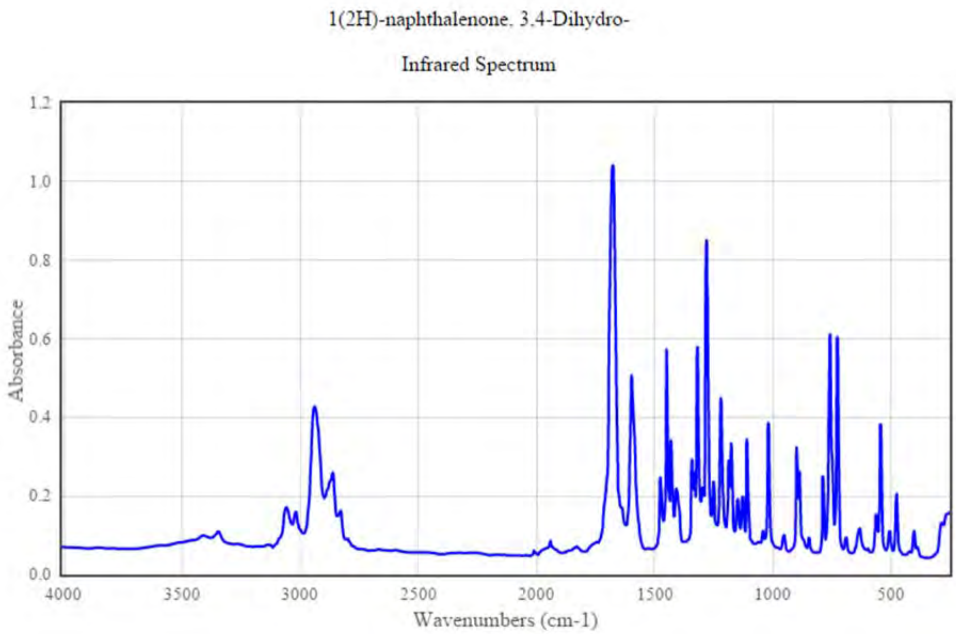

Figure 10.12: Reference FTIR spectrum of 1-tetralone (108)

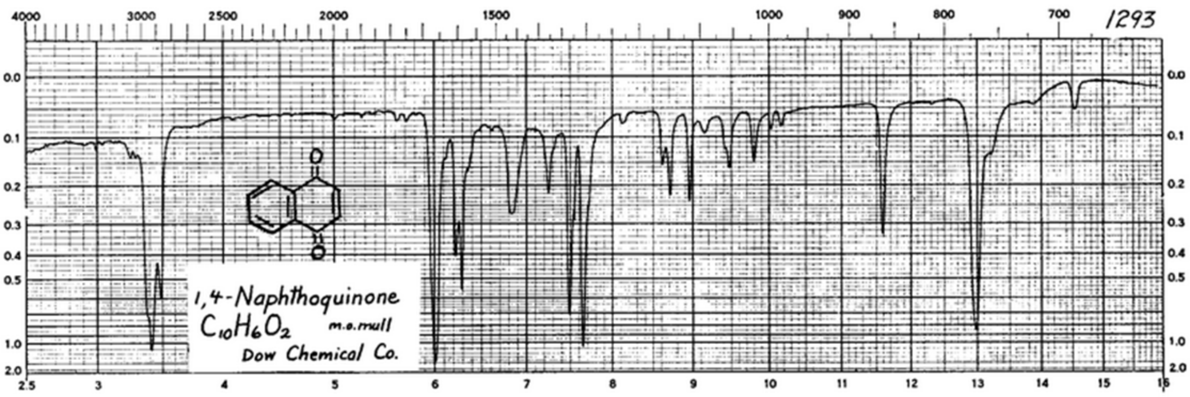

Figure 10.13: Reference FTIR spectrum of 1,4-naphthoquinone 1 (108)

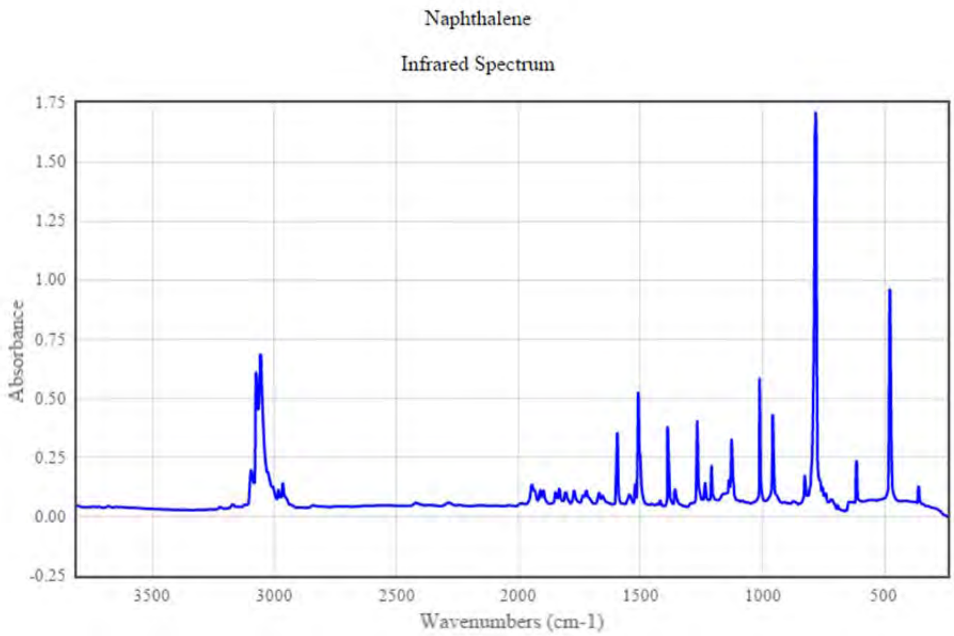

Figure 10.14: Reference FTIR spectrum of 1,4-naphthoquinone 2 (108)

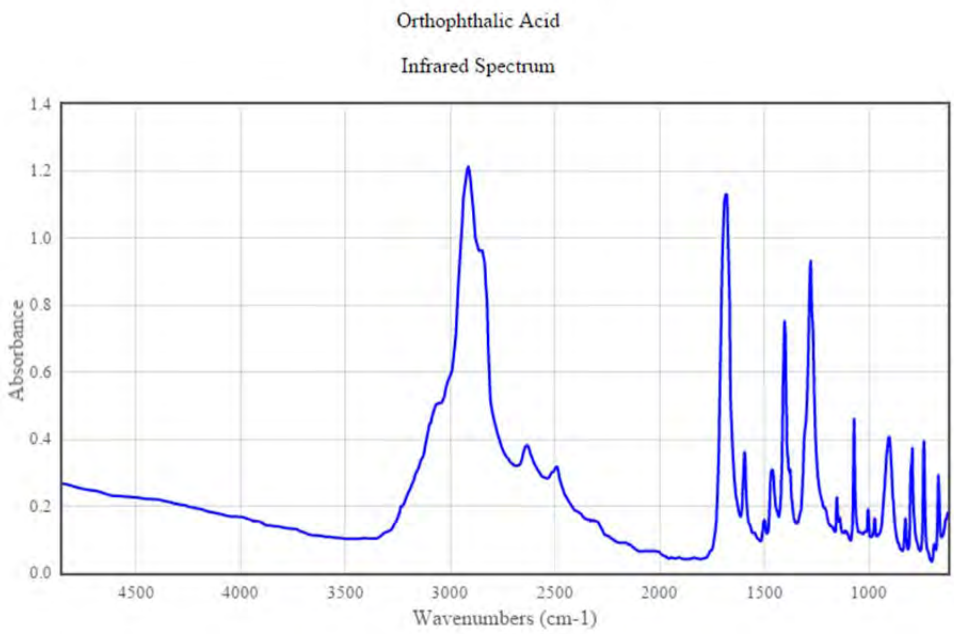

Figure 10.15: Reference FTIR spectrum of 1,2-benzenedicarboxylic acid (o-phthalic acid) (108)

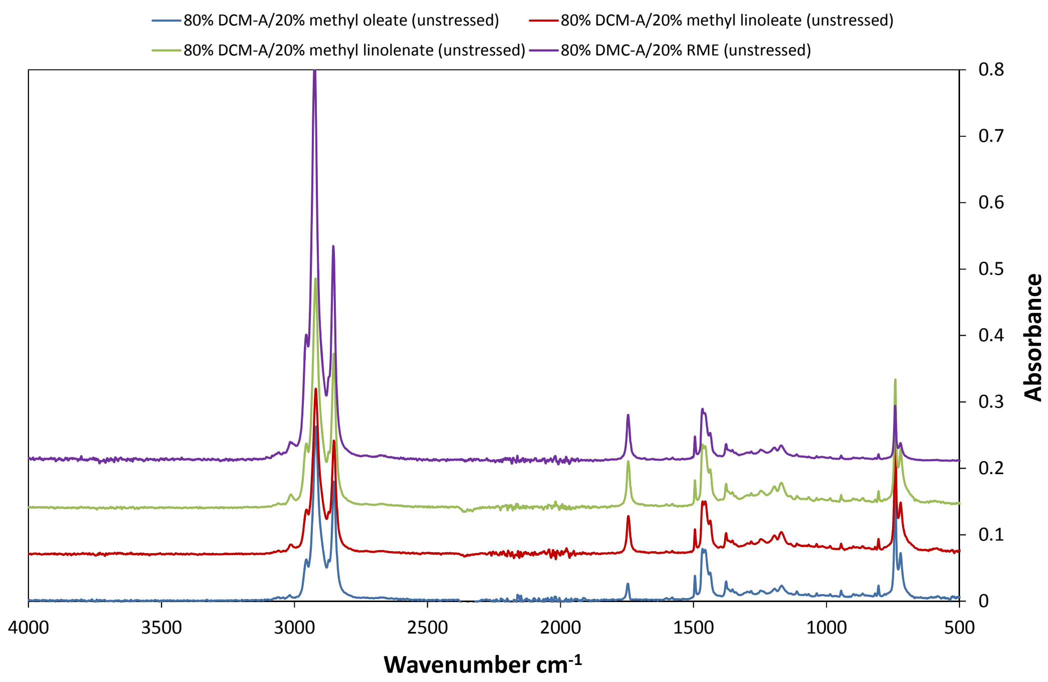

Figure 10.16: Comparison of the FTIR spectra of unstressed FAME model compounds and RME.

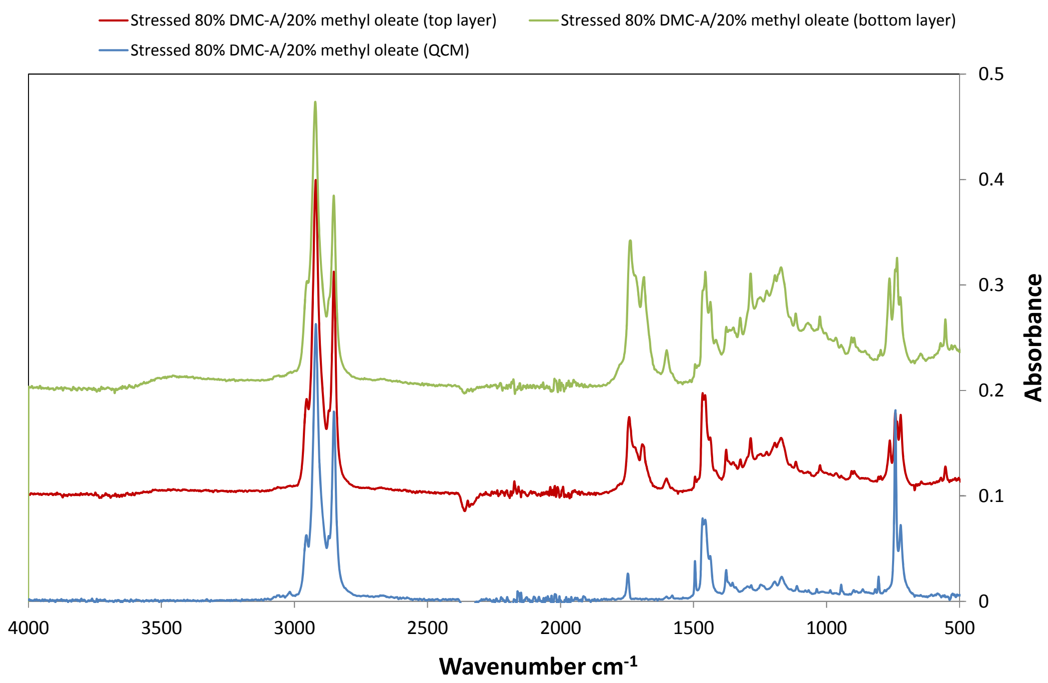

Figure 10.17: Comparison of the FTIR spectra of 80% DMC-A/20% methyl oleate blends stressed in a QCM-stressed and the two layers formed after 24h oxidative stressing of this blend at 140^{o}C in an open flask. Spectra are offset for clarity.

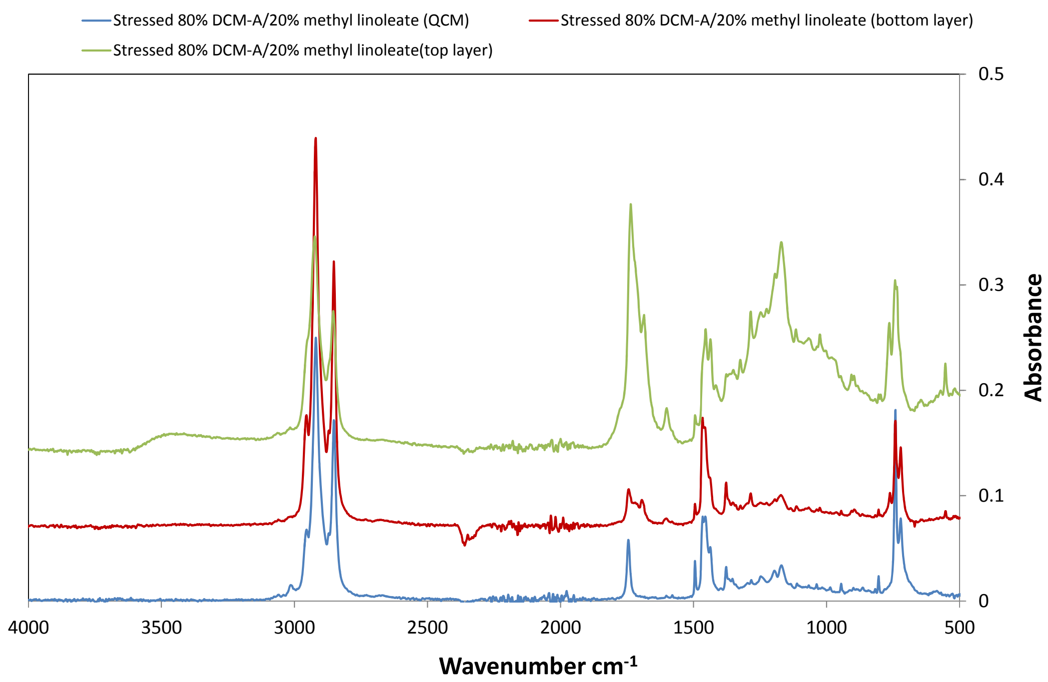

Figure 10.18: Comparison of the FTIR spectra of 80% DMC-A/20% methyl linoleate blends stressed in a QCM-stressed and the two layers formed after 24h oxidative stressing of this blend at 140^{o}C in an open flask. Spectra are offset for clarity.

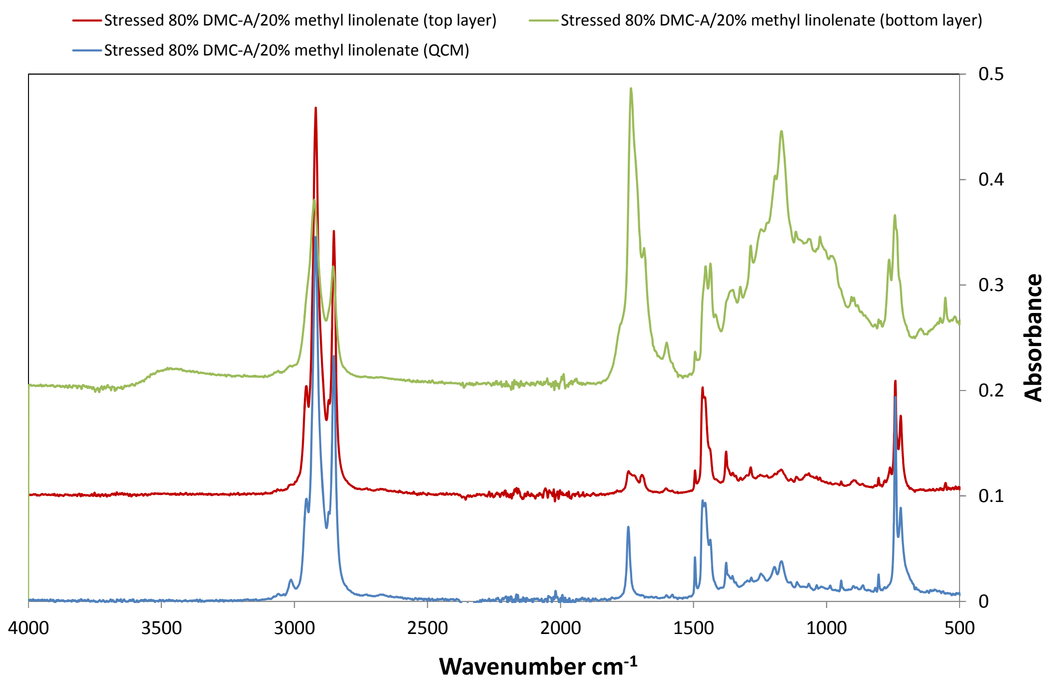

Figure 10.19: Comparison of the FTIR spectra of 80% DMC-A/20% methyl linolenate blends stressed in a QCM-stressed and the two layers formed after 24h oxidative stressing of this blend at 140^{o}C in an open flask. Spectra are offset for clarity.

10.4 GC-MS results

Table 10.3: Identification of major components of stressed DMC-A after QCM oxidation. Highest MS matches are reported.

Retention time (min)	Area	Compound name
4.389	**4269330**	**Tetralin**
4.559	784142	Naphthalene
4.795	58876	4-Hexenyl benzene
4.850	71783	1-Ethyl-1-propenylbenzene
5.769	1491493	1-Tetralol
5.938	749313	1-Tetralone
6.567	379745	n-Tetradecane
6.959	1587078	2-Methyl tridecane
7.258	**17612080**	***n*-Hexadecane**
7.749	608105	*n*-Octadecane
8.183	95567	1,3-Dimethylcyclopentanol
8.291	2687427	Icosane
8.367	167574	2-Hexadecanol
10.575	309394	1-Ethyl tetralin
10.695	347560	1-Propyl tetralin
11.510	100429	1,1-*bis*(dodecyloxy)-*n*-hexadecane

Table 10.4: Identification of major components of stressed DMC-B after QCM oxidation. Highest MS matches are reported

Retention time (min)	Area	Compound name
3.526	**12412850**	***trans*-Decalin**
3.884	**8736969**	***cis*-Decalin**
4.390	**12530163**	**Tetralin**
4.557	2745857	Naphthalene
5.241	180005	3,7,-Dimethyl decane
5.765	2982526	1-Tetralol
5.935	1145356	1-Tetralone
6.564	834855	n-Tetradecane
6.954	3201354	2-Methyl tridecane
7.175	5877699	Alkyl tridecane
7.266	**29927175**	***n*-Hexadecane**
7.744	2144004	*n*-Octadecane
8.286	2256812	Icosane
8.358	430659	2-Hexadecanol
10.567	555201	1-Ethyl tetralin
10.689	667099	1-Propyl tetralin

Table 10.5: Identification of major components of stressed DMC-C after QCM oxidation. Highest MS matches are reported

Retention time (min)	Area	Compound name
3.527	**12452919**	***trans*-Decalin**
3.886	**8975152**	***cis*-Decalin**
4.369	**6893091**	**Tetralin**
4.551	1670837	Naphthalene
4.907	129208	Octahydronaphthalen-4a(2*H*)-ol
5.764	1987838	1-Tetralol
5.934	1087246	1-Tetralone
6.562	1001077	n-Tetradecane
6.954	2214097	2-Methyl tridecane
7.175	5680657	4-Methyl-1-undecene,
7.256	**34092354**	**n-Hexadecane**
7.744	2311217	n-Octadecane
8.286	2786126	Icosane
8.358	525229	2-Hexadecanol
10.568	216150	1-Ethyl tetralin
10.692	283440	1-Propyl tetralin

Table 10.6: Identification of major components of stressed RME after QCM oxidation. Highest MS matches are reported

Retention time (min)	Area	Compound name
5.476	411688	E,E-2,4-decadienal
6.235	213582	Methyl 9-oxononoate
6.745	145623	Methyl dodecanoate
7.909	577259	Methyl palmitoleate
8.308	88024	Dodec-5-Z-enal
8.372	135889	Methyl Z-13-tetradecenoate
8.450	252937	Methyl pentadecanoate
8.865	5437644	Methyl oleate (methyl Z-9-octadecenoate)
8.980	1774154	Methyl hexadecanoate
9.258	1618037	Z-11-Hexadecen-1-ol/methyl-9-oxo nonanoate
9.353	1970537	Methyl Z-10-heptadecenoate
9.468	857669	Methyl heptadecanoate
9.885	9321223	Methyl linoleate, methyl Z,Z-9,12-octadecadienoate
9.947	6724627	Z-9-Octadecenal
10.015	15483669	Methyl Z,Z-9,15-octadecadienoate
10.282	4242455	Methyl nonadecanoate
10.334	1856764	Methyl Z-10-octadecenoate
10.425	2624339	Methyl cis-4-(1,5-dimethyl-3-oxohexyl cyclohexanecarboxylate
10.642	4031377	Methyl Z,Z,Z-11,14,17-eicosatrienoate
10.717	16024246	Methyl *cis*-3-pentyloxiraneundecanoate
10.821	12800915	Methyl 18-methylnonadecanoate
10.923	3409166	13-Z-docosenoic acid
11.094	2530370	Isopropyl linoleate
11.230	1692334	Methyl 2-nonyl-undecanoate
11.366	1722488	Unidentified
11.537	4394624	Methyl Z-13-docosenoate
11.631	5291165	Methyl docosanoate
11.930	288714	Methyl 7-hexadecenoate
12.014	368228	Methyl tricosanoate
12.345	5572896	3-hydroxypropyl oleate
12.431	2835506	Methyl tetracosanoate

Table 10.7: Identification of major components of stressed DMCA-A/methyl oleate blends after QCM oxidation. Highest MS matches are reported

Retention time (min)	Area	Compound name
2.932	1646574	2-Methyl pentane
4.384	**13976065**	**Tetralin**
4.560	2182874	Naphthalene
5.772	1364456	1-Tetralol
5.943	1533594	1-Tetralone
6.569	966153	n-Tetradecane
6.748	11350756	Methyl dodecenoate
6.958	2781514	2-Methyl tridecane
7.261	**7731316**	**n-Hexadecane**
7.750	4581295	n-Octadecane
7.852	4743355	Methyl myristoleate, methyl Z-9-tetradecenoate
7.916	13045821	Methyl palmitoleate
8.250	831795	Methyl pentadecanoate
8.295	4996748	Icosane,
8.375	900802	2-Hexadecanol
8.455	916209	Methyl pentadecanoate
8.780	2019854	14-Methyl pentadecanoate
8.872	**33096665**	**Methyl oleate; methyl Z-9-octadecenoate**
8.973	4196570	Methyl hexadecanoate
9.352	11849701	Methyl Z-10-heptadecenoate
9.467	1449033	Methyl heptadecanoate
9.808	9498795	Methyl linoleate, methyl Z,Z-9,12-octadecadienoate
9.857	12168416	Methyl Z-11-octadecenoate
9.942	1950077	Methyl octadecanoate
10.044	9751081	Methyl Z,Z-14,17-Octadecadienoate
10.119	7146503	Hexyl-Z-9-Octadecenoate
10.240	4092180	Octyl-Z-10-undecenoate
10.283	2682292	Methyl nonadecanoate
10.710	7860521	Methyl *cis*-3-pentyloxiraneundecanoate

Table 10.8: Identification of major components of stressed DMC-B/methyl linoleate blends after QCM oxidation. Highest MS matches are reported

Retention time (min)	Area	Compound name
3.849	342189	*cis*-Decalin
4.385	**15435093**	**Tetralin**
4.560	2412187	Naphthalene
4.800	110027	Benzenepentanol
4.851	194179	1-Ethyl-1propenylbenzene
5.480	198379	E,E-2,4-Heptadiene
5.772	639264	1-Tetralol
5.943	423249	1-Tetralone
6.238	593455	Methyl-9-oxo nonanoate
6.569	1507293	n-Tetradecane
6.960	2712727	2-Methyl tridecane
7.252	**7907232**	**n-Hexadecane**
7.751	3846829	n-Octadecane
8.293	4073924	Icosane
8.366	746360	2-Hexadecanol
9.257	1064241	E/Z-13-Heptadecen-1-ol/methyl-9-oxo nonanoate
9.844	**25345163**	**Methyl linoleate (methyl Z,Z-9,12-octadecadienoate)**
10.092	5063178	Methyl Z,Z-n,(n+3)-octadecadienoate
10.150	8244041	Methyl Z,Z-n,(n+3)-octadecadienoate
10.231	1126130	Z,Z-14,17-octadecadien-1-ol
10.650	5033420	Methyl Z,Z-7,10-eicosadienoate
10.690	6509600	Methyl ricinoleate, methyl 12-hydroxy-Z-9-octadecenoate
10.866	925235	Methyl Z,Z-7,10-eicosadienoate

Table 10.9: Identification of major components of stressed DMC-A/methyl linolenate blends after QCM oxidation. Highest MS matches are reported

Retention time (min)	Area	Compound name
3.846	67752	*cis*-Decalin
4.384	**3917519**	**Tetralin**
4.557	**1369594**	**Naphthalene**
4.675	996318	2,4,6-Trimethyl- phenol
4.792	629596	3-Phenyl cyclohexanone
4.848	146604	1-Ethyl-1-propenyl benzene
5.767	312185	1-Tetralol
5.937	178356	1-Tetralone
6.234	258478	Methyl 9-oxononanoate
6.564	475906	n-Tetradecane
6.956	1887527	2-Methyl tridecane
7.257	**16225324**	**n-Hexadecane**
7.746	1662162	n-Octadecane
8.289	1400401	Icosane
8.361	313012	2-Hexadecanol
8.762	280956	Ethyl tridecyl ester of carbonic acid
9.251	1048502	Linolenic acid/ methyl-9-oxo nonanoate
9.873	**5842357**	**Methyl linolenate (methyl Z,Z,Z-9,12,15-octadecatrienoate)**
10.089	1819514	Methyl gamma linolenate
10.146	3073485	Methyl Z,Z,Z-n,(n+3),(n+6)-octadecatrienoate
10.233	920025	Methyl Z,Z-n,(n+3)-octadecadienoate
10.648	2373836	Methyl Z,Z,Z-11,14,17-eicosatrienoate
10.686	2589466	Methyl ricinoleate, methyl 12-hydroxy-Z-9-octadecenoate
10.858	656446	2,3-dihydroxypropyl Z,Z,Z-9,12,15-octatridecenoate
11.930	599704	Campesterol
13.156	780977	Cholest-8-en-3-*beta*-ol acetate

Table 10.10: Identification of major components of stressed 80% DMC-B-20% RME after QCM oxidation. Highest MS matches are reported

Retention time (min)	Area	Compound name
3.521	**10334936**	***trans*-Decalin**
3.881	**7594420**	***cis*-Decalin**
4.364	**5664801**	**Tetralin**
4.551	1101927	Naphthalene
5.766	306285	1-Tetralol
5.938	312839	1-Tetralone
6.563	488761	n-Tetradecane
6.955	908809	2-Methyl tridecane
7.254	**24904307**	**n-Hexadecane**
7.743	2695372	n-Octadecane
7.909	2025914	Methyl palmitoleate
8.287	1149655	Icosane
8.860	4058727	13-Heptadecyn-1-ol/Methyl oleate (methyl Z-9-octadecenoate)
8.968	3996867	Methyl hexadecanoate
9.800	7706641	Methyl n,(n+3)-9,12-octadecadienoate
9.869	11986794	Methyl linoleate (methyl Z,Z-9,12-octadecadienoate)
9.939	2489551	Methyl octadecanoate
10.635	520078	Methyl Z,Z,Z-5,8,11-eicosatrienoate
10.704	11052530	Methyl Z-11-eicosenoate/methyl cis-3-pentyloxiraneundecanoate
10.810	5039872	Methyl 18-methylnonadecanoate
11.532	1481048	Methyl Z-13-docosenoate
11.625	2166212	Methyl docosanoate
12.334	752006	Methyl 15-tetracosenoate
12.427	555445	Methyl tetracosanoate

Table 10.11: Identification of major components stressed DMC-B after open flask oxidation. Highest MS matches are reported

Retention time (min)	Area	Compound name
3.517	**12063455**	***trans*-Decalin**
3.875	**7978126**	***cis*-Decalin**
4.358	**6628441**	**Tetralin**
4.550	4982902	Naphthalene
4.850	1404203	2-Methyl-3-phenyl-2-propenal
4.908	16399576	*trans*-Octahydronaphthalen-4a(2*H*)-ol
5.167	9068697	*cis*- Octahydronaphthalen-4a(2*H*)-ol
5.267	7255137	1-Decalol
5.375	5407756	*trans*-1-Decalone
5.450	2784566	*cis*-1-Decalone
5.525	1087562	1,2-Benzenedicarboxylic acid
5.567	2189879	*trans*-2-Decalol
5.658	4861593	*cis*-2-Decalol
5.800	34584875	1-Tetralol
5.958	55216563	1-Tetralone
6.058	11135801	1,11-Dodecadiene
6.225	10312208	1,4-Naphthoquinone
6.300	5173900	*cis*-1-Methyl-decalin
6.367	7159246	*trans*-2-Methyl decalin
6.405	4447074	*cis*-2-Methyl decalin
6.558	11199439	2-Tridecyl benzene acetate
6.692	8062722	*trans*-*p*-Menth-2-en-9-ol
6.775	16984473	3-(4-Methylphenyl)-2-propenal
6.883	8109371	3-(3-Hydroxyphenyl)propionic acid
6.950	7551249	2-Methyl tridecane
7.250	**33336319**	**n-Hexadecane**
7.742	1106820	n-Octadecane
8.050	1833977	E-3-Eicosene
8.183	26297274	6-Hexadecanone
8.292	38160975	E-3-Eicosene
8.358	19679992	2-Hexadecanol
8.750	2910249	1,1-*bis*(dodecyloxy) hexadecane
8.933	2163286	11-Heneicosanol
9.117	11221924	Tetradecyl methoxyacetate
9.333	10481064	Hexadecyl oxirane
10.200	2009565	1-Ethyl tetralin
10.642	2241252	1-Propyl tetralin
10.833	602804	2-(Phenylmethyl)-tetralin
11.025	1772602	1-Methyl-2-(1-methyl-2-propenyl)-benzene
11.783	1877606	2-Benzylidene-1-heptanol
11.933	1181388	Methyl *o*-[(1,2,3,4-tetrahydro-2-naphthyl)methyl]-hydrocinnamate

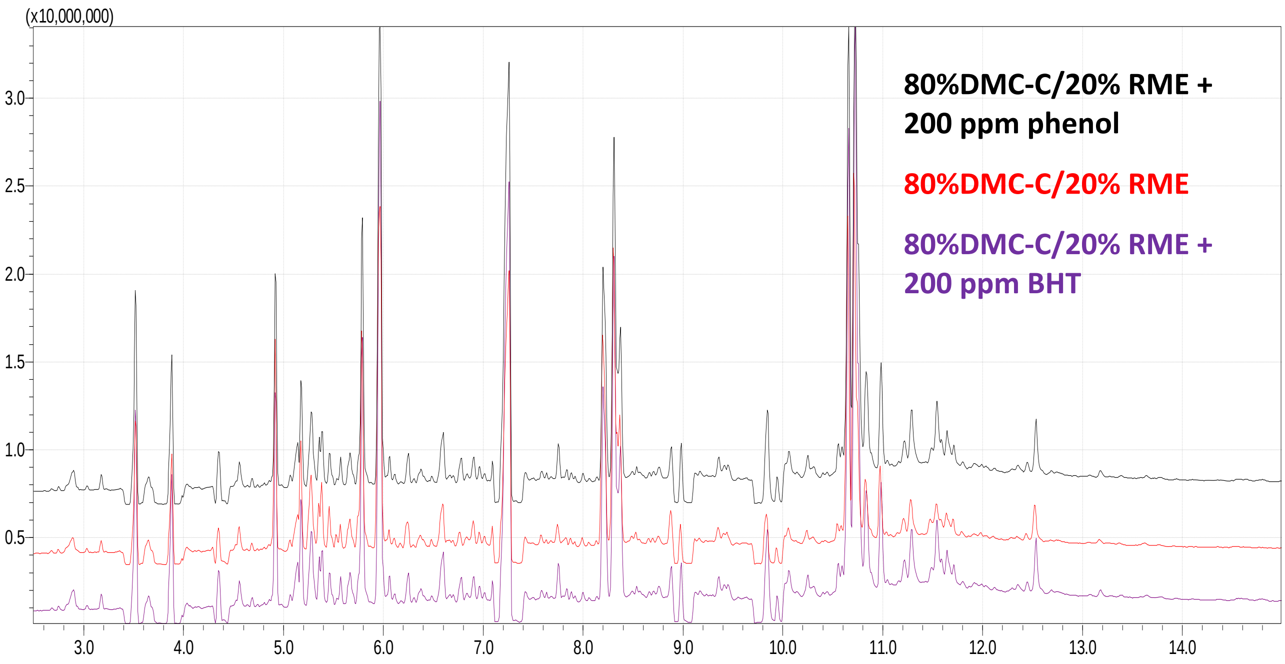

Figure 10.20: GC-MS chromatograms DMC-C/RME blends, both neat and doped with 200 ppm BHT and phenol, after 24h thermo-oxidative stressing at 140^{o}C in an open flask reactor

Figure 10.20 shows that after 24h, the effect of the antioxidant, BHT, when blending RME with diesel was small. All three chromatograms are very similar. This is likely the result of BHT being consumed well before 24h allowing significant oxidation to occur.

10.5 GC-FID results

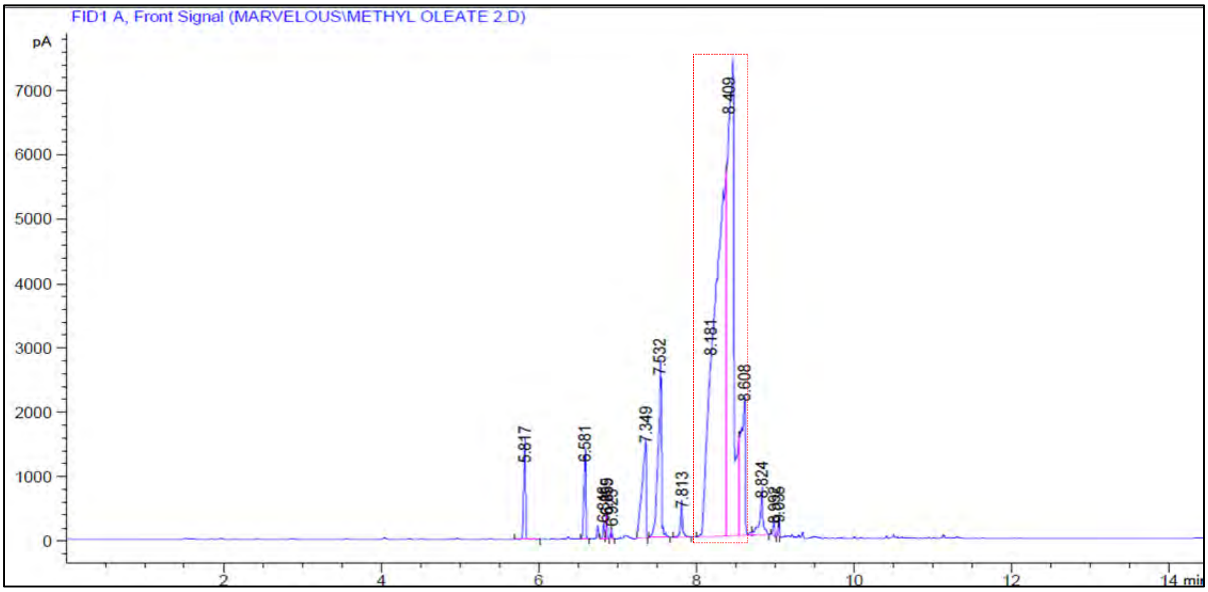

Figure 10.21: GC-FID chromatogram of neat methyl oleate

The methyl oleate used was 70% pure with the other components being longer and shorter chain monounsaturated fatty acids.

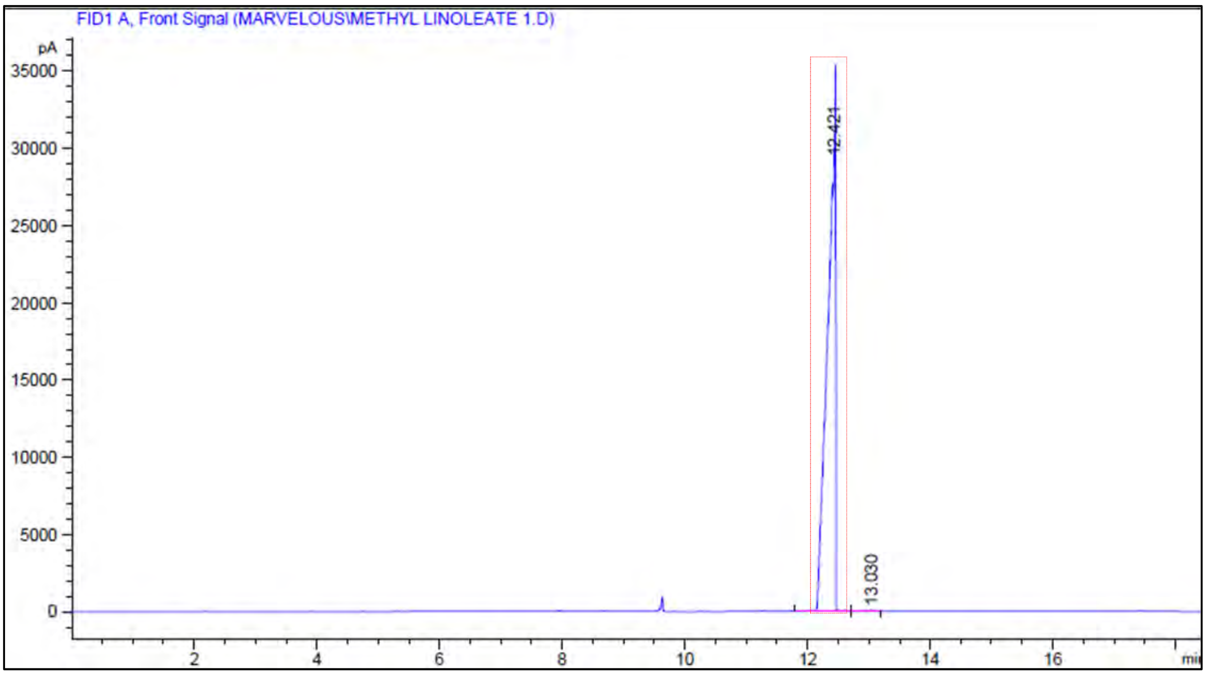

Figure 10.22: GC-FID chromatogram of neat methyl linoleate

The presence of one major peak indicates the high purity of this raw material.

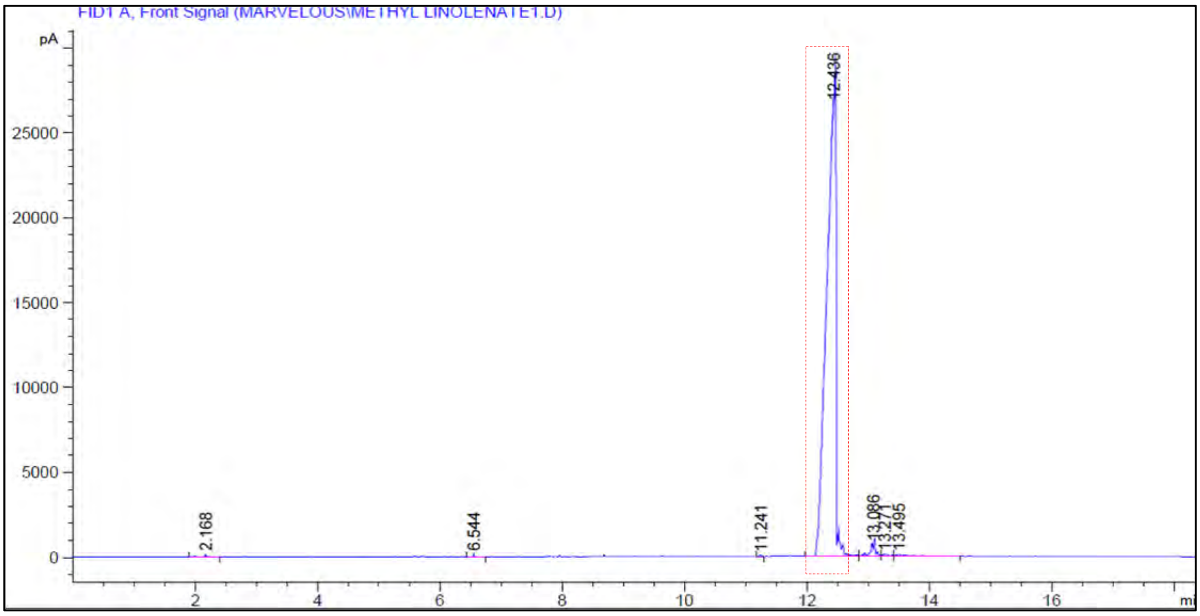

Figure 10.23: GC-FID chromatogram of neat methyl linolenate

This product was sold as 70% pure. Some higher molecular weight esters were observed. Comparison of Figure 10.22 with Figure 10.23 reveals that methyl linoleate and methyl linolenate have very similar retention times. The impurities in the methyl linolenate are thus likely to be primarily methyl linoleate.

10.6 UV spectra

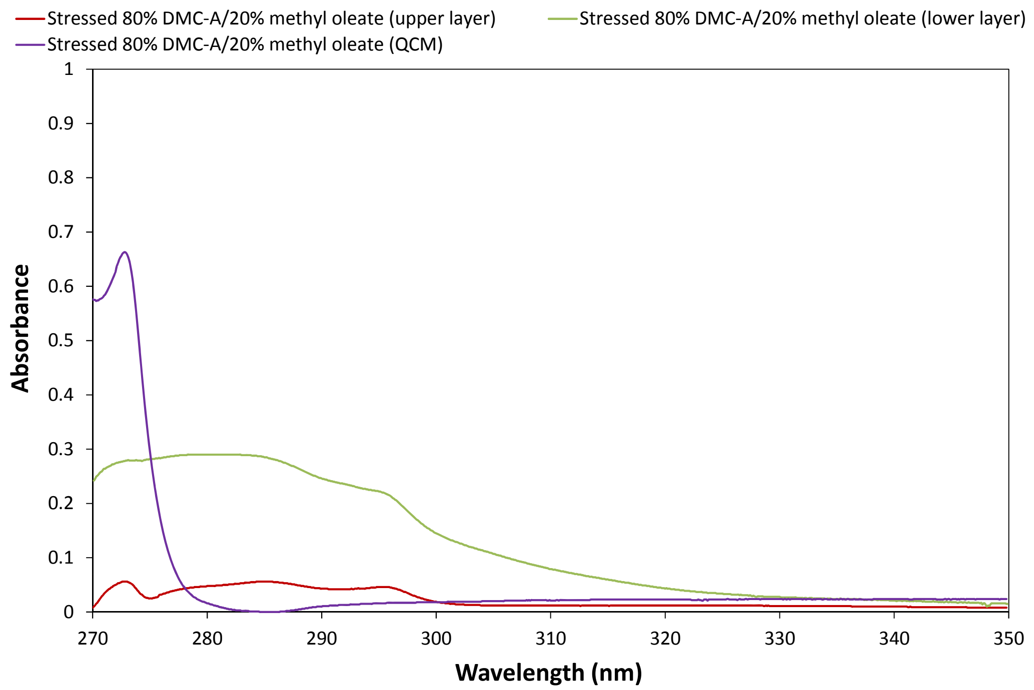

Figure 10.24: UV absorbance spectra of stressed 80% DMC-A/20% methyl oleate after oxidative stressing at 140°C for 24h in a QCM and in an open flask

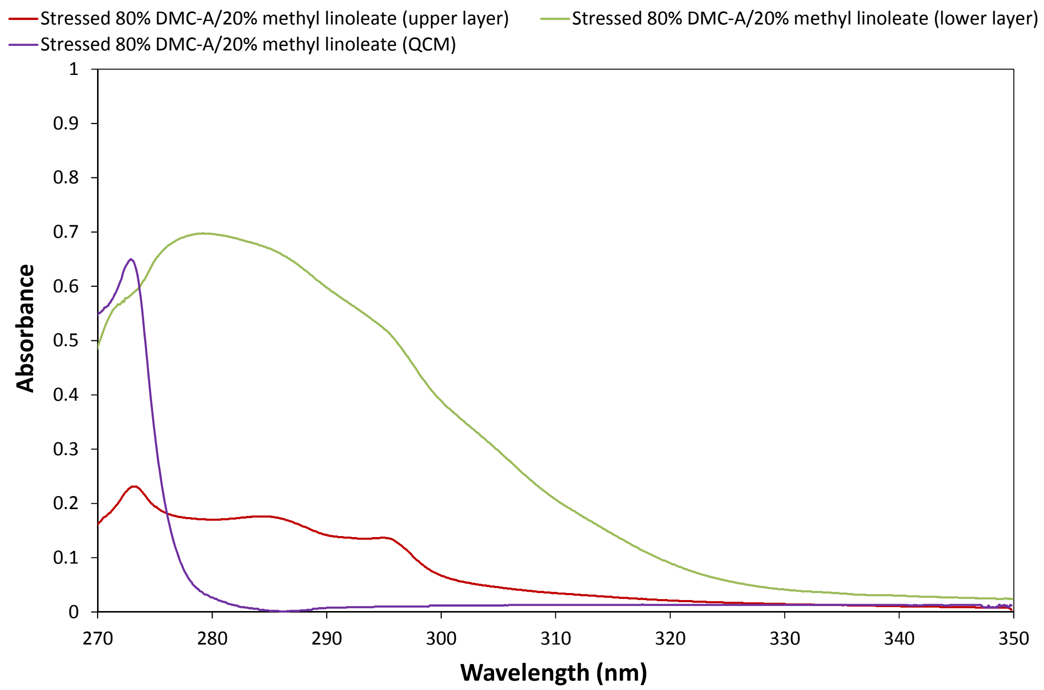

Figure 10.25: UV absorbance spectra of stressed 80% DMC-A/20% methyl linoleate after oxidative stressing at 140°C for 24h in a QCM and in an open flask

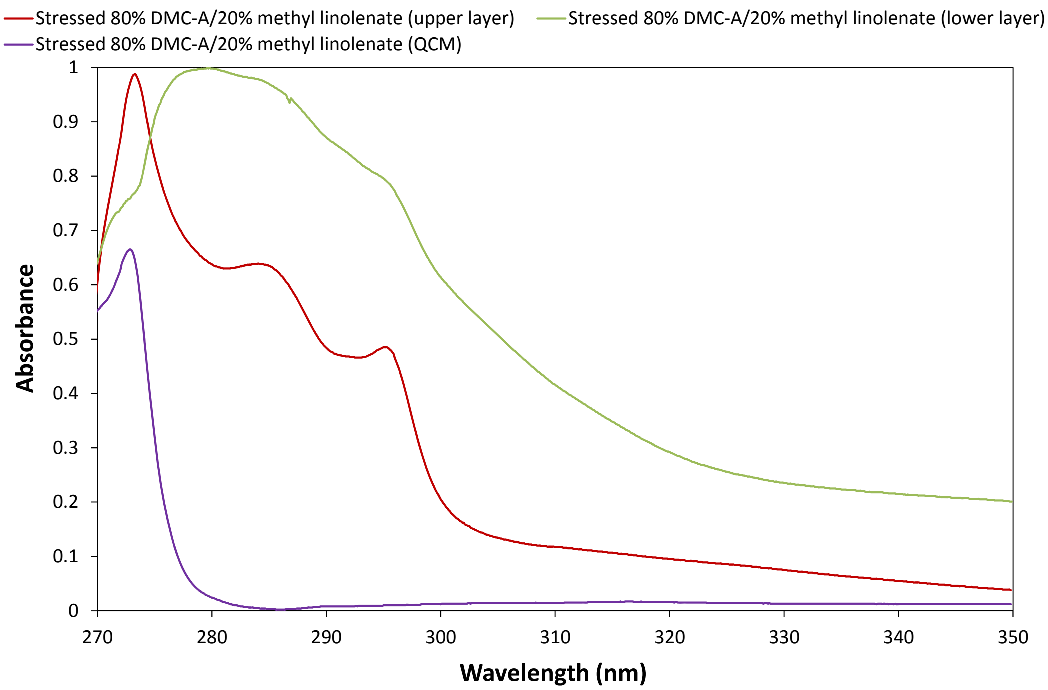

Figure 10.26: UV absorbance spectra of stressed 80% DMC-A/20% methyl linolenate after oxidative stressing at 140^{o}C for 24h in a QCM and in an open flask

10.7 ESI-MS spectra

10.7.1 QCM oxidation

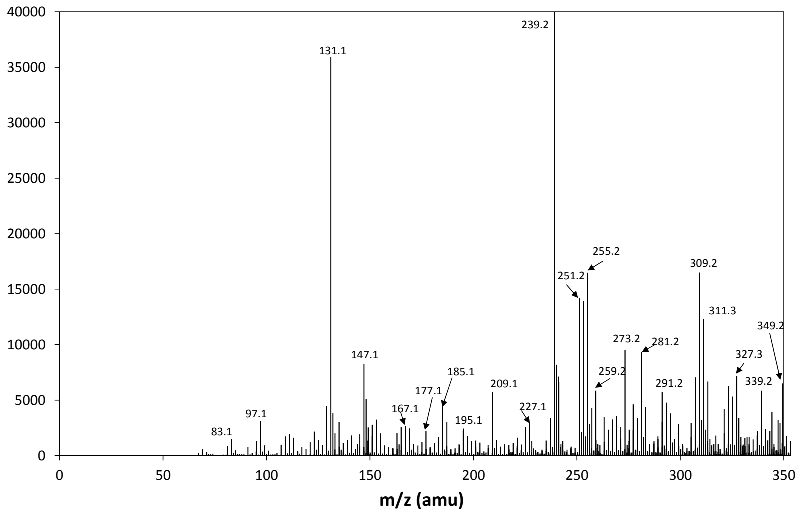

Figure 10.27: ESI-MS(+) spectrum for DMC-A after oxidation at 140°C in a QCM for 24h (0-350 amu)

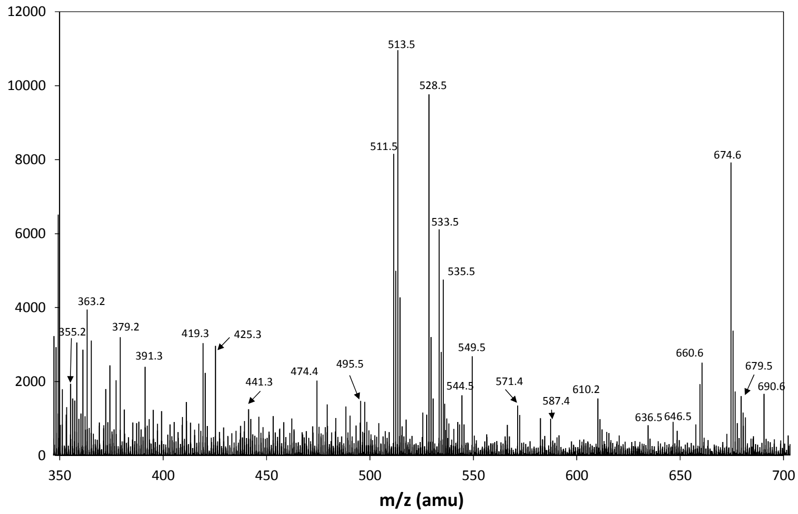

Figure 10.28: ESI-MS(+) spectrum for DMC-A after oxidation at 140°C in a QCM for 24h (350-700 amu)

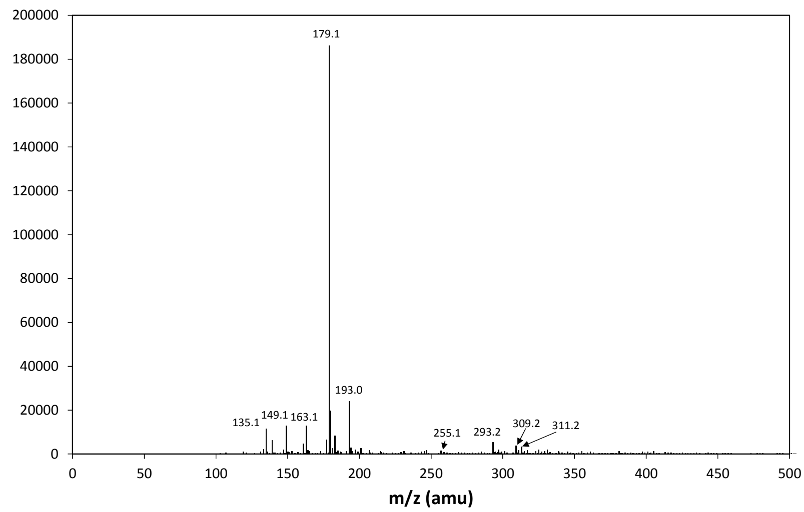

Figure 10.29: ESI-MS(-) spectrum for DMC-A after oxidation at 140^{o}C in a QCM for 24h (100-500 amu)

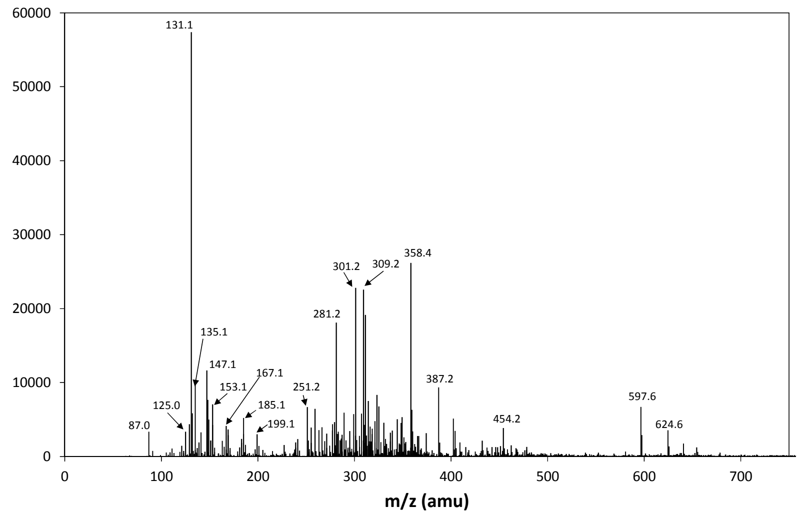

Figure 10.30: ESI-MS(+) spectrum for DMC-B after oxidation at 140^{o}C in a QCM for 24h (0-500 amu)

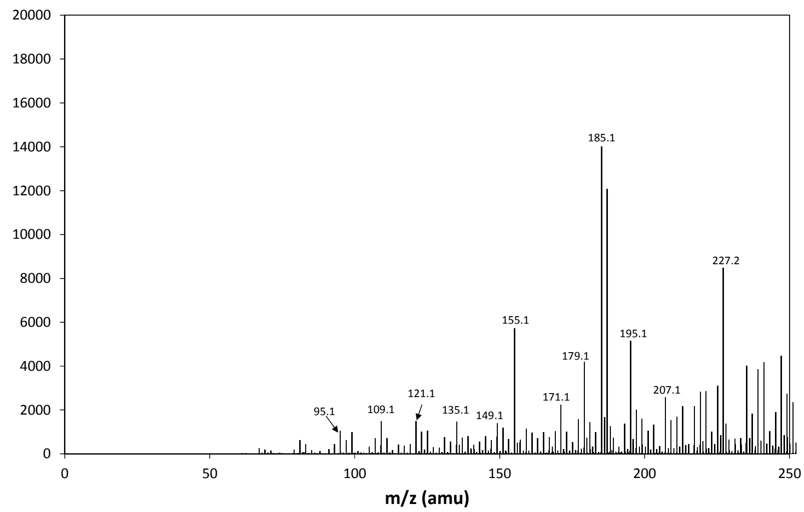

Figure 10.31: ESI-MS(+) spectrum for RME after oxidation at 140^{o}C in a QCM for 24h (0 -250 amu)

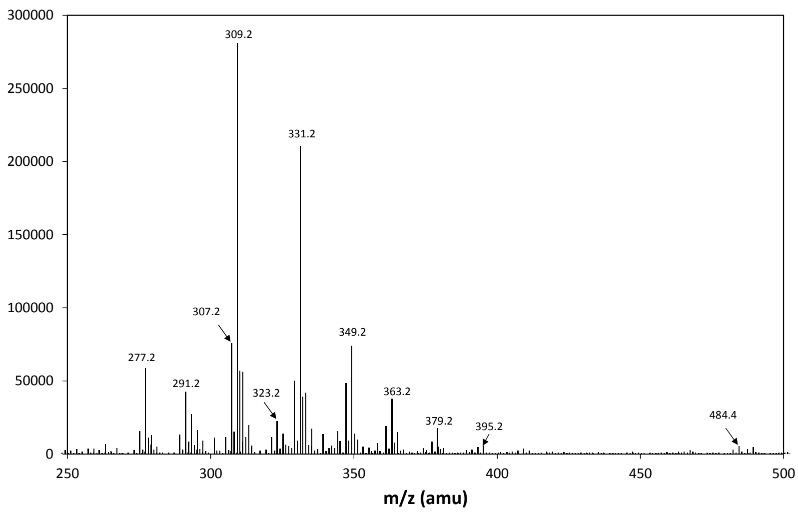

Figure 10.32: ESI-MS(+) spectrum for RME after oxidation at 140^{o}C in a QCM for 24h (250-500 amu)

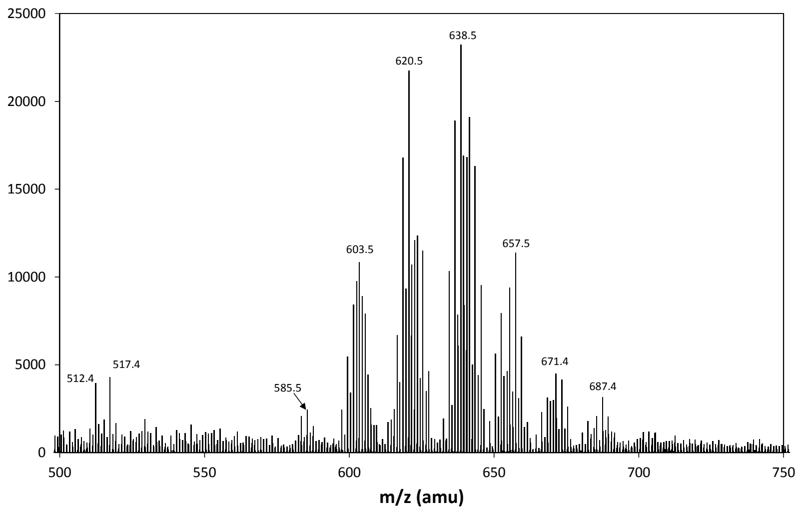

Figure 10.33: ESI-MS(+) spectrum for RME after oxidation at 140^{o}C in a QCM for 24h (500-750 amu)

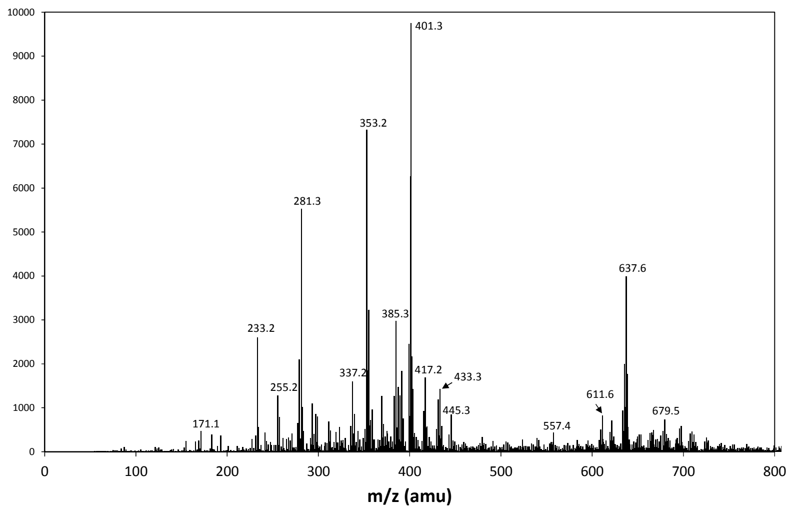

Figure 10.34: ESI-MS(-) spectrum for RME after oxidation at 140^{o}C in a QCM for 24h (0-800 amu)

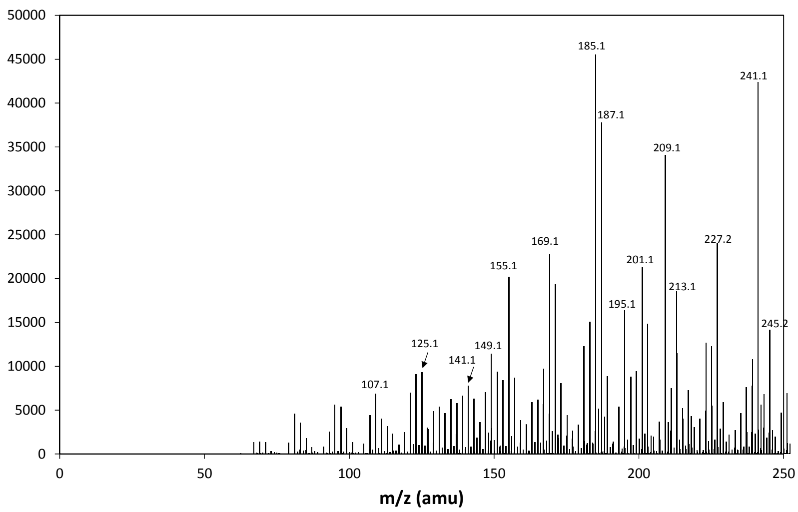

Figure 10.35: ESI-MS(+) spectrum for the 80% DMC-A/20% RME after oxidation in a QCM at 140^{o}C for 24h (0-250 amu)

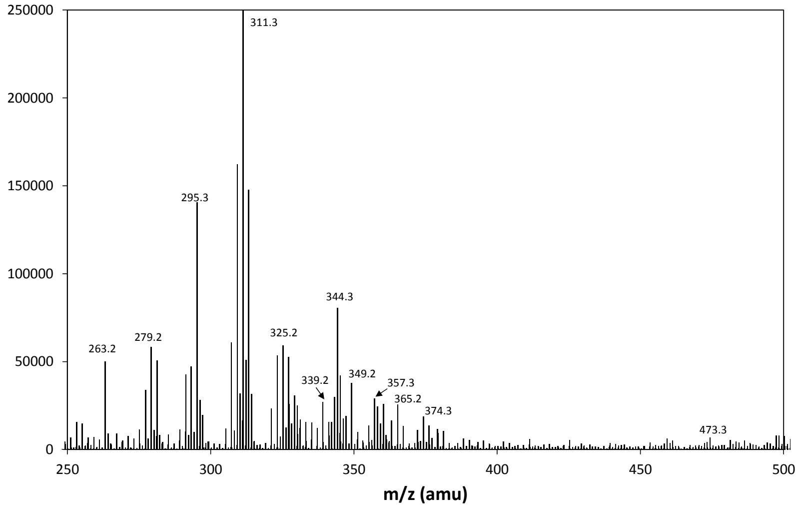

Figure 10.36: ESI-MS(+) spectrum for the 80% DMC-A/20% RME after oxidation in a QCM at 140^{o}C for 24h (250-500 amu)

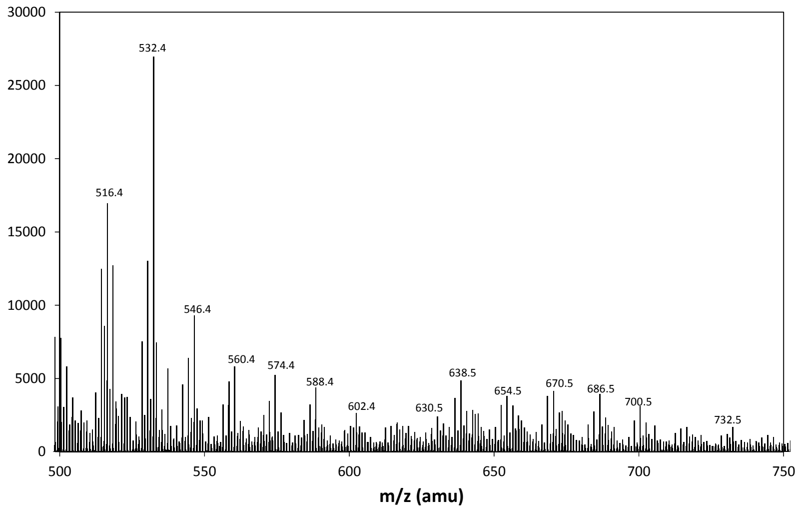

Figure 10.37: ESI-MS(+) spectrum for the 80% DMC-A/20% RME after oxidation in a QCM at 140^{o}C for 24h (500-750 amu)

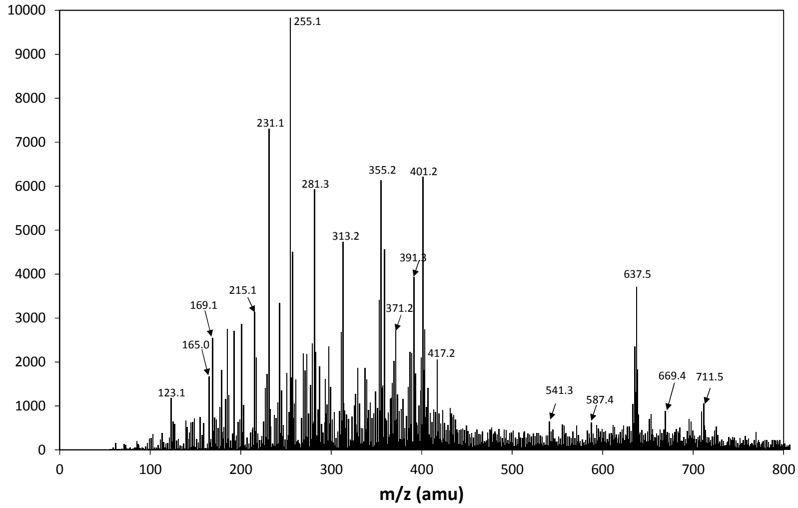

Figure 10.38: ESI-MS(-) spectrum for the 80% DMC-A/20% RME after oxidation in a QCM at 140°C for 24h (0-800 amu)

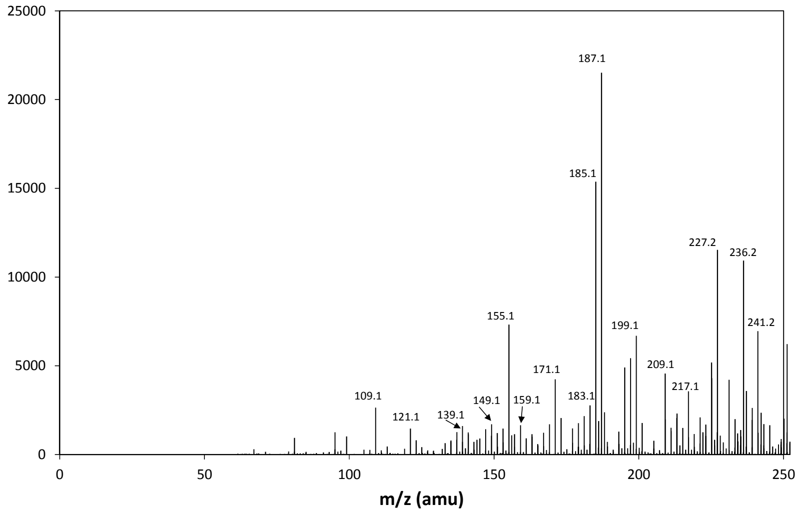

Figure 10.39: ESI-MS(+) spectrum for the 80% DMC-A/20% methyl oleate after oxidation in a QCM at 140°C for 24h (0-250 amu)

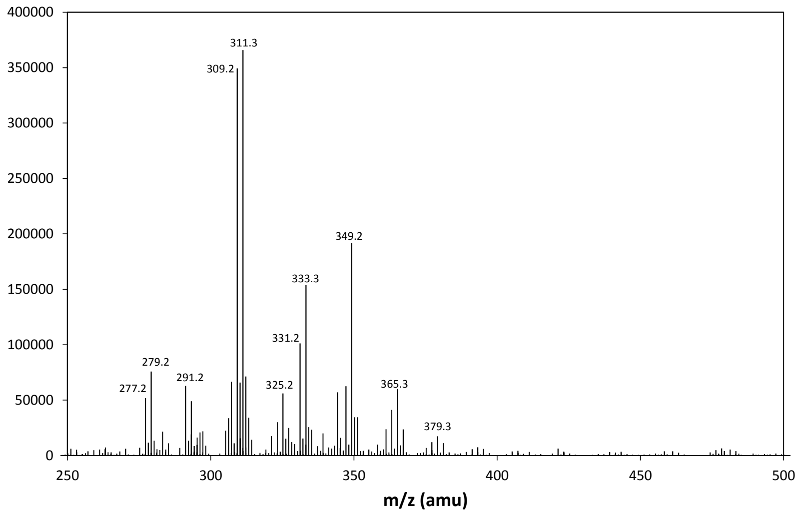

Figure 10.40: ESI-MS(+) spectrum for the 80% DMC-A/20% methyl oleate after oxidation in a QCM at 140°C for 24h (250-500 amu)

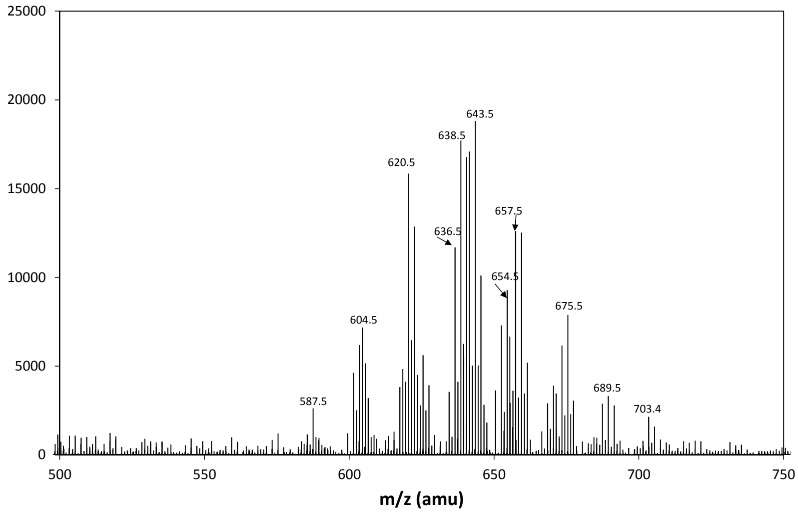

Figure 10.41: ESI-MS(+) spectrum for the 80% DMC-A/20% methyl oleate after oxidation in a QCM at 140^{o}C for 24h (500-750 amu)

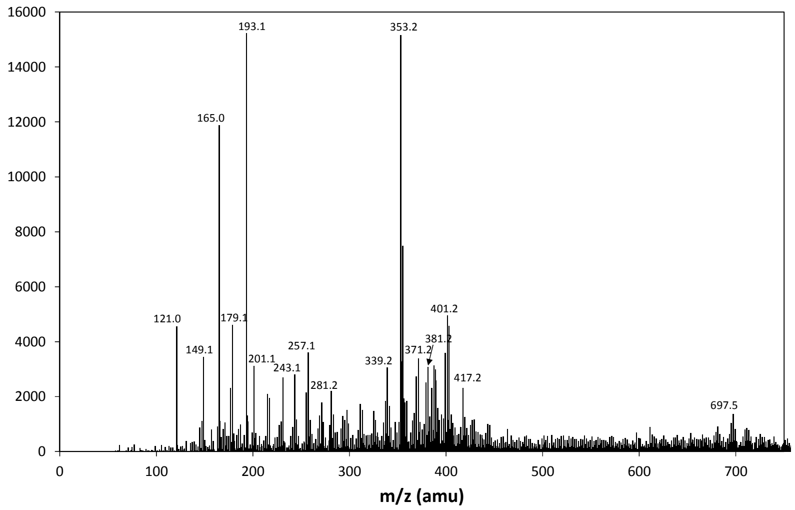

Figure 10.42: ESI-MS(-) spectrum for the 80% DMC-A/20% methyl oleate after oxidation in a QCM at 140^{o}C for 24h (0-750 amu)

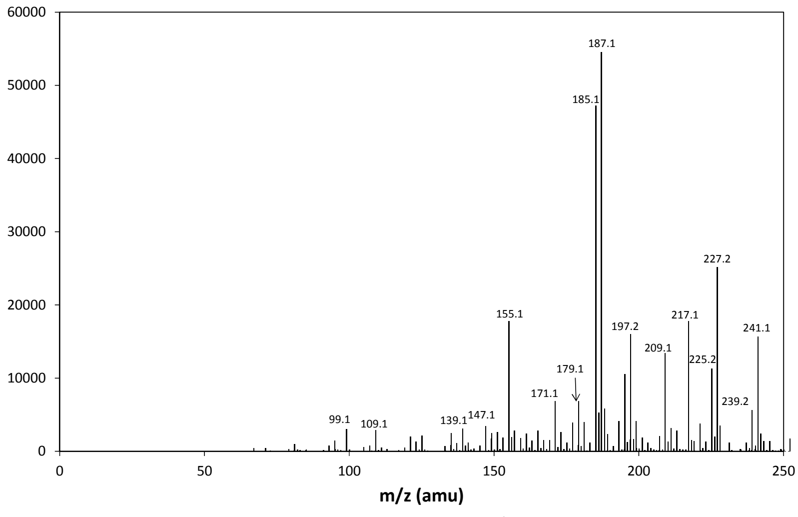

Figure 10.43: ESI-MS(+) spectrum for the 80% DMC-A/20% methyl linoleate after oxidation in a QCM at 140^{o}C for 24h (0-250 amu)

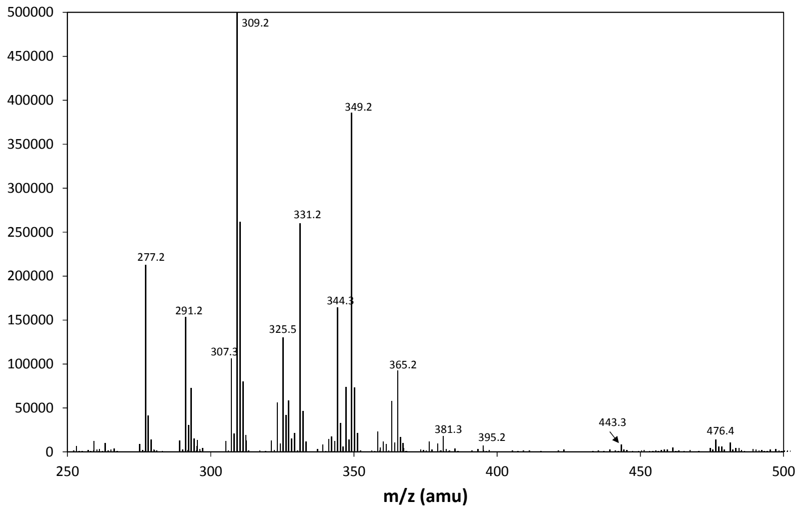

Figure 10.44: ESI-MS(+) spectrum for the 80% DMC-A/20% methyl linoleate after oxidation in a QCM at 140^{o}C for 24h (250-500 amu)

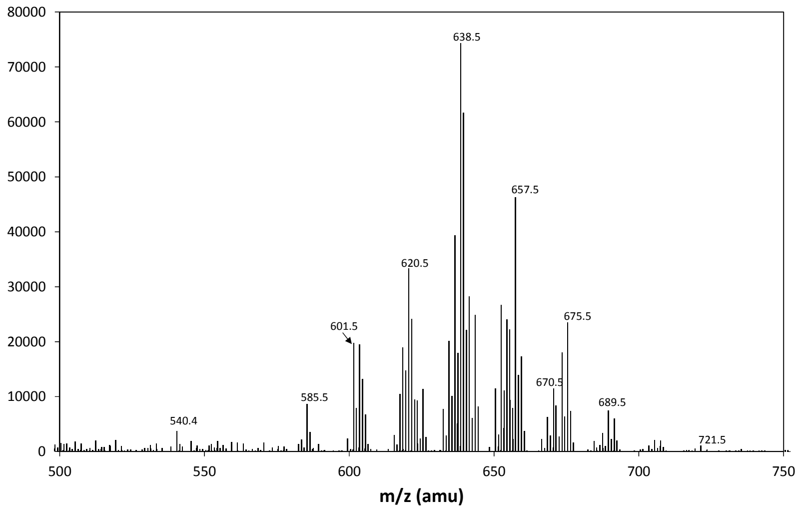

Figure 10.45: ESI-MS(+) spectrum for the 80% DMC-A/20% methyl linoleate after oxidation in a QCM at 140^{o}C for 24h (500-750 amu)

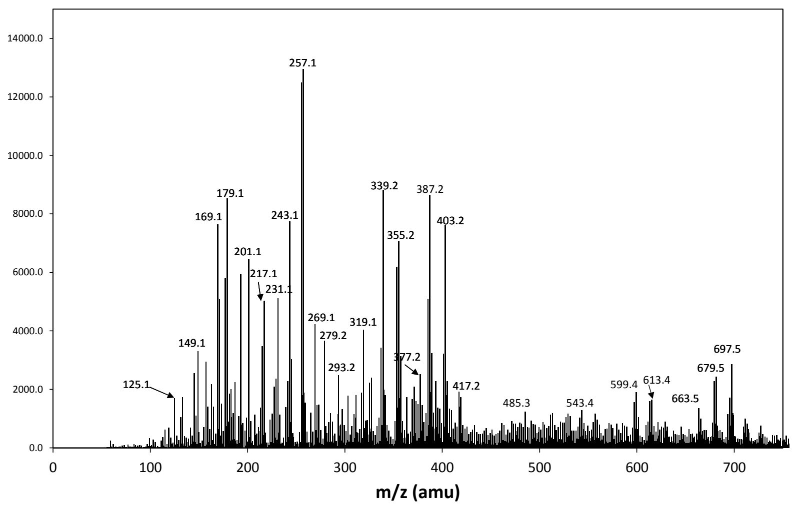

Figure 10.46: ESI-MS(-) spectrum for the 80% DMC-A/20% methyl linoleate after oxidation in a QCM at 140^{o}C for 24h (0-750 amu)

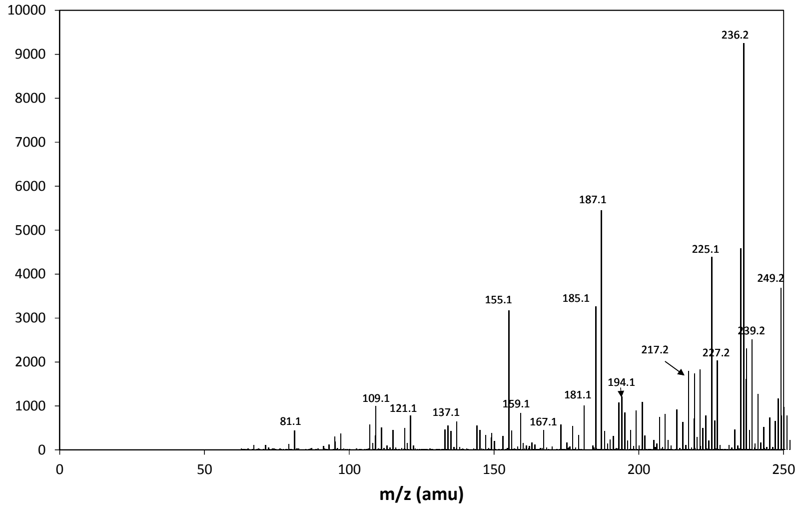

Figure 10.47: ESI-MS(+) spectrum for the 80% DMC-A/20% methyl linolenate after oxidation in a QCM at 140^{o}C for 24h (0-250 amu)

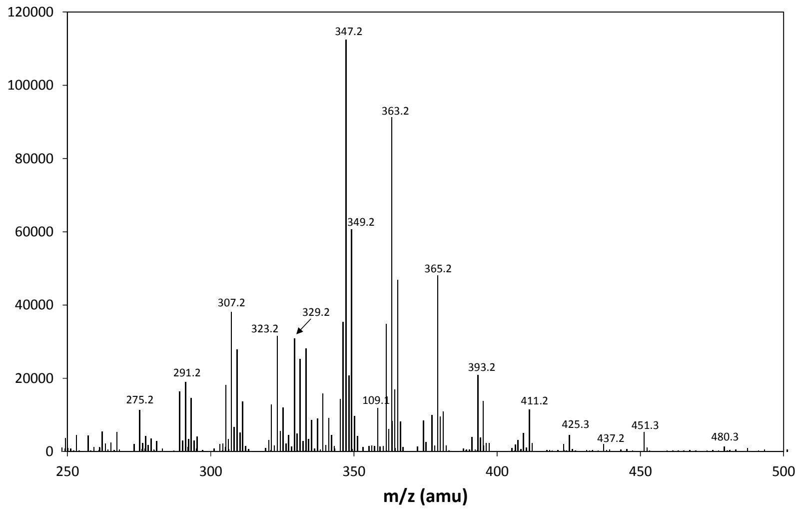

Figure 10.48: ESI-MS(+) spectrum for the 80% DMC-A/20% methyl linolenate after oxidation in a QCM at 140^{o}C for 24h (250-500 amu)

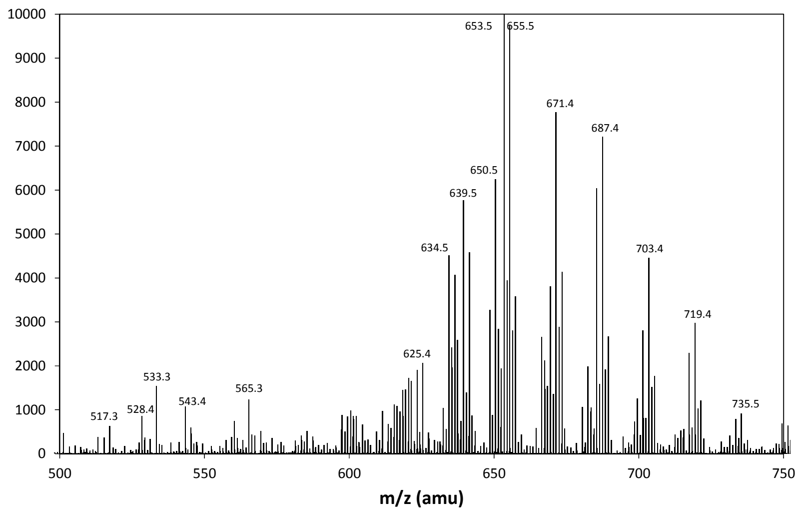

Figure 10.49: ESI-MS(+) spectrum for the 80% DMC-A/20% methyl linolenate after oxidation in a QCM at 140^{o}C for 24h (500-750 amu)

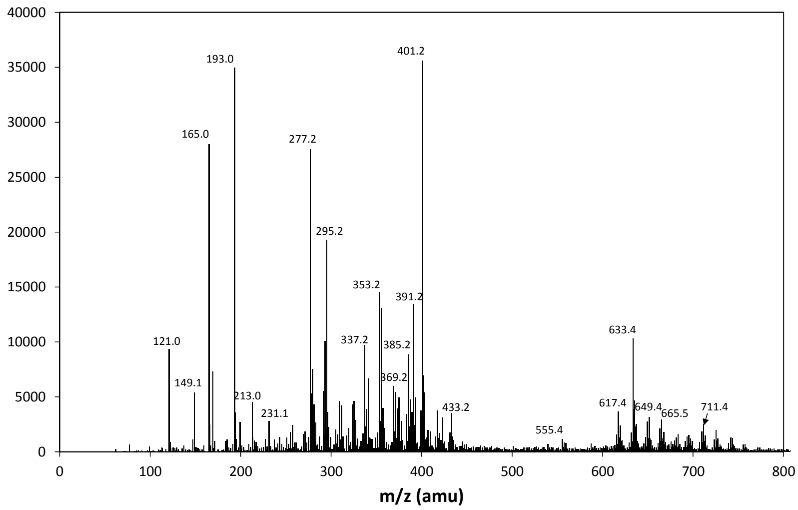

Figure 10.50: ESI-MS(-) spectrum for the 80% DMC-A/20% methyl linolenate after oxidation in a QCM at 140^{O}C for 24h (0-800 amu)

10.7.2 Flask oxidation

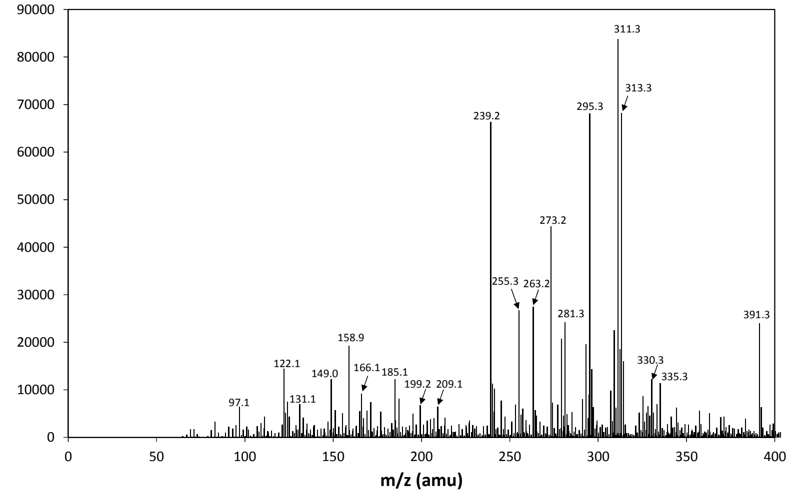

Figure 10.51: ESI-MS(+) spectrum for the upper layer from DMC-A after oxidation at 140^{o}C in a QCM for 24h (0-400 amu)

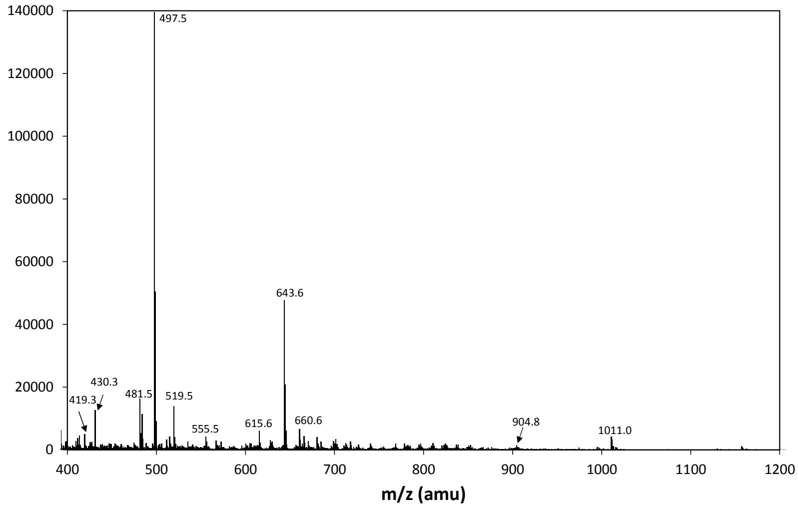

Figure 10.52: ESI-MS(+) spectrum for the upper layer from DMC-A after oxidation at 140^{o}C in a QCM for 24h (400-1200 amu)

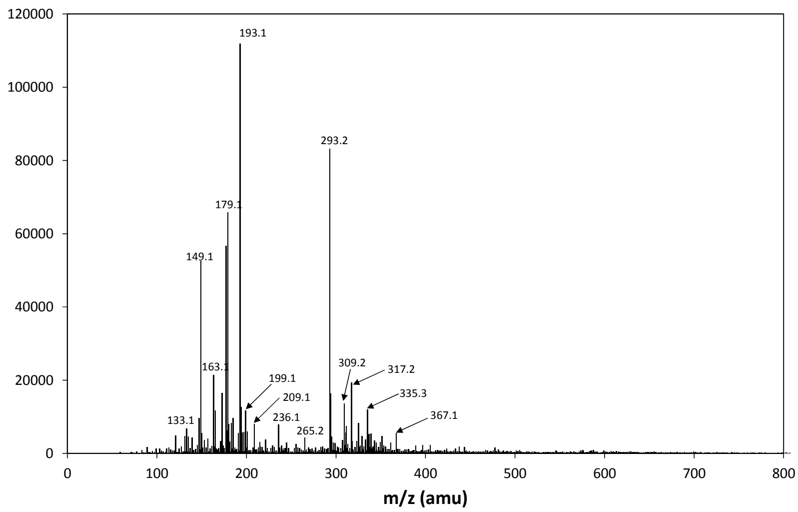

Figure 10.53: ESI-MS(-) spectrum for the upper layer from DMC-A after oxidation at 140^{o}C in a QCM for 24h (0-800 amu)

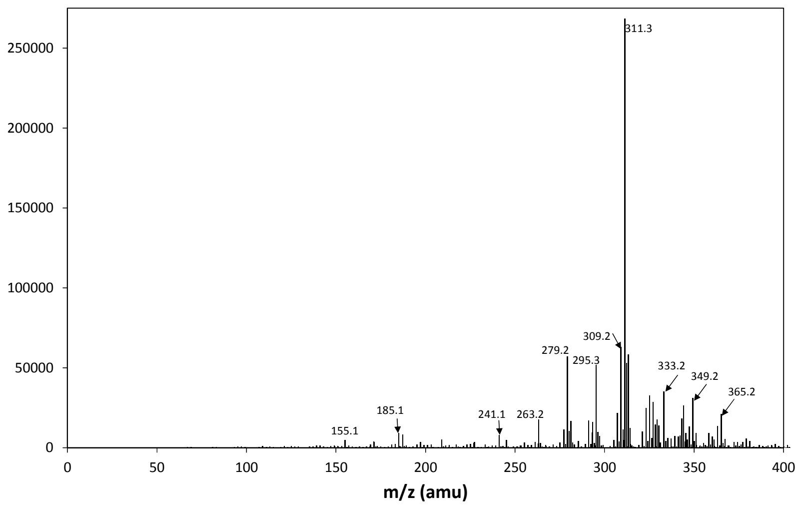

Figure 10.54: ESI-MS(+) spectrum for RME after oxidation at 140^{o}C in an open flask for 48h (0-400 amu)

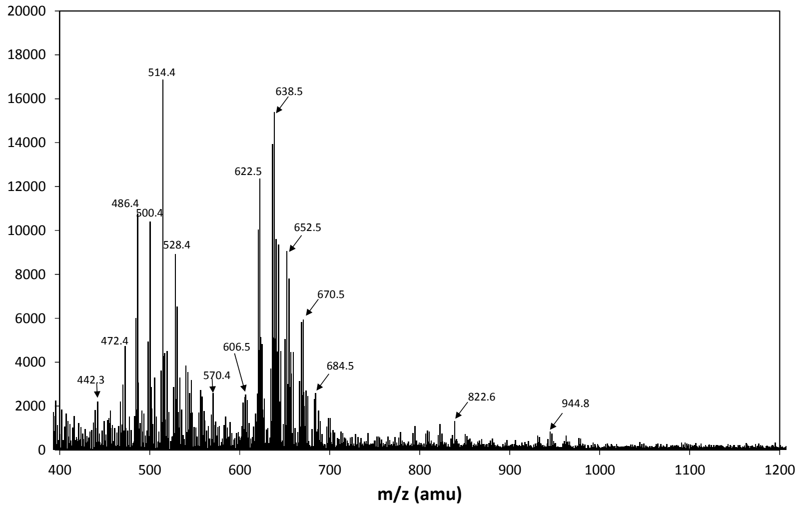

Figure 10.55: ESI-MS(+) spectrum for RME after oxidation at 140^{o}C in an open flask for 48h (400-1200 amu)

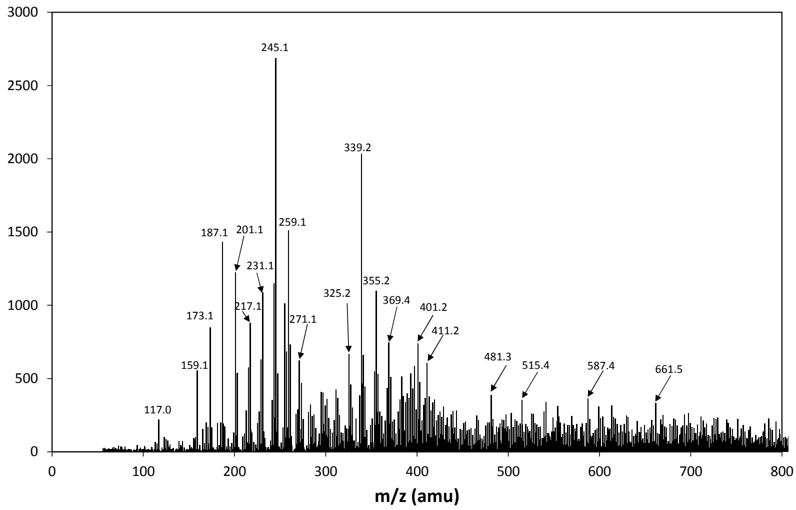

Figure 10.56: ESI-MS(-) spectrum for RME after oxidation at 140^{o}C in an open flask for 48h (0-800 amu)

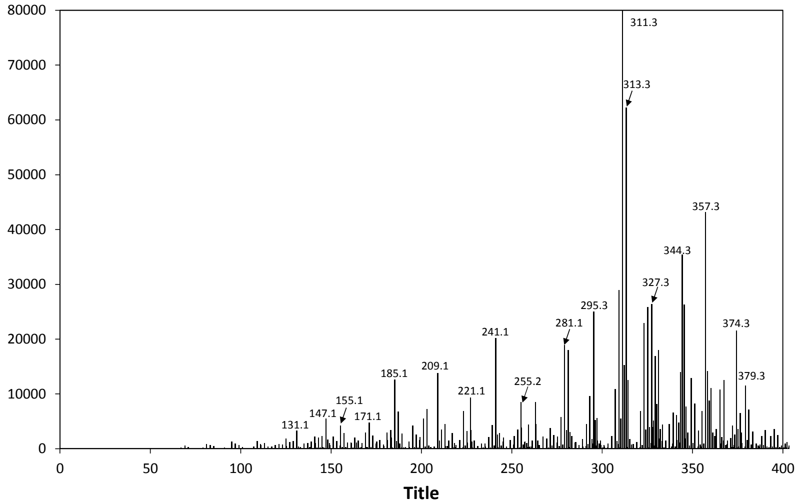

Figure 10.57: ESI-MS(+) spectrum for the lower layer of 80% DMC-A/20% RME after oxidation at 140^{o}C in a QCM for 24h (0-400 amu)

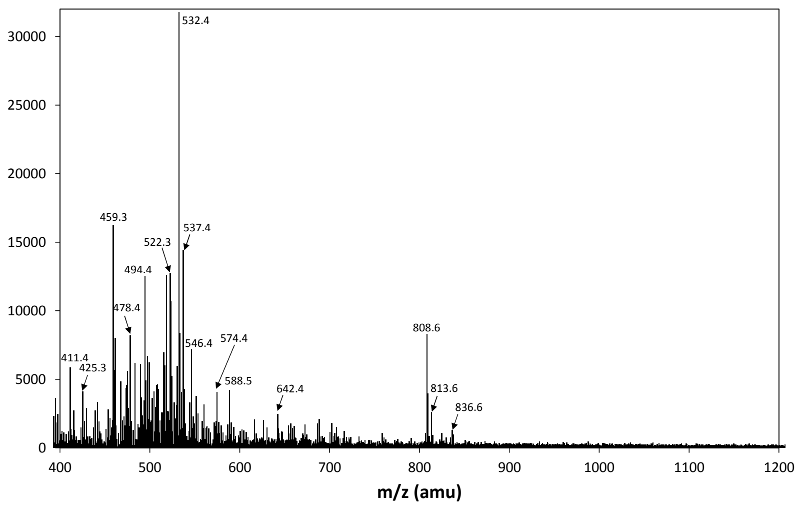

Figure 10.58: ESI-MS(+) spectrum for the lower layer of 80% DMC-A/20% RME after oxidation at 140^{o}C in a QCM for 24h (400-1200 amu)

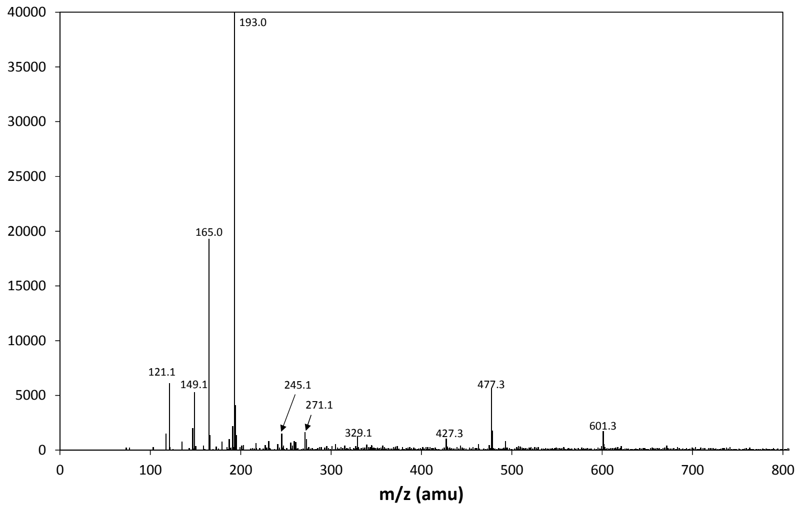

Figure 10.59: ESI-MS(-) spectrum for the lower layer of 80% DMC-A/20% RME after oxidation at 140^{o}C in a QCM for 24h (0-800 amu)

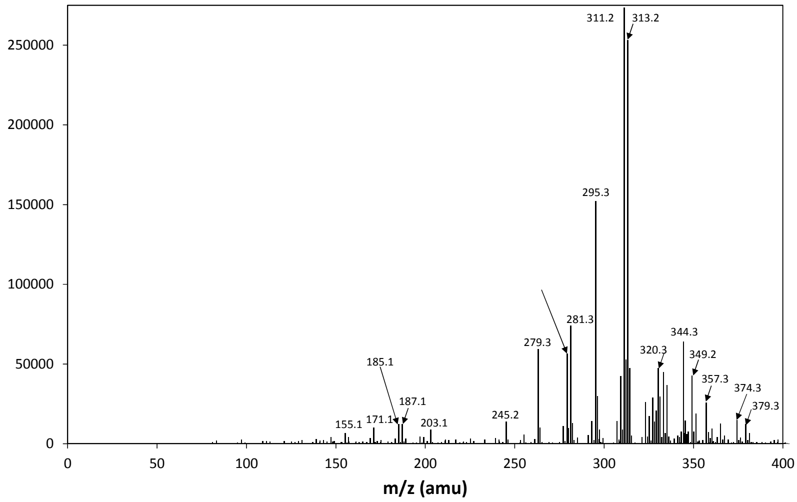

Figure 10.60: ESI-MS(+) spectrum for the upper layer of 80% DMC-A/20% RME after oxidation at 140^{o}C in a QCM for 24h (0-400 amu)

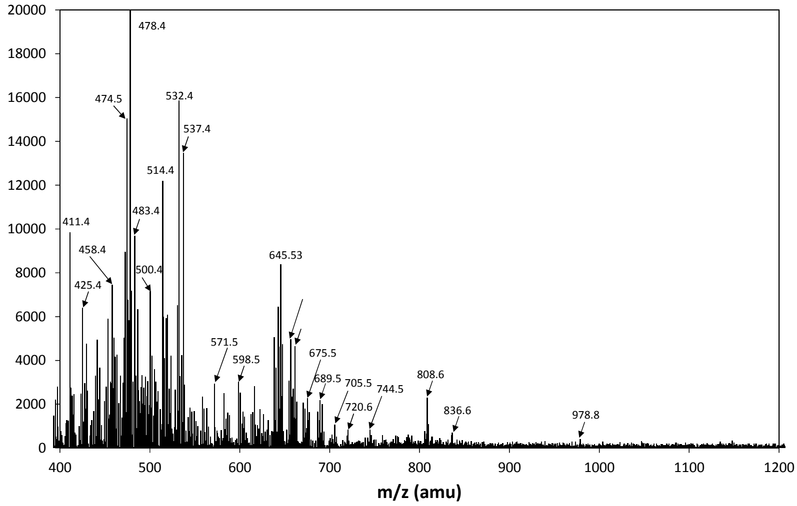

Figure 10.61: ESI-MS(+) spectrum for the upper layer of 80% DMC-A/20% RME after oxidation at 140^{o}C in a QCM for 24h (400-1200 amu)

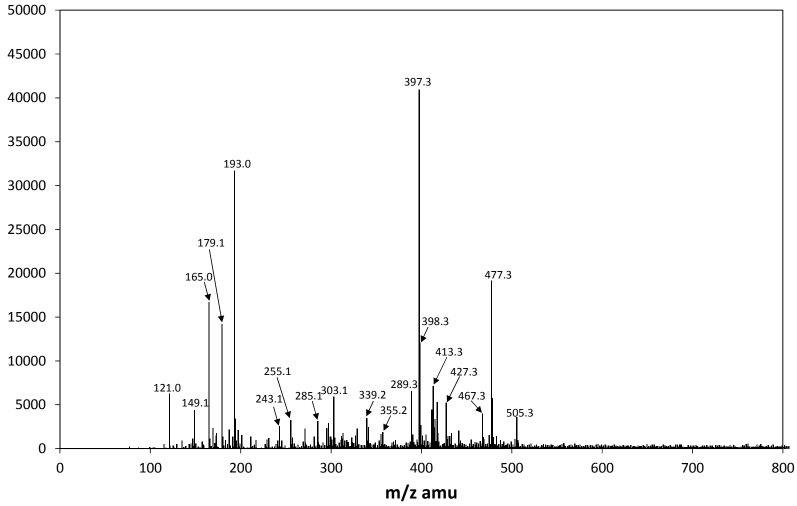

Figure 10.62: ESI-MS(-) spectrum for the upper layer of 80% DMC-A/20% RME after oxidation at 140^{o}C in a QCM for 24h (0-800 amu)

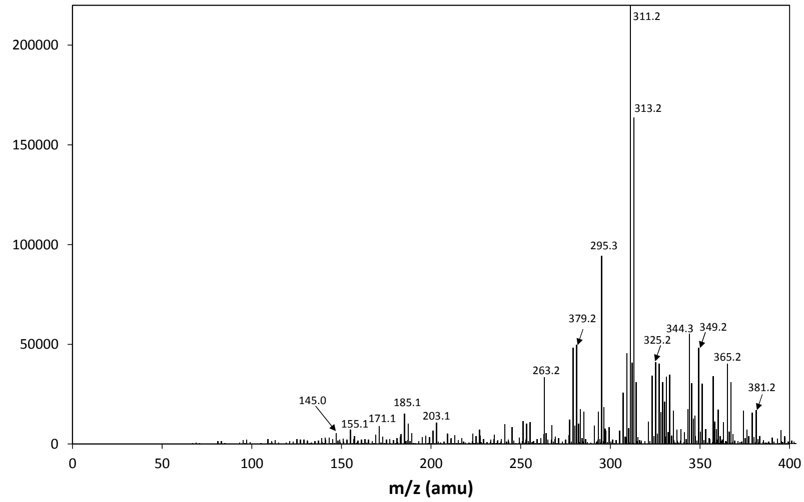

Figure 10.63: ESI-MS(+) spectrum for the lower layer of 80% DMC-A/20% methyl oleate after oxidation at 140^{o}C in an open flask for 24h (0-400 amu)

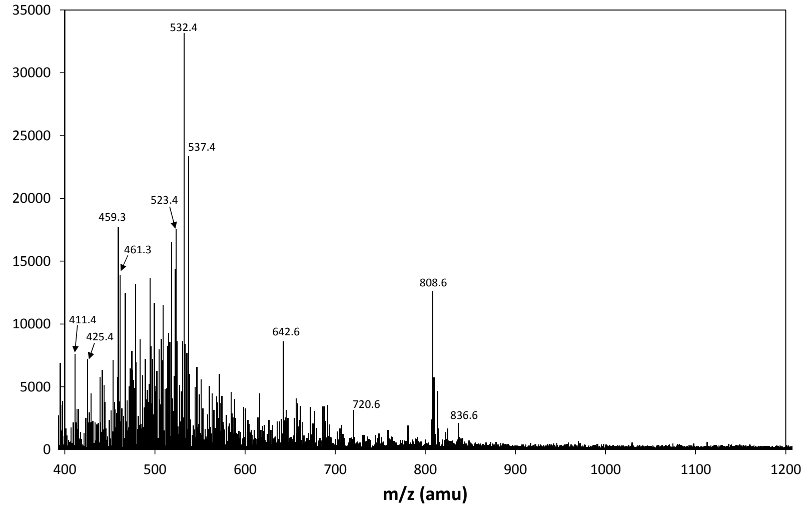

Figure 10.64: ESI-MS(+) spectrum for the lower layer of 80% DMC-A/20% methyl oleate after oxidation at 140^{o}C in an open flask for 24h (400-1200 amu)

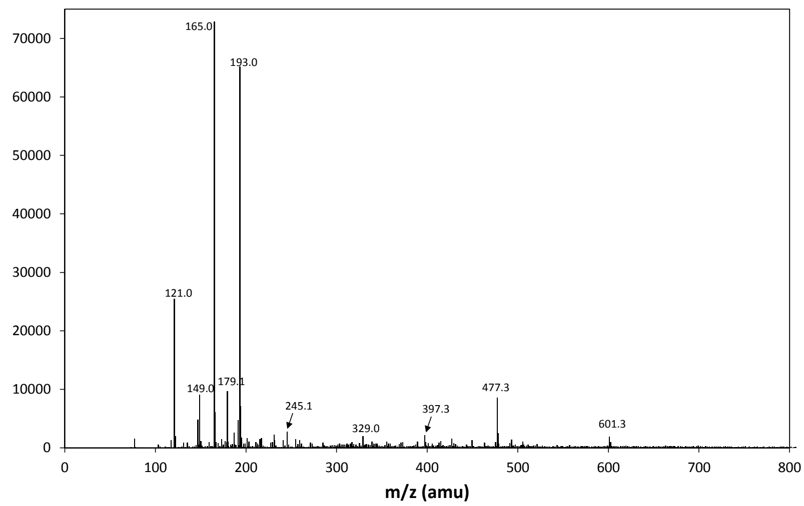

Figure 10.65: ESI-MS(-) spectrum for the lower layer of 80% DMC-A/20% methyl oleate after oxidation at 140^{o}C in an open flask for 24h (0-800 amu)

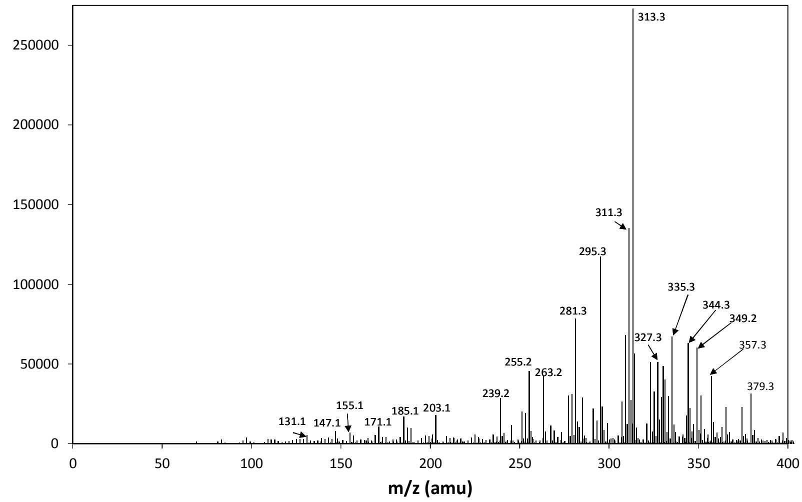

Figure 10.66: ESI-MS(+) spectrum for the upper layer of 80% DMC-A/20% methyl oleate after oxidation at 140^{o}C in an open flask for 24h (0-400 amu)

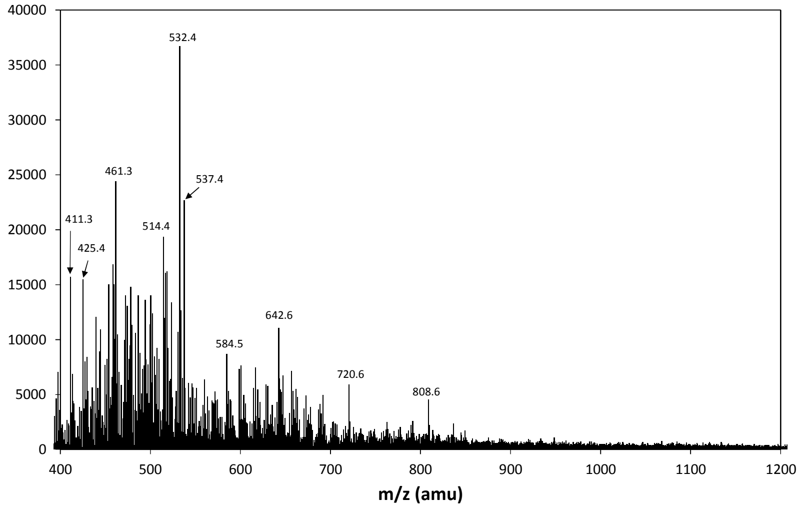

Figure 10.67: ESI-MS(+) spectrum for the upper layer of 80% DMC-A/20% methyl oleate after oxidation at 140^{o}C in an open flask for 24h (400-1200 amu)

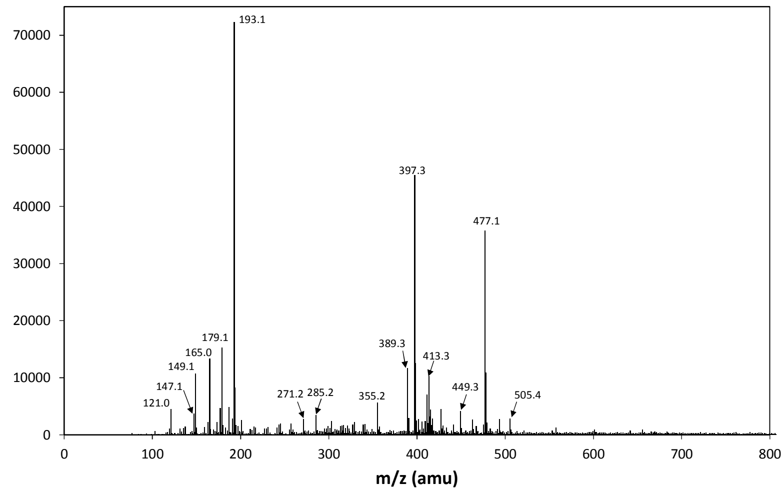

Figure 10.68: ESI-MS(-) spectrum for the upper layer of 80% DMC-A/20% methyl oleate after oxidation at 140^{o}C in an open flask for 24h (0-800 amu)

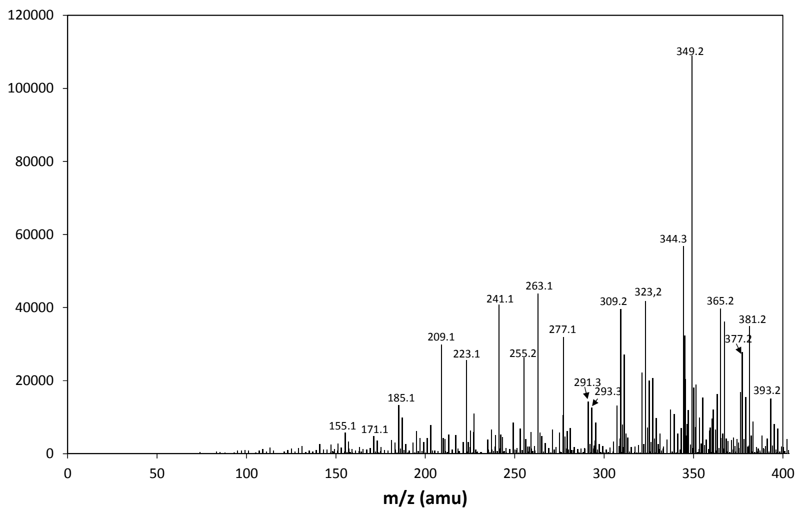

Figure 10.69: ESI-MS(+) spectrum for the lower layer of 80% DMC-A/20% methyl linoleate after oxidation at 140^{o}C in an open flask for 24h (0-400 amu)

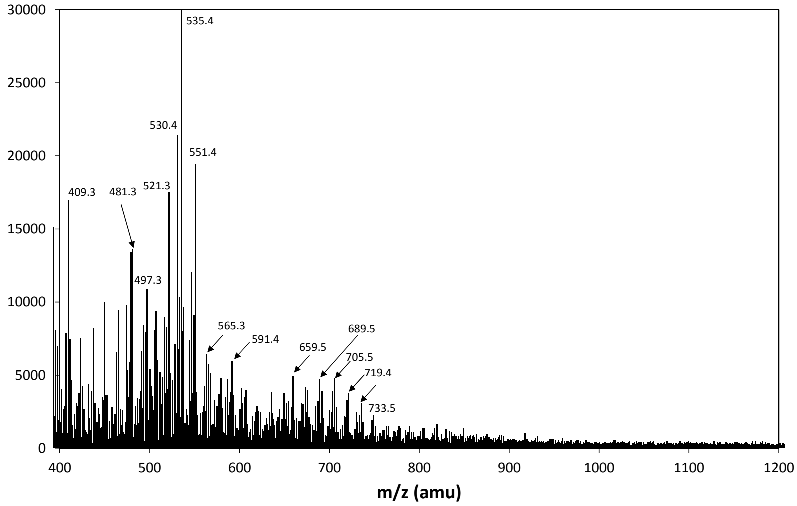

Figure 10.70: ESI-MS(+) spectrum for the lower layer of 80% DMC-A/20% methyl linoleate after oxidation at 140^{o}C in an open flask for 24h (400-1200 amu)

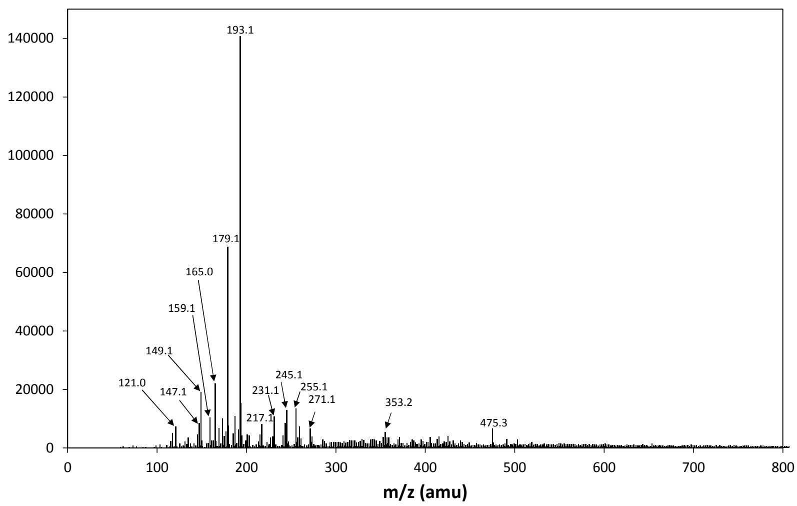

Figure 10.71: ESI-MS(-) spectrum for the lower layer of 80% DMC-A/20% methyl linoleate after oxidation at 140^{o}C in an open flask for 24h (0-800 amu)

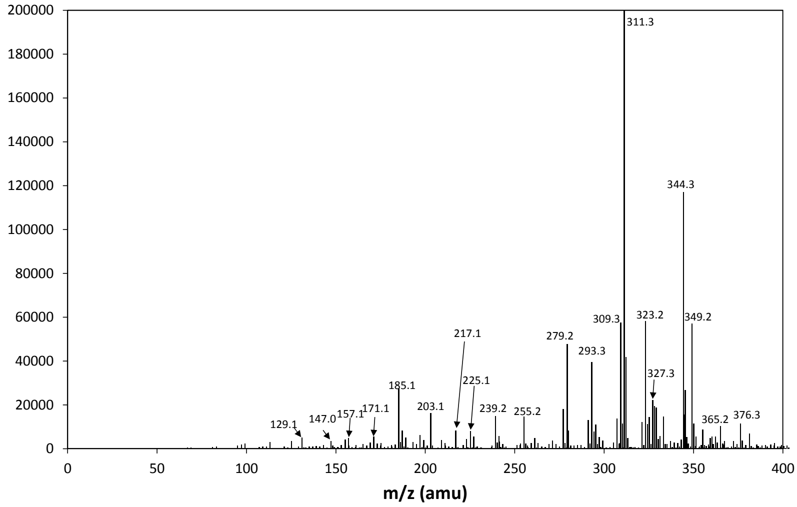

Figure 10.72: ESI-MS(+) spectrum for the upper layer of 80% DMC-A/20% methyl linoleate after oxidation at 140^{o}C in an open flask for 24h (0-400 amu)

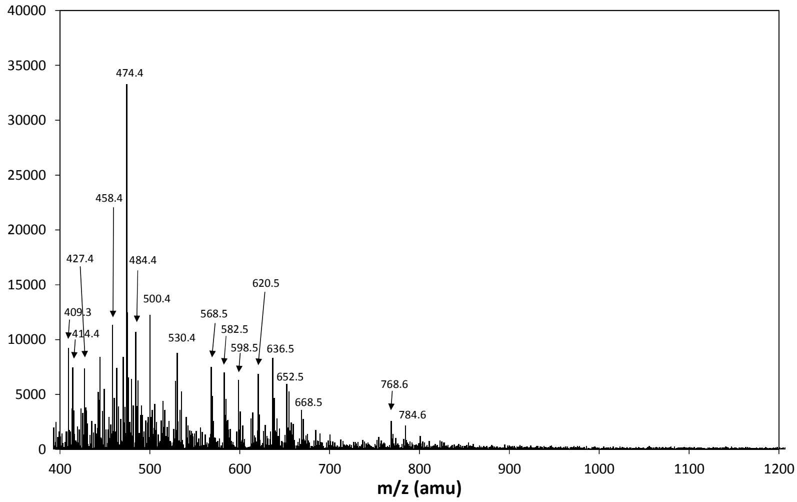

Figure 10.73: ESI-MS(+) spectrum for the upper layer of 80% DMC-A/20% methyl linoleate after oxidation at 140^{o}C in an open flask for 24h (400-1200 amu)

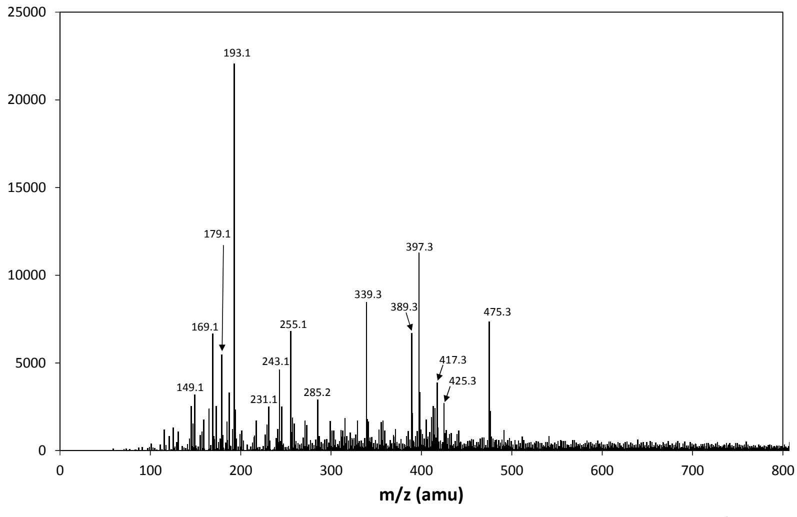

Figure 10.74: ESI-MS(-) spectrum for the upper layer of 80% DMC-A/20% methyl linoleate after oxidation at 140^{o}C in an open flask for 24h (0-800 amu)

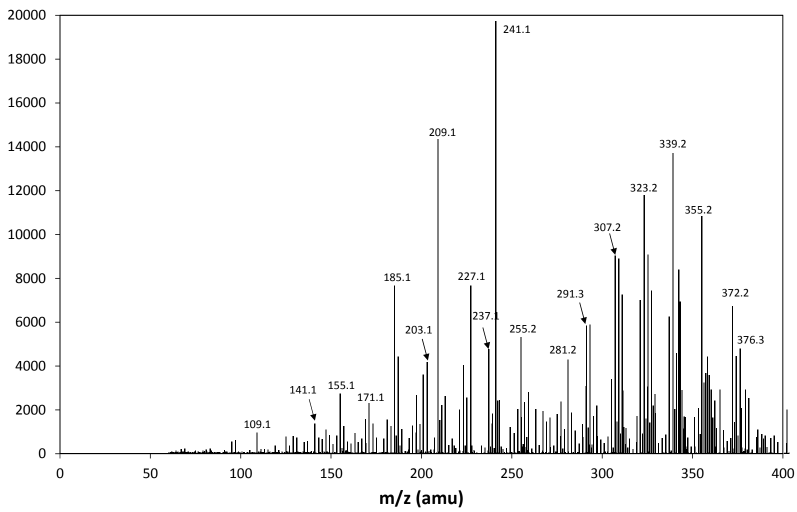

Figure 10.75: ESI-MS(+) spectrum for the lower layer of 80% DMC-A/20% methyl linolenate after oxidation at 140^{o}C in a QCM for 24h (0-400 amu)

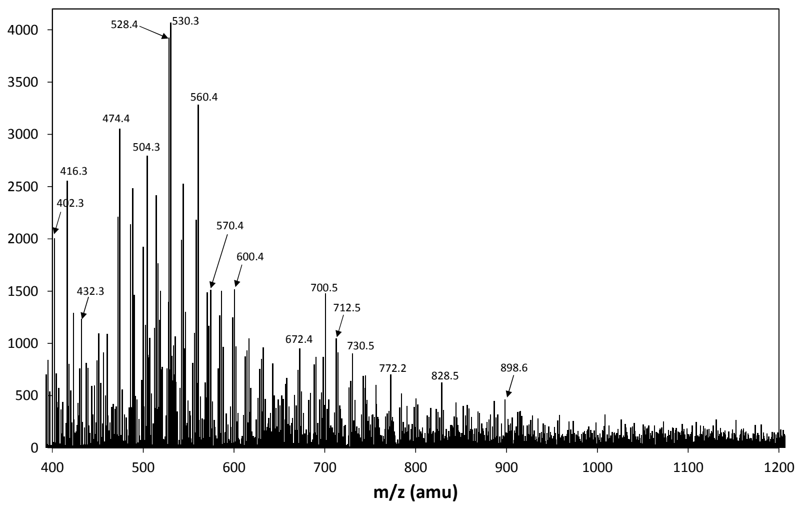

Figure 10.76: ESI-MS(+) spectrum for the lower layer of 80% DMC-A/20% methyl linolenate after oxidation at 140^{o}C in a QCM for 24h (400-1200 amu)

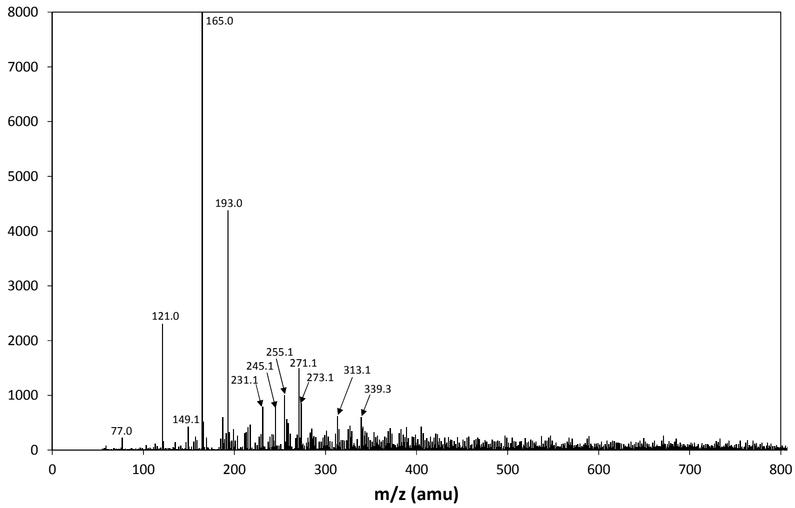

Figure 10.77: ESI-MS(-) spectrum for the lower layer of 80% DMC-A/20% methyl linolenate after oxidation at 140^{o}C in a QCM for 24h (0-800 amu)